DOCTOR OF PHILOSOPHY

Engineering novel antibody-based molecules to probe the role of the immunoglobulin hinge and generate a potential cancer vaccine

Leong, Tein Foong

Award date:
2017

Engineering novel antibody-based molecules to probe the role of the immunoglobulin hinge and generate a potential cancer vaccine

Tein Foong Leong

A thesis submitted for the degree of

Doctor of Philosophy

University of Dundee

May 2017

TABLE OF CONTENTS

LIST OF FIGURES

CHAPTER ONE

CHAPTER THREE

CHAPTER FOUR

CHAPTER FIVE

CHAPTER SIX

CHAPTER SEVEN

LIST OF TABLES

CHAPTER TWO

CHAPTER THREE

CHAPTER FOUR

CHAPTER FIVE

CHAPTER SIX

CHAPTER SEVEN

ACKNOWLEDGEMENTS

Firstly, I would like to thank my supervisor, Prof. Jenny Woof, for her guidance, advice and encouragement throughout my PhD project. I am very grateful to her because of her generosity in supporting my study through provision of laboratory materials and aiding my participation in conferences. I cannot thank her enough for what she had provided me throughout these four years.

I am indebted with many people within Division of Cell Signalling and Immunology and Division of Cancer Research for their support and advice. They have provided me with crucial materials that have aided the progression of this project. Without their materials, this project may not be completed successfully. Ask around and they will provide you with all the things you need. I would also like to thank Saira Ashraf and Timothy Wilson from Oligonucleotide Synthesis Service, University of Dundee, for their help and teaching as well as allowing me to use their equipment to carry out my experiments.

A special thanks to my fellow lab-mates, Lois Paton and Ruby, for being great friends and companions throughout my time in the lab. Both our happy and difficult times together shall always be remembered.

Finally, a great thank you to some of the people that are very precious to me. Thank you to my parents, Danny Leong Chee Kheong and Ho Yin Leng, for their unconditional and endless love and support. To both my siblings, Leong Yu Ting and Leong Wan Er, your stories have kept me entertained all this while. And to Phoebe Su Wan Tyng, thank you for being by my side with your unwavering love and support in the challenges I faced.

Thank you.

DECLARATION

I hereby declare that the candidate below is the author of this thesis, that all the references cited have been consulted by the candidate, that the work of which the thesis is a record has been carried out by the candidate, except where clearly stated, and has not previously been presented for the award of any other degree.

Signed:

Tein Foong Leong

I hereby declare that Tein Foong Leong has carried out his research under my supervision, and has fulfilled the conditions of the relevant Ordinance and Regulations of the University of Dundee, so that he is qualified to submit the following thesis in application for the degree of Doctor of Philosophy.

Signed:

Professor J. M. Woof
Professor and Associate Dean (Quality & Academic Standards)
Division of Cell Signalling and Immunology
University of Dundee

SUMMARY OF CONTENTS

In different immunoglobulin (Ig) isotypes, the hinge region, which separates the antigen-binding Fab region from the Fc region, varies considerably in length. The hinge region is believed to provide flexibility for the Ig to conduct better positioning for antigen binding via the Fab arms or better receptor association via the Fc region. However, the reason for the difference in hinge length among different Igs is not fully understood. In this project it is hypothesised that the longer the upper hinge length of an IgG the further the distance that the antigen binding sites at the tips of Fab arms are able to reach between neighbouring antigens.

In order to investigate the relation between upper hinge region of IgG and the distance between antigen binding sites, human IgG1 mutants specific for the hapten NIP which featured different upper hinge lengths were generated. Rigid bivalent ligands or "molecular rulers" (dsNIP-DNA) comprising defined lengths of double stranded DNA with NIP covalently attached to both ends were produced. ELISA tests demonstrated that anti-NIP human IgG1 bound to dsNIP-DNA. Through employment of molecular rulers of different lengths, surface plasmon resonance experiments indicated that the maximum distance between antigen binding sites is influenced by the length of the upper part of the IgG hinge. In addition, the role of upper hinge length on the ability of IgG to bridge between antigen on a target cell surface and Fc receptors on the surface of a phagocyte was investigated. Rosette formation between antibody-coated erythrocytes and Fc receptor-positive effector cells was utilised as an assay for this bridging. When anti-NIP human IgG1 hinge mutants were compared to wildtype IgG1, differences in rosette formation efficiency

were observed indicating that the upper hinge region has a role in facilitating the bridging between an antigenic target cell and effector cell.

In a second IgG engineering approach, potential cancer vaccines that feature the Fc region of IgG fused to the tumour associated cancer-testis antigen, MAGE-A, were generated and tested. Such vaccines are designed to promote formation of immune complexes, which are preferentially taken up by dendritic cells via their FcRn receptors, with the aim of stimulating a strong anti-tumour immune response. Human MAGE-A2 fused to either human IgG1 Fc or mouse IgG2a Fc had been successfully produced and purified using Protein-G Sepharose. Results from Coomassie staining and western blotting analyses suggested that the Fc fusion proteins were suffering from protein aggregations and possibly protein degradations. To test if MAGE-A2 Fc fusion protein can be a potential cancer vaccine, an 8 amino acid peptide sequence, SIINFEKL, was incorporated into MAGE-A2 protein of the Fc fusion protein containing mouse IgG2a Fc. IgG-immune complexes of SIINFEKL incorporated Fc fusion protein were incubated with bone marrow derived dendritic cells (BMDC) and corresponding cytotoxic T cells, B3Z, to investigate the induction of antigen cross presentation. Unfortunately, SIINFEKL incorporated Fc fusion protein was unable to activate B3Z T cells. Further investigation showed that BMDC seems to have a low expression of FcRn receptor, which is crucial for inducing an effective antigen cross presentation, and might be the reason for the unsuccessful antigen cross presentation assay. As a result, further investigations are required to determine if MAGE-A2 Fc fusion protein can be a potential cancer vaccine. More studies are also required to understand the characteristics of MAGE-A2 Fc fusion protein to minimise protein aggregations or protein degradations.

ABBREVIATIONS

0.5HA	anti-NIP mutant human IgG1 heavy chain with half hIgA1 hinge inserted
1HA	anti-NIP mutant human IgG1 heavy chain with full hIgA1 hinge inserted
ADCC	antibody dependent cell mediated cytotoxicity
ADCP	antibody dependent cellular phagocytosis
AHA	anti-hinge antibodies
Ala	alanine
APC	antigen presenting cells
Asn	asparagine
Asp	aspartic acid
BCR	B-cell receptor
BiTE	bispecific T cell engager
BMDC	bone marrow derived dendritic cells
bp	base pairs
BSA	bovine serum albumin
ºC	degrees Celsius
CD	cluster of differentiation
CDC	complement-dependent cytotoxicity
CDRs	complementarity determining regions
CH	constant domain of immunoglobulin heavy chain
CHO	Chinese hamster ovary
CL	constant domain of immunoglobulin light chain
cRPMI	complete RPMI medium

Cys	cysteine
DC	dendritic cells
DNA	deoxyribonucleic acid
DNP	2,4-Dinitrophenol
dsDNA	double stranded DNA
E.coli	*Escherichia coli*
ELISA	enzyme-linked immunosorbent assay
EM	electron microscopy
Ep-CAM	epithelial cell adhesion molecule
Fab	fragment antigen binding
Fc	fragment crystallisable
FcγR	Fc gamma receptor
FDA	US Food and Drug Administration
Gly	glycine
HEK	Human embryonic kidney
HPLC	High Performance Liquid Chromatography
HRP	horseradish peroxidase
HSV-2	herpes simplex virus type-2
His	histidine
IC	immune complex
Ig	immunoglobulin
Ile	isoleucine
kDa	kilo Dalton

LB	Luria-Bertani
Leu	leucine
MAC	membrane attack complex
MAGE	melanoma-associated antigens
MFc	MAGE-A2 fused with IgG Fc protein
MHC	major histocompatibility complex
Mono-Strep	monovalent streptavidin
NIP	3-nitro-4-hydroxy-5-iodophenylacetate
NK cells	natural killer cells
nM	nano Molar
ONeg	Anti-NIP O-linked negative mutant human IgG1 heavy chain with mutated half hIgA1 hinge inserted
PBS	phosphate buffered saline
PBS-T	phosphate buffered saline-Tween
PCR	polymerase chain reaction
PDB	Protein Data Bank
PMN	polymorphonuclear leukocytes
PPR	pattern recognition receptors
Pro	proline
RBC	red blood cell
RNA	ribonucleic acid
scFv	single chain Fv region
Ser	serine
SDC	spleen derived dendritic cells

SDS	sodium dodecyl sulfate
SIIN-MFc	MAGE-A2 Fc fusion protein incorporating SIINFEKL
siRNA	sequence interfering RNA
SPR	surface plasmon resonance
TAE	Tris-acetate-EDTA
TBE	Tris-borate-EDTA
TCR	T cell receptor
Thr	threonine
Val	valine
VH	variable domain of immunoglobulin heavy chain
VL	variable domain of immunoglobulin light chain
wt	wild type

CHAPTER ONE
GENERAL INTRODUCTION

CHAPTER 1: GENERAL INTRODUCTION

1.1 The immune system

Our immune system can be categorised into two different systems, specifically the innate and adaptive immune systems (Dempsey *et al*., 2003; Janeway *et al*., 2001c). Both immune systems defend and protect our body from the various challenges imposed by foreign organisms or dangerous compounds. The innate immune system consists of a range of components including the skin barrier, mucous secretions, different types of leukocytes (white blood cells), different types of cytokines and the complement protein system. The skin barrier and mucous secretions form a first line of defence which prohibits the entry of foreign microorganisms into the body. However, if a microorganism manages to breach through the initial defence and gain entry into the body, it will have to survive attack by leukocytes. There are different types of leukocytes in the immune system, the key ones being known as monocytes, macrophages, dendritic cells, eosinophils, neutrophils, basophils and lymphocytes (Dempsey *et al*., 2003; Janeway *et al*., 2001c). Lymphocytes can be divided into B cells, T cells, and natural killer cells (NK cells). Monocytes express a receptor family known as pattern recognition receptors (PPRs) on their cell surface which can recognise certain bacterial/viral molecules such as carbohydrates, peptides and nucleic acids leading to receptor activation (Dempsey *et al*., 2003; Janeway *et al*., 2001c). Once activated, the PPRs trigger a series of downstream signaling mechanisms that lead to the production and secretion of cytokines that contribute and mediate other defence mechanisms, such as leukocyte recruitment and activation. In addition, neutrophils, macrophages and monocytes are capable of phagocytosing microorganisms, containing them within a phagosome and subsequently killing them

by fusion of the phagosome with a lysosome loaded with different types of lethal enzymes. The components of the microorganism are digested and presented on a protein complex known as the major histocompatibility complex (MHC) (Dempsey *et al*., 2003; Janeway *et al*., 2001c). There are two classes of MHC protein complex, namely MHC class I and MHC class II. Both are responsible for linking the innate immune system to the adaptive immune system. The major difference between the innate and adaptive immune systems is that adaptive immunity displays specificity and memory whereas innate immunity does not (Janeway *et al*., 2001c). Specificity refers to the ability to recognise specific structural motifs (epitopes) that are either displayed by MHC complexes or expressed on the surface of pathogens/cells and distinguish foreign from self. Memory is the ability of generating a long-lived response, which is usually faster and stronger, to an antigen that has previously been encountered.

1.2 The adaptive immune system

The adaptive immunity is divided into two categories, specifically cellular and humoral immunity (Dempsey *et al*., 2003; Janeway *et al*., 2001c). The main factor that distinguishes these from each other is the involvement of proteins known as antibodies. Antibodies, also called immunoglobulins, are responsible for the clearance of foreign pathogens. Antibodies bind to the target pathogen and initiate effector mechanisms which usually result in the destruction of the target pathogen via mechanisms such as antibody-dependent cell-mediated cytotoxicity (ADCC), antibody-dependent cellular phagocytosis (ADCP) and complement-dependent cytotoxicity (CDC) (Burton, 1987; Janeway *et al*., 2001e; Janeway *et al*., 2001c; Schroeder Jr and Cavacini, 2010).

Cellular immunity is not mediated by antibodies, rather it is the activation of lymphocytes coordinated via the secretion of cytokines to further strengthen the immune response. T lymphocytes (or T cells), named as such because they mature in the thymus, originate from common precursors known as haematopoietic stem cells and are often categorised into two major sub-populations, namely cytotoxic T cells and T-helper cells. Both sub-populations are differentiated by the expression of cell surface molecules classified by CD (cluster of differentiation) number. Cytotoxic T cells express CD8, and thus are also known as $CD8^+$ T cells, whereas T-helper cells express CD4, gaining the name $CD4^+$ T cells. Besides that, both $CD8^+$ and $CD4^+$ T cells express an important receptor known as the T cell receptor (TCR), which is highly specific in epitope recognition, to carry out their main immunological functions. $CD8^+$ T cells use their TCR to bind to a complex of foreign antigen with MHC class I molecules that are present in all nucleated cells and thereby decide if a lethal response should be initiated. On the other hand, $CD4^+$ T cells use their TCR to bind to a complex of foreign antigen with MHC class II molecules that are only present on antigen presenting cells such as monocytes and B cells. Such interaction initiates secretion of a variety of cytokines to help the activation and differentiation of other immune cells, most importantly B cells. In addition, a sub-population of activated T cells form memory T cells which can stimulate a stronger and more rapid immune response if the same antigen is encountered.

In contrast, humoral immunity involves antibodies that are found to be present in various body fluids, including blood, saliva and mucous secretions (Dempsey *et al*., 2003; Burton, 1987; Schroeder Jr and Cavacini, 2010). Antibodies are produced and secreted by B cells when they are activated, usually via antigen binding and with the

help of $CD4^+$ T cells. B cells, named as such because they mature in the bone marrow and spleen, also originate from haematopoietic stem cells and express membrane-bound antibodies as receptors, known as B-cell receptors (BCR). Each BCR is also highly specific in epitope recognition and is key to B cell activation which occurs upon BCR binding to its target antigen along with appropriate stimulation from $CD4^+$ T cells (Janeway *et al*., 2001c). Following activation, B cells may differentiate into antibody secreting B cells or memory B cells. The former produce and secrete antibodies that have the same specificity for the target antigen that the BCR previously bound to. On the other hand, memory B cells are long lived cells that provide immunological memory towards the antigen that the BCR recognised. They are able to proliferate at a higher response rate if the same antigen is encountered again.

One interesting fact is that each T and B cell expresses only one kind of TCR or BCR; no two are the same unless they originate from a common ancestor (Janeway *et al*., 2001c). Similarly, an activated B cell will only secrete antibody of one specificity and this never changes. The unique antigen recognition of TCR and BCR govern the specificity of the adaptive immune response whereas the long lived memory B and T cells and their rapid response are responsible for the memory function of the adaptive response.

1.3 Immunoglobulin classes

All immunoglobulins (Ig) are formed from a basic unit of four polypeptide chains which comprise two identical light chains and two identical heavy chains held

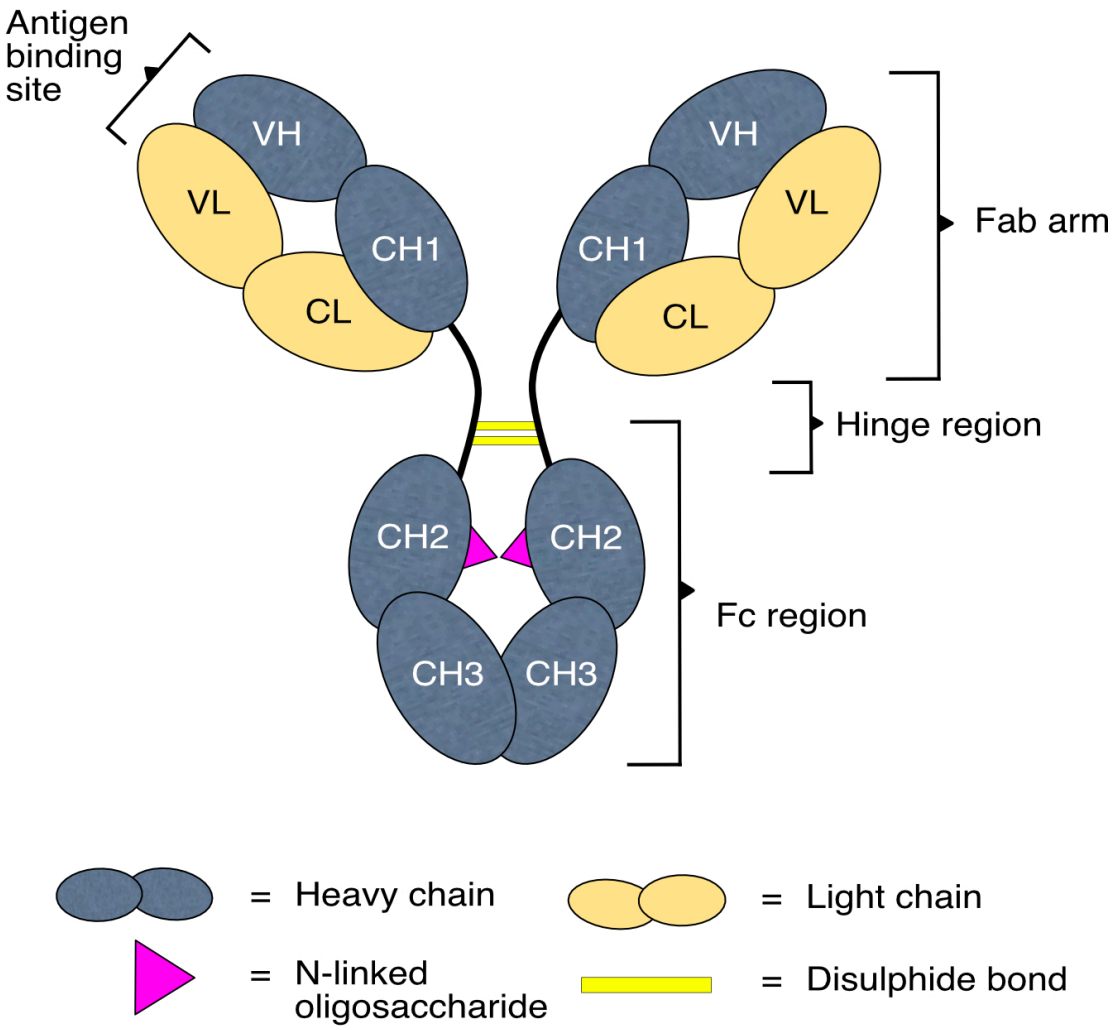

Figure 1.1: A diagram illustrating the general structure of human IgG1. IgG is formed from two heavy chains (grey) and two light chains (yellow), which are linked together by disulphide bonds. The IgG structure is divided into different regions: two identical Fab arms, hinge region and Fc region. Each heavy chain consists one variable domain (VH) and three constant domains (CH1-3). Each light chain consists one variable domain (VL) and one constant domain (CL). Each CH2 domain carries an N-linked oligosaccharide attached at asparagine 297. The antigen binding sites are located at the tip of the Fab arms.

together by disulphide bonds (Dempsey *et al*., 2003; Burton, 1987; Schroeder Jr and Cavacini, 2010), as shown in Figure 1.1. The number and arrangement of disulphide bonds varies between the different antibody classes and subclasses. Light chain exists in two different forms, termed kappa (κ) and lambda (λ), and both have a

molecular weight of approximately 25kDa. An individual antibody molecule will always have either kappa or lambda light chains, never both. Different heavy chains account for the five different Ig classes, and are named alpha (α), gamma (γ), epsilon (ε), mu (μ) and delta (δ), which determine the five antibody classes IgA, IgG, IgE, IgM and IgD respectively. Heavy chains have a molecular weight of 50-75kDa depending on the antibody class. Only one class of light chain will be expressed by a differentiated B cell. In contrast, the expression of heavy chain may change by a process known as isotype switching (Janeway *et al*., 2001d). A B cell always begins its antibody expression with IgM. IgD is usually expressed at the same time. In the later immune response, the process of isotype switching allows the B cell to change it heavy chain expression to either IgG, IgE or IgA. However, one rule of isotype switching is that B cell can only change its heavy chain expression in the following sequence IgM > IgD > IgG > IgE > IgA (Janeway *et al*., 2001d). For example, if the B cell switches to IgE at the beginning, it can only further switch to IgA in a later immune response and can never switch back to IgM, IgD or IgG.

In humans, IgA has two subclasses, namely IgA1 and IgA2, and is often characterised as a secretory antibody since it is the most abundant antibody in exocrine secretions, such as saliva, milk, and secretions of the intestinal and respiratory tracts. More importantly, IgA is usually found as a dimer in secretions, where two IgA monomers are joined together by a protein known as joining chain or J chain and a polypeptide known as secretory component. However, in the serum, IgA exists mainly as monomers (Woof and Russell, 2011).

IgG is the most abundant antibody in the serum but is often found in secondary

immune responses when an antigen is encountered for a second or subsequent time. In humans, there are four subclasses of IgG, known as IgG1, IgG2, IgG3 and IgG4. Among all human antibody classes, IgG is the only one that can cross the placenta into the foetal blood circulation, and helps to protect newborn infants until they begin to make their own IgG. Similar to IgM, IgG is capable of complement fixation via the classical pathway that greatly improves pathogen clearance.

IgM is the first antibody, along with IgD, to be expressed by naïve B cell as BCR and is produced in a primary immune response when a particular antigen is first encountered. IgM exists in polymeric form, usually as a pentamer where five IgM subunits are linked together by J chain. Hexamers of IgM also occur (Petrušić *et al*., 2011). IgM is considered the most efficient antibody in complement fixation due to its polymeric format.

In most individuals, IgE has an extremely low concentration in the serum. However, some individuals make IgE responses to harmless environmental antigens, often known are allergens. In these individuals IgE is often found bound to a specific receptor, known as FcεRI that is expressed on the surface of mast cells. When receptor-bound IgE binds to target allergen, mast cell degranulation is induced resulting in the symptoms associated with allergy. Thus, IgE is responsible for majority allergic reactions. IgE also plays an important role in protection against helminths and other parasites (Gould *et al*., 2003).

IgD remains as a rather mysterious antibody as not much is known about it. There is very little IgD in serum; however, it is expressed together with IgM, on the surface

of naïve B cells, acting as a BCR. The main role of IgD is still unclear but recent studies have suggested that IgD may have an immunological function involving basophil activation in the respiratory tract (Chen and Cerutti, 2011).

1.4 General features of antibody structure

An immunoglobulin molecule is divided into the three different regions, namely the Fab regions (which will be referred to also as Fab arms), Fc region and hinge region (Burton, 1987; Schroeder Jr and Cavacini, 2010). All immunoglobulins share the same basic structure in which the Fab regions are separated from the Fc region by the hinge region, as shown in Figure 1.1. The Fab arms and the Fc region are formed by different domains of the antibody. In detail, each of the light and heavy chains fold into several domains, each of which is formed by two β-sheets packed against each other via hydrophobic and other non-covalent interactions and further stabilised by a disulphide bond (Burton, 1987; Schroeder Jr and Cavacini, 2010; Janeway *et al*., 2001e). Such folding is also known as the "immunoglobulin fold" which is illustrated in Figure 1.2. All immunoglobulins have two different types of domain termed the variable and constant domains. The variable domain is located at the N-terminus and the constant domains form the subsequent domains. Variable domains are designated as VL, for that in the light chain, and VH, for that in the heavy chain. Constant domains are designated as CL, for that in the light chain, and CH1, CH2, CH3 and CH4, for those in the heavy chain. The immunoglobulin fold of variable domains is formed from 9 β-strands whereas that of constant domains is formed from 7 β-strands as indicated in Figure 1.2.

An antibody has two Fab arms and they are formed by the pairing of the VH and

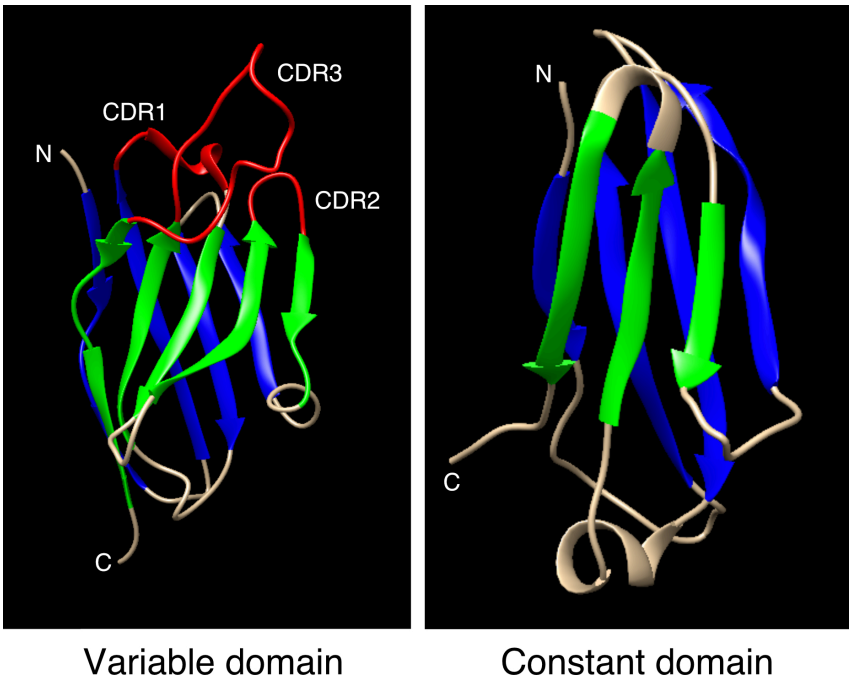

Figure 1.2: A diagram illustrating the structure of the immunoglobulin fold of typical variable and constant domains of an immunoglobulin. **LEFT**) The variable domain is formed from two β-sheets (green and blue) which consist of nine anti-parallel β-strands. Complementary determining regions 1 (CDR1), 2 and 3, are shown in red. **RIGHT**) Constant domains are formed from two β-sheets (green and blue) which consist of seven anti-parallel β-strands (green and blue). N, N-terminus; C, C-terminus. Image generated from the X-ray crystal coordinates of VH domain of chain K and CH1 domain of chain H of B12 human IgG1 heavy chain (PDB ID 1HZH) and modified using Chimera software.

CH1 domains of the heavy chains with the VL and CL domains respectively of the light chains. On the other hand, the Fc region refers to the CH2 and CH3 homodimer region and the lower hinge section of the antibody as indicated in Figure 1.1. Finally, the hinge region separates the Fab arms and the Fc region. Notably, the hinge region of IgM and IgE is replaced with an additional pair of constant domains. In contrast, the hinge regions of IgD and the subclasses of IgG and IgA vary in length. It is believed that the hinge region provides flexibility to the antibody molecule and allows both the Fab arms and Fc region to adopt a variety of conformations that aid protein-protein/antigen interactions, which will be explained in section 1.7 below.

In the case of IgG, the inter-heavy chain disulphide bonding occurs at the hinge region which aids assembly into the homodimer structure shown in Figure 1.1. The

role of each region will be described in more detail in other sections below.

1.5 Fab arms

Fab is the abbreviation for "fragment antigen-binding" and each antibody has two Fab arms as shown in Figure 1.1. The Fab arm functions as an antigen recognition site and this is mediated through its paired variable domains, located at the tip of the Fab arms. The VH and VL each have three complementarity determining regions (CDRs), shown in Figure 1.2, which are further supported within each V domain by four framework regions (FRs). The six CDRs together form the antigen binding site which binds with high specificity and affinity to antigen which has a complementary three dimensional structure. CDRs are highly variable in sequence and length due to the mechanism regulating the random selection of the genes encoding the variable region, also known as VDJ recombination (Kumagai and Tsumoto, 2002; Burton, 1987; Janeway *et al*., 2001b). In brief, the variable region is encoded by three different gene segments known as V (variable) segment, D (diversity) segment (only in heavy chains) and J (joining) segment (Janeway *et al*., 2001b; Kumagai and Tsumoto, 2002). There are multiple V, D or J gene segments that are available for the formation of both heavy and light chain variable domain. For example, the human heavy chain locus contains about 65 V gene segments, 27 D gene segments and 6 J gene segments (Janeway *et al*., 2001b). Selection of each segment to generate the final VDJ (heavy chain) or VJ (light chain) combination is completely random. As a result, this produces a huge diversity of specificities capable of recognising a huge variety of different antigens. It has been estimated that the human antibody repertoire is at least 10^{11} or more (Janeway *et al*., 2001b).

1.6 Fc region

Fc is the abbreviation for "fragment crystallisable". The Fc region contains several binding sites for different endogenous proteins which are required for the initiation of effector mechanisms such as CDC and ADCC and for prolonging plasma half-life. CDC is activated when C1q, a protein of the complement system, binds to the CH2 domain of the Fc region of either IgG or IgM to initiate the complement cascade (Duncan and Winter, 1988; Idusogie *et al*., 2000; Schneider and Zacharias, 2012). The activation of the classical complement cascade via antibody initiation is dependent on the binding of at least two of the C1q globular heads to the CH2 domains of the Fc regions of IgG or IgM antibodies (Idusogie *et al*., 2000). IgM is a very efficient complement activator mainly due to its natural state as a pentamer. Once IgM has undergone a conformational change from planar to staple conformation upon binding to an antigenic surface, it exposes sufficient binding sites for efficient binding of C1q (Schroeder Jr and Cavacini, 2010). On the other hand, IgG exists as a monomer in the serum. Thus, it is believed that multiple IgG molecules binding to a target pathogen and localised close together are required to activate complement. Recently, investigations by Diebolder and colleagues showed that IgG molecules are capable of assembling into hexamers via Fc-Fc interactions and such hexamers can bind Clq (Diebolder *et al*., 2014). Binding of C1q then promotes a series of protein cleavages and recruitments which ultimately promotes the formation of a membrane attack complex (MAC) on the target cell surface (Janeway *et al*., 2001a). MAC forms a pore in the target cell membrane and causes cell death by the influx of water and removal of electrolytes from the cell (Janeway *et al*., 2001a). The complement cascade mechanism driven by antibodies is summarised in Figure 1.3.

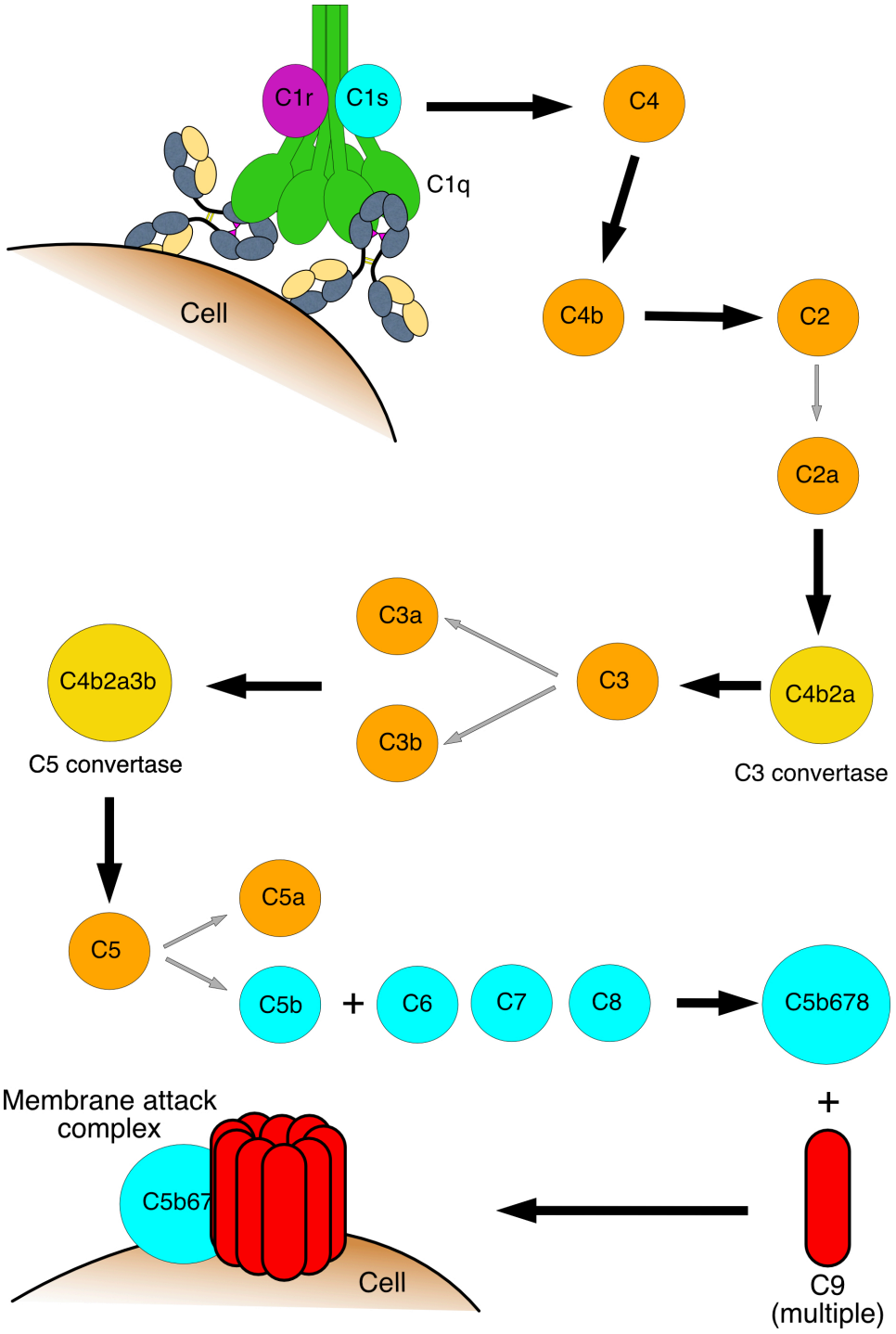

Figure 1.3: A diagram illustrating the mechanism of antibody activation of the complement cascade, initiated by the binding of C1q to IgG Fc region. C1q associates with C1r and C1s to form the C1 complex. This process activates C1s to cleave C4 into C4b that recruits C2, which is subsequently cleaved into C2a and forms the C3 convertase (C4b2a). C3 convertase acts on C3 to produce C3a and C3b. C3b is later recruited to the cell surface forming C5 convertase (C4b2a3b) which cleaves C5, generating C5b that then associates with C6 and C7 to recruit C8. The complex, C5b678, induces polymerisation of several C9 molecules to form a ring structure that penetrates the lipid bilayer and generates the membrane attack complex (MAC) (C5b6789). MAC forms a pore in the cell surface thereby killing the target cell.

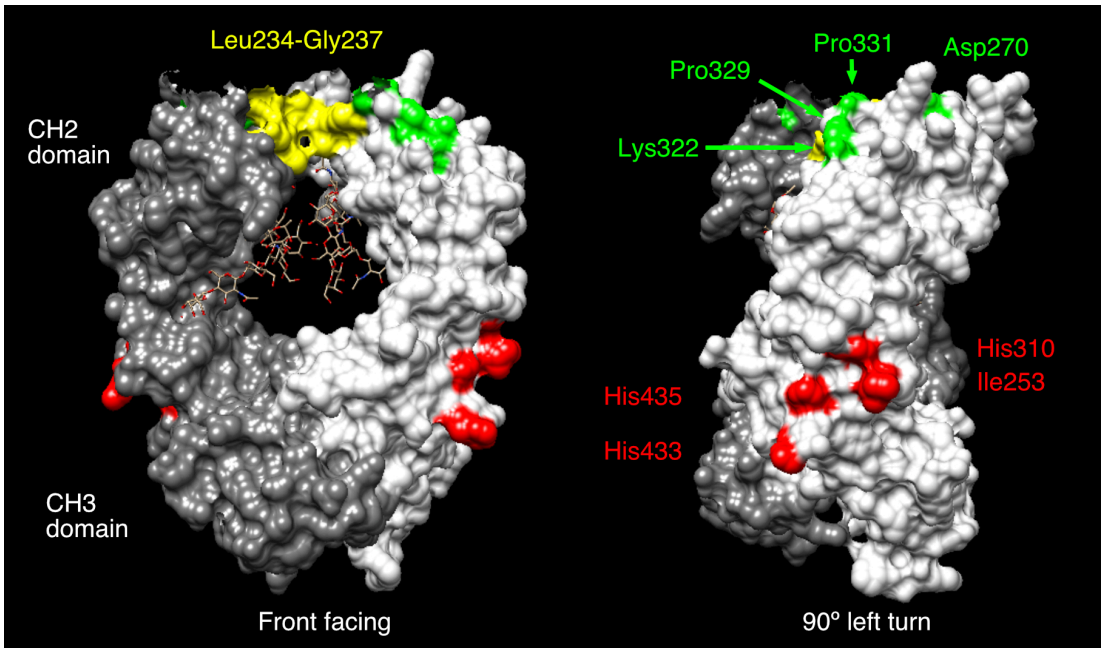

Figure 1.4: A diagram illustrating the key residues located in the hIgG1 Fc region which are required for effector mechanisms. One heavy chain of the Fc is shown in white and the other in grey. N-linked oligosaccharides are shown in stick format. Residues in yellow are crucial for the binding to Fcγ receptors. Residues in green are crucial for the binding of C1q and complement activation. Residues in red are crucial for binding to FcRn. The crystal structure is of the Fc region of human IgG1 (B12) (PDB ID: 1HZH). The image was generated using Chimera.

Duncan and Winter identified the CH2 domain residues critical for binding of C1q to mouse IgG2b to be Glu318, Lys320 and Lys322 (Duncan and Winter, 1988). However, these residues did not seem to apply to human IgG (hIgG) since they are conserved in all hIgG subclasses yet the subclasses exhibit different complement activation capabilities. Idusogie and colleagues later reported that the critical residues for C1q binding by hIgG1 were Asp270, Lys322, Pro329, and Pro331 (Idusogie *et al*., 2000), indicated in Figure 1.4. As a result, the authors further suggested that there might be species differences in C1q binding by IgG (Idusogie *et al*., 2000).

On the other hand, effector cell functions such as ADCC, ADCP, respiratory burst, and enzyme or mediator release are mediated through cell surface Fc receptor

binding (Daëron, 1997; Burton, 1987; Schroeder Jr and Cavacini, 2010). Importantly, each antibody class has its own Fc receptors and the binding sites for each Fc receptor differs (Woof and Burton, 2004). For IgA1, the binding site for its specific receptor Fcα receptor I (FcαRI) is located at the interface of the CH2 and CH3 domains of the IgA Fc region (Carayannopoulos *et al*., 1996; Pleass *et al*., 1999). The crystal structure of IgA Fc in association with FcαRI showed that only one heavy chain, out of two, of IgA1 was bound to a single FcαRI, therefore, it is possible that a single IgA1 is capable of binding to two FcαRI, although the physiological relevance is unclear (Woof and Burton, 2004; Herr *et al*., 2003). In contrast, the binding site on IgG for Fcγ receptors (FcγRs) was shown to centre of the lower hinge region, Leu234-Gly237, of the CH2 domain (Woof *et al*., 1986; Duncan *et al*., 1988; Shields *et al*., 2001), indicated in Figure 1.4. In the solved crystal structures of IgG Fc in complex with either FcγRI, FcγRII or FcγRIII, residues Leu234-Gly237 were proven to be critical in making direct contact with the FcγRs and the stoichiometry of IgG:FcγR was found to be 1:1 (Lu *et al*., 2015; Kiyoshi *et al*., 2015; Sondermann *et al*., 2000; Radaev *et al*., 2001; Ramsland *et al*., 2011). The different types of FcγRs will be described in subsequent section 1.7.1.

Another important feature about the Fc region is the presence of N-linked oligosaccharides and for IgG this glycosylation occurs at Asn297 (Burton, 1987; Schroeder Jr and Cavacini, 2010). Glycosylation at Asn297 is particularly important in maintaining optimal binding to FcγRs (Tao and Morrison, 1989; Jefferis, 2005) It was described that the affinity of IgG1 and IgG3 for FcγRI was reduced by 2 orders of magnitude upon aglycosylation, while binding to FcγRII and FcγRIII was

completely abolished (Lund *et al*., 1990). On the other hand, other studies have reported smaller effects of IgG aglycosylation on Clq binding and complement activation (Leatherbarrow *et al*., 1985). More importantly, the composition of the oligosaccharide attached at Asn297 displays strong heterogeneity and studies have shown that the effector mechanisms of IgG were affected by the different types of glycan present on Asn297 (Anthony *et al*., 2012; Forthal *et al*., 2010; Raju, 2008). For example, afucosylated hIgG1 which lacks the addition of fucose to the IgG core glycan, displays binding to FcγRIIIa with increased binding affinity by up to 50 fold (Anthony *et al*., 2012). Similarly, Li and colleagues showed that core fucosylated IgG had a reduced ADCC activity in NK cell activation assay compared to afucosylated IgG. In addition, the authors demonstrated that when the core of the glycan is fucosylated, the presence of terminal sialylation significantly decreased ADCC activity in cell-based assay. In contrast, sialylation had no significant impact in ADCC activity when the core glycan is afucosylated (Li *et al*., 2017). Recently, Dekkers and colleagues reported the selective production of IgG with different glycan composition by manipulating the addition of substrates and the expression of glycosyltransferases, which should further improve the understanding of the role of different glycan moieties in antibody functionality (Dekkers *et al*., 2016).

Finally, the Fc region of IgG is also responsible for prolonging the plasma half-life through association with an Fc receptor known as FcRn. The role of FcRn will be discussed in section 1.7.2 below.

1.7 Fc receptors

1.7.1 Fcγ receptors (FcγRs)

As mentioned before, key effector mechanisms of IgG are highly dependent on the interaction with FcγRs. In humans, there are three classes of FcγR, namely FcγRI (CD64), FcγRII (CD32) and FcγRIII (CD16), as indicated in Figure 1.5. FcγRI has three extracellular domains while the other FcγRs have two. More importantly, FcγRI has the highest binding affinity for IgG and is capable of binding to monomer IgG (Boross *et al*., 2008). The expression of FcγRI on monocytic and myeloid cells can be upregulated by stimulation with interferon γ (IFN-γ) and interleukin 10 (IL-10) (Perussia *et al*., 1983; Velde *et al*., 1993). On the other hand, both FcγRII and FcγRIII have a lower binding affinity than that of FcγRI, shown in Figure 1.5, and only interact with aggregated IgGs such as immune complexes (IC) (Boross *et al*., 2008). The interaction of IgG-IC or IgG-coated targets with FcγRs leads to the transduction of either an activating or inhibitory signal. The activating signal is mediated through the immunoreceptor tyrosine-based activation motif (ITAM) which is located either in the cytoplasmic domain of the receptor, as in the case of FcγRIIa and FcγRIIc, or the associated FcR γ chain homodimer, as is the case for FcγRI and FcγRIIIa, as shown in Figure 1.5. On the other hand, FcγRIIb is the only receptor that transmits an inhibitory signal via the immunoreceptor tyrosine-based inhibitory motif (ITAM) that is located in the cytoplasmic domain of the receptor (Boross *et al*., 2008; Guilliams *et al*., 2014). It has been reported that Fcgriib (the gene encoding FcγRIIb) knockout mice generate a stronger immune response both *in vivo* and *in vitro* (Nimmerjahn and Ravetch, 2008). In addition, dendritic cells (DC) demonstrated a spontaneous maturation when they were deficient in FcγRIIb

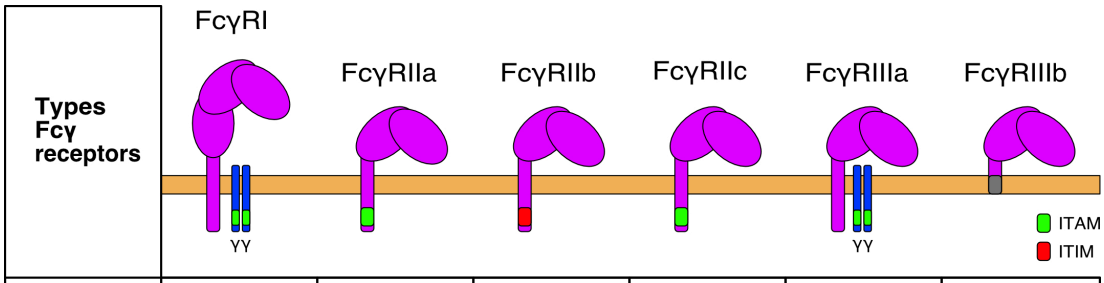

Types Fcγ receptors	FcγRI	FcγRIIa	FcγRIIb	FcγRIIc	FcγRIIIa	FcγRIIIb
Equilibrium dissociation constant with IgG (K_d)	10^{-8} – 10^{-7} M	10^{-7} – 10^{-5} M	10^{-6} – 10^{-4} M	10^{-6} – 10^{-4} M	10^{-7} – 10^{-4} M	10^{-6} – 10^{-5} M
Immune cell expression	Monocytes Macrophages Dendritic cells Eosinophils	Monocytes Macrophages Dendritic cells PMN cells	Macrophages Dendritic cells Eosinophils B cells	NK cells	Macrophages NK cells	PMN cells

Figure 1.5: A diagram illustrating the expression of different human Fcγ receptors (FcγRs) by different immune cells and their binding affinity. Based on their function, different FcγRs can mediate either activating signals via ITAM (green box) or inhibiting signals via ITIM (red box). FcγRIIIb is a glycosylphosphatidylinositol (GPI)-linked activating receptor that has no intracellular tail. PMN cells are polymorphonuclear leukocytes, such as NK cells, eosinophils and basophils.

expression (Nimmerjahn and Ravetch, 2008).

The diversity of FcγRs is further extended by the presence of polymorphisms in their extra- and intra-cellular domains. For example, two single amino acid substitutions at position 27 and 131 of the extracellular domain of human FcγRIIa gave rise to two variants, namely low-responder (Trp27 and His131) and high responder (Glu27 and Arg131), which reacted differently to mouse IgG1 (Warmerdam *et al*., 1990). On the other hand, it was found that the cytoplasmic domain of FcγRIII expressed by NK cells had an extension of 21 amino acids when compared to the FcγRIII expressed by PMN cells and that this difference was due to a change in the expression of a transcript which replaced the UGA termination codon to CGA and extended corresponding protein translation (Ravetch and Perussia, 1989). Finally, Bruhns and colleagues sensationally investigated the specificity and affinity of different human

FcγRs, including polymorphic variants, for all human IgG subclasses (Bruhns *et al*., 2009). The authors demonstrated that most human FcγRs had a measureable affinity for all IgG subclasses except for FcγRI, which did not bind IgG2, and FcγRIIIb, which did not bind IgG2 and IgG4, when binding to either monomeric or IC form of IgG (Bruhns *et al*., 2009). In addition, different binding affinities were observed for all IgG subclasses on different FcγRs. For instance, IgG3 bound FcγRIIIb with an affinity 25-fold higher than IgG4 and IgG1 bound FcγRIIa approximately 5 fold higher affinity than IgG3. It was also shown that FcγRIIIa$_{V158}$ is a high affinity receptor for IgG3 but not IgG1, IgG2 and IgG4 (Bruhns *et al*., 2009). These findings suggests that the binding affinity and specificity of FcγRs to IgG is dependent not only on the different types of receptor or IgG subclasses but also on the polymorphism on the receptor and IgG subclasses .

1.7.2 Neonatal Fc receptor (FcRn)

In human, IgG1, IgG2 and IgG4 have a long plasma half-life of around 21 days except IgG3 which is around 7 days (Morell *et al*., 1970; Janeway *et al*., 2001d) when compared to the other antibodies (5-8 days for IgA and IgM) (Janeway *et al*., 2001d). The reason for the shorter half life of IgG3 is due to a key amino acid residue substitution which affected FcRn binding and will be explained below. More importantly, IgG is the only antibody that is transferred from the mother to the foetus via the placenta to provide short term immunity (Roopenian and Akilesh, 2007; Brekke and Sandlie, 2003). The long plasma half-life and specific transport of IgG are found to be associated with a unique Fc receptor known as the neonatal Fc receptor (FcRn) (Roopenian and Akilesh, 2007; Burmeister *et al*., 1994).

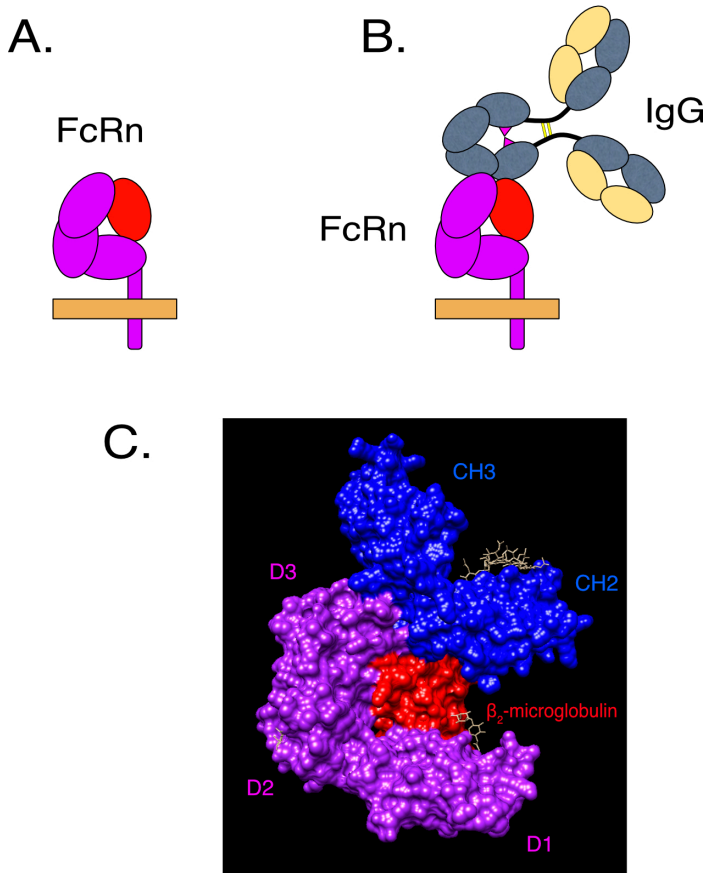

Figure 1.6: A schematic diagram illustrating the characteristics of neonatal Fc receptor (FcRn). **A**) The general structure of FcRn. The FcRn heavy chain (purple), that consists of three extracellular domains, pairs with β_2-microglobulin (red). **B**) FcRn binds to the CH2-CH3 domain interface of IgG Fc region. **C**) The solved crystal structure of rat FcRn: human IgG Fc complex (PDB ID: 1FRT). Different domains of each of the proteins are highlighted in different colours. Purple, FcRn heavy chain; Red, β_2-microglobulin; Blue, single heavy chain of human IgG Fc region.

FcRn is expressed by different cell types, such as epithelial cells, endothelial cells, placental syncytiotrophoblasts, dendritic cells and macrophages, within the endosome and also on the cell surface (Boross *et al*., 2008; Roopenian and Akilesh, 2007). The general structure of FcRn is similar to that of MHC Class I molecule in that the FcRn is a heterodimer consisting of a MHC Class I-like heavy chain associating with a β_2-microglobulin, as shown in Figure 1.6A. The crystal structure of rat FcRn with human IgG Fc complex had been solved and the binding site of FcRn on IgG Fc region is located at the CH2-CH3 domain interface as shown in Figure 1.6 (Roopenian and Akilesh, 2007; Burmeister *et al*., 1994). More importantly,

the authors observed that the stoichiometry of FcRn:IgG was 2:1 (Burmeister *et al*., 1994). Uniquely among different Fc receptors, the association of FcRn with IgG is strictly dependent on pH. At normal physiological pH 7.4, FcRn does not bind to IgG. However at an acidic pH of 6.0-6.5 FcRn will interact strongly with IgG (Roopenian and Akilesh, 2007). The key residues in IgG that are involved in the association with FcRn are Ile253, His310, His433 and His435, indicated in Figure 1.3. Notably, His310, His433 and His435 get protonated at acidic pH 6-6.5 and form salt bridges with anionic residues Glu117, Glu132 and/or Glu135 and Asp137 on the heavy chain of FcRn. On the other hand, hydrophobic residue Ile253 interacts with Trp133 of FcRn (Roopenian and Akilesh, 2007). For IgG3, the amino acid in position 435 was found to be an arginine instead of histidine (Stapleton *et al*., 2011). This substitution of H435 to R435 of IgG3 does not abolish FcRn-mediated recycling but the FcRn dependent recycling activity was significantly inhibited when IgG1, which has H435, is present (Stapleton *et al*., 2011). Further findings demonstrated that IgG3 allotype which contained H435 had a comparable FcRn binding to IgG1 (Stapleton *et al*., 2011). At physiological pH 7.4, the histidine residues are deprotonated and it is possible that the interaction of Ile253 alone is not sufficient to maintain a secure binding. Thus, the interaction of FcRn/IgG Fc is abolished. Nonetheless, it is this pH dependent manner of FcRn that helps to prolong IgG plasma half-life and transport IgG across the placenta. For placental transfer, as indicated in Figure 1.7A, it is expected that syncytiotrophoblasts which are bathed in maternal blood internalise serum maternal IgG into endosomes. The endosomes are gradually acidified and when the pH drops to pH 6.0-6.5 FcRn binds to the IgG Fc. The IgG containing endosome then transports the FcRn bound IgG by fusing with the cellular membrane surface lining the foetal blood circulation. At physiological pH 7.4, the association of

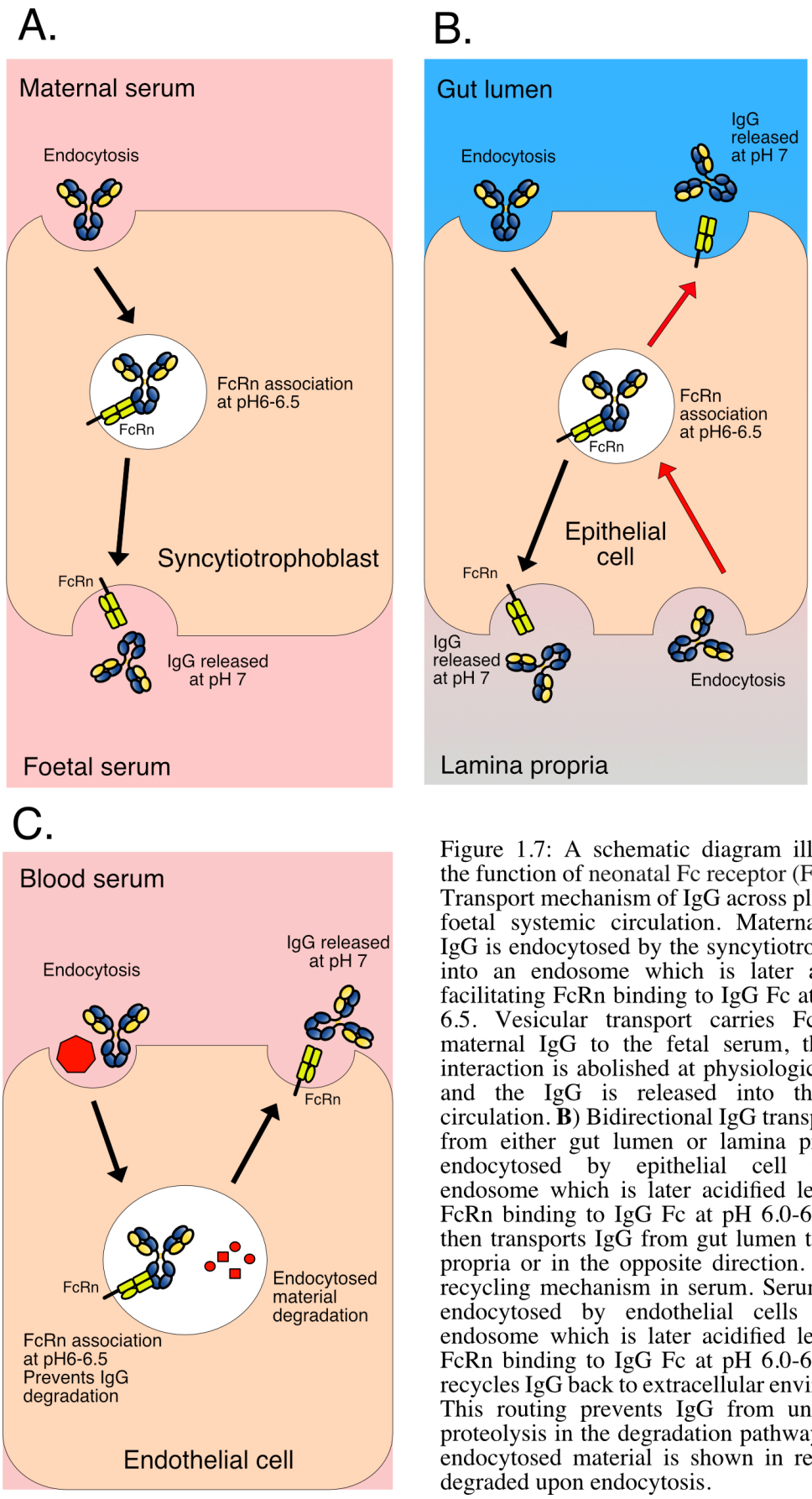

Figure 1.7: A schematic diagram illustrating the function of neonatal Fc receptor (FcRn). **A**) Transport mechanism of IgG across placenta to foetal systemic circulation. Maternal serum IgG is endocytosed by the syncytiotrophoblast into an endosome which is later acidified, facilitating FcRn binding to IgG Fc at pH 6.0-6.5. Vesicular transport carries FcRn and maternal IgG to the fetal serum, the FcRn interaction is abolished at physiological pH 7, and the IgG is released into the foetal circulation. **B**) Bidirectional IgG transport. IgG from either gut lumen or lamina propria is endocytosed by epithelial cell into an endosome which is later acidified leading to FcRn binding to IgG Fc at pH 6.0-6.5. FcRn then transports IgG from gut lumen to lamina propria or in the opposite direction. **C**) IgG recycling mechanism in serum. Serum IgG is endocytosed by endothelial cells into an endosome which is later acidified leading to FcRn binding to IgG Fc at pH 6.0-6.5. FcRn recycles IgG back to extracellular environment. This routing prevents IgG from undergoing proteolysis in the degradation pathway. Other endocytosed material is shown in red and is degraded upon endocytosis.

FcRn with IgG is abolished and the maternal IgG is released into the foetal blood circulation.

In the context of immune defence system, IgG in lamina propria is endocytosed by FcRn expressing epithelial cells lining the mucosal site or gut lumen and the subsequent association with FcRn in acidified endosomes protects the IgG from degradation and allows the IgG to be transported to the extracellular environment to encounter foreign antigens (Pyzik *et al*., 2015; Dickinson *et al*., 1999), as shown in Figure 1.7B. More importantly, antigens that are bound by IgG forming IC can be endocytosed by the same epithelial cells lining the mucosal site or gut lumen (Pyzik *et al*., 2015; Dickinson *et al*., 1999). Using the similar transport mechanism involving FcRn, the IgG IC are transported from the gut lumen or mucosal sites across the FcRn-expressing epithelial cell into the lamina propria in which dendritic cells are present (Pyzik *et al*., 2015). Such a mechanism allows the presentation of foreign antigens to dendritic cells which could stimulate a suitable immune response as a defensive mechanism to prevent foreign pathogen invasion.

In normal circulation, as indicated in Figure 1.7C, serum IgG is expected to be internalised via endocytosis by endothelial cells lining the blood vessels into endosomes. The endosomes are gradually acidified and when the pH drops to pH 6.0-6.5 FcRn binds to the IgG Fc and prevents it from being degraded. Weflen and colleagues showed that unbound FcRn and FcRn bound to monomeric IgG were sorted into recycling sorting tubules, which emerged from early endosomes, and directed the FcRn receptor and IgG away from lysosomal degradation pathway(Weflen *et al*., 2013), which other endocytosed materials are destined to

enter. In contrast, cross linking of FcRn by IgG-IC was demonstrated to enter the lysosomal pathway and be degraded (Weflen *et al*., 2013). Monomeric IgG which bound to FcRn is then recycled and transported back to extracellular surface where it is released at pH 7.4. This process prolongs the plasma half-life of IgG (Roopenian and Akilesh, 2007).

Finally, FcRn was recently found to be involved in promoting antigen cross presentation to activate cytotoxic T cells (Baker *et al*., 2013; Baker *et al*., 2011; Baker *et al*., 2014). More details on the role of FcRn in promoting antigen cross presentation will be described in Chapter 6. In brief, a similar mechanism of IgG recycling was identified. However, instead of recycling IC containing IgGs and their antigen, the IC were sorted into antigen processing vesicles after the FcRn association. In the process, antigen digestion will occur and derived peptides can be presented on MHC-Class I molecules, leading to cytotoxic T cell activation (Baker *et al*., 2013; Baker *et al*., 2011; Baker *et al*., 2014).

1.8 Hinge region

The hinge region separates the Fab arms from the Fc region. Notably the hinge length varies considerably between immunoglobulin isotypes, even those of the same class. For example, the hinge of human IgG1 (hIgG1) comprises 17 amino acids, human IgA2 has a hinge of 7 amino acids, while that of human IgG3 is much longer, stretching to 63 amino acids (Burton, 1987). More importantly, the variability of the differences in hinge length applies to other immunoglobulins from different species as well.

For IgG, the hinge region can be divided into three sections, the upper hinge, the middle hinge and the lower hinge, as defined by Burton (1987). The upper hinge starts immediately after the cysteine residue that forms the disulphide bond with light chain and continues until the amino acid residue immediately before the subsequent cysteine residue, which forms the disulphide bond with heavy chain. The middle hinge, also known as the core hinge, starts from the first cysteine residue that forms an inter heavy chain disulphide bond and continues to the last cysteine residue that forms such a bond. Finally, the lower hinge starts immediately after the last cysteine residue of the middle hinge and continues until the start of the CH2 domain. Using human IgG1 as an example, the upper hinge is formed by Asp221-Thr225, the middle hinge consists of Cys226-Cys229 and the lower hinge is made up of Pro230-Gly237, as shown in Figure 1.8A. On the other hand, the hinge region of human IgA is not categorised into different sections as human IgG1 because after the Cys220 that forms disulphide bonding with light chain, the next cysteine residue, Cys241, is located at the start of the CH2 domain. As a result, the entire section from Cys220 to Cys241 of human IgA1 is considered as the hinge region of the antibody (Burton, 1987), as shown in Figure 1.8B.

To enable a better look into the diversity and variation of the hinge region of different antibodies, a comparison of the hinge regions of different IgG and IgA antibodies of different species is shown in Figure 1.8. For IgG antibodies, human IgG1 is used as a guide to align all other different IgG antibodies together, according to the amino acid residues mentioned earlier which define the three hinge sections. As indicated in Figure 1.8A, the hinge regions of different IgG antibodies differ greatly in both the upper and middle hinges. Notably, the middle hinge of human

A. Different IgG hinge region sequences

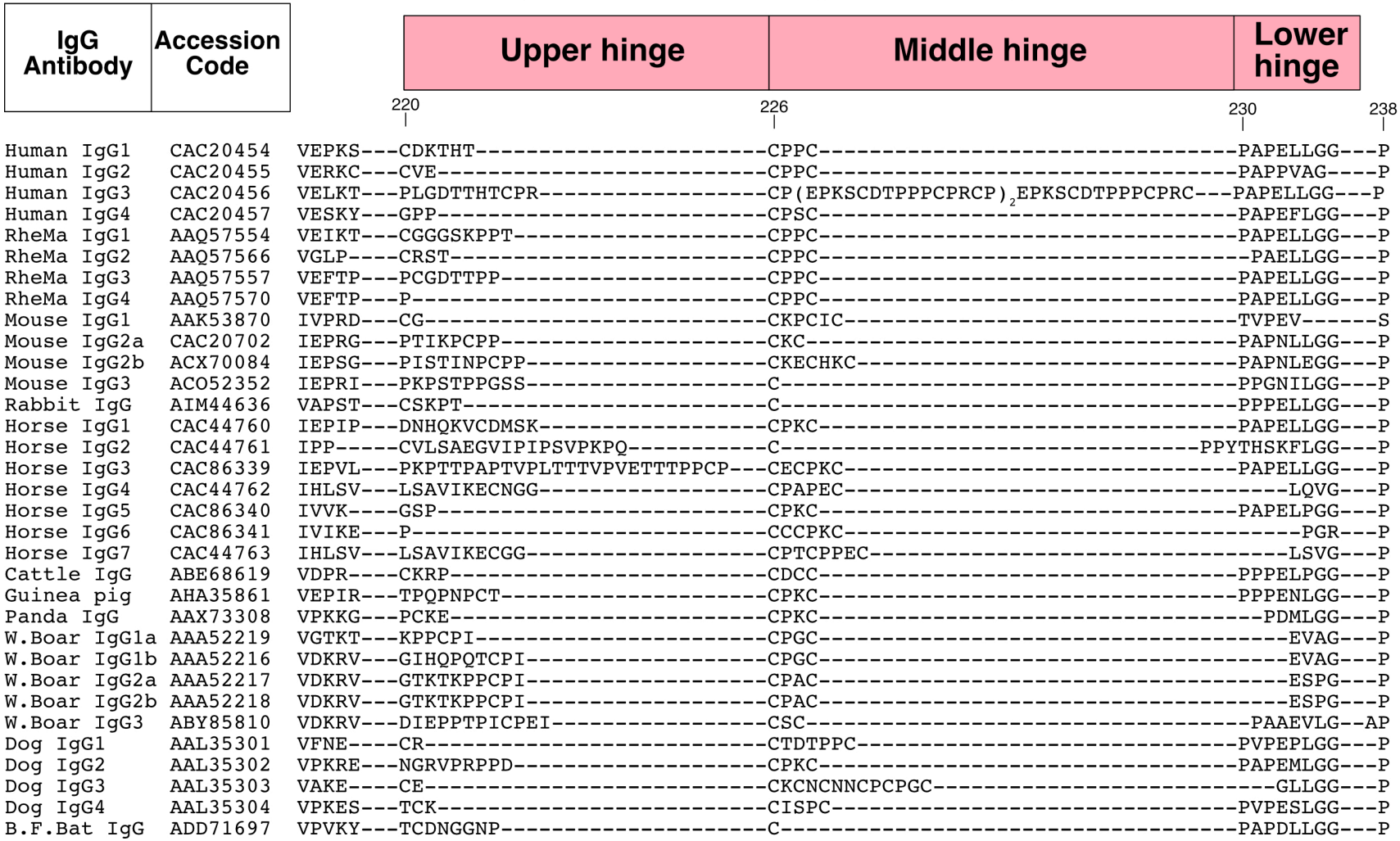

B. Different IgA hinge region sequences

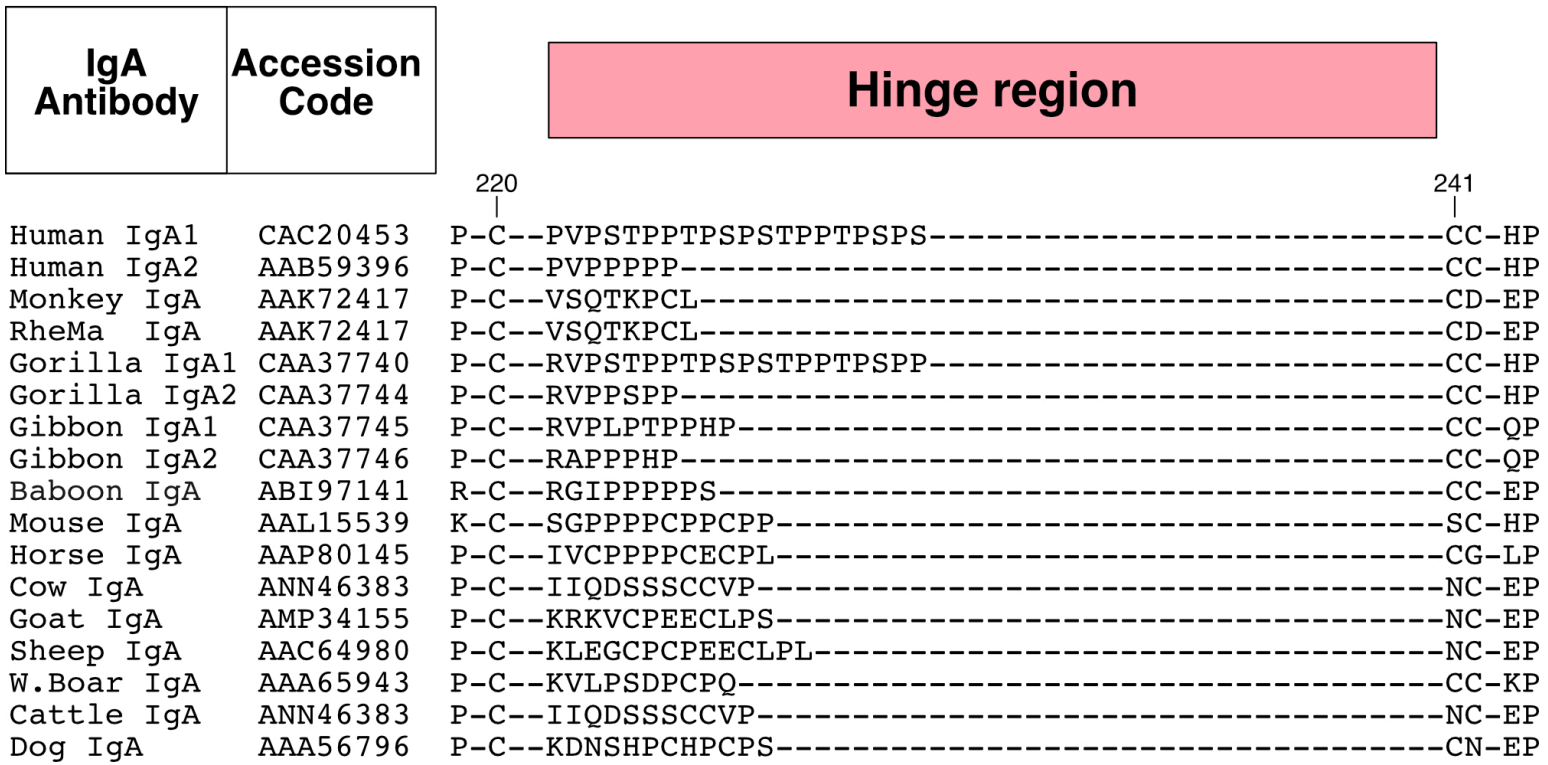

Figure 1.8: Alignment of the amino acid sequences of the hinge region of different immunoglobulins from various species using COBALT (https://www.stva.ncbi.nlm.nih.gov/tools/cobalt/cobalt.cgi?CMD=Web). **A**) Different IgG antibodies from various species are aligned with human IgG1. The hinge region of IgG is divided into three sections; upper hinge, middle hinge and lower hinge. Upper hinge starts after Cys220 that forms a disulphide bond with light chain and ends before Cys226 that forms the first inter-heavy chain disulphide bond. Middle hinge starts with Cys226 and ends with Cys229 that forms the last inter-heavy chain disulphide bond**.** Lower hinge starts with Pro230 and ends just before Pro238 which is the start of the CH2 domain. **B**) Different IgA antibodies from various species are aligned with human IgA1. The hinge region of IgA1 starts at Cys220 that forms a disulphide bond with light chain and ends just before Cys241 which is the start of CH2 domain. The numbering listed is according to the EU numbering of human IgG1 and the BUR numbering of IgA1 (Putnam *et al*., 1979). RheMa, Rhesus macaque; W.Boar, Wild Boar ; B.F. Bat, Black fruit bat.

IgG3 is significantly longer than that of any other IgG antibodies. On the other hand, the lower hinge region seems to be quite conserved between different IgG antibodies in which the lower hinge consists of different combinations of prolines (P), glutamic acid (E), leucine (L) and glycine (G). In particular, the region Leu234-Gly237 of human IgG1 which is critical for binding to FcγRs seems to be partly conserved across IgGs of different species. However, some IgGs exhibited 1-2 amino acids substitutions as shown in Figure 1.8A which have been shown to have major impact on FcγR binding (Woof *et al*., 1986). In contrast, according to the hinge of human IgA1 the hinge region can be defined as starting after Cys220 that forms a disulphide bond with light chain and ending with the subsequent cysteine residue, Cys241, that forms a disulphide bond with heavy chain and which is located at the start of the CH2 domain. Different IgA antibodies are aligned based on the hinge region of human IgA1 as indicated in Figure 1.8B.

The hinge region is particularly important because it keeps the Fab arms distanced away from the Fc region thereby allowing access by C1q and FcγRs to the upper parts of the Fc region. Hinge deleted human IgG1 antibodies such as Mcg (Guddat *et al*., 1993), Dob (Silverton *et al*., 1977) and Lec (Rivat *et al*., 1976) have been shown to be unable to activate complement or bind Fcγ receptors (Klein *et al*., 1981). All these mutant antibodies have a 15 amino acid hinge deletion which starts after Val216, resulting in complete loss of the upper and middle hinge (Rivat *et al*., 1976; Guddat *et al*., 1993; Steiner and Lopes, 1979). The lower hinge region which contains the core binding site for FcγRs, as described earlier, was not deleted. However, the failure of all three antibodies to associate with FcγRs was suggested to be due to the obstruction at the FcγR binding site due to close approach of the CH1

and CH2 domains because of the hinge deletion (Guddat *et al*., 1993; Silverton *et al*., 1977). The same reasoning was suggested for failure in complement fixation of Mcg, Dob and Lec as the binding site for C1q was located at the top region of CH2 domain, as indicated in Figure 1.3. Such studies support the notion that separation of the Fab arms away from the Fc region by the hinge region is one of the major factors in initiating proper Ig effector mechanisms.

1.8.1 Antibody flexibility involving the hinge region

The flexibility of an antibody can be divided into two categories, segmental flexibility and hinge flexibility, as shown in Figure 1.9. Segmental flexibility involves the region between two domains, such as the region that connects VH to CH1 or CH2 to CH3, which is a very small region that consists of around 5-6 amino acid residues. It is believed that this small domain-connecting region grants small free movements to the connected domains as a whole to move about, as indicated in Figure 1.9A, for better positioning to conduct antibody function such as antigen or receptor interaction. For the region involving VH-CH1, segmental flexibility is likely to help in coordinating a more precise match with epitope orientation leading to a more secure antigen binding. In contrast, segmental flexibility of the region involving CH2-CH3 in IgG is likely to help in exposing the histidine residues critical for association with FcRn.

The importance of segmental flexibility was established by structural analysis of IgM and IgE because both these antibodies lack the hinge region. Instead they possess an additional constant domain (CH2), and therefore, any structural bending observed is most likely due to segmental flexibility. Feinstein and Munn used electron

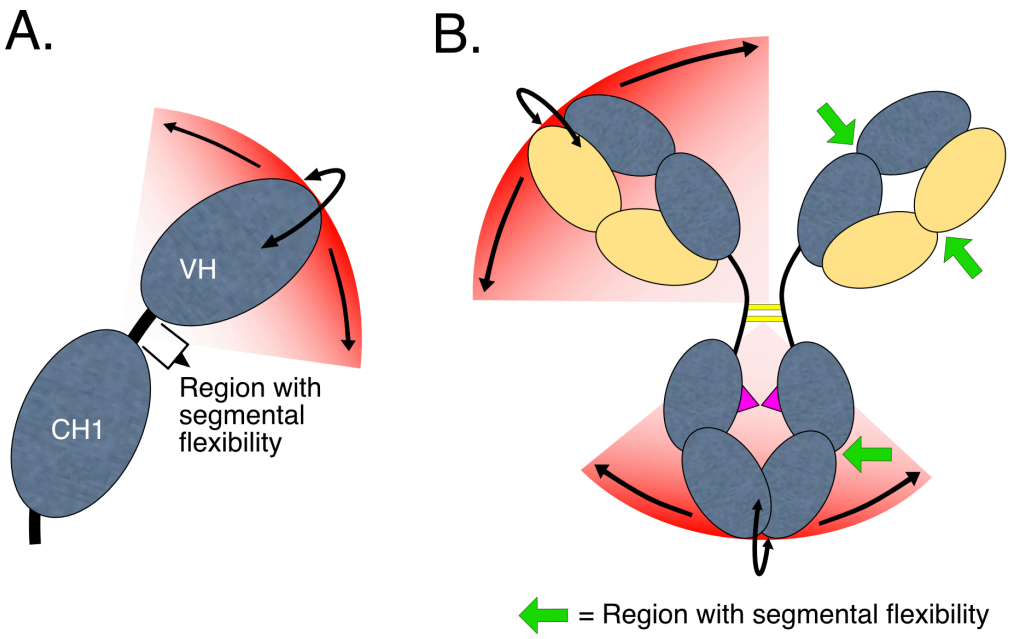

Figure 1.9: A schematic diagram illustrating the potential flexibility of a human IgG1 molecule. **A**) Segmental flexibility which occurs at the region that connects two domains together and allows small free movements to each of the connected domains as a whole. **B**) Hinge flexibility uses the middle hinge which contains the interchain disulphide bonds as a central point and grants the upper and lower hinge region certain flexibility to enable both Fab arms and Fc region to take up different positions conducive to better antigen/receptor binding. Hinge flexibility assumes that the hinge region is flexible rather than having rod-like rigidity. Arrow in green represents regions with segmental flexibility.

microscopy to analyse the structural features of pentameric IgM and showed that upon binding to *Salmonella* flagella the pentameric IgM adopted a conformational structure resembling a "table" in which the Fab arms were bent about 90º to the Fc region (Feinstein and Munn, 1969). Although the exact location of the bend was not reported, the only possible position for the bend was the region connecting the domains together. On the other hand, Drinkwater and colleagues used several techniques such as molecular dynamics and protein crystallisation and showed that IgE could adopt both linear or bent conformations in solution, which further demonstrated the presence of segmental flexibility (Drinkwater *et al*., 2014). Finally, segmental flexibility is also shown by studies analysing the angle, termed the elbow angle, between two domains (Saphire *et al*., 2001; Stanfield *et al*., 2006; Guddat *et al*., 1993). It was reported that the elbow angle between pairs of variable and

constant domains of different crystallised antibodies were 118º for Mcg (hingeless hIgG1), 147º for Dob (hingeless hIgG1) and 174º for Kol (hIgG1) while those recorded of B12 (hIgG1) were 170º and 174º (Saphire *et al*., 2001; Guddat *et al*., 1993). In addition, Stanfield and colleagues developed a programme which used the crystallised Fab 8F5 fragment as a standard and aligned up to 536 different crystallised Fab fragment structures deposited in the RCSB Protein Data Bank (PDB) to analyse the diversity of the elbow angles of antibody Fab regions (Stanfield *et al*., 2006). The authors reported that the elbow angle ranged from 115º to 225º and that the majority of Fab fragments containing lambda light chains showed a greater elbow angle than those containing kappa light chains (Stanfield *et al*., 2006). All these reported different elbow angles suggest that segmental flexibility might be an important structural feature in antibody functionality, such as antigen or receptor binding.

On the other hand, hinge flexibility is granted by the hinge region and refers to the flexibility of the antibody which uses the core hinge that contains the interchain disulphide bonds as central point and enables both the Fab arms, via upper hinge flexibility, and Fc region, via lower hinge flexibility, to take up different positions conducive for better antigen/receptor binding, as indicated in Figure 1.9B. These flexibilities are highly dependent on the upper hinge and lower hinge amino acid residue compositions and it is assumed that both regions are flexible rather than rigid rod-like structures. Hinge flexibility, presumably upper hinge flexibility, was elegantly demonstrated by Roux and colleagues in a study utilising various wildtype and hinge modified mutant antibodies of identical antigen specificity (idiotype). These antibodies were incubated with a specific anti-idiotypic monoclonal antibody

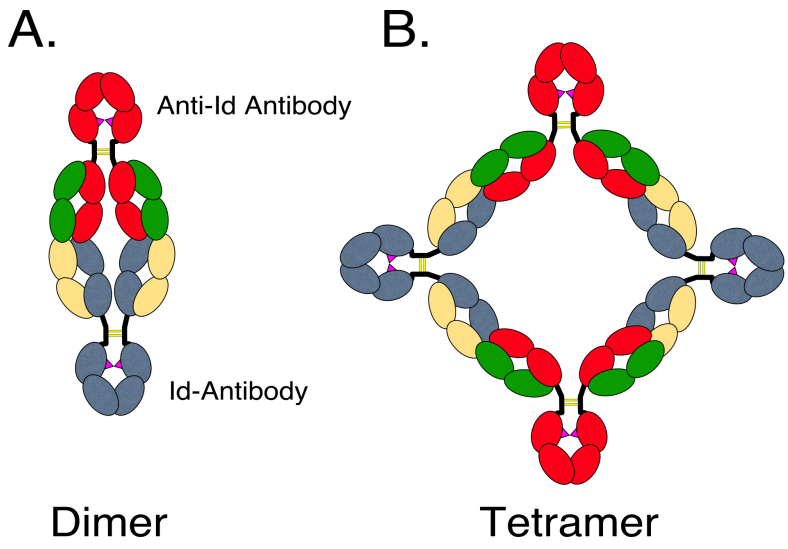

Figure 1.10: A schematic diagram illustrating the different immune complexes formed, due to different Fab arms arrangements. **A**) Formation of dimeric immune complex due to the Fab arms being "close" together, causing a bivalent binding of one anti-Id antibody to a single Id-antibody. **B**) Formation of tetrameric immune complex due to the Fab arms being more "open", allowing each anti-Id antibody to bind two different Id antibodies. Idiotype (Id) antibody, blue and yellow. Anti-Id specific antibody, red and green.

to form polymeric complexes and it was shown that they formed different complexes ranging from dimers to tetramers or higher polymers, using electron microscopy (Roux *et al*., 1998). This observation suggested that the upper hinge region has a certain degree of flexibility because higher polymeric complexes such as tetramers were expected to form only when the Fab arms are more "open", as indicated in Figure 1.10B. In addition, the crystal structure of the anti-HIV human IgG1, B12, showed that the Fab arms adopted an asymmetrical conformational structure which suggests that the upper hinge had a certain degree of flexibility (Saphire *et al*., 2001). On the other hand, the flexibility of the lower hinge region of IgG was shown by the crystal structure of human IgG1 Fc in complex with FcγRIII in which the lower hinge region was bent to a certain angle relative to the Fab for successful association with FcγRIII (Sondermann *et al*., 2000). Finally, hinge flexibility was demonstrated in the studies performed by Sandin and colleagues in which they used cryo-electron tomography to analyse the conformation of murine IgG2a in solution (Sandin *et al*.,

2004) . The authors aligned the Fc region of four different IgG2a structures together and showed that the Fc regions were very similar to each other. However, the Fab arms of each of the IgG2a molecules demonstrated different conformational structures and positions, strongly suggesting the presence of hinge flexibility (Sandin *et al*., 2004). In a different study, the angle between two Fab arms, termed hinge angle, of several crystallised antibodies had been compared together (Saphire *et al*., 2002). It was reported that the hinge angle of B12 (hIgG1) was 148º, Mcg (hingeless hIgG1) was 185º and Kol (hIgG1) was 132º while that of a murine IgG2a, 231, and a murine IgG1, 61.1.3, were 172º and 115º respectively (Saphire *et al*., 2002). These reported hinge angles hint at the diversity of the different conformers that the Fab arms of an antibody can adopt at different times due to the flexible movement granted, most likely, by the upper hinge region.

1.8.2 Hinge proteolysis

Antibodies form one of the major defences against bacterial pathogens. As a result, some bacterial pathogens have evolved to produce proteases which target immunoglobulins, causing lost of functionality. The hinge region is the site mainly targeted by different proteases. In particular, the hinge region of human IgA1 is found to contain several bacterial protease cleavage sites (Mistry and Stockley, 2011), as shown in Figure 1.11. IgA1 proteases seemingly have only one purpose which is to abolish the effector function of IgA1 in mucosal secretions by cleaving the antibody into three fragments, i.e. two Fab and one Fc fragments. The Fab fragments may still bind to target pathogen, however, elimination mechanisms such as respiratory burst or phagocytosis cannot be initiated due to the absence of the Fc fragment. Thus, the survival and invasion rates of the protease-secreting pathogen is

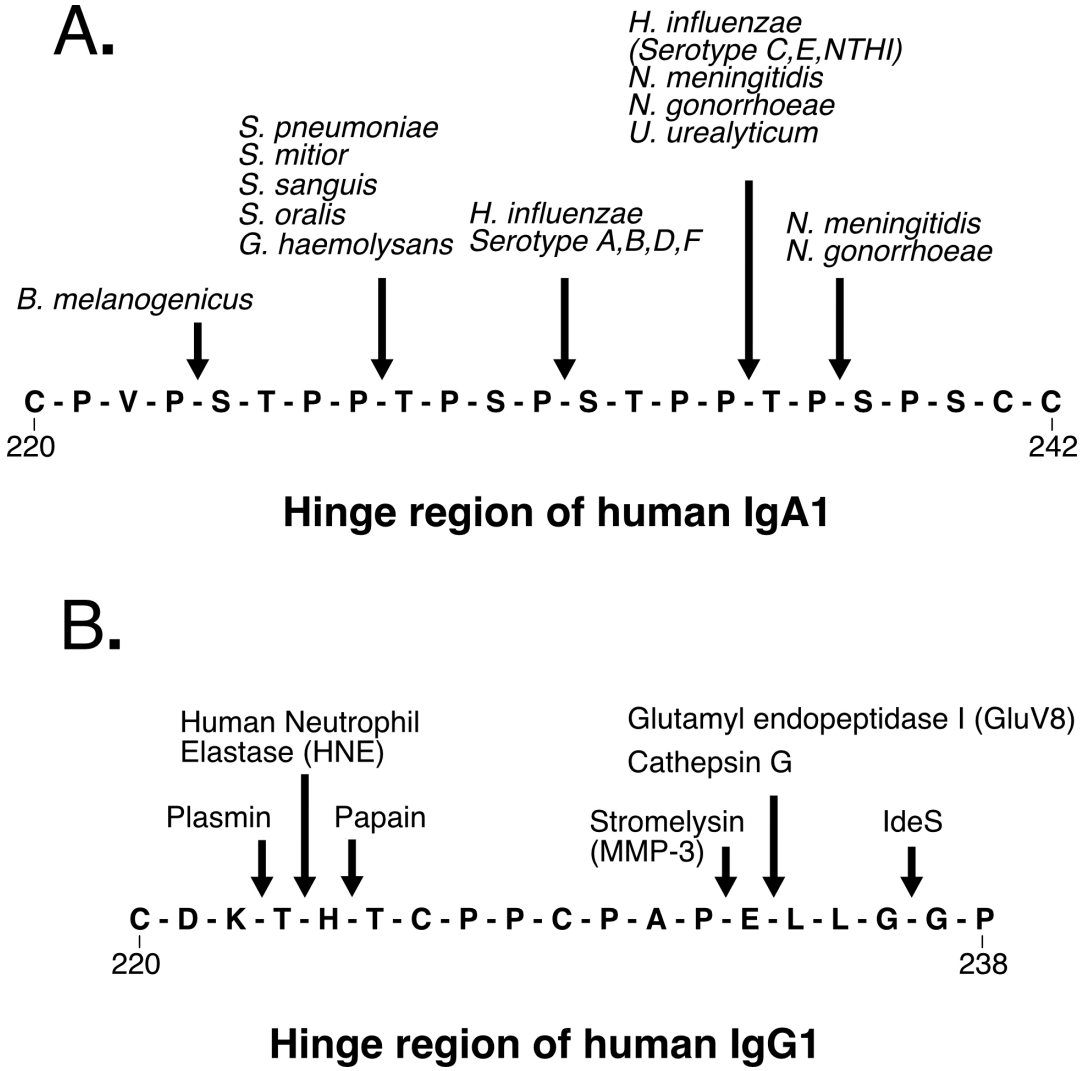

Figure 1.11: A schematic diagram illustrating sites in the hinge regions of human IgA1 and IgG1 that are susceptible to cleavage. **A**) Identified cleavage sites for bacterial proteases within the hinge region of human IgA1. **B**) Identified cleavage sites within the hinge region of human IgG1 for different proteases. Diagram adapted from (Mistry and Stockley, 2011; Janeway *et al*., 2001c) and (Brezski and Jordan, 2010).

greatly increased.

The hinge region of IgA1 mainly consists of a mixture of proline, serine and threonine residues. Notably, all identified IgA1 proteases cleave the hinge region at sites C-terminal to a proline residue, such as proline-serine or proline-threonine bonds, as indicated in Figure 1.11A. Intriguingly, the presence of protease binding sites within the hinge do not necessarily always lead to cleavage as it seems that

there are certain requirements for the cleavage to happen (Senior *et al*., 2000; Senior and Woof, 2005). In brief, Senior and colleagues generated a human IgA2/A1 mutant antibody by inserting a seven amino acid sequence derived from human IgA1 into the hinge region of human IgA2 and carried out enzyme cleavage on the IgA2/A1 antibody. The new hinge sequence of IgA2/A1 contained cleavage sites for the IgA1 proteases of *S. pneumoniae* and *S. oralis*. However, only the protease from *S. pneumoniae* and not *S. oralis* was able to cleave the IgA2/A1 antibody, suggesting that the protease of *S. oralis* required additional factors to mediate efficient cleavage (Senior *et al*., 2000). The same group later performed different combinations of amino acid substitutions and subtractions at the hinge region of the IgA2/A1 antibody and showed that some IgA1 proteases required a certain distance between Fab and Fc region to carry out the protease cleavage (Senior and Woof, 2005). Notably, some proteases that cleave at the IgA1 hinge region were found to require certain recognition sites within the CH3 domain of IgA1 in order to carry out the cleavage activity (Chintalacharuvu *et al*., 2003; Senior and Woof, 2006).

On the other hand, human IgG has also been identified to contain several cleavage sites for different proteases (Brezski and Jordan, 2010; Virella and Yeh, 1977; Baici *et al*., 1982), as indicated in Figure 1.11B. Notably, some of the proteases that cleave human IgG are endogenous enzymes, such as plasmin, Cathepsin G and Human Neutrophil Elastase (HNE). As an example, plasmin is an enzyme found in the blood and is involved in wound healing mechanisms. Similarly, IgG is also highly found in the blood. Thus, the presence of plasmin might be considered as a threat to antibody functionality. However, it is not known if the cleavage of IgG by plasmin happens spontaneously *in vivo*. Intriguingly, Virella and Yeh showed that

although the same classes of different monoclonal human IgGs were used during the plasmin cleavage experiment, different monoclonal antibodies showed different susceptibility to plasmin cleavage (Virella and Yeh, 1977). For instance, when three different monoclonal hIgG1s, WEI, GIA and STO, were incubated with plasmin for up to 72 hours, both WEI and GIA were cleaved by plasmin but not STO (Virella and Yeh, 1977). Similar to the case with IgA1, pathogenic bacteria have developed certain proteases to cleave human IgG as a means to survive. Such proteases include glutamyl endopeptidase V8 (GluV8) of *Staphylococcus aureus* and immunoglobulin-degrading enzyme of *Streptococcus pyogenes* (IdeS) (Brezski and Jordan, 2010). For example, IdeS was shown to cleave IgG at the Gly236-Gly237 bond that is located within the IgG lower hinge region crucial for FcγR binding (von Pawel-Rammingen *et al*., 2002). Indeed, IdeS treatment of *S. pyogenes* that had been pre-incubated with immune plasma prevented the bacteria being killed when they were further incubated with phagocytes. The survival of *S. pyogenes* is most likely due to the abolishment of IgG effector function after IgG Fc region cleavage by IdeS. In comparison untreated *S. pyogenes* were readily killed (von Pawel-Rammingen *et al*., 2002). Interestingly, it was later discovered that IdeS has a second binding site at the IgG Fc region and that this IgG Fc binding is required for the cleavage activity of IdeS at the lower hinge region of IgG (Vincents *et al*., 2004). Interestingly, such a finding is reminiscent of the requirement of certain hIgA1 proteases for Fc elements in order to drive efficient substrate cleavage, as mentioned above.

The cleavage of immunoglobulins not only abolishes their effector function but can also result in induction of an antibody response against the cleaved Fab and Fc fragments. Antibodies capable of recognising cleaved Fab and Fc fragments were

found to be very specific in their antigen recognition which is against the cleaved site of the fragments, especially the C-terminal neoepitopes of Fab or F(ab´)$_2$ (Ryan *et al*., 2008; Falkenburg *et al*., 2017; Terness *et al*., 1995). As a result, these antibodies are also known as anti-hinge antibodies (AHA). AHA were reported to be found in the serum of healthy individuals and patients suffering from rheumatoid arthritis (RA) or systemic lupus erythematosus (SLE) (Falkenburg *et al*., 2017). In addition, AHA were also identified in the synovial fluid of patients with rheumatoid arthritis (Ryan *et al*., 2008). The immunogenic effect of these Fab and Fc fragments along with AHA is not entirely clear yet. However, studies had shown that the immune complexes formed by Fab fragments and AHA seems to have a role in complement amplifications (Fumia *et al*., 2008). The CH1 domain of IgG contains a binding site, mainly Ser132, for the complement cascade protein, C3b. However, the formation of C3b-IgG is considered to be a rare event (Vidarte *et al*., 2001; Shohet *et al*., 1993). To investigate the link between Fab fragment, AHA, and complement amplification, Fumia and colleagues generated F(ab´)$_2$ fragments by utilising pepsin digestion and incubated these with AHA purified from pooled whole human IgG to generate F(ab´)$_2$-IC. Using ^{125}I-iodinated C3 to monitor C3 activation, the authors showed that F(ab´)$_2$-IC had a stronger C3 activation when compared to control IgG-IC (Fumia *et al*., 2008). More importantly, a weak C3 activation was observed when F(ab´)$_2$ was incubated in AHA depleted plasma. However, when AHA was reintroduced into the plasma the activation of C3 was dramatically increased (Fumia *et al*., 2008), suggesting that the AHA played a major role in complement amplification. It is suggested that the formation of F(ab´)$_2$-IC increased the overall conformational stabilisation of F(ab´)$_2$ and allowed a higher probability of C3b activation due to more concentrated binding sites being available within F(ab´)$_2$-IC (Fumia *et al*., 2008;

Lutz and Fumia, 2008).

1.9 Different antibody formats and engineering

With the increasing knowledge on antibody biology, modification of the structural features of immunoglobulins, also known as antibody engineering, has been vastly conducted with the ultimate aim of improving antibody functionality for therapeutic applications.

The identification that the antigen binding site is governed by the CDR generated the idea of grafting the CDRs of a mouse monoclonal antibody, (i.e. homogeneous antibody derived from a single clone), into a human IgG for therapeutic purposes (Queen *et al*., 1989; Carter *et al*., 1992; Harding *et al*., 2010). For example, Queen and colleagues attempted to transfer the CDRs of a mouse monoclonal anti-human interleukin 2 receptor (IL-R2) to a human IgG1 that had high homology to the original mouse antibody within the framework regions (Queen *et al*., 1989). The authors reported that the so-called humanised antibody had a binding affinity for IL-R2 about 1/3 of that of the murine antibody (Queen *et al*., 1989). This approach has greatly enhanced the use of humanised antibodies in clinical applications. However, some humanised antibodies are reported to be immunogenic (Getts *et al*., 2010; Harding *et al*., 2010). It was believed that the murine/rodent CDRs grafted into human antibodies contain epitopes that can stimulate the production of host antibodies and/or be presented on MHC Class II molecules which activate T helper cells, causing the production of cytokines that result in upregulation of an undesired immune response (Getts *et al*., 2010; Harding *et al*., 2010). To tackle this obstacle, Lee and colleagues inserted the entire human immunoglobulin variable region

repertoire into the genome of mouse embryonic stem cells and silenced the mouse variable region genes (Lee *et al*., 2014). This approach resulted in the generation of unique mice which are capable of producing antibodies with human variable regions and mouse constant domains (Lee *et al*., 2014). More importantly, the variable region of these antibodies can be cloned and fused with different human immunoglobulin constant domains to generate fully human antibodies with minimal immunogenicity for therapeutic purposes. Over the years, besides the improvement in the generation of humanised monoclonal antibodies, different antibody formats have been generated through antibody engineering and some them are described in Figure 1.12.

Sometimes the antigen epitope that is targeted is well hidden within a tissue structure and accessibility to the epitope might be hindered by neighbouring structural features. In such a scenario, the full length antibody might be too large to gain access to the target epitope. However, the antibody could be cleaved at the hinge region to produce smaller antigen binding fragments, such as $F(ab')_2$ or Fab fragments, to achieve better penetration into tissues to reach the target epitope. Indeed, the use of $F(ab')_2$ and Fab fragments has yielded promising results for radioimmunotherapy in mouse models when compared to full length monoclonal IgG antibody. This outcome was reasoned to be due to an improved and homogenous tumour uptake because of the smaller molecular size of $F(ab')_2$ and Fab fragments (Behr *et al*., 2000; Sandström *et al*., 2012).

An scFv molecule has a molecular weight even smaller than that of an Fab fragment since it comprises only the variable domains of both light and heavy chain linked

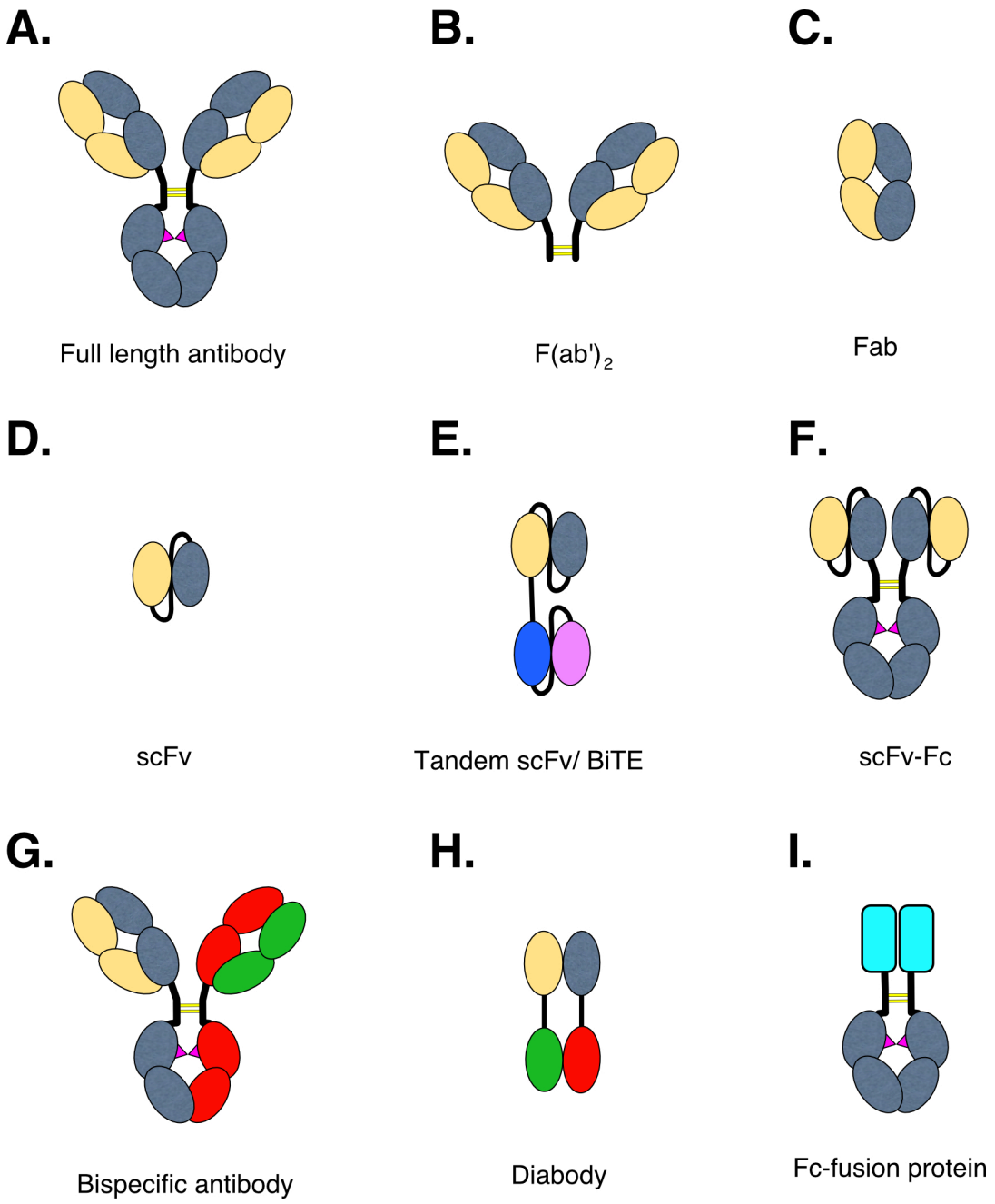

Figure 1.12: A schematic diagram illustrating the different antibody formats that have been engineered. **A**) Full length antibody. **B**) Full length antibody is cleaved at the lower hinge region to produce $F(ab')_2$. **C**) Full length antibody is cleaved at the upper hinge region to produce two Fabs. **D**) Both variable domains of light and heavy chains are joined together by a linker peptide to produce scFv. **E**) Two scFvs are joined together by a linker peptide to produce a tandem scFv. When one of the scFv is targeting a T cell receptor, the molecule is also known as a Bi-specific T-cell engager (BiTE). **F**) Two scFvs are fused to the Fc region of an antibody to produce scFv-Fc. **G**) A full length antibody capable of recognising two different target antigens is known as a bispecific antibody. **H**) Four different variable domains of light and heavy chains are joined together to produce a diabody which can bind two different target antigens**. I**) A desired protein fused to the Fc region of an antibody to produce an Fc-fusion protein.

together by a peptide chain, and yet it retains the original antigen binding capability (Chames *et al*., 2009). The development of scFv started when Inbar and colleagues could produce the Fv demonstrated that cleavage of a Fab fragment of murine IgA under acidic conditions fragment and yet still retain the antigen binding capability (Inbar *et al*., 1972). scFv is a very small monovalent molecule and was reported to have a plasma half-life of only around 2 hours (Chames *et al*., 2009). Thus, it is expected that scFv may have limited clinical application. As a result, scFv is usually fused to other proteins to achieve a target specific homing mechanism. For example, Lorenzo and colleagues fused human anti-ErbB-2 receptor scFv to human RNase and showed that cell toxicity was achieved in a dose dependent manner in ErbB-2-positive cells (Lorenzo *et al*., 2004). In addition, two scFvs can be fused together to generate a product called a tandem scFv, as indicated in Figure 1.12. One of the significant achievements based on tandem scFv was the development of Bi-specific T-cell engagers (BiTE) (Huehls *et al*., 2015; Smits and Sentman, 2016). BiTE molecules are bispecific tandem scFv in which one of the target antigens is a T cell-specific molecule, usually the T cell receptor component CD3, while the other target antigen is a tumour-specific molecule (Huehls *et al*., 2015; Smits and Sentman, 2016). It appears that both antigen binding sites of BiTE must be associated with target antigens to stimulate cytotoxicity activity from T cells. Indeed, no expression of cytokines related to the activation of T cells, such as interferon gamma and tumour necrosis factor alpha (TNF-α), were observed in the absence of dual antigen binding (Smits and Sentman, 2016). In 2014, Blinatumomab (anti-CD19 and anti CD3) was the first BiTE to be approved by the US Food and Drug Administration (FDA) to treat Philadelphia chromosome–negative relapsed or refractory precursor B-cell acute lymphoblastic leukaemia (R/R ALL) (Przepiorka *et al*., 2015).

Although these different small fragments derived from antibody engineering have shown rewarding results in terms of tumour penetration and specific protein homing mechanisms, they all suffer from short plasma half-life mainly due to the absence of the IgG Fc region which could associate with FcRn to prolong plasma half-life, as described in earlier sections. Therefore, there are also different engineered antibody formats that preserved the IgG Fc region such as bispecific antibodies and Fc-fusion proteins. A bispecific antibody has dual antigen specificity as the name suggests. In the past, bispecific antibodies were generated by quadroma technology which is the fusion of two different hybridomas. One popular bispecific antibody called Triomab, is a fusion between rat IgG2b and murine IgG2a, enabling easy purification and the capability of activating human FcγRs (Lindhofer *et al*., 2011; Lindhofer *et al*., 1995). At present, many different techniques have been developed to improve the generation of bispecific antibodies, such as “knobs-into-holes” engineering (Ridgway *et al*., 1996) and Fab-arm exchange technology (Labrijn *et al*., 2013). 'Knobs-into-holes' engineering utilises a single amino acid change of T366Y to generate the “knob” in the CH3 domain of one heavy chain and another mutation Y407T to generate the “hole” in the CH3 domain of the other heavy chain (Ridgway *et al*., 1996). The authors reported that the generation of bispecific antibody due to the pairing of “knobs-into-holes” technology represented up to 92% of the protein pool when compared to the pairing of wildtype heavy chains, which was up to 57% (Ridgway *et al*., 1996). On the other hand, Fab-arm exchange technology introduces single matched point mutations of K409R at one heavy chain and F405L in the other heavy chain to achieve a strong heterogeneous CH3 domain dimerization between two different heavy chains following mild reduction (Labrijn *et al*., 2013). Finally, Fc fusion proteins represent a unique from of antibody engineering because the Fab

region of the antibody is replaced with an unrelated protein while the Fc region is retained, indicated in Figure 1.12I. Further details on Fc-fusion proteins are described in the next section.

1.10 Fc-fusion proteins

As mentioned above, Fc-fusion proteins involve the fusion of a desired protein to the Fc region of an antibody, usually hIgG1 Fc, although the use of IgA and IgM Fc has also been attempted (Czajkowsky *et al*., 2012). The reason for this is mainly to take advantage of the long plasma half-life of IgG through association with FcRn (Roopenian and Akilesh, 2007; Czajkowsky *et al*., 2012) and to obtain a slower renal clearance due to a larger size granted by the Fc region (~50kDa) (Kontermann, 2011). Alternatively, because of the presence of the intact IgG Fc in Fc-fusion proteins, the effector function capability of IgG can be taken advantage of. For example, Fc-fusion proteins can interact with FcγRs to induce ADCC activity (Deng *et al*., 2015; Sioud *et al*., 2015).

There are several Fc-fusion proteins that have reached the clinic such as etanercept, alefacept, belatacept, aflibercept and abatacept (Czajkowsky *et al*., 2012). Intriguingly, all the Fc-fusion proteins listed above function as protein inhibitors. As an example, etanercept is a TNF-α inhibitor in which the TNF receptor is fused to the Fc region of human IgG1 (Haraoui and Bykerk, 2007). TNF-α is a trimeric cytokine produced mainly by activated macrophages and T cells and has a major role in immune regulatory responses (Haraoui and Bykerk, 2007). Two distinct cell surface TNF receptors, termed p55 and p75, exist and can be cleaved to produce soluble monomeric TNF receptor, which acts as natural TNF-α inhibitor (Haraoui

and Bykerk, 2007). Fusion of monomeric TNF receptor, p75, to IgG1 Fc generates a dimeric TNF-α binding protein (etanercept) due to IgG Fc being a homodimer protein itself (Mohler *et al*., 1993). As a result, and given the trimeric nature of TNF-α, the avidity of etanercept is expected to be stronger than natural soluble monomeric TNF receptors. Indeed, etanercept was shown to have an increased binding affinity for TNF-α of up to 50-fold higher than that of monomeric TNF receptor. As a result, it has been shown to be able to prevent killing by a normally lethal dose of lipopolysaccharides (LPS) in mouse models, mainly by inhibiting the effector mechanisms of TNF-α (Mohler *et al*., 1993). More importantly, it was reported that the elevated serum levels of TNF after injection of LPS alone or LPS with human IgG (control) lasted for around 2 hours whereas it lasted at least 4 hours in mice injected with LPS and etanercept (Mohler *et al*., 1993), which is most likely due to the recycling capability of etanercept via FcRn association.

Using conventional techniques, generation of an antigen-specific antibody suitable for clinical therapy takes a long time, because of the requirement for antigen immunisation, purification of antigen-specific antibodies from animal models, selection of suitable antibody with superior antigen specificity and high affinity, and humanisation of the monoclonal antibody before it can be used in clinical therapy. The production of antigen-specific Fc-fusion proteins allows one to bypass these procedures because the natural ligand/receptor of the target antigen may already have been identified, such as TNF-α and TNF receptor for etanercept. Thus, the fusion of this natural ligand/receptor to the antibody Fc is all it that is necessary to generate an "antibody-like" molecule that could bind specifically to targeted antigen and initiate antibody effector functions. Indeed, Deng and colleagues successfully generated a

Fc-fusion protein, termed NKp80-Fc, by fusing the natural killer cell-activating receptor (NKp80) to hIgG1 Fc because the availability of an antibody specific to the natural ligand of NKp80, activation-induced C-type lectin (AICL), was lacking (Deng *et al*., 2015). The authors reported that NKp80-Fc could direct NK cells to AICL-expressing leukaemia cells and trigger ADCC killing activity of NK cells *in vitro* (Deng *et al*., 2015). In an *in vivo* experiment, the introduction of a combination of NK cells and NKp80-Fc was shown to be able to inhibit tumour progression from AICL-expressing U937 xenografts in mouse models, in comparison to control, a combination of NK cells alone, or NK cells and hIgG (Mohler *et al*., 1993). Such findings suggest that Fc-fusion proteins may serve as an attractive alternative option to replace antibody-based therapies.

Alternatively, Fc-fusion protein has also been used as a mode of transport to deliver antigenic vaccine across the mucosal barrier (Ye *et al*., 2011). Such transport is believed to be mediated mainly via FcRn. Ye and colleagues had fused the herpes simplex virus type-2 (HSV-2) glycoprotein gD to murine IgG2a Fc, hereby named as gD-Fc. Following immunisation of mice with the generated Fc-fusion protein via the mucosal pathway, they demonstrated that the immunised mice showed an efficient induction of antibody, B and T cell immune responses and could survive a lethal challenge with the relevant virus. It is most likely that gD-Fc was endocytosed by FcRn-expressing epithelial cells and upon introduction onto the mucosal surface and is transported across the epithelial barrier after associating with FcRn, as described earlier in Figure 1.7B. The gD-Fc is then expected to form immune complexes due to host antibody recognising the HSV-2 gD protein and being phagocytosis by nearby dendritic cells via FcγR-mediated phagocytosis. Finally, the gD-Fc is then digested

and presented on both MHC Class I and II, thus initiating a specific anti HSV-2 immune response.

In summary, all these findings suggest that the outcome of using Fc-fusion protein can be quite rewarding. However, many investigations have to be carried out upon generation of a new Fc-fusion protein to confirm the characteristics of the fused protein partner and the molecule as a whole in terms of its stability, binding affinity, and toxicity.

1.10.1 Factors affecting the selection of fusion partner

Although Fc fusion proteins are emerging as an alternative option in the generation of new therapeutic drugs due to some of the advantages mentioned earlier, there are certain factors that one has to take into consideration in the selection of the Fc fusion partner. One of the factors is the stability of the selected protein after fusion with IgG Fc and in secreted soluble formation. If the protein partner becomes unstable after Fc fusion, it will not be able to carry out its intended function and might not be secreted because unstable protein usually suffers from protein misfolding and aggregation which ultimately leads to protein degradation (Del Pozo-Yauner *et al*., 2015). For example, light-chain amyloidosis (AL) is one of the diseases that is caused by protein misfolding and aggregation which could ultimately leads to organ proteotoxicity and dysfunction. Thus, the stability of the fused protein has to be confirmed to avoid a similar outcome (Cooley *et al*., 2014). Secondly, the binding affinity of the fused partner for its targeted antigen has to taken into consideration because the binding affinity of natural ligand/receptor interactions varies and might be rather low. The antibody Fc is a homodimeric molecule, and therefore the

generation of Fc fusion protein is expected to result in a slight increase in antigen avidity due to doubling of the binding sites for targeted antigen, which is similar to the structural feature of etanacept mentioned earlier. However, if the binding affinity of the dimeric fused protein is still low, one option is to generate a polymeric Fc-fusion protein to increase overall binding avidity (Nagashima *et al*., 2011; Mekhaiel *et al*., 2011). Mekhaiel and colleagues successfully induced the formation of a hexameric Fc-fusion protein in an attempt to increase the association with FcγRII and FcγRIII, which only bind aggregated IgG IC, by inserting the 18 amino acid tailpiece of human IgM and mutating Leu309 to cysteine to enhance the formation of polymers (Mekhaiel *et al*., 2011). Therefore, this technique may be used in the case of low binding fusing partners to generate hexameric Fc-fusion proteins with improved overall binding avidity.

1.11 Recombinant antibody technology

Since the generation of a hybridomas capable of producing an infinite supply of identical monoclonal antibody (Kohler and Milstein, 1975), the technology in antibody production has expanded enormously. Currently, specific oligonucleotides can be used to clone the DNA sequences of the variable domains of an antibody and fuse these with the DNA sequences of different antibody heavy chain constant regions (Karu *et al*., 1995), including those of different species, to produce a desired complete monoclonal antibody DNA sequence. Subsequently, such DNA sequences are usually cloned into an expression vector and transfected into suitable host cells to drive the expression of the antibody. These techniques are known as “recombinant antibody technology”. Currently, there are a variety of both prokaryotic and eukaryotic hosts available for antibody production as reviewed by Frenzel *et al*.

(2013). In brief, *Escherichia coli* (*E. coli*) is one of the popular choices for a prokaryotic host since recombinant antibody expression in *E. coli* can yield up to several grams per litre of extracellular production (Frenzel *et al*., 2013). However, there are certain limitations in bacterial antibody expression. For instance, antibody fragments can only be produced in *E. coli* in the non-native state which is due to the incompetent protein folding mechanism that involves disulphide bonds (Skerra and Pluckthun, 1988; Frenzel *et al*., 2013). However, this obstacle can be overcome if the antibody fragment is directed to the oxidative periplasm of the bacterium which favours the formation of disulphide bonds (Skerra and Pluckthun, 1988; Frenzel *et al*., 2013). The production of the full length 150kDa antibody is quite challenging in bacterial expression due to the need of the correct homodimer pairing of the Fc region which involves disulphide bonding. Therefore, *E. coli* is usually selected for the expression of scFv due to its smaller molecular size and the fact that it does not require homodimer pairing (Skerra and Pluckthun, 1988). In addition, due to difference in post-translation modifications between prokaryotic and eukaryotic hosts, the successful expression of full length antibody is usually in an aglycosylated version in *E. coli* (Simmons *et al*., 2002; Mazor *et al*., 2007). One of the major problems with aglycosylated antibody is the significant reduction in the binding affinity for FcγRs and C1q as mentioned earlier (Jefferis, 2005; Mazor *et al*., 2007; Simmons *et al*., 2002). Therefore, one has to consider the importance of the effector functions of the antibody product if *E. coli* is selected as the expression host.

In regards to eukaryotic expression systems, almost 95% of clinically approved recombinant antibodies are produced by mammalian cells. This choice is because mammalian cells have sufficient protein production machineries to handle

mammalian protein folding, post-translational modification and protein secretion, which makes the produced antibody almost indistinguishable from those expressed in the human body (Frenzel *et al*., 2013). As a result, the immunogenicity of the antibody protein is significantly lowered, which is a major advatange for therapeutic purposes. Chinese hamster ovary (CHO) and human embryonic kidney cell line (HEK293) are two of the main mammalian cell lines used for antibody expression (Frenzel *et al*., 2013; Karu *et al*., 1995). Although not from a human origin, the N-linked glycosylation profile of proteins produced in CHO cells are very close to those made by human cells as both cell lineages express the same N-linked glycan core structures but may differ in the expression of the extra glycan moieties on the core structure (Higel *et al*., 2016; Hossler and Khattak, 2009). However, numerous studies had been carried out to overcome such obstacles which include the use of sequence interfering RNA (siRNA) to prevent expression of the enzyme fucosyltransferase, that is required for fucosylation, generating mutant CHO cells which do not express fucosyltransferase, or upregulating the expression of the enzyme sialyltransferase, that is required for sialylation (Butler and Spearman, 2014). As a result, the difference in the N-linked glycosylation profile between antibodies generated in CHO cells and those found in humans is greatly reduced. On the other hand, due to the human origin of HEK293, it is expected that the glycosylation profile of antibodies expressed in HEK293 will be very similar to those found in natural human serum. As a result, HEK293 cells are also widely used for transient antibody expression for many research purposes (Frenzel *et al*., 2013; Vink *et al*., 2014). Recently, Vink and colleagues reported the transient expression of an antibody produced from a modified HEK-293 cell line known as FreeStyle™ 293-F (HEK-293F) at up to 400 mg/ml in less than 7 days (Vink *et al*., 2014). As a result,

the transient expression of antibody from mammalian cell lines seems to be a good choice for a quick and efficient way to obtain sufficient amounts of antibody for research purposes.

1.12 Project aims

Over the years, there have been very many investigations to expand understanding of antibody biology. However, there are still areas regarding the structural features of antibodies that remain to be discovered. Notably, the hinge region of different antibodies varies considerably, but the precise impact of such variations on function is still incompletely understood. Alongside this, recombinant antibody technology and antibody engineering has allowed development of novel antibody formats which may be tested for their value for therapeutic use. Each of the novel antibody formats has demonstrated their own advantages and limitations and further expanded understanding of antibody biology. The research work of this thesis similarly aimed to expand knowledge of antibody biology. The main hypotheses and aims of this project are listed below:

1. It was hypothesised that a mutant human IgG1 antibody with an extended upper hinge length would have an increased antigenic binding distance, i.e. the distance between two neighbouring antigens bound by the Fab arms of the antibody. To test this hypothesis, this project aimed to a) engineer various human IgG1 mutants with different upper hinge lengths to investigate the relationship between the upper hinge length and the antigenic distance of an antibody and b) to develop a novel molecular distance measuring system to calculate the antigenic distance of an antibody.

2. It was hypothesised that Fc-fusion proteins designed to promote antigen cross presentation via FcRn engagement and subsequent activation of cytotoxic T cells against cancer cells might serve as potential cancer vaccines. To test this hypothesis, this project aimed to fuse a protein which is specifically expressed by cancer cells to IgG Fc. Upon successful production of the Fc-fusion protein, the aim was to characterise the protein and investigate the possibility of inducing antigen cross presentation in dendritic cells.

CHAPTER TWO
MATERIALS AND METHODS

2.1 GENERAL MATERIALS

2.1.1 Chemicals

All chemicals used in the laboratory were purchased from Sigma-Aldrich or VWR International unless otherwise stated.

2.1.2 General solutions and buffers

Water

Deionised water from a Milli-Q Ultra-Pure system (Millipore) was used. For tissue culture usage, Milli-Q water was autoclaved prior to use.

Phosphate buffered saline (PBS)

A 10X stock solution of PBS (1.37M NaCl, 27mM KCl, 100mM Na_2HPO_4, 18mM KH_2PO_4, pH7.2) was prepared and autoclaved. This stock solution was diluted to 1X with Milli-Q water prior to use.

PBS-Tween (PBS-T)

0.05% (v/v) Tween 20 was added to PBS.

2.2 ANTIBODIES AND OTHER DETECTING SUBSTANCES

A list of antibodies and other detecting agents that were used during protein analyses were included in Table 2.1 along with details of host species and clonality (if known), conjugation (if any), manufacturer (if known) and their final concentration used in the protein analyses application.

Table 2.1: List of antibodies and other detecting compounds used

	Antibody/ Detecting agent (Product Code)	Host species and clonality	Conjugation	Manufacturer	Final protein concentration in application
	Characterisation of antibodies				
1.	Anti mouse lambda light chain (A90-121P)	Goat polyclonal	HRP	Bethyl Laboratories, Inc.	1 µg/ml - Blot 0.2 µg/ml - ELISA
2.	Anti human IgG (P0214)	Rabbit polyclonal	HRP	DAKO	1 µg/ml - Blot 0.2 µg/ml - ELISA
3.	Biotinylated jacalin (B-1155) (Gift from Riccardo Trapannone)	-	Biotin	Vector Laboratories	0.2 µg/ml - ELISA
4.	Streptavidin Horseradish Peroxidase Conjugate (43-4323)	-	HRP	Invitrogen	0.2 µg/ml - ELISA
	Detection of human Fcγ receptors				
5.	Anti human CD64 antibody [10.1] FITC (ab93500)	Mouse monoclonal	FITC	Abcam	1.25 µg/ml per $1x10^5$ - $1x10^8$ cells - Flow cytometry
6.	Anti human CD32 antibody [AT10] FITC (ab30356)	Mouse monoclonal	FITC	Abcam	10 µg/ml per 10^6 cells - Flow cytometry

	Characterisation of antigen presentation pathway				
7.	Anti mouse CD64 (FcγRI) - PE (130-103-808)	Recombinant human monoclonal	PE	MACS Miltenyi Biotec	3 µg/ml - Flow cytometry
8.	Anti mouse CD32/CD16/ FcγRIIB (AF1460)	Goat Polyclonal	-	R&D Systems	10 µg/ml - Flow cytometry
9.	Anti mouse FcRn (PB9867)	Rabbit polyclonal	-	Boster Biological Technology Co., Ltd.	0.25 µg/ml - Flow cytometry
10.	$F(ab')_2$ anti rabbit IgG (whole molecule) (F-1262)	Goat Polyclonal	FITC	Sigma	20 µg/ml- Flow cytometry
11.	Anti sheep/ goat IgG (S078-201)	Polyclonal	FITC	SAPU	50 µg/ml - Flow cytometry
12.	Anti human IgA, α-chain specific (I-0884)	Goat polyclonal	-	Sigma	10 µg/ml - Flow cytometry
13.	Anti actin (A2103)	Rabbit polyclonal	-	Sigma	0.5 µg/ml - Blot
14.	Anti rabbit IgG (whole molecule) (A0545)	Goat polyclonal	HRP	Sigma	4 µg/ml - Blot
15.	Anti chicken ovalbumin	Rabbit polyclonal	-	Bioss Antibodies	12.5 µg/ml - Assay
16.	Anti mouse IgG (whole molecule) (M7023)	Rabbit polyclonal	-	Sigma	25-34 µg/ml - Assay

	Characterisation of MAGE A2-Fc fusion protein				
17.	Anti human MAGE-A2, clone 1H4 (D7121-1H4)	Mouse monoclonal	-	Sigma	12.5 µg/ml - Assay 0.47 µg/ml - Blot
18.	Anti human MAGE-A, clone 6C1 (sc-20034) (Gift from Bianca Ihrig)	Mouse monoclonal	-	Santa Cruz Biotechnology, Inc.	0.2 µg/ml - Blot
19.	Anti mouse kappa light chain (A90-119P)	Goat polyclonal	HRP	Bethyl Laboratories, Inc.	1 µg/ml - Blot 0.2 µg/ml - ELISA
20.	Anti mouse IgG (Fc specific) (A2554)	Goat polyclonal	HRP	Sigma	Concentration not available. 1:5000 dilution -Blot

2.3 MOLECULAR BIOLOGY MATERIALS

2.3.1 Buffers, solutions and materials

Tris-acetate-EDTA (TAE)

A 50X stock solution of TAE buffer (2M Tris, 1M glacial acetic acid, 50mM EDTA (disodium salt), pH 8) was prepared and autoclaved. This stock solution was diluted to 1X with Milli-Q water prior to use.

Tris-Borate-EDTA (TBE)

TBE buffer (89mM Tris Base, 89mM Boric acid, 2mM EDTA) was prepared and autoclaved.

Luria-Bertani (LB) Broth

LB Broth was prepared using LB Broth (Sigma) according to manufacturer's guide, 20g in 1 litre of Milli-Q water, and autoclaved. Ampicillin (Sigma) was added to a final concentration of 100 μg/ml if required. Completed LB Broth is stored at 4ºC and warmed to room temperature prior to use.

Luria-Bertani (LB) agar plates

LB Broth with 1.5% Bacto™ Agar (Becton, Dickson and Company) was prepared by adding 15g of Bacto™ Agar to 1 litre of LB Broth and autoclaving. The solution was allowed to cool to room temperature before adding ampicillin to a final concentration of 100 μg/ml.

LB agar plates were prepared by pouring the final LB Broth solution in to 90mm Petri Dishes (Thermo Fisher Scientific) and allowed to cool and solidify. LB agar plates were stored at 4ºC prior to use.

2.3.2 Restriction enzymes

All restriction enzymes were purchased from New England Biolabs or Invitrogen, Thermo Fisher Scientific.

2.3.3 DNA Ligase

T4 DNA Ligase (Invitrogen, 15224-017) was purchased from Thermo Fisher Scientific.

2.3.4 DNA Molecular weight markers

Quick-Load® Purple 2-Log DNA Ladder (0.1-10.0 kb) (N0550) molecular weight markers were purchased from New England Biolabs.

2.3.5 DNA Polymerase

KOD Hot Start DNA polymerase kit (Novagen, 71086-3) was purchased from EMD Millipore.

2.3.6 Competent cells

Subcloning Efficiency™ DH5α™ competent cells (Invitrogen, 18265-017) were purchased from Thermo Fisher Scientific. 50µl cells were aliquoted into sterile 1.5ml microfuge tubes on ice and stored at -80ºC prior to use.

2.3.7 Primers

Primers were purchased from Eurofins Genomics. All primers are reconstituted to a final concentration of 100 pmol/µl with Milli-Q water and stored at -20ºC.

Table 2.2: List of amplifying primers used

	Name of primer	Direction	DNA sequence (5´- 3´)
	Restoration of lost amino acids (See Chapter 3)		
1.	DS3	Forward	AGGACTCTACTCCCTCAGCAGC
2.	GUHIAS	Reverse	AGTTTTGTCACAAGATTTGGGCTCAAC TTTCTTGTCCACCTTGGTGTTGC
3.	GUHIS	Forward	GAGCCCAAATCTTGTGACAAAACTCCC TCAACTCCACCTACCCCATC
4.	AG3´NEW	Reverse	GCGCGCGCGAATTCGCTTTATTTCCAT GCTGGGC

	Generation of O-linked negative mutant (See Chapter 3)		
5.	OlinkNegForw	Forward	CCACCTGCTCCAGCTCCGGGCGCACCA CCTGGACCAGCACCCGGCTGCCCACCG TGCCCAGGTAAGCC
6.	OlinkNegRev	Reverse	CAGGTGGTGCGCCCGGAGCTGGAGCA GGTGGGCCTGCGGGTCCTTTGTCACAA GATTTGGGCTCAAC
	Generation of MAGE A2-Fc fusion protein (See Chapter 6)		
7.	MAGEForwShort	Forward	GCGCGCAAGCTTATGGGATGGAGCTGT ATC
8.	MAGERev	Reverse	ACTGCTACTCCCTCCGCTACTGCCTCCA CCACTGCTACCCTCTTCTCCCTCTCTCA AAGC
9.	MAGEForwLong	Forward	GCGCGCAAGCTTATGGGATGGAGCTGT ATCATCCTCTTCTTGGTAGCAACAGCT ACAGGTGTCCACTCCATGCCTCTTGAG CAGAGG
10.	IgGForw	Forward	TAGCGGAGGGAGTAGCAGTGACAAAA CTCACACATG
11.	MAGE-Fc Kosak	Forward	GCGCGCAAGCTTCCACCATGGGATGGA GCTG
12.	MouseFcForw	Forward	CAGTAGCGGAGGGAGTAGCAGTCCTCC ATGCAAATGCCCAGCA
13.	MouseFcRev	Reverse	GCGCGCGAATTCTGAGCTCATTTACCC GGAGTC
14.	Siinfekl1	Reverse	CAATGAGGGCCCTGAGTTTCTCGAAGT TAATGATTGATGGACCCCACAGGAACT C

Table 2.3: List of sequencing primers used

	Name of primer	Direction	DNA sequence (5´- 3´)
1.	CGamma1BacSeq	Reverse	GATTCACGTTGCAGATGTAGG
2.	VNIPSEQ1	Forward	GCTGATGCAGACAGACATCCTCAGC
3.	UPIgGCH2Forw	Forward	CACGTCCACCTCCATCTCTTC
4.	3'VHIgGSCG1	Reverse	CTTGCACTTGTACTCCTTGCC
5.	UPHindIIIForw	Forward	GCTGTTAACGGTGGAGGGCAG
6.	pEIgGENDRev	Reverse	GAAGTATGTACAGGGGGTACG
7.	MidMAGEForw	Forward	CTGCTCCTCAAGTATCGAGCC

8.	MIDMageFcRev	Reverse	CCACTTCCACCACCTCAATGC
9.	MidIgG2aRev	Reverse	GCTGGGAGGTCTTTGTTGTTG
10.	MidIgG2aFor	Forward	CACAAACCCATAGAGAGGATTAC

2.4 MOLECULAR BIOLOGY METHODS

2.4.1 Restriction digestion

DNA was digested with restriction enzymes to yield suitable DNA fragments for further analyses or experiments. The standard reaction setup for a restriction digest is listed below in Table 2.4. The mixture was gently mixed and incubated at an appropriate temperature, according to manufacturer's protocol, in a water bath for at least 1 hour. Double restriction digests were performed using a reaction buffer suitable for both restriction enzymes and the reaction setup were adjusted accordingly. If the optimal temperature for the restriction enzymes differed, the reaction was incubated at the lower optimal temperature for an hour before increasing to the higher optimal temperature for another hour. Digested DNA was then subjected to agarose gel electrophoresis, section 2.4.4, for further analysis or purification.

Table 2.4: Reaction mix for restriction digestion

Component	Volume added
10X Reaction Buffer (suitable for particular restriction enzyme(s))	3µl
Restriction enzyme	1µl
Plasmid DNA (1-2 µg) or purified PCR product	As required depending on plasmid concentration
Milli-Q water	To bring volume to 30µl
Total	**30µl**

2.4.2 Polymerase Chain Reaction (PCR) DNA amplification

Desired DNA fragments could be amplified using the technique termed Polymerase Chain Reaction (PCR). The standard reaction setup using KOD Hot Start DNA polymerase, section 2.3.5, is listed below in Table 2.5. All components listed, except primers, DNA template and Milli-Q water, were provided with the enzyme. The standard reaction conditions used to carry out PCR amplification are shown in Table 2.6. Steps 2-4 were repeated 30 times. PCR reactions were performed using a Mastercycler personal machine (Eppendorf).

Table 2.5: Reaction condition for PCR DNA amplification

Component	Volume	Final Concentration/Amount
10X Reaction Buffer	5µl	1X
25mM $MgSO_4$	3µl	1.5mM
dNTPs (2mM each)	5µl	0.2mM (each)
Sense (5´) Primer (10µM)	1.5µl	0.3µM
Anti-sense (3´) Primer (10µM)	1.5µl	0.3µM
KOD Hot Start DNA polymerase (1 Unit/µl)	1µl	0.02 Unit/µl
DNA template	X µl	10ng
Milli-Q water	Y µl	To bring volume to 50µl
Total reaction volume	**50µl**	-

Table 2.6: List of steps for typical PCR DNA amplification

	Step	Incubation
1.	KOD Hot Start polymerase activation	95ºC for 2 minutes
2.	Denaturation of DNA	95ºC for 20 seconds
3.	Annealing of primers	At Tm of primer with lowest Tm for 10 seconds
4.	DNA extension	72ºC for 50 seconds

Note: Primer Melting Temperature (Tm) is defined as the temperature at which half of the DNA duplex will dissociate into single stranded formation.

2.4.3 Agarose gel electrophoresis

DNA molecules of different lengths can be separated by performing agarose gel electrophoresis. 1% (w/v) UltraPure™ Agarose (Invitrogen, 16500) in 1X TAE buffer was prepared and heated using a microwave to dissolve the agarose powder. The solution was allowed to cool before adding SYBR® Safe DNA Gel Stain (Invitrogen, S33102) to a final concentration of 1X. The final solution was poured into a casting tray with the comb inserted and allowed to solidify at room temperature. Once the gel was ready, the comb was removed and the gel was placed into a suitable electrophoresis tank (Bio-Rad). The tank was then filled with 1X TAE buffer and DNA samples were prepared. An appropriate volume of 10X BlueJuice™ Gel Loading Buffer (Invitrogen, 10816-105) was added to DNA samples to a final concentration of 1X prior to loading into the gel. 7µl of DNA molecular weight marker, see section 2.3.4, at 100 ng/µl was loaded into a well on each gel for size referencing. Loaded DNA was electrophoresed using a Power Pack 3000 (Bio-Rad) at 100V for 60-90 minutes depending on the size of the DNA sample that needed to be resolved. Upon completion of electrophoresis, the positions of DNA products within the gel were visualised using a GelVue UV Transilluminator (Syngene) and imaged using GeneFlash (Syngene) or FluorChem™ System (Alpha Innotech).

2.4.4 DNA Purification from agarose gel

Upon completion of agarose gel electrophoresis, the gel was viewed using a UV transilluminator, UVT-28M (HeroLab), or Safe Imager™ 2.0 Blue-Light Transilluminator (Invitrogen). DNA product with the correct size was extracted using a sterile scalpel and weighed. The DNA product was purified from the agarose gel using QIAquick® Gel Extraction Kit (Qiagen, 28704) according to

manufacturer's protocol. In the final step, the digested DNA fragments were eluted with 30µl of Milli-Q water whereas DNA plasmids were eluted with 50µl of Milli-Q water and stored at -20ºC prior to use.

2.4.5 DNA Ligation

Fragments of purified DNA were ligated together using T4 DNA Ligase (section 2.3.3). The standard reaction setup is listed in Table 2.7. The reaction was mixed gently and incubated overnight at room temperature, prior to use for transformation of competent *E. coli*.

Table 2.7: Reaction conditions for DNA ligation

Components	Requirements
5X Ligase Reaction Buffer	4µl
Vector DNA	1-2 µl
Insert DNA	3-6 µl
T4 DNA Ligase (1 Unit/µl)	1µl
Milli-Q water	to make mixture up to 20 µl
Total	**20µl**

Note: The volume of Vector DNA, Insert DNA and Milli-Q water varied depending on the concentration of the DNAs. However, a molarity ratio of 1:3 Insert:Vector was maintained for all ligation reactions. The final total volume of the ligation reaction was made up to 20µl with Milli-Q water.

2.4.6 Transformation of competent DH5α cells

50µl of competent DH5α *E. coli* cells (section 2.3.6) were taken from storage at -80ºC and thawed on ice. Cells were mixed by gently tapping before introducing DNA. 1-5µl (1-10ng) of plasmid DNA or 1-2µl of ligation product (section 2.4.6) was added to cells and mixed gently before incubating on ice for 30 minutes. Cells were then heat shocked for 20 seconds in a 42ºC water bath and placed on ice for another 2 minutes. Subsequently 950µl of pre-warmed LB broth medium was added

to the cells and incubated at 37ºC for 1 hour, with shaking at 50g. Cells were centrifuged at 800g for 3 minutes and 700µl of supernatant was discarded. Cells were resuspended in the remaining LB broth medium and pipetted onto an LB agar plate with ampicillin (section 2.3.1), previously warmed to room temperature. A sterile L-shaped spreader (Greiner Bio-One, 730190) was used to spread the cells evenly across the plate, which was then incubated at 37ºC overnight to allow formation of bacterial colonies.

2.4.7 Plasmid DNA amplification

Plasmid DNA was amplified by inoculating bacteria that carry the correct plasmid into a large volume of selective growth medium. All plasmids described in this thesis carried an ampicillin resistance gene, allowing ampicillin to be used as the selective agent. For a smaller scale of amplification, such as for a DNA miniprep, transformed bacterial colonies on LB agar plates (section 2.3.7) were picked into different 30ml polypropylene tubes containing 5ml LB broth with ampicillin and incubated overnight at 37ºC, with shaking at 200 rpm. Upon completion of incubation, cells were ready for plasmid DNA extraction (section 2.4.9) unless a larger scale of plasmid DNA amplification was required. For a larger scale amplification, such as for a DNA maxiprep, 5ml of overnight bacterial culture was added to a larger volume (200-500ml) of LB broth with ampicillin and cultured overnight at 37ºC, with shaking at 200 rpm. Bacterial culture was ready for plasmid purification (section 2.4.9) after incubation.

2.4.8 Plasmid DNA extraction

Miniprep

Plasmid DNA from 5ml of bacterial culture was extracted and purified using a QIAprep® Spin Miniprep Kit (Qiagen, 27106), according to manufacturer's protocol. In the final step, plasmid DNA was eluted with 50µl of Milli-Q water and stored at -20ºC.

Maxiprep

Plasmid DNA from larger volumes of bacterial culture (200-500ml) was extracted and purified using a QIAGEN® Plasmid Maxiprep Kit (Qiagen, 12163), according to manufacturer's protocol. In the final step, plasmid DNA was reconstituted with 500µl of Milli-Q water and transferred to a 1ml microfuge tube to be stored at -20ºC.

2.4.9 DNA Concentration and purity

The concentration and purity of purified DNA was measured using a ND-1000 Spectrophotometer (NanoDrop). The concentration of sample DNA was calculated by loading 1µl of sample into the device. With regards to DNA purity, the sample absorbance at 230nm, 260nm and 280nm were measured. A value of ~1.80 for the 260/280 ratio and one of 2.0-2.2 for the 260/230 ratio was considered to be indicative of a highly pure DNA sample. A ratio that was either higher or lower than the ratios stated above was considered to be (partially) contaminated with protein, phenols or other contaminants.

2.4.10 DNA Sequencing

All plasmid DNA along with appropriate sequencing primers were submitted to DNA Sequencing and Services Unit, University of Dundee for automated sequencing.

2.5 TISSUE CULTURE MATERIALS

2.5.1 Cell lines and growth conditions

All reagents and supplements used for cell line culture were purchased from Gibco, ThermoFisher Scientific.

Table 2.8: List of cell culture conditions and details of each cell line used

Cell line	Origin	Cell type	Growth medium	Cell maintenance
THP-1 (Tsuchiya *et al*., 1980)	Available in the lab	Human monocyte-like	RPMI-1640 10% Foetal Bovine Serum 1X Penicillin-Streptomycin	Below 1 x 10^6 cells/ml at 37ºC, 5% CO_2
FreeStyle 293-F (Vink *et al*., 2014)	Thermo Fisher Scientific	Human embryonic kidney cell	FreeStyle™ 293 Expression Medium 1X Penicillin-Streptomycin	Below 2.5 x 10^6 cells/ml at 37ºC, 8% CO_2
B3Z (Karttunen *et al*., 1992)	Gift from Prof. Colin Watts	Murine cytotoxic T cell	RPMI-1640 1X Kanamycin 1X Sodium Pyruvate 1X Non-Essential Amino Acids 1X L-Glutamine 50 μM β-Mercaptoethanol (Sigma)	Below 5 x 10^5 cells/ml at 37ºC, 5% CO_2

Note: 1X Penicillin-Streptomycin = 10 Units/ml Penicillin and 10 μg/ml Streptomycin
1X Kanamycin = 100 μg/ml Kanamycin
1X Sodium Pyruvate = 1mM Sodium Pyruvate
1X Non-Essential Amino Acids = A mixture of 7 amino acids, 0.1mM of each amino acid
1X L-Glutamine = 2mM L-Glutamine

2.5.2 Plasticware

25 cm^2 (T25), 75 cm^2 (T75) and 175 cm^2 (T175) tissue culture flasks were purchased from Greiner-Bio-One. 125ml Erlenmeyer Flasks were purchased from Corning.

2.6 TISSUE CULTURE METHODS

2.6.1 Thawing of frozen cells

A 30ml universal tube containing 5ml of suitable medium, preincubated at 37ºC, was prepared for each cell line. A vial containing the desired cells was removed from liquid nitrogen storage and thawed with gentle shaking in a 37ºC water bath. After spraying the exterior of the vial with 70% (v/v) ethanol, the contents were decanted into the universal tube and centrifuged at 500g for 5 minutes. Supernatant was discarded and cells were resuspended in 1 ml of suitable medium before seeding either a T25 or T75 tissue culture flask filled with suitable medium.

2.6.2 Cell maintenance or expansion

When cells were approaching the cell maintenance threshold, Table 2.8, they were split into similar sized tissue culture flasks for maintenance or larger flasks for cell expansion if a high number of cells were required for experiments.

2.6.3 Harvesting cells

Once the number of cells per ml had been determined using a haemocytometer, the desired volume of cell suspension was pipetted into a 30ml universal tube and centrifuged for 5 minutes at 500g. Supernatant was discarded and the cell pellet was washed 3 times with PBS or medium by resuspending and centrifuging for 5 minutes

at 500g each time. Finally, the supernatant was discarded and the cells were resuspended in PBS or medium at the desired final cell density.

2.6.4 Freezing cells for storage

Normally between 1 x10^6 and 1 x10^7 cells per vial were frozen. Cells were harvested and centrifuged at 500g for 5 minutes. The supernatant was discarded and the cells were resuspended at between 1 x10^6 and 1 x10^7 cells/ml in suitable freezing medium, Table 2.9. 1ml aliquots were added into CryoTube vials (Nunc) and labelled. The cryotubes were then placed in a biological freezer (Taylor Wharton) and allowed to freeze slowly in the liquid nitrogen vapour phase for ~5 hours or overnight. Alternatively, a CoolCell® Cell Freezing Container (Biocision) was used to freeze the cells at a controlled rate of -1°C/minute in a -80°C freezer overnight. All cryotubes were transferred into liquid nitrogen freezers for long-term storage.

Table 2.9: Details of the medium used for freezing different cell lines

Cell line	Freezing medium
THP-1	90% FBS, 10% DMSO
FreeStyle 293-F	90% FreeStyle™ 293 Expression Medium, 10% DMSO
B3Z	90% RPMI, 10% DMSO

2.7 PROTEIN ANALYSIS MATERIALS

2.7.1 Buffers and solutions

SDS Running buffer

A 10X stock solution of SDS running buffer (0.25M Tris, 1.92M glycine, 1% SDS, pH 8.3) was prepared. This stock solution was diluted to 1X with Milli-Q water prior to use.

Non-reducing sample buffer (2X)

Milli-Q water	2.8 ml
Glycerol	2.0 ml
1.0M Tris, pH 6.8	1.2 ml
10% SDS	4.0 ml
Bromophenol Blue (Bio-Rad)	0.01%

Reducing sample buffer (2X)

Milli-Q water	1.8 ml
Glycerol	2.0 ml
1.0M Tris, pH 6.8	1.2 ml
10% SDS	4.0 ml
14.3M β-Mercaptoethanol	1.0 ml
Bromophenol Blue (Bio-Rad)	0.01%

Transfer buffer

25mM Tris, 192mM glycine, 20% methanol, pH 8.3

2.7.2 Protein molecular weight markers

Precision Plus Protein™ All Blue Prestained Protein Standards (161-0373) were purchased from Bio-Rad.

2.8 PROTEIN ANALYSIS METHODS

2.8.1 Preparation of dialysis tubing

Dialysis tube (19mm with a molecular weight cut-off at 12-14 kDa), was purchased from Scientific Laboratory Supplies Ltd (TUB2008). An appropriate length of tubing was cut and incubated in PBS for at least 1 hour prior to use.

2.8.2 Preparation of Protein G Sepharose

Protein G Sepharose™ 4 Fast Flow, 17061801, was purchased from GE Healthcare. The protein G Sepharose was mixed gently and 500µl was pipetted into a 30ml universal tube. To wash the resin, 5ml binding buffer (a mix of 577ml 20mM Na_2HPO_4 and 424ml 20mM NaH_2PO_4, pH 7.0 per litre) was added and mixed gently, followed by centrifugation at 500g for 5 mins. The liquid was discarded and the washing process was repeated 3 times. After the final wash, the protein G Sepharose was ready to be used.

2.8.3 Antibody purification on Protein G Sepharose

25ml transfected FreeStyle 293-F cell suspension was collected into a 30ml universal tube. Cells were centrifuged at 500g for 5 minutes. The supernatant was transferred to a universal tube containing washed protein G Sepharose (section 2.8.2) and incubated overnight on a roller (Spiramix 5 (Dentley)) at 4ºC. The next day, a 5 ml disposable polypropylene column (Pierce 29922, Thermo Fisher Scientific), was prepared according to manufacturer's guide. The column was flushed with PBS prior to use. The protein G Sepharose mixture was poured into the column and allowed to flow by gravity to separate the resin from the liquid. The liquid solution was collected and stored at 4ºC. The protein G Sepharose was washed several times with binding buffer before adding 10ml elution buffer (0.1M glycine, pH 3.0). The eluted antibody was collected into a 30ml universal tube and immediately neutralised with neutralising buffer (1M Tris-HCl, pH 8.0) to give a final pH of 7.0-7.5.

2.8.4 Protein dialysis

Protein preparations such as purified antibody (section 2.8.3) were pipetted into

dialysis tubing (section 2.8.1). After sealing with a clip, the tubing was placed into a beaker filled with PBS for dialysis overnight at room temperature or 4ºC with at least one change of buffer.

2.8.5 Protein concentration

Protein concentration was performed using Amicon Ultra-15 Centrifugal Filter Units, of 50kDa molecular weight cut off, purchased from Millipore. Upon completion of dialysis, protein preparations were centrifuged in filter units at 700g for ~10 minutes until a final volume of 300-400µl was retained. The concentrated protein was transferred to a 1.5ml microfuge tube and its protein concentration determined.

2.8.6 Antibody and Fc-fusion protein concentration determination

To minimise loss of protein, a 10X dilution was used for determination of absorbance at 280nm, measured using a UV spectrophotometer (Ultrospec 2000, Pharmacia Biotech). The concentration of the protein sample was calculated using the formula below.

$$A = \varepsilon c l$$

A = Absorbance at 280nm
ε = extinction coefficient (1.5 for IgG)
c = protein concentration (mg/ml)
l = path length in cm (1 cm in the cuvette used)

With regards to the above formula, a formula to calculate protein concentration could be derived where, c in mg/ml = (A/ ε l) x (dilution factor)

2.8.7 SDS-Polyacrylamide gel electrophoresis (SDS-PAGE)

Proteins could be analysed by separating on the basis of molecular weight using SDS- PAGE. For antibody and Fc-fusion protein analysis, a 10% separating gel was

used. The recipe listed below was used to make one gel.

Stacking gel

Milli-Q water	2.1 ml
Acrylamide/ Bis-acrylamide, 37:1 ratio (A6050, Sigma)	0.5 ml
1.0M Tris, pH 6.8	0.38 ml
10% (w/v) SDS	30 µl
10% (w/v) ammonium persulphate (freshly made)	30 µl
TEMED	3 µl

Separating gel (10%)

Milli-Q water	4.0 ml
Acrylamide/ Bis-acrylamide, 37:1 ratio (A6050, Sigma)	3.3 ml
1.5M Tris, pH 8.8	2.5 ml
10% SDS	100 µl
10% ammonium persulphate (freshly made)	100 µl
TEMED	3 µl

A gel-running apparatus (Bio-Rad Mini Protean II) was set up according to manufacturer's instructions. 8ml of separating gel solution was poured into gel plates and overlaid with isopropanol before allowing it to set for 15-20 mins. Once the gel had solidified, the isopropanol was discarded and the exposed section of the gel was washed with Milli-Q water. Stacking gel solution was poured on top on the separating gel and the comb was inserted before allowing the gel to set for 10-15 minutes. The gel plates, which contained the gel, were then placed into the apparatus and the tank was filled with fresh SDS running buffer (section 2.7.1). The comb was removed and the gel was ready for protein sample loading. Samples were prepared in 1.5ml microfuge tubes. About 1-2 µg of protein was required to be loaded into each well. Once the appropriate dilutions were made, an equal volume of non-reducing sample buffer or reducing sample buffer (section 2.7.1) was added to each prepared protein sample to give a final concentration of 1X sample buffer. The protein

samples were then incubated in a heat block at 90ºC for 10 minutes to fully denature the proteins. Once completed, the protein samples were centrifuged for 5 seconds and allowed to cool to room temperature before loading into their respective wells. 7µl of protein molecular weight marker (section 2.7.2) was loaded for size referencing. After protein loading, protein samples were electrophoresed using a Power Pack 3000 (Bio-Rad) at 100V for 10-13 minutes to be properly stacked before entering the separating gel. The voltage was then increased to 180V and the protein samples were run until the bromophenol blue almost reached the end of the gel. The gel plates were removed from the tank and dismantled to expose the gel. The gel was then ready to proceed to western blotting or Coomassie staining.

2.8.8 Western blotting

After SDS-PAGE electrophoresis, the proteins embedded in the gel were transferred to nitrocellulose membrane for further analysis using a Bio-Rad transfer device. Nitrocellulose Blotting Membrane (Protran, 0.45 µm pore size, GE Healthcare) and filter paper (Whatman 3MM) cut to the size of the gel, were presoaked along with transfer sponges in transfer buffer (section 2.7.1) for at least 5 mins prior to use. The nitrocellulose membrane was placed on top of the protein gel and sandwiched between filter papers and transfer sponges before placing into the transfer tank. Once the apparatus was set up, the transfer tank was filled with transfer buffer and an ice block was placed in the tank to prevent overheating. The proteins were transferred at 100V for 60 minutes. After disassembling, the nitrocellulose membrane was blocked with 5% (w/v) non-fat milk in PBS-T (section 2.1.2) for 1 hour at room temperature with shaking. The nitrocellulose membrane was then washed three times with PBS-T for 5 minutes each wash. The nitrocellulose membrane was then incubated with the

desired primary antibody for 1 hour or overnight followed by three 5 mins washes with PBS-T. If the primary antibody was unconjugated, the membrane was incubated with a suitable secondary antibody for 1 hour followed by three further washes as before, and developed using an appropriate substrate. If the primary antibody was conjugated, the membrane was ready to be developed using an appropriate substrate. Since detecting antibodies were HRP conjugated, TMB Membrane Peroxidase Substrate (Kirkegaard & Perry Laboratories Inc.) or Pierce® ECL Western Blotting Substrate (Thermo Fisher Scientific) was used to develop the reaction. Developed protein bands were imaged using FluorChem™ System (Alpha Innotech), Canon iR-ADV C5030i or Li-Cor Odyssey Fc (Li-Cor Bioscience UK Ltd).

2.8.9 Coomassie staining and destaining of SDS gels

After SDS-PAGE, the gel was placed into a suitable container/tray and rinsed once with Coomassie destaining solution (25% (v/v) methanol, 7% (v/v) acetic acid). The gel was then incubated with Coomassie staining solution (0.25% (w/v) Coomassie Brilliant Blue R-250 (Sigma, B-0149), 50% (v/v) methanol, 10% (v/v) acetic acid) overnight at room temperature with shaking. The gel was subsequently incubated in Coomassie destaining solution at room temperature on a shaker. Destaining solution was changed as frequently as required until the gel was completely destained. The gel was then imaged using FluorChem™ System (Alpha Innotech) or Canon iR-ADV C5030i.

2.8.10 ELISA

All ELISA analyses were carried out using 96 well MaxiSorp ELISA plates (Nunc). Appropriate concentrations of proteins (e.g. ~10μg/ml of NIP-BSA) were prepared in

freshly made ELISA coating buffer (15mM Na_2CO_3, 35mM $NaHCO_3$, pH 9.6). 100µl of final ELISA coating solution was pipetted into wells and incubated overnight at 4ºC. For control wells, ELISA coating buffer was used alone. When the coating was completed, the plate was washed 5 times with tap water. Each well was then blocked with 200µl of 5% (v/v) non-fat milk in PBST (section 2.1.2) for 1 hour. After repeating the washing process 100µl of selected primary detecting antibody, prepared in PBST at a concentration shown in Table 2.1, was added to desired wells. The plate was incubated on a shaker at room temperature for 1 hour before being washed 5 times as before. If required, 100µl of selected secondary detecting antibody, prepared in PBST at a concentration shown in Table 2.1, was added to desired wells, and the palate incubated as previously. After washing as before, 200µl SureBlue™ TMB Microwell Peroxidase Substrate (Kirkegaard & Perry Laboratories Inc.) was added to each well and colour allowed to develop for at least 20 minutes. Absorbance was measured at 630nm on a ELx808 Absorbance Microplate Reader (BioTek).

CHAPTER THREE
GENERATION OF ANTI-NIP WILDTYPE HUMAN IgG1 AND DIFFERENT HINGE MUTANT ANTIBODIES

CHAPTER 3. GENERATION OF ANTI-NIP WILDTYPE HUMAN IgG1 AND DIFFERENT HINGE MUTANT ANTIBODIES

3.1 INTRODUCTION

The length of the hinge region and in particular the distance between the end of the CH1 domain and the first inter-heavy chain disulphide bridge varies between antibody classes and subclasses (Burton, 1987). As an example, the number of amino acids in this particular region of hIgA1 is 20 whilst in hIgG1 it is only 5. The length and flexibility of this region is expected to play a role in allowing the Fab arms to attain better positioning to achieve efficient antigen binding, as described earlier in Figure 1.9B. In brief, a better flexibility at the region between the end of the CH1 domain and the first inter-heavy chain disulphide bridge would improve the overall free movements of the Fab arms to achieve better positioning for antigen binding whilst a longer length of this region would distance the Fab arms further away from the Fc region to allow better antigenic reach. Exactly how modification of this particular region might improve antibody functionality has not been very well studied. However, extending the length of this region is expected to improve, at least, the antigenic reach of an antibody, as mentioned earlier. In human IgG, this particular region is also known as the upper hinge region, as indicated earlier in Figure 1.8A. This chapter aimed to generate a range of IgG mutant antibodies with different upper hinge lengths which could be tested in various analyses to improve understanding of the role of the upper hinge region on antibody functionality.

3.1.1 Bivalent antigenic distance of an antibody

Bivalent antigenic distance is defined in this thesis as the maximum distance between two antigens bound by both the Fab arms of an antibody as shown in Figure 3.1. This

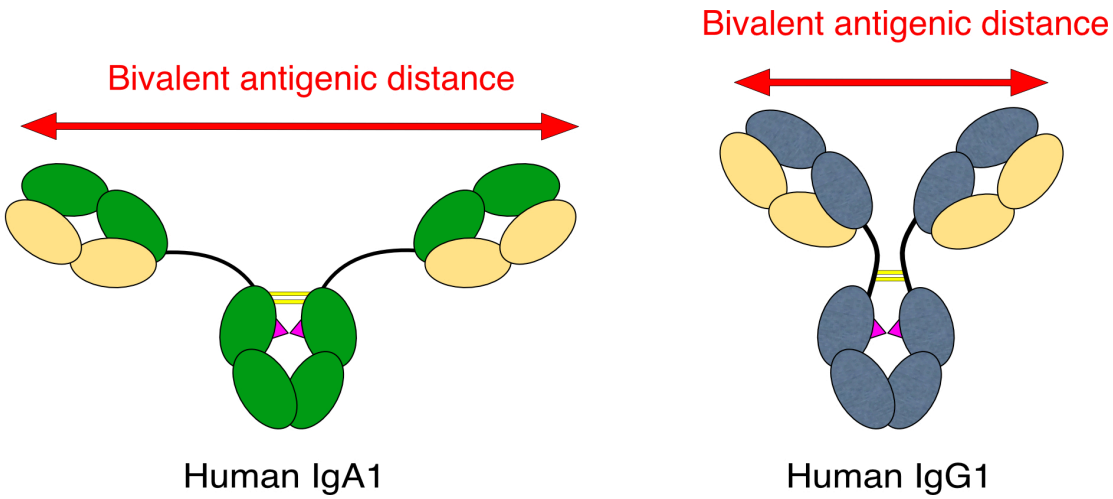

Figure 3.1: A schematic diagram illustrating the bivalent antigenic distance of antibodies. The bivalent antigenic distance of an antibody is the maximum distance between two antigens bound by both the Fab arms and is expected to be dependent on the length and flexibility of the hinge region. The hinge region of human IgA1 consists of 20 amino acid residues whilst the upper hinge region of human IgG1 consists of only 5 amino acid residues. Thus, it is expected that IgA1 will have a greater bivalent antigenic distance than IgG1.

distance is expected to depend heavily on the flexibility and length of the hinge region, in particular, the distance between the end of the CH1 domain and the first inter-heavy chain disulphide bridge which governs the movement of Fab arms. hIgG1 and hIgA1 are two good examples to describe the difference in bivalent antigenic distance likely to arise as a result of the difference in the number of amino acid residues in their hinge regions, as illustrated in Figure 1.8. In brief, the hinge region of hIgA1 consists of 20 amino acid residues whereas the upper hinge region of hIgG1 consists of 5 amino acid residues. Thus, it is expected that hIgA1 will have a greater bivalent antigenic distance than hIgG1. Indeed, observations from the derived hIgA1 structure model suggested that the bivalent antigenic distance of hIgA1 was 17nm (Boehm *et al*., 1999) whereas the bivalent antigenic distance of the crystallised hIgG1 Kol was estimated to be 146Å (14.6nm) (Huber *et al*., 1976).

Previous studies have reported the Fab tip to tip distance of several different antibodies. This distance is likely to be closely related to bivalent antigenic distance

but it can be determined in the absence of antigen whereas bivalent antigenic distance cannot. These Fab tip to tip calculations were mainly based on electron microscopy, neutron/X-ray scattering and/or crystallography of the relevant antibodies (Valentine and Green, 1967; Marquart *et al*., 1980; Sosnick *et al*., 1992). Valentine and Green incubated bivalent DNP ligands with anti-DNP rabbit IgGs and allowed the formation of immune complexes (Valentine and Green, 1967). Using electron microscopy, the authors noticed that the majority of the immune complexes formed a ring structure consisting of 2-3 antibody molecules (4-6 Fab arms). The mean Fab tip to tip distance was reported to be 120Å and did not exceeded 150Å (Valentine and Green, 1967). In a different scenario, Sosnick and colleagues used neutron and X-ray scattering analysis and deuterated antigen to measure the antigen binding distance in solution between the two Fab arms of murine IgG1, IgG2a and IgG2b and reported that the mean distance was around 117Å - 134Å for all three subclasses (Sosnick *et al*., 1992). Finally, Marquart and colleagues calculated the Fab tip to tip distance of Kol (a human IgG1) from its crystal structure and reported a distance of 145Å (Marquart *et al*., 1980). In contrast, the average Fab tip to tip distance of human IgA1 was reported to be 17nm (170Å) according to molecular models build on the basis of small angle X-ray and neutron scattering measurements (Boehm *et al*., 1999). In a different study, Roux and colleagues generated an antigenic idiotype (Id) matched set of genetically engineered human IgG1, -2, -3 and -4 subclass antibodies to investigate the differences in immune complex formation due to hinge-mediated differences in flexibility by incubating the generated IgGs with two different anti Id-specific murine monoclonal antibodies (Roux *et al*., 1997a). The authors reported that each IgG subclass exhibited different ranges of Fab-Fab angle in which IgG1 was 30º-210º; IgG2 was 60º-190º; IgG3 was 20º-270º and IgG4

was 30º-210º and that the hinge mediated flexibility of different human IgG subclasses was ranked as lgG3 > lgGl > lgG4 > lgG2 (Roux *et al*., 1997a). Although the Fab tip to tip distances of different generated human IgGs were not calculated in the studies of Roux et al. (1997), the authors demonstrated the different ranges of Fab-Fab angle distance that each IgG could adopt which in turn contributes to the diversity of the Fab tip to tip distance of each different IgG subclass.

The differences in the reported Fab tip to tip distances of different antibodies described earlier is hypothesised to be due to the different lengths of their hinge regions. However, this hypothesis is yet to be proven. In addition, the distance between Fab arms of different antibodies when bound to antigen have not been identified. As a result, this chapter aimed to generate novel IgG hinge mutant antibodies to investigate if the length of the upper hinge region affected the bivalent antigenic distance. Using antibody recombinant technology, the length of the upper hinge of wild type human IgG1 (wt hIgG1) was extended by the addition of amino acids to generate hIgG1 hinge mutants with different upper hinge lengths, as shown in Figure 3.2, so that an antigen binding comparison can be made with wt hIgG1 to identify if the length of upper hinge of hIgG1 would affect the overall bivalent antigenic distance of hIgG1. Rather than randomly adding different amino acids to extend the upper hinge length of IgG, it was decided to utilise the hinge region of hIgA1 as a choice of peptide chain extension. One of the main reasons for using hIgA1 is because the hinge region of hIgA1 is very long at 20 amino acids, compared to other human antibodies. More importantly, it is a naturally evolved hinge region, and therefore the generated hinge mutants containing such a hinge insertion should be very stable during and after protein production. Secondly, based on the structure

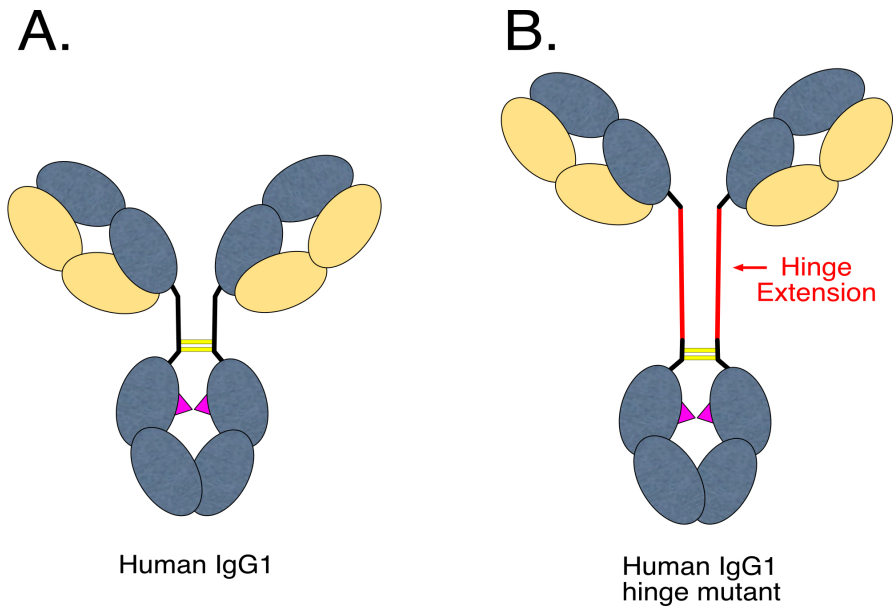

Figure 3.2: A schematic diagram illustrating the differences in lengths of the upper hinge region of different human IgG antibodies. **A**) Wildtype human IgG1 with normal upper hinge length. **B**) Human IgG1 hinge mutant with extended upper hinge length (shown in red).

of hIgA1 that was modelled based on small angle X-ray and neutron scattering, the hinge region of IgA1 had been proposed to adopt an open and extended conformation (Boehm *et al*., 1999), as illustrated in Figure 3.1A. Bonner and colleagues later modelled the structure for dimeric hIgA1 based on solution scattering studies and proposed a similar conformation in which the Fab arms of the antibody were quite extended away from the Fc region, most likely due to the long hinge (Bonner *et al*., 2008). As a result, using the hinge region of hIgA1 for hinge extension of IgG1 was reasoned as likely to provide an open and extended conformation with a greater bivalent antigenic distance. Further details of the hinge region of hIgA1 will be described in another section below. In summary, by extending the length of the upper hinge of hIgG1 while retaining identical constant domains identical would allow a comparison of the hIgG1 hinge mutants with wt hIgG1 to be made. Hence, any significantly different outcomes exhibited by the hinge mutants are most likely to be due to the upper hinge extension.

3.1.2 The disulphide bond between heavy (H) and light (L) chains

In this project, a previously constructed hinge mutant hIgG1, TAHG (described below), was used as a starting point for generation of novel hinge mutants. The TAHG mutant carries part of the hinge sequence of human IgA1 but has lost the 8 amino acid sequence EPKSCDKT which comprises the N-terminal portion of the original IgG1 hinge region. This sequence is critical since the cysteine residue which it contains is responsible for disulphide bond linkage to the light chain (Liu and May, 2012; Edelman *et al*., 1969). As mentioned in Chapter 1, an antibody is composed of two light chains and two heavy chains bound together by disulphide bonds. Appropriate association of heavy and light chains, stabilized by a disulphide bridge, is important so that both the variable domain of the light chain and that of the heavy chain come into close contact to form the complete antigen binding site located at the tip of the Fab arms. Some antibodies, especially IgA, were secreted onto the mucosal lining where extreme pH may be encountered, e.g. in the gastrointestinal tract (Mantis *et al*., 2011). The disulphide bonding between light and heavy chain may prove crucial in holding both chains together as the extreme pH within the environment may tend to affect the protein structure leading to the disruption of light and heavy association.

The heavy chains of the different antibody classes form disulphide bonds with light chains at different locations. For human IgG1, the disulphide bond with light chain was formed between the fifth cysteine residue of the IgG1 heavy chain (Cys220) and the C-terminal cysteine of the light chain (Cys214) (Liu and May, 2012). However, for human IgG2, IgG3 and IgG4 the H-L disulphide bond is formed between the third cysteine residue (Cys131) of the heavy chain and Cys214 of light chain (Liu

and May, 2012). In the case of human IgA1, the disulphide bond to light chain involves the third cysteine residue, Cys133, of the α heavy chain constant region (Chintalacharuvu and Morrison, 1996). Human IgA2 is slightly different as it lacks a Cys at position 133, (it is replaced by an aspartic acid), but at least for the IgA2m(2) allotype, it is still capable of forming an H-L disulphide bond (Chintalacharuvu *et al*., 2002). The IgA2m(1) allotype is exceptional. An early study reported that there were no disulphide bonds found between light and heavy chains in this allotype (Tsuzukida *et al*., 1979). However, further studies have reported H-L disulphide bonds in some IgA2m(1) molecules. Seemingly, the efficiency of formation of that linkage is greatly reduced (Chintalacharuvu and Morrison, 1996; Chintalacharuvu *et al*., 2002). In contrast, there had been no reports of intact human IgGs that lack H-L disulphide bonding. Since an aim of this project was to investigate the impact of antibody structure in relation to its function, the restoration of the 8 IgG hinge amino acids into the TAHG construct was necessary in order to more closely resemble the natural hIgG1 antibodies in terms of H-L assembly.

3.1.3 The benefits of introns and their removal by mRNA splicing

All the antibody heavy chain constant region DNA sequences used in this project aim were not cDNAs but gene sequences that contained both introns and exons. Often, expression of protein from cDNA is preferred as it significantly reduces the size of the encoding DNA which makes transfection easier. Moreover, the cDNA option is often considered less complicated as it removes any concern about correct mRNA splicing to remove introns. However, the usage of introns in antibody expression systems had several advantages. One of the advantages is the associated enhancement in antibody expression. Gaurav and colleagues constructed several

antibody expression plasmids to test different types of promoter as well as the addition or removal of an intron and found that with the addition of a single intron, the antibody expression level increased by almost two fold (Backliwal *et al*., 2008). Increased expression levels of proteins due to the addition of introns have been reported by other groups also (Buchman and Berg, 1988; Nott *et al*., 2003). Thus, it has been found beneficial to include introns in order to obtain improved antibody expression. Another benefit of the inclusion of introns relates to the possibility to introduce useful restriction sites within introns without affecting the actual protein transcription and translation. For antibodies, this creates an easy approach for domain swapping, addition or deletion, which has proved highly beneficial for understanding antibody structure and its functionality. However, the mRNA splicing signals encoded in an intron must not be disrupted in order to ensure all introns are spliced out and all exons are joined correctly. An intron usually starts with the sequence GT at the 5′ end and ends with AG at the 3′ end (Clancy, 2008). These consensus sequences, also known as splice sites, are crucial and any changes in their sequence would result in splicing failure (Clancy, 2008). Another important requirement apart from the splice sites is the branch site which is located upstream of the 3′ end splice site (Clancy, 2008). The branch site always contains an adenine and usually adopts the sequence YNYYRAY, where Y is a pyrimidine (C or T), N is any nucleotide, R is a purine (A or G) and A is adenine (Clancy, 2008). In this chapter, all the antibody constructs used were found to contain an intron deletion, which is most likely a PCR artifact, that included a small part of the starting sequences of the CH1 domain. The missing 3′ intron splice site located before the start of CH1 domain coding sequence might cause the CH1 domain exon to be mistakenly signaled as an intron and completely spliced out, resulting in the loss of the CH1

domain in the mature protein. Therefore, restoration of the lost intron and the CH1 domain splice site was necessary.

3.1.4 The hinge region of human IgA1 and its O-linked glycans

As mentioned in section 3.1.1 above, this project developed novel hIgG1 hinge mutants with hIgA1 hinge insertions. The structure for hIgA1 has been proposed to adopt an open and extended conformation (Boehm *et al*., 1999; Bonner *et al*., 2008), in which the extra long hinge of hIgA1 may have contributed to this structural conformation. Another factor that might contribute to the conformation of the hIgA1 hinge is the presence of O-linked glycans (Mattu *et al*., 1998; Baenziger and Kornfeld, 1974; Novak *et al*., 2000). As mentioned in Chapter 1, the hinge region of hIgA1 displays a repeated sequence of proline, serine and threonine and the O-linked glycosylation on hIgA1 was reported to occur on both serine and threonine residues within the hinge region (Baenziger and Kornfeld, 1974). There are a total of nine potential sites for O-linked glycosylation at the hinge region of hIgA1 but not all sites appear to be glycosylated, as indicated in Figure 3.3. Usually three to five sites are glycosylated (Baenziger and Kornfeld, 1974; Mattu *et al*., 1998), but up to six have been described (Tarelli *et al*., 2004). The presence of glycans at the hinge region might create steric hindrance which prevents the Fab arms of hIgA1 from coming close in contact, thus, an open conformation might be more optimal for hIgA1. The roles of O-linked glycans at the hinge region of hIgA1 are not exactly clear yet but some believe that they provide a certain degree of structural rigidity which stabilises the long hinge (Arnold *et al*., 2007). Similarly, hIgD which has a longer hinge than hIgA1 is also O-glycosylated at the hinge region (Takahashi *et al*., 1982). In contrast, hIgG3 also has a very long hinge but it does not contain any

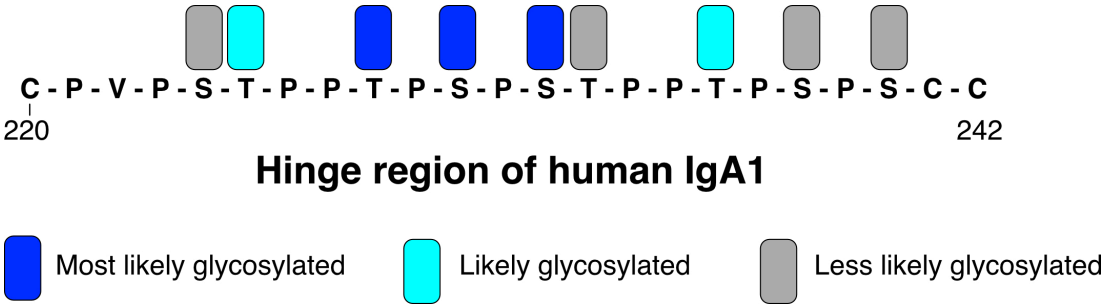

Figure 3.3: A schematic diagram illustrating the nine potential O-linked glycosylation sites located at the hinge region of human IgA1. O-linked glycosylation occurs only at serine or threonine residues. There are nine potential sites but not all are glycosylated. Blue, most likely glycosylated sites; Aqua blue, likely glycosylated sites; Grey, less likely glycosylated sites.

O-linked glycans. Instead, the structural rigidity is provided by eleven inter-chain disulphide bonds between the two hIgG3 heavy chains (Liu and May, 2012). Thus, it seems that hIgA1 and hIgD have evolved to be glycosylated in their hinge regions as an alternative way to ensure structural integrity whilst attaining a higher degree of reach, and possibly flexibility, in antigen binding. In addition to extra hinge length, the hIgA1 hinge region displays heterogeneity in its O-linked glycosylation (Novak *et al*., 2000). Royle and colleagues analysed the glycan structures from pooled normal human secretory hIgA1 and found that O-linked glycans present at the hinge region of secretory hIgA1 had a wide range of interaction sites that could interact with bacterial adhesins (Royle *et al*., 2003). Looking at the proposed model of hIgA1, the open conformation that hIgA1 is proposed to adopt actually provides an easy access for bacterial adhesins to the hinge O-linked glycans. Therefore, the O-linked glycans might have a role in immune system defensive approaches. As a result, the present project also aimed to investigate whether the removal of hinge O-linked glycans would have any effect on antibody structure and function. To achieve that aim, the O-glycosylation of a hinge mutant was prevented by mutating all the serine and threonine residues at the hinge region to alanine and/or glycine residues.

3.1.5 Jacalin, an O-linked glycan binding lectin

Lectins are a class of proteins that bind specifically to different sugars. Among different plant lectins, jacalin originates from the seeds of jackfruit (*Artocarpus heterophyllus*) and has a high specificity for the disaccharide galactose (β1, 3) N-acetylgalactosamine, which is the most common core of O-linked glycans (Kabir, 1998). Due to such high specificity, jacalin had been used to isolate hIgA1 and hIgD from other immunoglobulins because these two immunoglobulins have O-linked oligosaccharides at their hinge regions (Kabir, 1998). In this project, jacalin was utilised to determine the presence of O-linked glycans on the different recombinant antibodies generated.

3.1.6 Anti-NIP variable domain

The use of matched sets of antibodies featuring identical antigen binding sites ensures that antigen binding affinity and epitope recognition is identical across all antibodies produced, allowing direct comparison of the impact of different antibody heavy chain features on function. In 1978, Reth and colleagues reported a murine hybridoma capable of producing antibodies which recognised the hapten 4-hydroxy-3-iodo-5-nitrophenyl acetic acid (NIP) (Reth *et al*., 1978). The chemical structure of NIP is shown in Figure 3.4. In the past, the NIP antigen system has been utilised by many groups to investigate antibody function by generating a variety of anti-NIP chimeric antibodies and comparing them in different functional analyses (Bindon *et al*., 1988; Garred *et al*., 1989; Lucisano Valim and Lachmann, 1991). In particular, Bindon and colleagues generated anti-NIP human IgG1, IgG2, IgG3, IgG4 and IgE and by derivatizing NIP onto the surface of human red blood cells they were able to study each antibody's ability to activate the complement cascade (Bindon *et al*., 1988). In a different scenario, Garred and colleagues conjugated NIP to BSA at

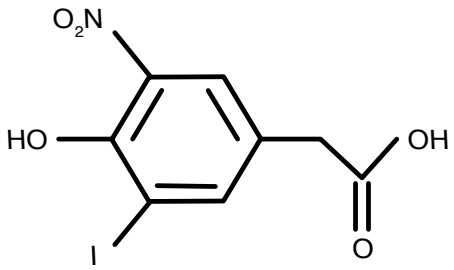

4-hydroxy-3-iodo-5-nitrophenyl acetic acid

Figure 3.4: Chemical structure of 4-hydroxy-3-iodo-5-nitrophenyl acetic acid (NIP) hapten.

different antigen densities in order to study the relationship between antigen availability and complement activation. Using different anti-NIP human antibodies they found that at a lower antigen density IgG3 was the best candidate in complement activation followed by IgG1 and IgG2 (Garred *et al*., 1989). In this project, the NIP recognition system was selected to study the impact of hinge length on the functionality of different human IgG1 antibodies as the NIP system is very well established in the Woof lab.

3.2 AIMS

This project hypothesised that an increase in the length of the upper hinge region will lead to an increase in the bivalent antigenic distance of an antibody. To test this hypothesis, this chapter aimed to generate a matched set of anti-NIP hIgG1 mutants with different upper hinge lengths by incorporating portions of the hinge region of hIgA1 into their upper hinge regions. This project also aimed to study the impact of O-linked glycans of an antibody in antigen binding, thus, the generation of an O-linked negative mutant will be attempted.

3.3 MATERIALS AND METHODS

3.3.1 MATERIALS

NIP-BSA

Bovine serum albumin derivatised with hapten NIP (NIP-BSA) was available in the Woof lab, having been made by past members of the lab.

3.3.2 PLASMIDS

pE1001

The pE1001 plasmid encoding the majority of the constant region of the heavy chain of wildtype human IgG1 (wt hIgG1) was available in the Woof lab. DNA sequencing showed that pE1001 lacked approximately 400 base pairs (bp) comprising part of the exon encoding the CH1 domain and the upstream intron.

pTAHG

The pTAHG plasmid, encoding the heavy chain of an anti-NIP hinge-modified human IgG1, was available in the Woof lab. The reason for using pTAHG is because pTAHG carried DNA sequence encoding the hinge region of human IgA1 inserted at the upper hinge region of wt hIgG1, resulting in an extension of 18 amino acids in the encoded heavy chain protein, which would generate a suitable hinge mutant candidate for this project. However, DNA sequencing showed that pTAHG lacked sequence encoding 8 amino acids, EPKSCDKT, which comprises the N-terminal portion of the original IgG1 hinge region. pTAHG also contained the CH1 domain

upstream exon deletion as described in pE1001.

pBSK-419bp

A plasmid, pBSK-419bp, containing a sequence of 419bp that encoded the correct intron sequence upstream of the CH1 domain of wt hIgG1 was purchased from Dundee Cell Products Ltd. The sequence contained two unique restriction sites that could be digested by HindIII and BstEII.

preλLC

An expression vector encoding a murine anti-NIP lambda light chain was available in the Woof lab.

3.3.3 CONSTRUCTION OF ANTI-NIP ANTIBODY PLASMIDS

3.3.3.1 Reintroducing missing sequence EPKSCDKT into the pTAHG expression vector

The procedure for reintroducing the sequence encoding the eight missing amino acids is illustrated in Figure 3.5. The PCR procedure was carried as described in section 2.4.3 using the appropriate primers and annealing temperatures to obtain the final desired DNA products. Primers DS3 and GUHIAS (Table 2.2, No.1 & 2) were used to amplify a fragment of approximately 140bp which contained a unique BstEII site, using pTAHG as template at an annealing temperature of 63ºC. Using pTAHG as template, primers GUHIS and AG3'NEW (Table 2.2, No.3 & 4) were used at an annealing temperature of 65ºC to amplify a DNA product of approximately 1100bp which contained a unique EcoRI site. PCR products were run on a DNA agarose gel

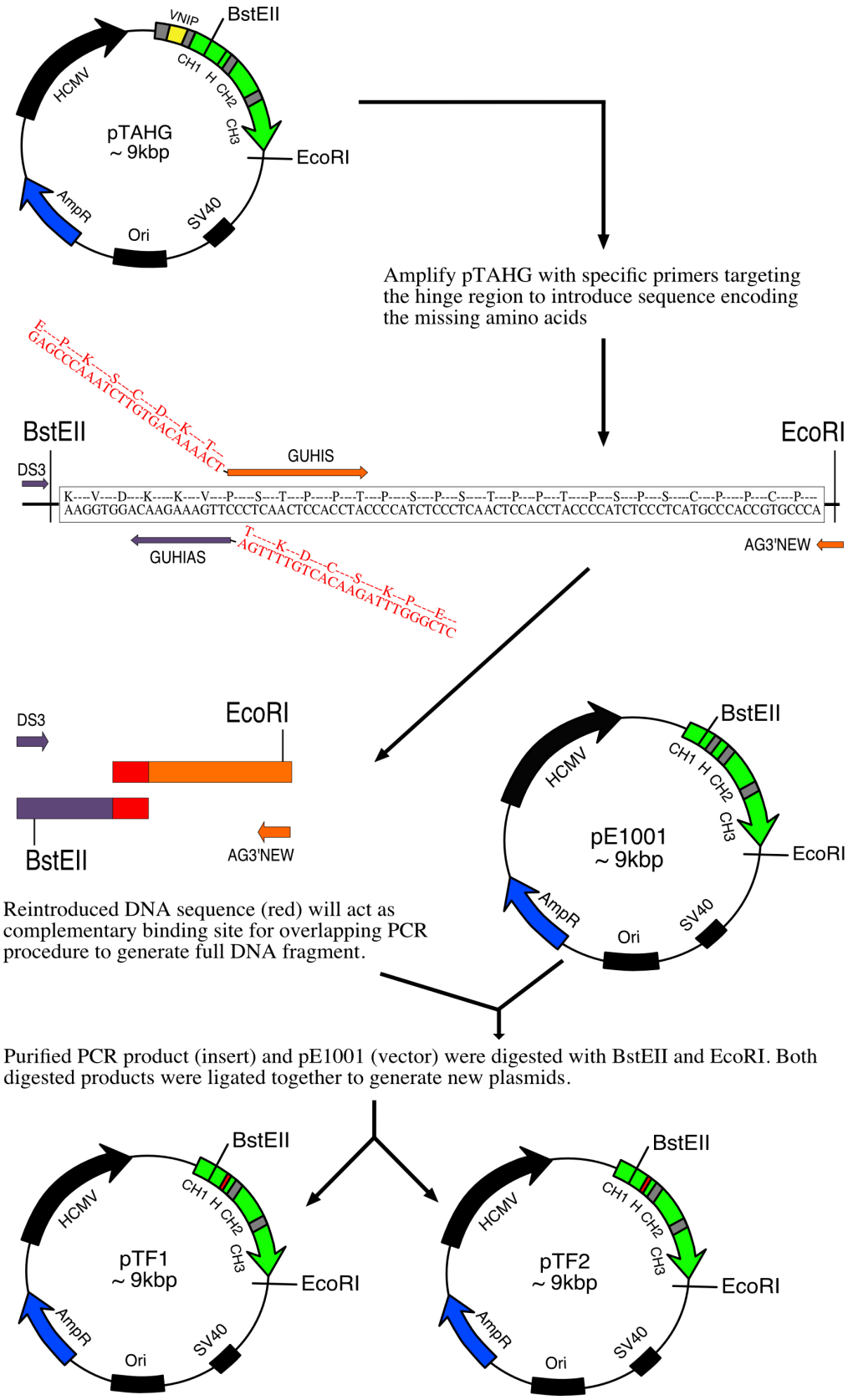

Figure 3.5: A schematic diagram illustrating the procedure to reintroduce sequence encoding the missing amino acids. The hinge region of the hinge mutant encoded in pTAHG was PCR amplified to reintroduce missing sequence. The missing sequence served as a complementary sequence during overlapping PCR. The new insert was inserted into digested pE1001 using the restriction enzymes BstEII and EcoRI. pTF1 is a plasmid with just half the hinge region from hIgA1 inserted due to primer mismatches during PCR amplification. In contrast, pTF2 is a plasmid with full hIgA1 hinge region insertion.

as described in section 2.4.4 and DNA bands of the correct sizes were extracted as described in section 2.4.5. Using a PCR procedure described in section 2.4.3, an overlap PCR extension was performed by using a mix of 2µl of each extracted DNA fragment as template and DS3 and AG3'NEW as primers (Table 2.2, No.1 & 4) at an annealing temperature of 63ºC, to produce a final DNA product of approximately 1240bp. Gel electrophoresis and DNA gel extraction were carried out subsequently. The purified DNA fragment and pE1001 were then digested with restriction enzymes BstEII and EcoRI as described in section 2.4.1. Gel electrophoresis and DNA gel extraction were performed to purify the digested DNA fragment at 1240bp (insert) and digested pE1001 at about 8000bp (vector). Both purified DNA fragments were then ligated as described in section 2.4.6 and transformed into competent DH5α *E. coli* as described in section 2.4.7. After purifying the plasmids from positive clones as described in section 2.4.9, DNA sequencing was carried out (section 2.4.11) to ensure the desired sequence was obtained. Plasmids with the correct DNA sequence were named as pTF1 and pTF2. pTF1 is a plasmid with just half the hinge region from hIgA1 inserted due to primer mismatches during PCR amplification and the reason for using pTF1 will be discussed in section 3.4.1, page 103. In contrast, pTF2 is a plasmid with full hIgA1 hinge region insertion.

3.3.3.2 Repairing the CH1 region of fixed pE1001, pTF1 and pTF2

The procedure for repairing the intron upstream to CH1 is illustrated in Figure 3.6. Plasmids pE1001, pTF1, pTF2 and pBSK-419bp were individually digested with restriction enzyme HindIII and BstEII at 37ºC and at 60ºC for 1 hour respectively as described in section 2.4.1. Gel electrophoresis and DNA gel extraction were performed to purify digested DNA fragments at about 8000bp (vector) respectively

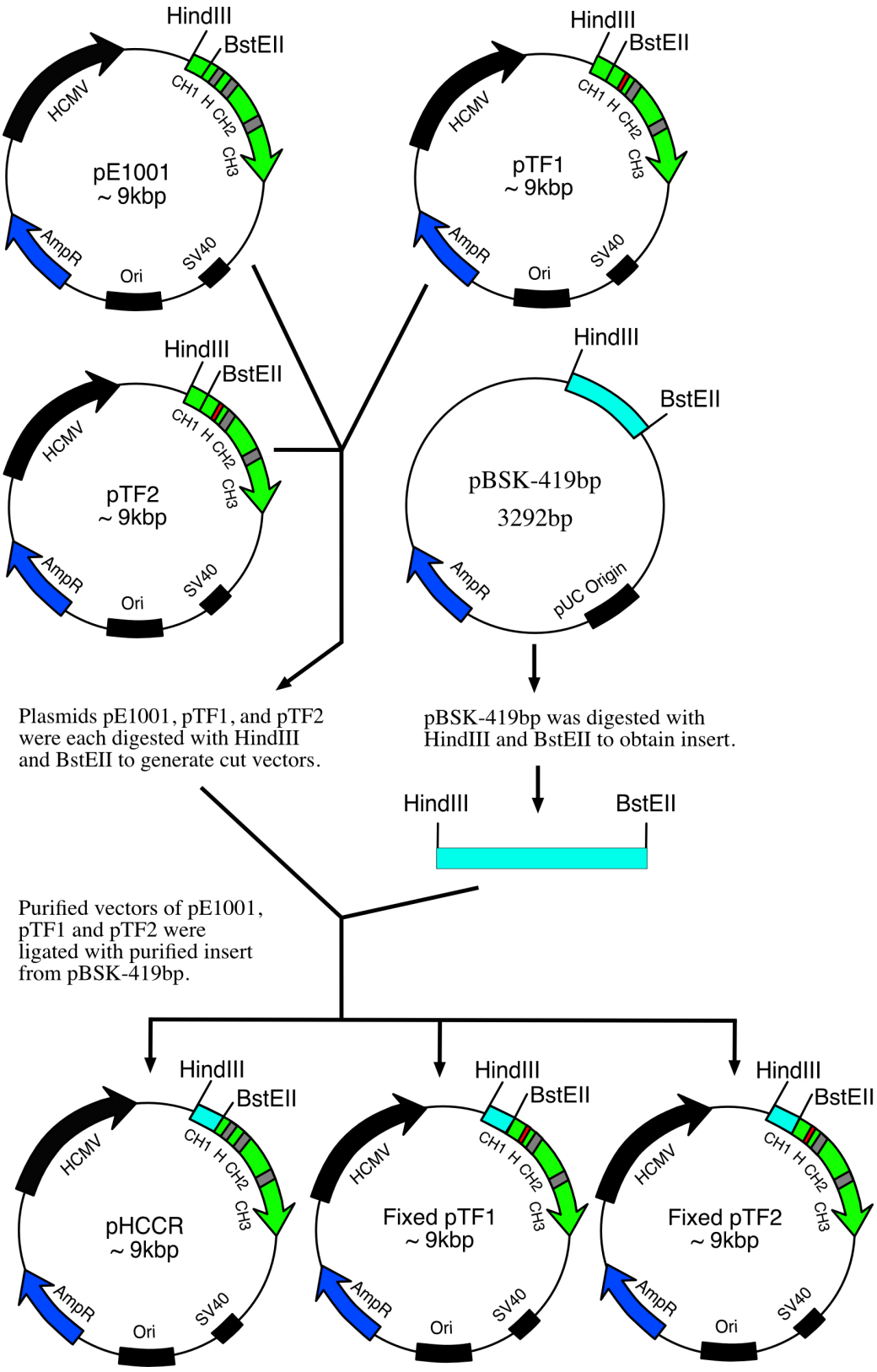

Figure 3.6: A schematic diagram of the repair of the exon upstream to CH1. pBSK-419bp was digested with HindIII and BstEII to obtained the insert encoding the correct DNA sequence of the upstream exon. pE1001, pTF1 and pTF2 were digested with HindIII and BstEII to obtain respective cut vectors and each was ligated with the insert obtained from pBSK-419bp.

for pE1001, pTF1 and pTF2, and at 419bp (insert) for pBSK-419bp. Purified DNA fragments were then ligated as described in section 2.4.6 and transformed into competent DH5α *E. coli* as described in section 2.4.7. After purifying the plasmids from positive clones as described in section 2.4.9, DNA sequencing was carried out (section 2.4.11) to ensure that the exon had been successfully repaired. Plasmids with correct DNA sequence were named respectively as pHCCR, Fixed pTF1 and Fixed pTF2.

3.3.3.3 Generation of O-linked negative mutant expression vector

The procedure for generating an expression vector for the heavy chain of the O-linked negative mutant is illustrated in Figure 3.7. Using Fixed pTF2 as template, primers DS3 and OlinkNegRev (Table 2.2, No.1 & 6) were used at an annealing temperature of 60ºC to amplify a DNA product of approximately 190bp which contained a unique BstEII site. Similarly, primers OlinkNegForw and AG3'NEW primers (Table 2.2, No.5 & 4) were used at an annealing temperature of 63ºC to obtain a DNA product of approximately 1100bp which contained a unique EcoRI site. These two sets of amplification are designed to mutate the sequence encoding serine and threonine amino acids in the hinge region of Fixed pTF2 to that encoding a mixture of glycine and alanine, thereby changing the hinge amino acid sequence from TPSTPPTPSPSTPPTPSPS to GPAGPPAPAPGAPPGPAPG. After DNA electrophoresis, DNA fragments of the correct sizes were extracted and purified. An overlap PCR extension was performed as described in section 2.4.3 on a mix of 2µl of each extracted DNA fragment for 30 cycles at an annealing temperature of 72ºC without the addition of primers. When the procedure ended, primers DS3 and AG3'NEW (Table 2.2, No.1 & 4) were added and the same PCR procedure was

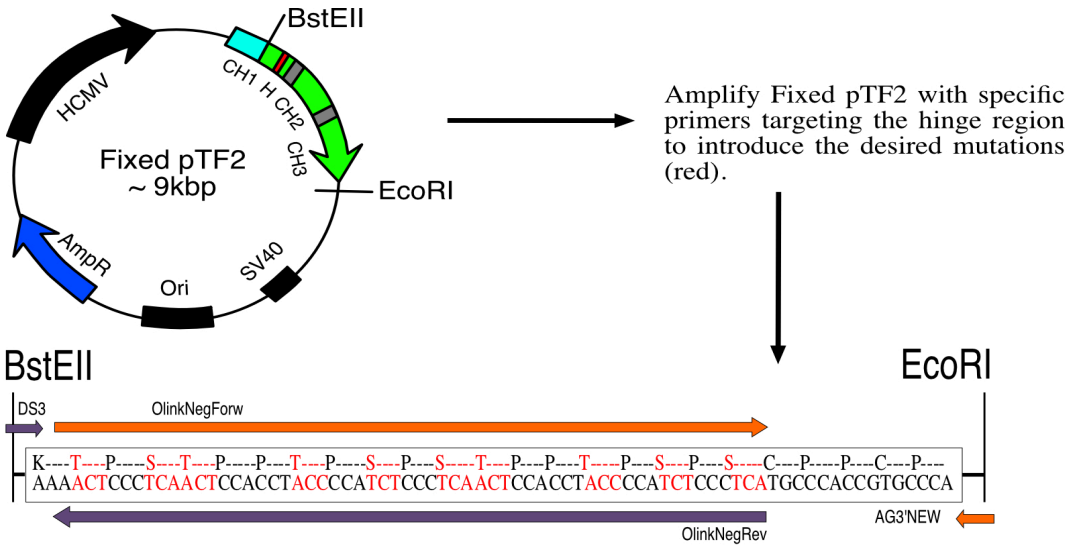

All serine and threonine amino acids encoded at the hinge region of Fixed pTF2 (above) were mutated into a mixture of alanine and glycine (below). Mutated DNA sequence will serve as a complementary binding site during overlapping PCR procedure to generate full DNA fragment.

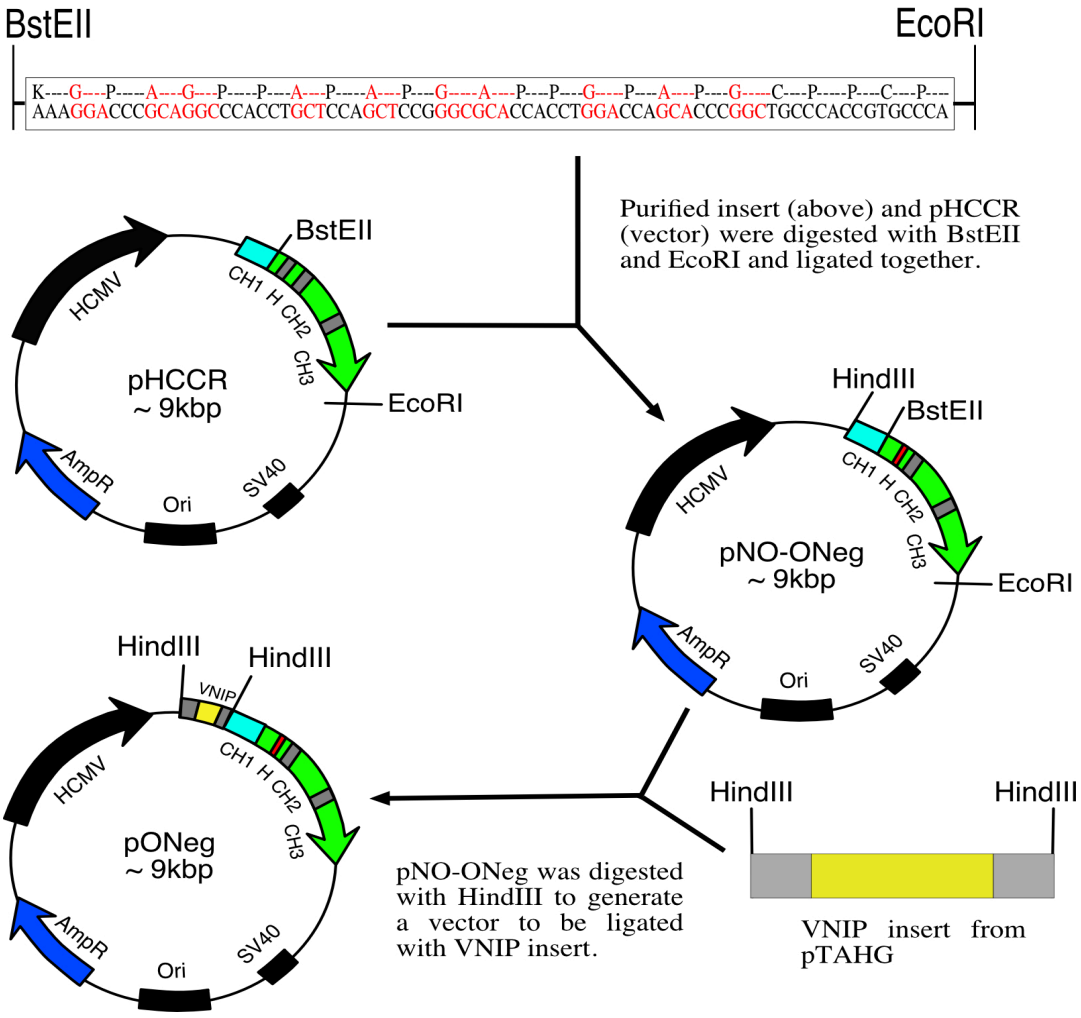

Figure 3.7: Generation of O-linked negative mutant heavy chain expression vector. The hinge region of the hinge mutant encoded in Fixed pTF2 was PCR amplified to introduce several mutations as shown above. The amplified DNA fragment was inserted into pHCCR using BstEII and EcoRI sites. pNO-ONeg was then digested with HindIII to allow insertion of VNIP obtained from pTAHG shown in Figure 3.8.

performed at an annealing temperature of 60ºC to obtain a final DNA product of approximately 1240bp. Gel electrophoresis and DNA gel extraction were carried out subsequently. Purified DNA fragment and plasmid pHCCR were then digested with restriction enzymes BstEII and EcoRI as described in section 2.4.1. Gel electrophoresis and DNA gel extraction were performed to purify the digested DNA fragment of 1240bp (insert) and digested pE1001 of about 8000bp (vector). Both purified DNA fragments were then ligated as described in section 2.4.6 and transformed into competent DH5α *E. coli* as described in section 2.4.7. After purifying the plasmids from positive clones as described in section 2.4.9, DNA sequencing was carried out (section 2.4.11) to ensure that the hinge region had been correctly mutated. Plasmid with correct DNA sequence was named as pNO-ONeg.

3.3.3.4 Insertion of sequence encoding murine anti-NIP variable heavy domain (VNIP)

The procedure for VNIP insertion is illustrated in Figure 3.8. pTAHG, pHCCR, Fixed pTF1, Fixed pTF2 and pNO-ONeg were digested individually with restriction enzyme HindIII at 37ºC for 1 hour as described in section 2.4.1. Gel electrophoresis and DNA gel extraction were performed to purify digested DNA fragment at about 8000bp (vector) for pHCCR, Fixed pTF1, Fixed pTF2 and pNO-ONeg and 750bp (VNIP insert) for pTAHG. In each case, purified vector and insert DNA fragments were then ligated as described in section 2.4.6 and transformed into competent DH5α *E. coli* as described in section 2.4.7. Due to both ends of the VNIP insert being flanked by HindIII sites, it was possible for the VNIP insert to ligate in two different orientations. However, the correct orientation could be determined by EcoRI digestion because VNIP carried a unique EcoRI restriction site located near 3´ end, shown in Figure 3.9. Thus a correct orientation should yield a fragment of 1929bp

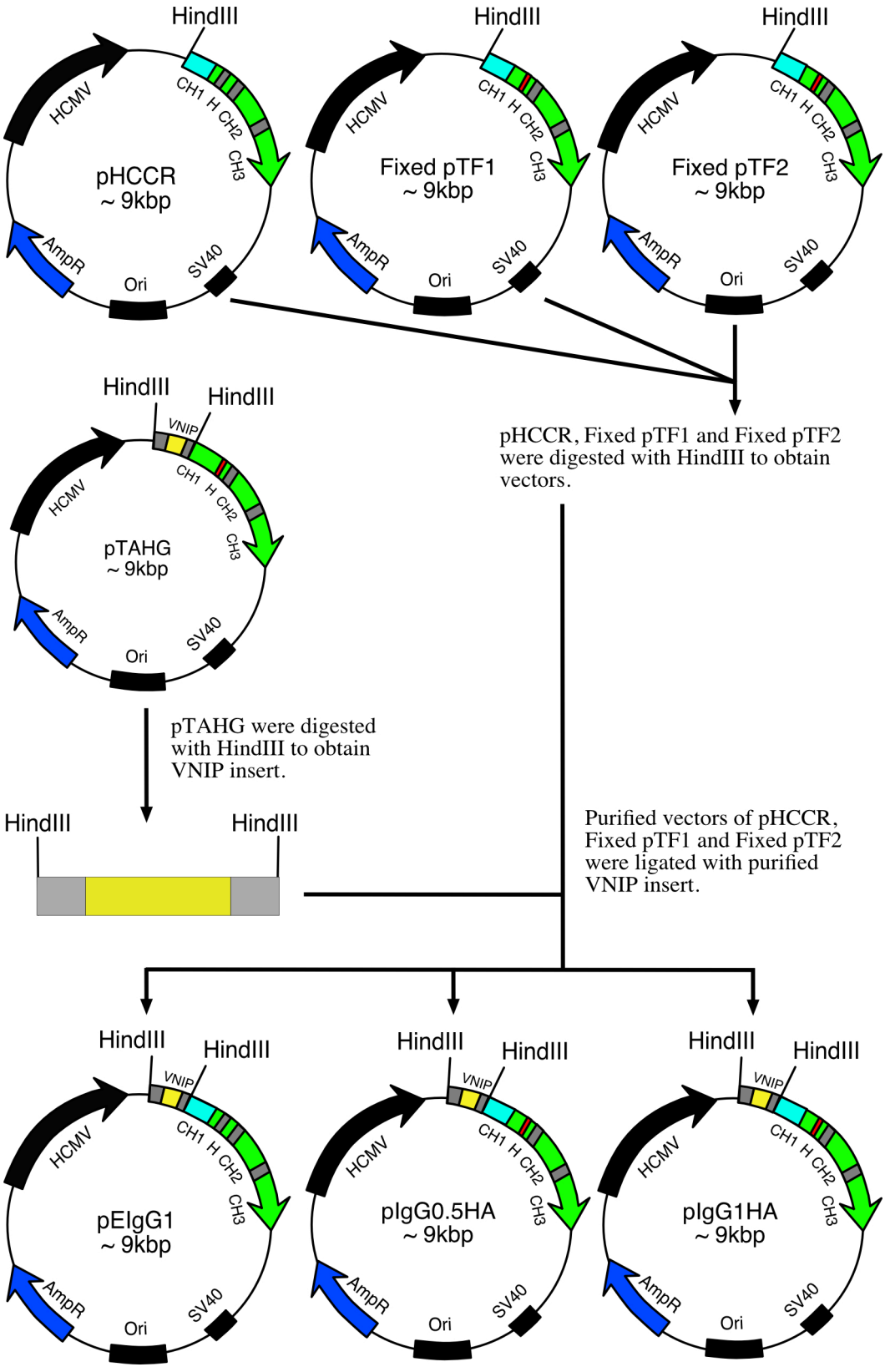

Figure 3.8: Anti-NIP variable heavy domain (VNIP) insertion. pTAHG was digested with HindIII to obtain VNIP insert. pHCCR, Fixed pTF1 and Fixed pTF2 were each digested with HindIII to obtain each respective vectors prior to ligation with VNIP insert.

for pHCCR and around 1600bp for Fixed pTF1, Fixed pTF2 and pNO-ONeg upon EcoRI digestion. After purifying the plasmids from positive clones as described in section 2.4.9, DNA sequencing was carried out (section 2.4.11) to verify that the VNIP insert was in the correct orientation. Plasmids with correct DNA sequences were named as pEIgG1 (derived from pHCCR), pIgG0.5HA (derived from Fixed pTF1), pIgG1HA (derived from Fixed pTF2) and pONeg (derived from pNO-ONeg) respectively. Amplification of plasmid DNA was then carried out as described in section 2.4.8.

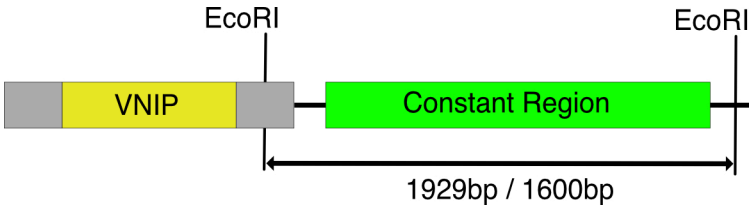

Figure 3.9: Determination of correct orientation of anti-NIP variable heavy domain (VNIP). Both VNIP and the constant region gene carried EcoRI sites near their 3´ termini. When digested with EcoRI, the correct VNIP orientation should yield 1929bp for pEIgG1 and around 1600bp for pIgG0.5HA, pIgG1HA and pONeg.

3.3.4 PRODUCTION AND CHARACTERISATION OF RECOMBINANT ANTIBODIES

3.3.4.1 Antibody production and purification from FreeStyle 293-F cells

Frozen FreeStyle 293-F cells were thawed and maintained in appropriate growth conditions as shown in section 2.6.2. Before the day of transfection, each flask of cells were split and seeded in a total volume of 25ml at 5 x 10^5 cells/ml in Erlenmeyer flasks, so that on the day of transfection total cells were 1 x 10^6 cells/ml at a viability of 90% or above. Five antibody plasmids, listed in Table 3.1, were used to transfect FreeStyle 293-F cells to generate the desired antibodies. For transfection, 293Fectin (Invitrogen) and Opti-MEM (1X) (Gibco Life Technologies) were brought

Table 3.1: Amount of DNA required for FreeStyle 293-F cells transfection

Type of DNA expression vector	Amount of DNA
Heavy chain	4.17μg
Light chain	16.67μg
pAdvantage vector (Promega)	4.17μg

Note: The total amount of DNA is kept at 25μg. The ratio is for each DNA is Heavy chain:Light chain:pAdvantage = 0.5:2.0:0.5.

Table 3.2: The type of antibody plasmid required for transfection

Plasmid	Antibody Code Name	Encoded Antibody Chain
pEIgG1	wt hIgG1	Anti-NIP wildtype human IgG1 heavy chain
pIgG0.5HA	1HA	Anti-NIP mutant human IgG1 heavy chain with full hIgA1 hinge inserted
pIgG1HA	0.5HA	Anti-NIP mutant human IgG1 heavy chain with half hIgA1 hinge inserted
pONeg	ONeg	Anti-NIP O-linked negative mutant human IgG1 heavy chain with mutated half hIgA1 hinge inserted
preλLC	LC	Anti-NIP murine lambda light chain

to room temperature. For a single transfection, two aliquots of 0.833ml of Opti-MEM (1X) were pipetted into two 30ml Universal tube. In one tube, the amount of DNA listed in Table 3.2 were added and mixed gently. In the other tube, 33.25μl of 293Fectin was added and allowed to incubate for exactly 5 minutes at room temperature before the addition of the DNA mixture prepared earlier. Once the DNA mixture was added, the solution was gently mixed and allowed to incubate for 20-30 minutes at room temperature. When completed, the solution was added to the FreeStyle 293-F cells and incubated on a shaker at 180rpm in an incubator in 8% CO_2 at 37ºC. Antibody was ready to be harvested and purified after 4 days as described in section 2.8.

3.3.4.2 Characterisation of antibody heavy and light chains

Antibody purifications were carried out as described in section 2.8. Purified antibodies were subjected to SDS-PAGE as described in section 2.8.6. Protein gels were stained with Coomassie as described in section 2.8.8 to determine the purity of the antibodies generated. To further analyse the purified proteins, they were subjected to western blotting as described in section 2.8.7. After the blocking and washing procedure, the membranes were incubated with detecting antibodies: polyclonal goat anti-mouse lambda light chain HRP conjugated (Table 2.1 No.1) or polyclonal rabbit anti-human IgG HRP conjugated (Table 2.1 No.2). All membranes were washed and developed with appropriate substrate.

3.3.4.3 Determination of NIP antigen recognition by ELISA

NIP-binding ELISA was carried out as described in section 2.8.9. Wells of 96 well Maxisorp ELISA plates (Nunc) were coated with NIP-BSA at 1-2 μg/ml overnight at 4°C. For certain control wells, buffer alone was used for coating. After the blocking and washing procedure, wells were incubated with 100μl of wt hIgG1, 0.5HA, 1HA and ONeg antibodies at 20 μg/ml for 60 minutes. For certain control wells, anti-NIP antibodies were replaced with PBST buffer only. The wells were washed as described and incubated with 100μl of detecting antibodies: polyclonal goat anti-mouse lambda light chain HRP conjugated (Table 2.1 No.1) or polyclonal rabbit anti-human IgG HRP conjugated (Table 2.1 No.2). All wells were washed and developed with appropriate substrate. Absorbance of each well were read at 630nm.

3.3.4.4 Determination of O-linked glycosylation by ELISA

NIP-binding ELISA was carried out as described in section 2.8.9. Wells of 96 well Maxisorp ELISA plates (Nunc) were coated with NIP-BSA at 1-2 μg/ml overnight at

4°C. For certain control wells, buffer alone was used for coating. 1% (w/v) BSA in PBST was used as blocking buffer instead of 5% (w/v) milk. After the blocking and washing procedure, wells were incubated with 100µl of wt hIgG1, 0.5HA, 1HA and ONeg antibodies at 20µg/ml for 60 minutes. 100µl of 20µg/ml human IgA1 produced from CHO cells (available in the Woof Lab) was used as positive control. The plates were washed as described and incubated with 100µl of biotinylated jacalin (Table 2.1 No.3) for 1 hour. For certain control wells, biotinylated jacalin were replaced with PBST buffer only. All wells were washed and further incubated with 100µl of streptavidin HRP conjugated (Table 2.1 No.4) for another hour. The wells were washed and developed with appropriate substrate. Absorbance of each well were taken at 630nm.

3.4 RESULTS

3.4.1 Restoration of missing DNA sequences

Using the primer combinations of DS3 and GUHIAS, and GUHIS and AG3'NEW, DNA amplified fragments of the correct sizes of 1100bp and 140bp respectively were obtained as shown in Figure 3.10 A. Although there were other non-specific bands being amplified, the bands were not at similar sizes when compared to the desired ones, thus, allowing an easy purification. The GUHIAS and GUHIS primers were specifically designed not only to restore the missing DNA sequence, shown in red in Figure 3.5, but also to generate complementary regions to aid overlapping PCR. The result of the subsequent overlapping PCR procedure was shown in Figure 3.10 B. The band obtained of approximately 1200bp indicated that the 1100bp and 140bp DNA fragments had annealed through their complementary regions leading to

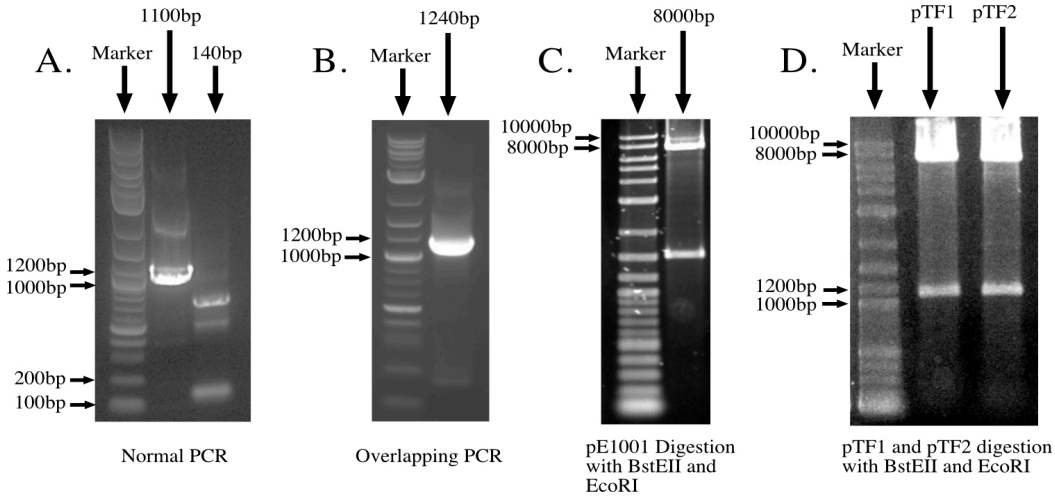

Figure 3.10: Results of molecular cloning for heavy chain repair. **A**) PCR amplifications to reintroduce missing DNA sequences. Lane 1100bp shows PCR amplification using DS3 and GUHIAS to obtain DNA fragment at 1100bp. Lane 140bp shows PCR amplification using GUHIS and AG3'NEW to obtain DNA fragment at 140bp. **B**) Overlapping PCR. Complementary DNA fragments of 1100bp and 140bp from A. were amplified using DS3 and AG3'NEW to to produce a fragment of 1240bp. **C**) Restriction digest of pE1001 to obtain cut vector at 8000bp. **D**) Restriction digests of purified plasmid from positive clones.

successful amplification. The PCR product and pE1001 vector were ligated together after digestion with BstEII and EcoRI restriction enzymes. After transforming the plasmids into *E.coli*, DNA plasmids were purified from positive clones and digested with BstEII and EcoRI and the presence of an insert size of 1240bp were confirmed as shown in Figure 3. 10 D. Subsequent DNA sequencing also confirmed that the previously missing DNA sequences had been successfully restored and the correct plasmid was named as pTF2.

Interestingly, the result of DNA sequencing of positive clones also identified another mutant that carried only 10 amino acids from the human IgA1 hinge rather than the expected 18 amino acids. This mutant was most likely due to a mismatch at the region encoding the hinge during the overlapping PCR procedure. The hIgA1 hinge region sequence PSTPPTPS**PSTPPTPS**PS, has a repeated sequence of 8 amino acids before ending with a proline and a serine. It was suspected that during the

overlapping PCR procedure, the DNA fragment had misaligned and bound to the second PSTPPTPS, skipping the primary repeat of this sequence, thus generating a mutant with about half the hIgA1 hinge. This mutant would be a useful comparison in this project, therefore, the plasmid was retained and named as pTF1. Finally, to repair the CH1 intron, pBSK-419bp was digested using the restriction enzyme HindIII and BstEII to obtain an insert of 419bp. The insert was then ligated into pTF1, pTF2 and pE1001 after performing a similar digestion to obtain suitably cut vectors. After transforming the plasmids into *E.coli*, DNA plasmids were purified from positive clones and subsequent DNA sequencing confirmed that the intron was successfully reintroduced (data not shown).

3.4.2 Generation of O-linked negative mutant heavy chain expression plasmid

Using the primer combinations of DS3 and OlinkedRev, and OlinkedForw and AG3'NEW, DNA amplified fragments of the correct sizes of 1100bp and 190bp were obtained as shown in Figure 3.11A. This suggested that although there were several nucleotide mismatches within the OlinkedRev and OlinkForw primers, the remaining complementary base pairs were sufficient for the primers to anneal at the targeted site. Overlapping PCR was performed after purifying the required DNA fragments and a successful amplification was indicated by generation of a DNA fragment with the correct size of 1290bp in Figure 3.11B. Amplified PCR product and pHCCR vector were ligated together after digestion with HindIII and BstEII restriction enzymes. After transforming the plasmids into *E.coli*, DNA plasmids were purified from positive clones and digested with HindIII and BstEII. The presence of an insert size of 1290bp were confirmed. Subsequent DNA sequencing also

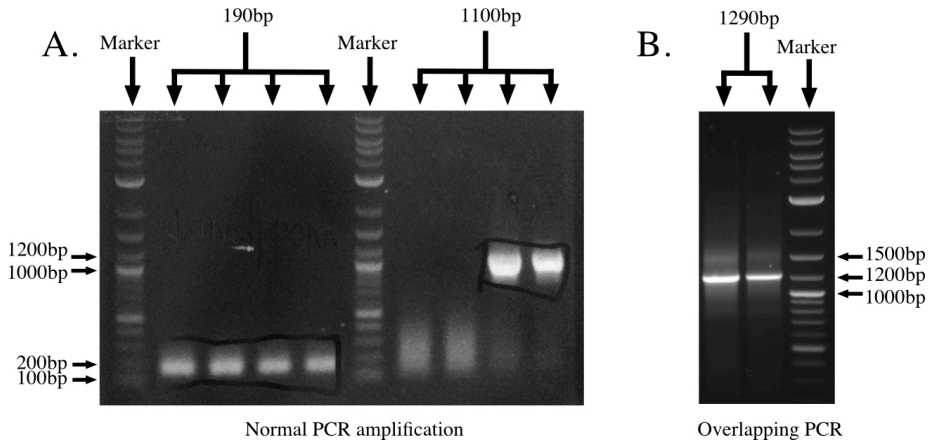

Figure 3.11: Results of molecular cloning for generating O-Linked negative mutant heavy chain expression plasmid. **A**) PCR amplifications to introduce several mutations using designated primers. Four repeat experiments (190bp) of PCR amplification using DS3 and OlinkRev primers. Four repeat experiments (1100bp) of PCR amplification using OlinkForw and AG3'NEW primers. The correct sized product is seen in the third and fourth repeats. **B**) Two repeat experiments (1290bp) of an overlapping PCR amplification using the DNA fragments obtained in A.

confirmed that the mutations shown in Figure 3.7 had been successfully incorporated (data not shown).

3.4.3 VNIP insertion

VNIP insert was successfully obtained from pTAHG by performing a restriction digest using HindIII enzyme. Suitable cut vectors were obtained by digesting pHCCR, Fixed pTF-1, Fixed pTF-2 and pNO-ONeg with EcoRI enzyme. Since VNIP was flanked by HindIII sites, it was able to ligate in two different orientations. Initially, it was observed that many of the obtained clones lacked VNIP insertions. After several ligation attempts, plasmid that carried VNIP insertion with the correct orientation was obtained and subsequent DNA sequencing confirmed the presence and orientation of VNIP. Figure 3.12 shows a representative result with pONeg of a correct VNIP insertion whereby the size of the insert was around 1600bp, as described in Figure 3.9.

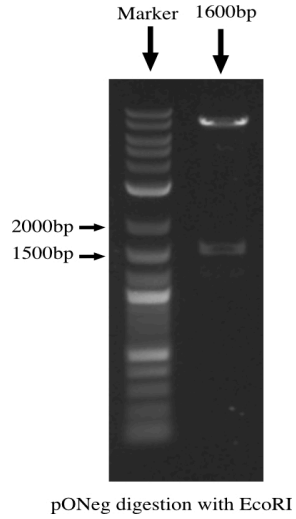

Figure 3.12: A representative result for determination of VNIP orientation. pONeg was digested with EcoRI enzyme and yielded an insert at around 1600bp which showed a correct orientation of the VNIP insert.

3.4.4 Amino acid sequence of the hinge region of different antibodies

The DNA sequencing result and the encoded amino acid sequence of the hinge region of each different hIgG1 antibody were shown in Table 3.3. In summary, wt hIgG1 has 5 amino acids, 0.5HA which incorporated only half the hinge region from hIgA1 has 13 amino acids, 1HA with the full hinge region from hIgA1 inserted has 21 amino acids, and ONeg which is similar to 1HA has 21 amino acids in their hinge regions respectively. Although having similar hinge length, the difference between 1HA and ONeg was that the residues corresponding to serine and threonine residues in the hinge region of 1HA were mutated to a mixture of glycine and alanine in ONeg, as shown in Table 3.3.

3.4.5 Production and characterisation of recombinant antibodies

Four antibody heavy chain constructs, pEIgG1, pIgG0.5HA, pIgG1HA and pONeg, were each transfected together with the light chain vector preλLC into FreeStyle 293-F cells. After 4 days, supernatants of the cell cultures were incubated with Protein G-Sepharose and the antibodies expressed were efficiently purified. The amount of antibody obtained from a single 25ml transfection was around 200-250μg

Table 3.3: DNA sequencing results and the translated protein sequences of the hinge region of different antibodies

The number of amino acids in the hinge is indicated. Cys residues involved in H-L and the most N-terminal H-H interchain disulphide bonds and their codons are shown in red.

Heavy chain Plasmid	Antibody	Hinge DNA sequence and translation	Number of amino acids
pEIgG1	wt hIgG1 (Wildtype human IgG1)	220 E--P--K--S--C--D--K--T--H--T--C--P--P--C--P-- GAGCCCAAATCTTGTGACAAAACTCACACATGCCCACCGTGCCCA GAGCCCAAATCTTGTGACAAAACTCACACATGCCCACCGTGCCCA	5
pIgG0.5HA	0.5 HA (Mutant with half human IgA hinge inserted)	E--P--K--S--C--D--K--T--P--S--T--P--P--T--P--S--P--S--C--P--P--C--P-- GAGCCCAAATCTTGTGACAAAACTCCCTCAACTCCACCTACCCCATCTCCCTCATGCCCACCGTGCCCA GAGCCCAAATCTTGTGACAAAACTCCCTCAACTCCACCTACCCCATCTCCCTCATGCCCACCGTGCCCA	13
pIgG1HA	1 HA (Mutant with full human IgA hinge inserted)	E--P--K--S--C--D--K--T--P--S--T--P--P--T--P--S--P--S--T--P--P--T--P--S--P--S--C--P--P--C--P-- GAGCCCAAATCTTGTGACAAAACTCCCTCAACTCCACCTACCCCATCTCCCTCAACTCCACCTACCCCATCTCCCTCATGCCCACCGTGCCCA GAGCCCAAATCTTGTGACAAAACTCCCTCAACTCCACCTACCCCATCTCCCTCAACTCCACCTACCCCATCTCCCTCATGCCCACCGTGCCCA	21
pONeg	ONeg (1HA Mutant with O-linked glycans removed)	E--P--K--S--C--D--K--G--P--A--G--P--P--A--P--A--P--G--A--P--P--G--P--A--P--G--C--P--P--C--P-- GAGCCCAAATCTTGTGACAAAGGACCCGCAGGCCCACCTGCTCCAGCTCCGGGCGCACCACCTGGACCAGCACCCGGCTGCCCACCGTGCCCA GAGCCCAAATCTTGTGACAAAGGACCCGCAGGCCCACCTGCTCCAGCTCCGGGCGCACCACCTGGACCAGCACCCGGCTGCCCACCGTGCCCA	21

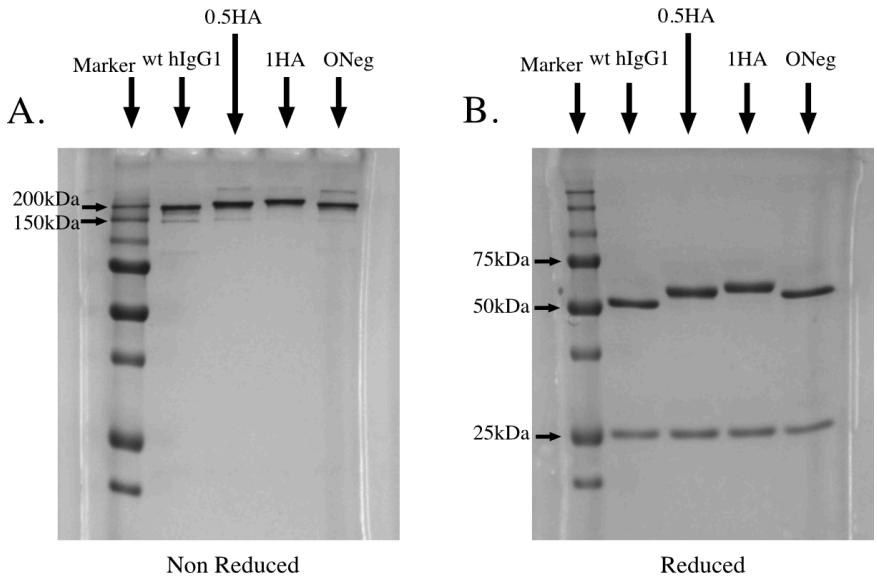

Figure 3.13: Coomassie staining of purified antibodies after SDS-PAGE. **A**) Antibodies run under non-reducing conditions. **B**) Antibodies run under reducing conditions. Molecular weight markers were run in the left hand lane in both cases. Wt hIgG1, wildtype human IgG1; 0.5HA, half hinge mutant; 1HA, represents full hinge mutant; ONeg, represents O-linked negative full hinge mutant.

for all antibodies. Purified antibodies were subjected to SDS-PAGE, as described in Section 2.8.6. Figure 3.13 shows the results of the SDS-PAGE under both non-reducing and reducing condition after Coomassie staining, and Figure 3.14 shows the western blotting results obtained when probing with anti-human IgG heavy chain HRP and anti-murine lambda light chain HRP detecting antibodies. As seen in Figure 3.13, the antibody preparations appear highly pure, with no obvious contamination with other proteins. There were some other faint bands below 150kDa seen under non-reducing conditions as shown in Figures 3.13A, 3.14A and 3.14C. However, under reducing conditions there were no bands observed other than the heavy chain band at 50-60kDa (Figures 3.13B and 3.14B) and the lambda light chain band at 25kDa (Figures (3.13B and 3.14D). This suggests that the faint bands seen under non-reducing conditions might be due to the presence of half molecules (HL or H-H), but these represent only a very minor proportion of the total antibody.

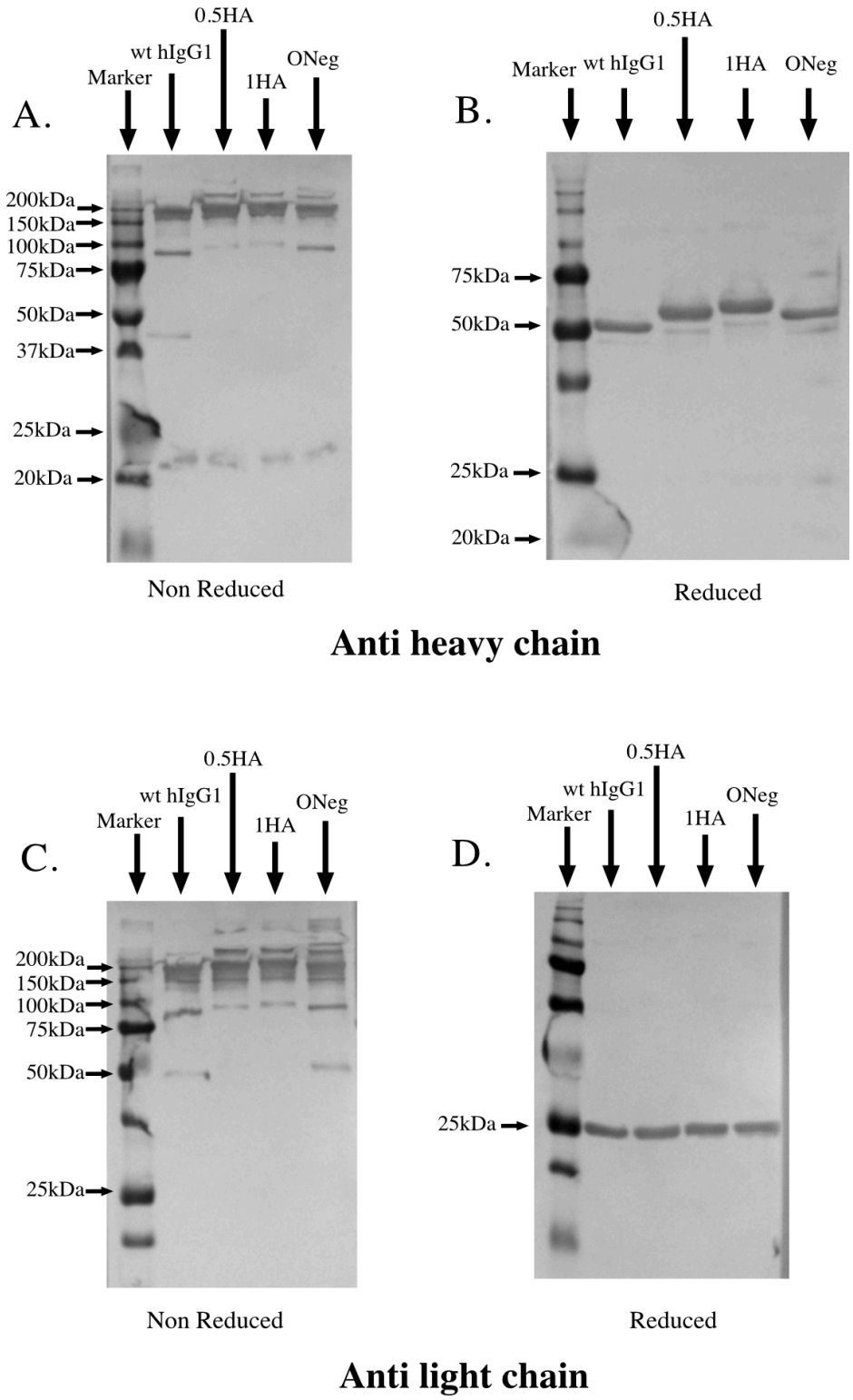

Figure 3.14: Western blotting of purified antibodies. **A**) Purified antibodies run under non-reducing conditions probed with anti-human IgG heavy chain detecting antibodies. **B**) Purified antibodies run under reducing conditions probed with anti-human IgG heavy chain detecting antibodies. **C**) Purified antibodies run under non-reducing conditions probed with anti-murine lambda light chain detecting antibodies. **D**) Purified antibodies run under reducing conditions probed with anti-murine lambda light chain detecting antibodies. Molecular weight markers were run in the left hand lane in each case. Wt hIgG1, wildtype human IgG1; 0.5HA, half hinge mutant; 1HA, full hinge mutant; ONeg, O-linked negative full hinge mutant.

The absence of protein bands below 50kDa under non-reducing conditions (Figure 3.13A) leads to the conclusion that the light chain formed the expected disulphide bonds with heavy chain and the restoration of the required cysteine residue had been successful. Although there were faint bands seen under non-reducing conditions with masses around 20-25kDa in blots probed with anti-heavy chain antibody (Figure 3.14A), these bands were absent under reducing conditions (Figure 3.14B). Therefore, the hypothesis that these bands were free light chain could be neglected. In addition, the presence of only the predicted light and heavy chain bands under reducing conditions (Figure 3.13 B), suggested that the mRNA splicing mechanism was working correctly and there were no alternative splice variants being produced. Hence it could be concluded that the restoration of the lost intron had been successful. Under reducing conditions, there were noticeable differences in the molecular weights of the heavy chain of each of the antibodies, as seen in Figure 3.13B and Figure 3.14B. With the longest hinge, the heavy chain of IHA had the highest molecular weight of these antibodies. The heavy chain of ONeg demonstrated a lower molecular weight than than that of 1HA even though they had the same numberof amino acids in their hinge region. This finding suggests the presence of O-linked glycosylation within the hinge regions of 0.5HA and 1HA but not that of ONeg, as anticipated.

3.4.6 NIP antigen recognition

In order to be able to directly compare the function of each antibody, all antibodies under test should have identical antigen recognition properties. This approach is designed to ensure that any differences observed can be attributed to structural differences. Therefore, in this project all antibodies had identical variable domains

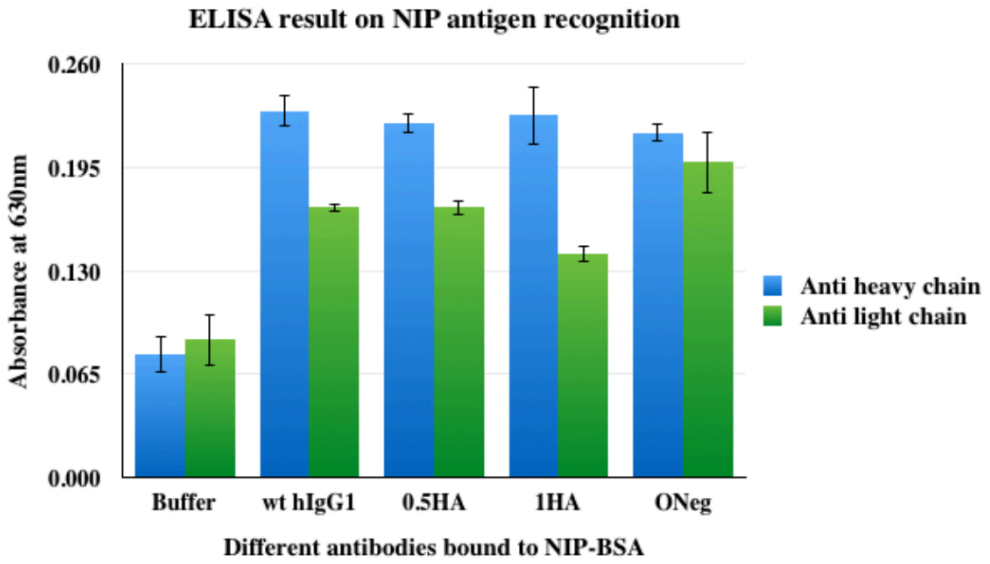

Figure 3.15: NIP binding ELISA. 10µg/ml of NIP-BSA was coated onto ELISA plate wells and different antibodies were added at 20µg/ml. Wells were then developed using suitable substrate after probing with anti-human IgG heavy chain HRP (blue) or anti-murine lambda light chain HRP (green). Buffer represents PBST only (negative control). Wt hIgG1, wildtype human IgG1; 0.5HA, half hinge mutant; 1HA, full hinge mutant; ONeg, O-linked negative full hinge mutant. The results show the mean of triplicate measurements. Bars represent standard deviation measurements.

that were expected to be able to specifically recognise NIP. To confirm such antigen recognition, NIP-BSA was coated onto ELISA plate wells and purified antibodies were incubated to allow antigen binding. Bound antibodies were then detected using suitable detecting antibodies. Figure 3.15 shows the results of NIP antigen recognition based on ELISA. As seen in Figure 3.15, all antibodies produced were able to recognise NIP antigen as expected. The detection levels for all antibodies were very similar, suggesting that the antigen recognition was similar for all antibodies, as might be expected given their identical variable domains. Results from Figure 3.15 also suggest that the incorporation of longer hinge regions had no or minimal impact on antigen recognition, thus, allowing comparison between each antibody in subsequent analyses.

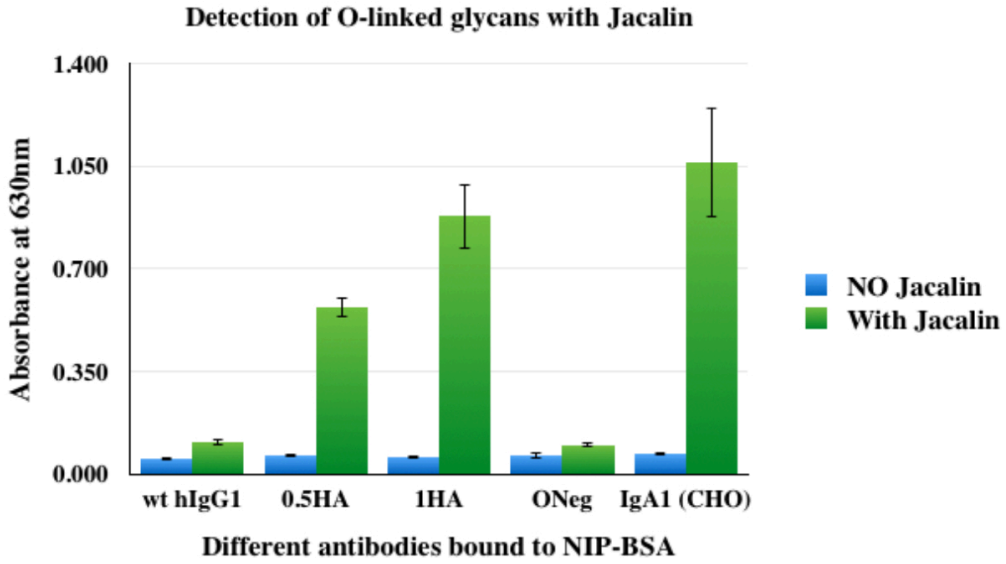

Figure 3.16: ELISA result of O-linked glycans detection using jacalin. 10µg/ml of NIP-BSA was coated onto ELISA plate wells and different antibodies were added at 20µg/ml. Biotinylated jacalin at 0.2µg/ml was then used as an O-linked glycans detecting agent. Wells were then developed using suitable substrate after incubation with streptavidin-HRP at 0.2µg/ml. Bars in blue represent the tests without jacalin (as negative control). Bars in green represent the tests with jacalin addition. Wt hIgG1, wildtype human IgG1; 0.5HA, half hinge mutant; 1HA, full hinge mutant; ONeg, O-linked negative full hinge mutant; IgA1 (CHO), human IgA1 produced from CHO cells used as a positive control. The results show the mean of triplicate measurements. Bars represent standard deviation measurements.

3.4.7 Determination of O-linked glycosylation

Due to the difference in the molecular weight observed between the heavy chains of 1HA and ONeg in Figure 3.13 B and Figure 3.13 B, the presence of O-linked glycans was investigated using the lectin jacalin which has a high specificity for a common core structure of O-linked glycans, as mentioned in section 3.1.5. When used to probe blots of purified antibodies the biotinylated jacalin was found to react with both the light and heavy chains of all antibodies including wt hIgG1 which had no O-linked glycans (data not shown). To resolve this issue of sensitivity, ELISA was applied because the antibodies were considered likely to retain their intact structure, rather than being denatured as in SDS-PAGE. Since it had been determined that all antibodies were able to recognise NIP when derivatised on BSA (Figure 3.15), a similar format was used to detect O-linked glycans using biotinylated jacalin. The

results of the investigation are shown in Figure 3.16. Using hIgA1 and wt hIgG1 as positive and negative control respectively, the investigation showed that 0.5HA and 1HA were indeed O-linked glycosylated and ONeg did not contain any O-linked glycans. It was noticed that there was a difference in the level of absorbance between 0.5HA and 1HA in which 1HA had a higher absorbance level, suggesting that more jacalin had bound to 1HA compared to 0.5HA. The reason for such observation was most likely due to a lower level of O-linked glycosylation in 0.5HA compared to 1HA because 0.5HA only contained half the hinge region of hIgA1, resulting in a fewer potential sites for O-linked glycosylation than 1HA which had the entire hinge region of hIgA1 incorporated. The absorbance level of ONeg was not significantly different from that of wt hIgG1, suggesting that the mutations of hinge region serines and threonines to alanines and glycines had indeed abolished O-linked glycosylation in the hinge region of ONeg. The low absorbance level of both wt hIgG1and ONeg also confirmed the specificity of jacalin for O-linked glycans and not N-linked glycans, since all antibodies were assumed to be similarly N-glycosylated.

3.5 DISCUSSION

The aim of this chapter was to generate upper hinge extended mutant hIgG1 antibodies with identical antigen recognition capabilities as tools to investigate the role of the upper hinge region in IgG structure and function. Rather than randomly adding different amino acids to extend the upper hinge length of hIgG1, this project had chosen to incorporate the naturally evolved hinge region from hIgA1 into the upper hinge of wt hIgG1. The process ensured that the IgG cysteines that were required for inter-heavy chain disulphide bonding were not disturbed, thus, all antibodies generated should retain the normal antibody structure of two heavy and

two light chains as described in Chapter 1. Using a naturally occurring hinge sequence is less likely to be immunogenic, should such a construct ever be considered for therapeutic application. However, one concern regarding the hinge mutants is the possibility of the generation of neoepitopes at the points where the hIgG1 and hIgA1 sequences meet. Anti-hinge antibodies that recognises protease-restricted neoepitopes located at the hinge region of human IgG or antiglycans antibodies specific to hIgA1 O-linked glycans had been found to be present in the serum of healthy individuals and patients suffering from various inflammatory diseases such as RA, SLE and IgA nephropathy respectively (Falkenburg *et al*., 2017; Ryan *et al*., 2008; Falkenburg *et al*., 2016; Tomana *et al*., 1999). For this project, the concern regarding immunogenicity can be neglected because the generated hinge mutants were not used for therapeutic purposes.

Modifying the hinge region of hIgG1 required care as the area around the hinge region, especially the lower hinge region, is crucial for antibody effector function through Fcγ receptor binding (Klein *et al*., 1981; Idusogie *et al*., 2000; Duncan *et al*., 1988; Sondermann *et al*., 2000; Radaev and Sun, 2001; Lu *et al*., 2015; Kiyoshi *et al*., 2015). In addition, since the CH2 domain is critical for binding of C1q and subsequent activation of the classical pathway of complement, structural changes to the hinge may also impact on complement activation. Hinge deleted mutants such as Dob, a human IgG1 cryoglobulin (Silverton *et al*., 1977), Mcg, a human IgG1 (Guddat *et al*., 1993) and Lec, a human IgG1 (Rivat *et al*., 1976) were unable to activate complement protein C1q or bind Fcγ receptors (Klein *et al*., 1981). The reason for this was because Dob, Mcg and Lec have a 15 amino acid hinge deletion which starts after Valine 216 resulting in a complete lack of the middle hinge (Rivat

et al., 1976; Guddat *et al*., 1993; Steiner and Lopes, 1979). Access to the binding sites for C1q and Fcγ receptors, the latter located in the lower hinge region (Idusogie *et al*., 2000; Duncan *et al*., 1988), were blocked presumably as a result of the Fab arms coming into close contact with the Fc region due to the hinge deletion (Guddat *et al*., 1993; Silverton *et al*., 1977). In marked contrast, all three hinge mutants generated in this project have a hinge extension. Thus, it was expected that the binding sites of C1q and Fcγ receptors were unlikely to be disrupted and to remain accessible, allowing studies into the role of hinge region on antibody effector function to be conducted.

Using recombinant antibody technology, several groups had generated different antibody hinge mutants to study the impact of the hinge region on antibody function (Roux *et al*., 1998; Klein *et al*., 2014; Sandlie *et al*., 1989; Horgan *et al*., 1993; Michaelsen *et al*., 1992). In particular, Horgan and colleagues generated different hIgG1 and hIgG4 molecules (with and without hinges) and demonstrated that there were no significant differences in antigen binding in both solution and solid phase antigen binding assays between the mutants of the same isotype (Horgan *et al*., 1993). In agreement with this finding, the mutant antibodies generated in this project demonstrated that hinge region modification did not appear to affect the antigen binding ability of the antibodies in the solid phase antigen binding assay as shown by the NIP-BSA ELISA result. In a different scenario, Roux and colleagues reported the generation of several human IgG3 hinge mutants that had reduced hinge lengths, in order to investigate the role of the hinge on antibody flexibility (Roux *et al*., 1998). It was found that hIgG3 mutants with hinge regions containing more prolines were able to form higher order immune complexes such as tetramers rather than dimers that

were preferred by wt hIgG3 (Roux *et al*., 1998), indicating the impact of the flexibility of the hinge. The hIgA1 hinge region incorporated into different hIgG1 mutants in this project contained several proline residues, leading to speculation that the hinge region of these hinge mutants may display a higher degree of flexibility compared to wt hIgG1.

Interestingly, other workers have reported expression of several hIgG1 hinge mutants with hIgA1 hinge region insertions, but with additional mutations, in HEK-6E cells. These mutants were used to investigate different linker flexibilities using dynamic light scattering (Klein *et al*., 2014). Their studies found that mutants with extra hinge incorporated from hIgA1 had a higher hydrodynamic radius when compared to wt hIgG1 (Klein *et al*., 2014), suggesting that the hinge mutants adopted a more open conformation compared to hIgG1. Although the same hIgA1 hinge region was used, the hinge mutants produced by Klein and colleagues were different from the hinge mutants generated in this project. Klein and colleagues had introduced several mutations including a single or several asparagine residues or a linker peptide to the hIgA1 hinge region (Klein *et al*., 2014). In contrast, this project inserted wt hIgA1 hinge region without any other mutations to generate the 1HA mutant. It would be interesting to investigate if the hinge mutants in this project behave in a similar way in dynamic light scattering studies to that reported by Klein and colleagues.

While there have been numerous hinge mutants generated with various hinge lengths as mentioned earlier, the ONeg mutant in this project is the first mutant antibody to have a hinge length more than 20 amino acids long synthesised *de novo* without the presence of any O- or N-linked glycans or disulphide bonds at the hinge region. In

the past, Gala and Morrison had used benzyl 2-acetamido-2-deoxy-α-D-galacto-pyranoside (BADG), which blocks the formation of O-linked glycans after the addition of first GalNac to serine of threonine residues, to inhibit the complete O-linked glycosylations of hIgA1 and hIgD (Gala and Morrison, 2002). The authors showed that the truncation of O-linked glycans did not inhibit the production and the secretion of hIgA1 and hIgD antibodies (Gala and Morrison, 2002). The successful production of the ONeg mutant in this chapter further improved the understanding on the role of O-linked glycans at the hinge region of antibodies by indicated that the presence of O-linked glycans of the hinge region is not an essential factor for antibody synthesis and secretion. As a result, whether the presence of the O-linked glycans on the hinge regions of hIgA1 and hIgD is evolved to maintain an open conformational structure for better antigen reach and to present lectin binding epitopes for trapping bacteria remains an open question. Nevertheless, the successful generation of different hinge mutants, 0.5HA, 1HA and ONeg, has opened up the possibility for further investigation in order to shed more light on the role of upper hinge length on IgG antibody function, as will be discussed in Chapter 5.

CHAPTER FOUR
PRODUCTION AND CHARACTERISATION OF dsDNA MOLECULAR RULERS

CHAPTER 4. PRODUCTION AND CHARACTERISATION OF dsDNA MOLECULAR RULERS

4.1 INTRODUCTION

As mentioned in the previous chapter, the Fab arms of an antibody are able to adopt a variety of positions at different times as suggested by the reported Fab-Fab angles exhibited by different IgG subclasses (Roux *et al*., 1997b; Saphire *et al*., 2002; Kilár *et al*., 1985). For example the observed Fab-Fab angles for antibodies studied by EM were 30º-210º for human IgG1; 60º-190º for IgG2; 20º-270º for IgG3 and 30º-210º for IgG4 (Roux *et al*., 1997b). In addition, different solved IgG crystal structures have exhibited different Fab-Fab angles, such as 148º by B12 (hIgG1), 132º by Kol (hIgG1), 185º by Mcg (hinge-deleted hIgG1), 172º by 231 (murine IgG2a) and 115º by 61.1.3 (murine IgG1) (Saphire *et al*., 2002).

It might be argued that within the antibody molecule, the Fab arms use the most N-terminal hinge disulphide bond as an anchor point to freely move around for better antigen binding, as described earlier in Chapter 1. Antigen binding occurs at the tips of the Fab arms, thus, the positioning of Fab arms is expected to have a direct effect on the bivalent antigenic distance of an antibody. For IgG, the length and flexibility of the upper hinge region is hypothesised to have a role in regulating the bivalent antigenic distance, as explained earlier. If this is true, one of the important features governed by the upper hinge of IgG would be the maximum bivalent antigenic distance. The maximum bivalent antigenic distance is a key feature of the antibody since it affects the monovalent and bivalent binding activity. However, this distance has rarely, if ever, been directly investigated. The importance of monovalent and bivalent binding of an antibody will be further described below in section 4.1.1.

Some Fab tip to tip distances of IgG antibodies have been reported in the past, such as that of rabbit IgG at around 120Å (Valentine and Green, 1967), those of murine IgG1, IgG2a and IgG2b at around 117Å - 134Å (Sosnick *et al*., 1992), that of human IgG1 (Kol) at 145Å (Marquart *et al*., 1980), and that of human IgA1 at 170Å (Boehm *et al*., 1999). However, these findings were derived from solved crystal structures or molecular models generated based on X-ray and neutron scattering and were not the actual functional bivalent antigenic distance of the antibodies. As a result, this thesis hopes to study the impact of the length of upper hinge on the functional bivalent antigenic distance of an IgG antibody.

This project hypothesised that the longer the region of amino acids at the upper hinge of IgG the greater the bivalent antigenic distance was likely to be. The generated hIgG1 hinge mutant antibodies with different upper hinge lengths, described in the previous chapter, are suitable candidates for testing this hypothesis. However, in order to test this hypothesis molecular "rulers" of known length are required. This chapter sought to test whether dsDNA might serve as a suitable framework for molecular "rulers". dsDNA offers the advantages that its length can be readily calculated and molecules of different length can be easily generated which will be further described in section 4.1.2.

4.1.1 Antibody maximum bivalent antigenic distance

Since all antibody molecules have two Fab arms, each antibody could bind monovalently or bivalently to a pathogen depending on the density of the target antigen on the surface of the pathogen. One of the important features of an antibody that regulates monovalent/bivalent antigen binding activity is the bivalent antigenic

distance. An antibody that has a greater bivalent antigenic distance is expected to be better able to achieve bivalent binding and remain associated with targeted antigen for a longer period of time compared to an antibody with a shorter bivalent antigenic distance, as shown in Figure 4.1. The reason for this phenomenon, as described in Figure 4.1, is because when the targeted antigen is at a low density and individual antigen molecules are spaced at relatively further apart, an antibody with a greater bivalent antigenic distance has the ability to reach two antigens simultaneously. Thus, such antibody will increase in overall avidity. In contrast, an antibody with a shorter bivalent antigenic distance would only be able to bind monovalently, hence, showing a lower avidity. In addition, when an antigenic dissociation occurs at one of the Fab arms of an antibody that is binding bivalently, the antibody remains localised at the area due to the association of the remaining Fab arm bound to target antigen. Such maintained association may allow the initiation of effector mechanisms or the dissociated Fab arm to rebind antigen. In constrast, when an antigenic dissociation occurs at the Fab arm of an antibody that is binding monovalently, the antibody is more likely to diffuse away from its targeted antigen and the antigen-antibody complex is lost. Obviously, the antigen binding affinity plays a major role as well. The disadvantage of monovalent binding described above will not be a major problem if the antigen binding affinity of the antibody is high because the rate of dissociation will be significantly reduced by high affinity binding. However, if the binding affinity is low then an antibody with a greater bivalent antigenic distance will have the advantage to bind bivalently to target antigens, improving overall binding avidity and reducing the rate of dissociation. As a result, it would be a great advantage if the bivalent antigenic distance of an antibody could be modified and extended to improve the chances of bivalent binding activity of an antibody.

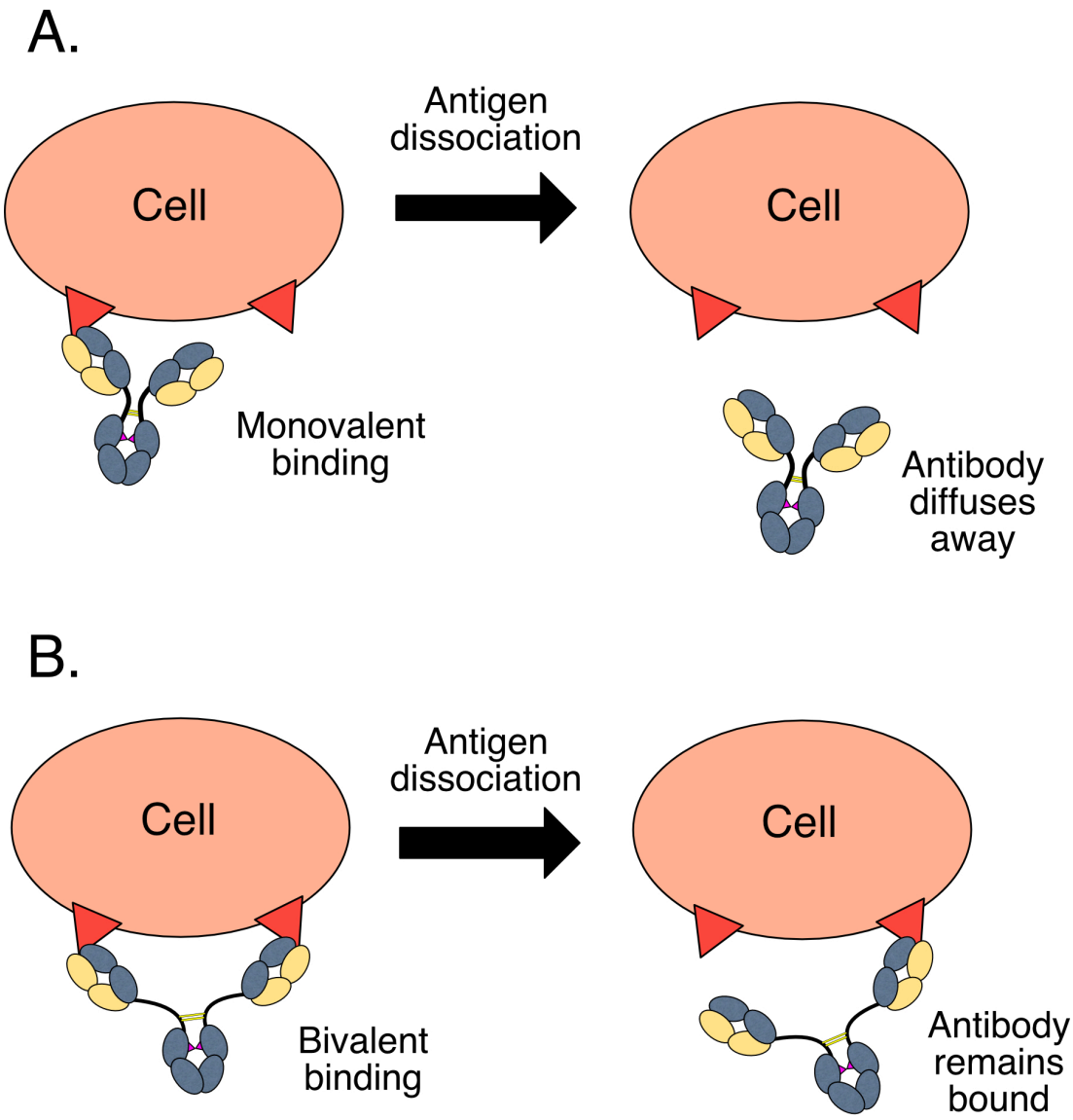

Figure 4.1: A diagram illustrating the advantage of an antibody which has a greater bivalent antigenic distance when the targeted antigen density is low and individual antigen molecules are spaced relatively far apart. **A**) An antibody with shorter bivalent antigenic distance will only bind monovalently to antigen. Upon a single Fab arm dissociation, the antibody would lose the association with target antigen and diffuse away. **B)** An antibody with greater bivalent antigenic distance will bind bivalently to antigen. Upon a single Fab arm dissociation, the antibody remains localised due the remaining Fab arm which may allow the dissociated Fab arm to regain antigen binding. Red triangle represents targeted antigen.

In the past, Tang and colleagues had generated different hIgG1 antibodies capable of recognising an identical epitope on the extracellular domain (ECD) of HER2/*neu* receptor (CD340) but with different antigen binding affinities. These were tested on different tumour cells, which had different expression levels of HER2/*neu* receptor,

to investigate the role of antigen binding affinity and antigen density on ADCC activation (Tang *et al*., 2007). The authors reported that the antibody variants C6.5 and H3B1 exhibited a different tumour surface retention profile in which C6.5 was lower than that of H3B1 after incubation with cells that expressed high levels of surface antigen. The authors suggested that this difference was due to differing antigen intrinsic binding affinity, in which C6.5 had a $K_d = 2.3x10^{-8}M$ whereas H3B1 had a $K_d = 5.6x10^{-10}M$. It was proposed that the higher intrinsic binding affinity of H3B1 allowed it a higher likelihood of bivalent binding due to slower dissociation rate and, in contrast, C6.5 was mainly monovalent binding because either one of the Fab arms was dissociating from its target antigen at a faster rate (Tang *et al*., 2007). Similarly, Velders and colleagues had compared the ADCC activity of two different murine monoclonal antibodies, 17-1A and 323/A3, which could recognise overlapping epitopes on epithelial cell adhesion molecule (Ep-CAM) (Velders *et al*., 1998). Interestingly, 323/A3 had a binding affinity 40-fold higher than 17-1A and by regulating the expression level of Ep-CAM on transfected cells and that the authors reported that 323/A3 outperformed 17-1A in all ADCC assays. It is very likely that the higher binding affinity of 323/A3 increased the antibody surface retention time and maximised antibody effector functions. From a different point of view, the antibody surface retention time could also be increased with improved bivalent binding activity. As a result, structural modifications which could increase the bivalent antigenic distance of an antibody may be highly beneficial.

4.1.2 dsDNA as a molecular "ruler" to measure antibody bivalent antigenic distance

As mentioned above, dsDNA was selected as the molecular "ruler". The reason for

this decision was that in order to accurately measure the bivalent antigenic distance of an antibody, the length of this ruler should be known and it should be possible to manipulate this length. Fortunately, the structure of dsDNA was solved by Watson and Crick in 1953 (Watson and Crick, 1953). Based on the solved structure of DNA, a single complete turn which consists of 10 nucleotides, was determined to have a length of 34Å (3.4nm) (Watson and Crick, 1953). Thus, in a stretch of DNA a single nucleotide would contribute a distance of 0.34nm. This information allows the calculation of the length of any DNA fragment provided the number of basepairs (nucleotides) is known. Since oligonucleotide synthesis can generate short DNA fragments of desired numbers of nucleotides, the length of the dsDNA molecules can be easily manipulated in order to obtain a desired length. dsDNA of short lengths is very stable and rigid in structure. A previous study reported that dsDNA has a persistence length of 50nm (Smith *et al*., 1992). The persistence length of dsDNA is defined as the maximum length of the dsDNA to maintain a rigid linear conformation (Smith *et al*., 1992; Hagerman, 1988). Since this distance was at least 3 fold longer than the reported bivalent antigenic distance of human IgG, dsDNA appears to have the potential as a suitable molecular "ruler" to measure antibody bivalent antigenic distance. Besides the advantage of ease of length modification, dsDNA also offers the capacity to conjugate the 5′ end of both the sense and antisense strands to different compounds such as fluorescent labels or antigens (Zearfoss and Ryder, 2012). In this project, this advantage allowed NIP hapten to be covalently conjugated to the 5′ end of each DNA strand, therefore, generating a bivalent ligand, as shown in Figure 4.2A. Such ligand should facilitate the binding of both Fab arms of an antibody molecule to bind to a single dsDNA fragment, and

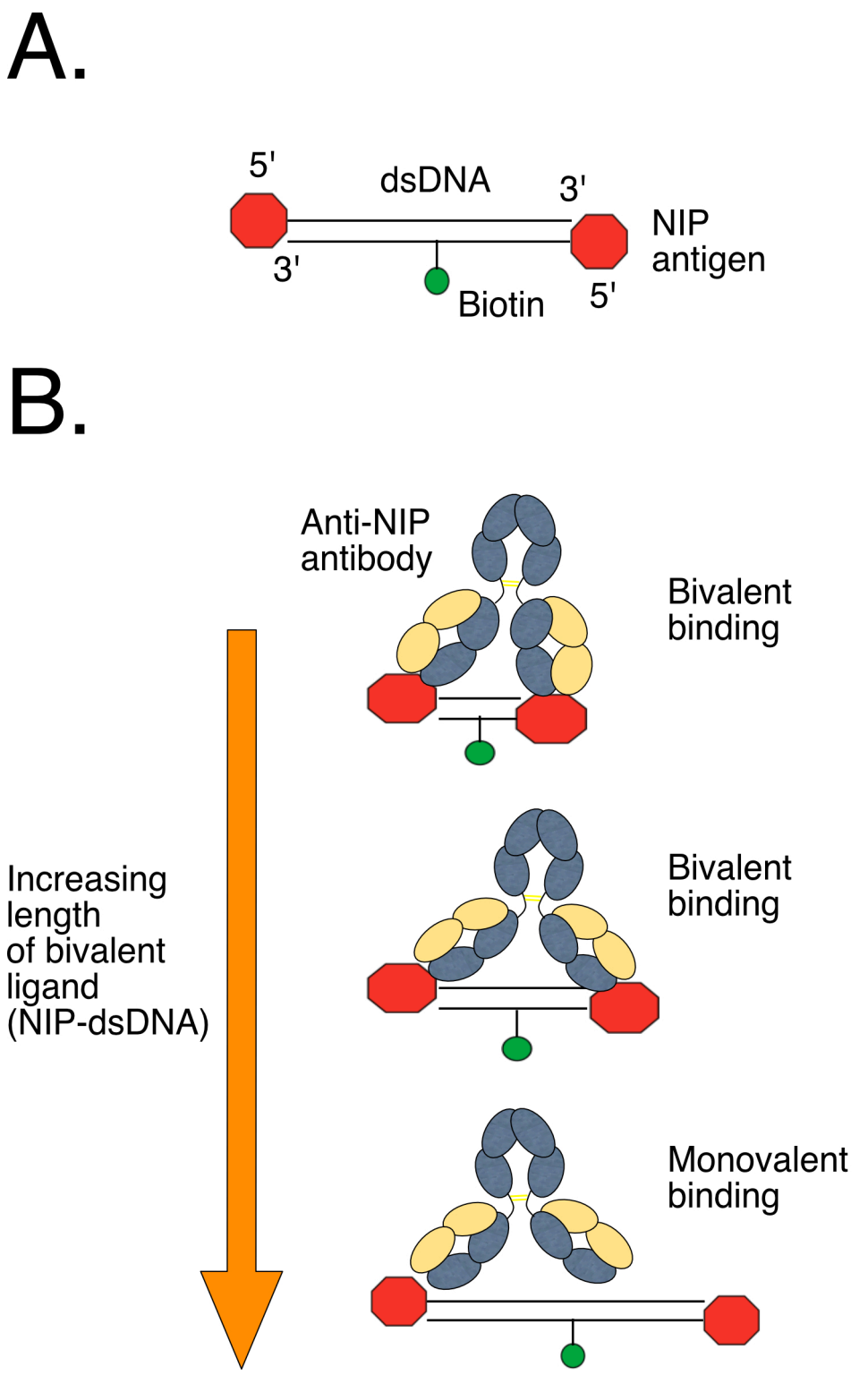

Figure 4.2: The concept of using dsDNA as a molecular "ruler" to measure the bivalent antigenic distance of an antibody. **A**) A bivalent ligand composed of biotinylated dsDNA with NIP antigen covalently attached to both 5´ ends. **B**) Anti-NIP antibody can bind bivalently to short dsDNA bivalent ligand. However, when the length of the dsDNA bivalent ligand is increased beyond the bivalent antigenic distance of the antibody, the binding will change from bivalent to monovalent, which will be an indication of the bivalent antigenic distance of the antibody.

hence, through the use of dsDNA molecules of differing lengths allow the measurement of the bivalent antigenic distance of an antibody by observing the dsDNA length at which binding was monovalent rather than bivalent, as described in Figure 4.2B. This approach gives us a chance to measure the actual functional bivalent antigenic distance which is distinctively different from, and more physiologically relevant than, the reported Fab tip to tip distances which were derived from crystal structures or molecular models.

Once produced, NIP-derivatized dsDNA fragments of desired length could be used in surface plasmon resonance (SPR) analysis (details are described in Chapter 5) that would require the dsDNA to be anchored onto sensor chips. It can be very difficult to immobilise dsDNA onto different surfaces due to its highly negative charge (Watson and Crick, 1953). In order for dsDNA molecules to be anchored in a controlled fashion onto sensor chips, incorporation of a biotinylated deoxythymidine nucleotide was required, shown in Figure 4.2A. The incorporated biotin molecule was designed to allow tight association with streptavidin immobilised onto different surfaces including sensor chips for SPR analysis (Liu and Wilson, 2010). The biotinylated deoxythymidine was positioned in the middle of the dsDNA molecule to minimise any disturbance to the antigen binding sites which were located at both ends of the dsDNA molecule.

4.1.3 Monovalent streptavidin and biotin association

Steptavidin and biotin association is a very tight interaction with a dissociation constant (K_D) in the femtomolar range (Howarth *et al.*, 2006). One streptavidin protein can bind up to 4 biotin molecules (Howarth *et al.*, 2006). As mentioned

above, the approach taken was to use streptavidin to anchor the dsDNA to SPR sensor chip surfaces after streptavidin/biotin association. However, having 4 dsDNAs anchored to each streptavidin molecule would not be ideal and would preclude the function as a molecular "ruler" because it would likely result in multiple antigens in close proximity, rendering any measurement of the bivalent antigenic distance inaccurate. Fortunately, Howarth and colleagues had generated a mutant streptavidin with only one biotin binding site per molecule, named monovalent streptavidin (Mono-Strep) (Howarth *et al*., 2006). Mono-Strep is similar to wildtype streptavidin but 3 of the 4 biotin binding sites had been mutated to abolish their association with biotin (Howarth *et al*., 2006). More importantly, the remaining biotin binding site retains the femtomolar binding affinity towards biotin (Howarth *et al*., 2006). With just one binding site for biotin yet retaining a strong association with biotin, Mono-Strep was the best candidate to be used to anchor the dsDNAs since it would overcome all the difficulties mentioned previously. However, whether the NIP antigens on dsDNA molecules remained accessible for antibody binding after associating with Mono-Strep had yet to be investigated.

4.2 AIMS

This project hypothesised that the longer the upper hinge region the greater the bivalent antigenic distance of an antibody was likely to be. To test this hypothesis, this chapter aimed to evaluate whether dsDNA might be a suitable molecular "ruler". The approach chosen was to generate several dsDNA molecules of different lengths with NIP antigen conjugated to each end and determine whether the NIP antigen could then be recognised by anti-NIP antibody after biotin incorporation and Mono-Strep association.

4.3 MATERIALS AND METHODS

4.3.1 MATERIALS AND BUFFERS

NIP-OSu

4-Hydroxy-3-iodo-5-nitrophenylacetic acid succinimidyl ester (NIP-OSu) was purchased from Cambridge Research Biochemicals.

DNA Annealing buffer

An annealing buffer of 10mM Tris, 50mM sodium chloride, 1mM EDTA, pH 7.5-8.0 was prepared and autoclaved.

5X TBE

A 5X TBE (89mM Tris, 89mM boric Acid, 2mM EDTA) stock was prepared. This stock solution was diluted to 1X with Milli-Q water prior to use.

Molecular weight marker

A suitable molecular weight marker comprising 0.02% (w/v) bromophenol blue and 0.02% (w/v) xylene cyanol in Milli-Q water was prepared.

20bp NIP-DNA oligonucleotides

Two DNA oligonucleotides listed in Table 4.1 were purchased from Biosearch Technologies. Both oligonucleotides were reconstituted at 1mM with Milli-Q water and stored at -20ºC prior to use.

Table 4.1: DNA sequence and modifications of purchased oligonucleotides

	Oligonucleotide	DNA sequence and modifications
1.	20bp	NIP-C6-ATCTCGGTGACGGGCAGGAC 3′
2.	20bp Biotin	NIP-C6-GTCCTGCCCGTCACCGAGAT 3′

Note: Red coloured T represents biotinylated thymidine. C6 represents an amine modified six carbon linker.

45bp and 55bp DNA oligonucleotides

Four DNA oligonucleotides listed in Table 4.2 were synthesised by the Oligonucleotide Synthesis Service (University of Dundee) at a scale of 1μM.

Table 4.2: DNA sequence and modifications of synthesised oligonucleotides

	Oligonucleotide	DNA sequence and modifications
1.	45bp	C6-ATCTCGGTGATCTACTATCGGCATGGCTTACAG TGCGGGCAGGAC 3′
2.	45bp-Biotin	C6-GTCCTGCCCGCACTGTAAGCCATGCCGATAGT AGATCACCGAGAT 3′
3.	55bp	C6-GTCTCGGTGCTCGATCGTACTATCGGCATGGCT TACAGTGCGGGTGAATCAGGAC 3′
4.	55bp-Biotin	C6-GTCCTGATTCACCCGCACTGTAAGCCATGCCG ATAGTACGATCGAGCACCGAGAC 3′

Note: Red coloured T represents biotinylated thymidine. C6 represents an amine modified six carbon linker.

Monovalent streptavidin

Monovalent streptavidin was a gift from Dr. Mark Howarth, University of Oxford.

4.3.2 GENERATION OF NIP-CONJUGATED DNA OLIGONUCLEOTIDES (45bp AND 55bp)

4.3.2.1 Cleavage of DNA oligonucleotide and deprotection of 5′ amino modifiers

Four DNA oligonucleotides listed in Table 4.2 were synthesised by the Oligonucleotide Synthesis Service (University of Dundee). Upon completion of a single DNA oligonucleotide synthesis, two sterile 2ml syringes, one filled with 2ml of 20% diethylamine (Sigma) in acetonitrile (Sigma), were attached to both ends of the synthesis column. The synthesis column was washed by performing a "push-pull" technique for 10 times and allowed to incubate at room temperature for 5 minutes to remove the cyanoethyl group that could react with the free amino group at the 5′ end of the DNA oligonucleotide during the subsequent deprotection procedure. The solution was then discarded and the synthesis column was washed with 2ml of acetonitrile using the same procedure. When done, the solution was discarded and the same procedure was repeated with 2ml volume of air to dry the synthesis column. Using a new pair of sterile 2ml syringes, subsequent cleavage of the DNA oligonucleotide and deprotection of the 5′ amino modifier was carried out simultaneously by performing the "push-pull" technique for 10 times with 2ml of ammonium hydroxide (Sigma) every hour for 3 hours and the synthesis column was kept in the dark at room temperature during the process. Upon completion, the DNA oligonucleotide-containing ammonium hydroxide solution was transferred to a 4ml glass vial (Wheaton®, 224802) and sealed with a cap (Sigma, Z106429). The glass vial was labeled and incubated at 65ºC using a heat block for 2 hours. The vial was then cooled on ice for 10 minutes before transferring the solution into a 2ml

microfuge tube and dried overnight using a SpeedVac Concentrator (SPD111V, ThermoFisher Scientific).

4.3.2.2 NIP hapten coupling

Dried DNA oligonucleotides were resuspended in 200µl of Milli-Q water and the concentration of each was measured using a NanoDrop machine (section 2.4.10). 20nmol of DNA oligonucleotide and 200nmol of NIP-OSu (a ratio of 1:10 DNA/Hapten) were used for the coupling reaction. Each reaction mixture, shown in Table 4.3, was set up in a 1.5ml microfuge tube and incubated overnight at room temperature with shaking at 200rpm on a shaker, Thermomixer F1.5 (Eppendorf).

Table 4.3: Reaction conditions for NIP hapten coupling

Reagent	Volume
Hapten NIP-OSu in DMSO (200nmol)	42 µl
0.1M Sodium tetraborate, pH 8.5	225 µl
DNA Oligonucleotide (20nmol)	12 µl
Milli-Q water	21 µl
Total	**300 µl**

4.3.2.3 DNA acrylamide gel electrophoresis purification

Due to the low molecular weight of the DNA oligonucleotides, a 14% acrylamide gel was used for purification after the coupling procedure. The recipe listed below was used to make one gel.

<u>14% acrylamide gel</u>

Denature gel stock (20% Acrylamide/Bis, 7M Urea in TBE)	42 ml
7M Urea in 1X TBE	18 ml
10% Ammonium persulfate	500 µl
TEMED	25 µl

A vertical slab gel apparatus (C.B.S. Scientific, SG-250-02) was set up according to the manufacturer's instructions. Acrylamide gel solution was poured between the gel plates and a comb was inserted before allowing it to set overnight. Once the gel was ready, the gel plates, which contained the gel, were placed into the apparatus and the tank was filled with fresh 1X TBE buffer. The comb was removed and the apparatus was run without any samples at 650V for 10 minutes to slightly warm up the gel. DNA samples was prepared by adding an equal volume (300µl) of formamide (Sigma) to the DNA oligonucleotide-hapten reaction mixture before being heated to 95ºC for 5 minutes in a heat block, then cooled on ice for 2 minutes. Samples were loaded into respective wells at a maximum volume of 150µl per well. 100µl of molecular weight marker (section 4.3.1) was loaded for size referencing. Samples were run at 650V until the sample marker xylene cyanol reached the bottom of the gel, in about 2.5-3 hours. When the electrophoresis process was completed, the gel plates were removed from the tank and dismantled to expose the gel.

4.3.2.4 DNA oligonucleotide extraction from acrylamide gel

After electrophoresis, the gel was placed on top of a glass TLC plate coated with fluorescent indicator (TLC Silica gel 60 F_{254}, Merck Millipore). The DNA oligonucleotide bands were then viewed using a compact UV lamp (UVGL-25, UVP) and cut out using sterile scalpels. In order to extract the DNA oligonucleotide from the excised gel piece, a Unidirectional Electroelutor (International Biotechnologies, Inc) was set up according to the manufacturer's instructions. The tank was filled with 1X TBE buffer while the reservoir for DNA collection was filled with 140µl of 8M ammonium acetate. The gel pieces containing DNA were placed onto their respective wells and the device was run at 150V for 45 minutes. Upon completion, DNA-

containing 8M ammonium acetate was recovered and transferred into a 1.5ml microfuge tube. 1ml of 100% ethanol was added to each tube and incubated at -20ºC for at least 1 hour to precipitate the oligonucleotide before being dried overnight using a SpeedVac Concentrator (SPD111V, ThermoFisher Scientific).

4.3.2.5 Purification of DNA using High Performance Liquid Chromatography (HPLC)

Dried DNA oligonucleotides were reconstituted in 200µl of 5% acetonitrile in 0.1M Triethylammonium acetate (TEAA). High Performance Liquid Chromatography (HPLC) was performed to separate the NIP-conjugated DNA oligonucleotides from the unconjugated ones. Details of the HPLC apparatus were listed in Table 4.4. 5% acetonitrile in 0.1M TEAA was used as the initial running buffer and 200µl of DNA sample was injected into the system and binding allowed to occur before being eluted with an increasing gradient of acetonitrile. The absorbance of the DNA sample was measured at 260nm. The fractions of DNA oligonucleotide that had successfully been conjugated to NIP hapten were collected into a 1.5ml microfuge tube. The tubes were then placed into a SpeedVac Concentrator (SPD111V, ThermoFisher Scientific) and allowed to dry overnight. Dried NIP-DNA oligonucleotides were reconstituted in 15µl of Milli-Q water and the concentration for each was determined using a NanoDrop machine (section 2.4.10).

Table 4.4: Details of the HPLC devices used

HPLC Components	Product details
Pump	Dionex P680 HPLC Pump
Detector	Dionex PDA-100 Photodiode Array Detector
Column	Ace 10 C18-300

4.3.3 CHARACTERISATION OF NIP-CONJUGATED DNA

4.3.3.1 Formation of dsDNA

To ensure that all biotin-derivatised ssDNA would form dsDNA, the unbiotinylated ssDNA strand was added in slight excess during the generation of dsDNA. In each case, 55µl of 20µM unbiotinylated oligonucleotide strand and 50µl of 20µM biotinylated DNA strand were prepared in DNA annealing buffer (section 4.2.1) in 0.5ml microfuge tubes respectively. Each strand was then mixed with its complementary strand to produce a final volume of 105µl of approximately 10µM DNA. To generate dsDNA, the DNA mixtures were then heated to 95ºC for 5 minutes, in a Mastercycler personal PCR machine (Eppendorf), and allowed to cool to room temperature for 1 hour. The tubes were then briefly centrifuged and were ready for analysis or to be stored at -20ºC.

4.3.3.2 DNA polyacrylamide gel electrophoresis

A Bio-Rad Mini Protean II apparatus was set up according to the manufacturer's instructions. 20% polyacrylamide gel solution, shown in Table 4.5, was poured into gel plates and a comb was inserted before allowing the solution to solidify. Once the gel had solidified, the gel plates were placed into the apparatus and the tank was filled with fresh 1X TBE buffer and the comb removed. An appropriate volume of 10X BlueJuice™ Gel Loading Buffer (Invitrogen, 10816-105) was added to 200ng of each prepared DNA sample to a final 1X concentration prior to loading into the gel. 10µl of molecular weight marker (section 4.3.1) was loaded for size referencing. The gel was electrophoresed using a Power Pack 3000 (Bio-Rad) at 170V for 2-3 hours.

Table 4.5: Recipe for 20% DNA polyacrylamide gel

Components	Volume required for 20% Gel
1X TBE	4.85 ml
Acrylamide/bis (30%)	10 ml
10% Ammonium persulfate	150 µl
TEMED	6 µl

4.3.3.3 Staining of DNA gel

When the electrophoresis process was completed, the gel plates were removed from the tank and dismantled to expose the gel. The gel was then incubated in 50ml 1X SYBR® Safe DNA gel stain (Invitrogen, S33102) for 1 hour before viewed using a GelVue UV Transilluminator (Syngene).

4.3.3.4 ELISA analysis

Different concentrations (0.0-1.0µM and 2.0µM) of 20bp NIP-dsDNA and Mono-Strep were prepared in ELISA coating buffer (section 2.7.1). For a single well, 50µl of 20bp NIP-dsDNA and 50µl of Mono-Strep were mixed together at the same molarity and allowed to associate for 1 hour at room temperature. When completed, the mixture was coated onto a well of a 96 well Maxisorp ELISA plates (Nunc) as described in section 2.8.9. ELISA coating buffer alone and 1µM Mono-Strep (without DNA) were used in control wells. ELISA analysis was carried out as described in section 2.8.9. 20µg/ml of anti-NIP wildtype hIgG1 was used as primary detecting antibody and anti-mouse lambda light chain HRP (Table 2.1, No.1) was used as secondary detecting antibody.

4.4 RESULTS

4.4.1 Conjugation of NIP-hapten to DNA and purification of NIP-DNA

The separation of NIP-conjugated and unconjugated DNA oligonucleotides during purification using HPLC might be anticipated to be challenging due to the small molecular weight of NIP, which was around 420Da, when compared to those of the 45bp and 55bp DNA oligonucleotides, which were around 14kDa and 17kDa respectively. To resolve this, both unconjugated and NIP-conjugated 45bp DNA oligonucleotide samples were injected to the HPLC system for a test run and the results of DNA sample elution were compared to determine if the HPLC system would be suitable for the DNA purification. The result of the DNA elution comparison from HPLC for unconjugated and NIP-conjugated 45bp DNA oligonucleotides is shown in Figure 4.3. Surprisingly, the elution times for the unconjugated and NIP-conjugated 45bp DNA oligonucleotides were significantly different, as shown in Figure 4.3, allowing for easy purification. Two defined peaks were observed for the NIP-conjugated sample indicating the presence of both residual unconjugated DNA and the major NIP-conjugated DNA product. As indicated in Figure 4.3, the DNA peak eluting at 12 minutes has the same elution time as the control unconjugated 45bp DNA oligonucleotide, confirming that the DNA eluted at this timepoint was unconjugated DNA. In comparison, the DNA peak that was eluted at 15 minutes had a higher molecular weight, consistent with the identity of this particular fraction being NIP-conjugated DNA.

After determining that the separation and purification of the NIP DNA samples was possible, HPLC purification of all four oligonucleotides, 45bp NIP DNA, 45bp NIP

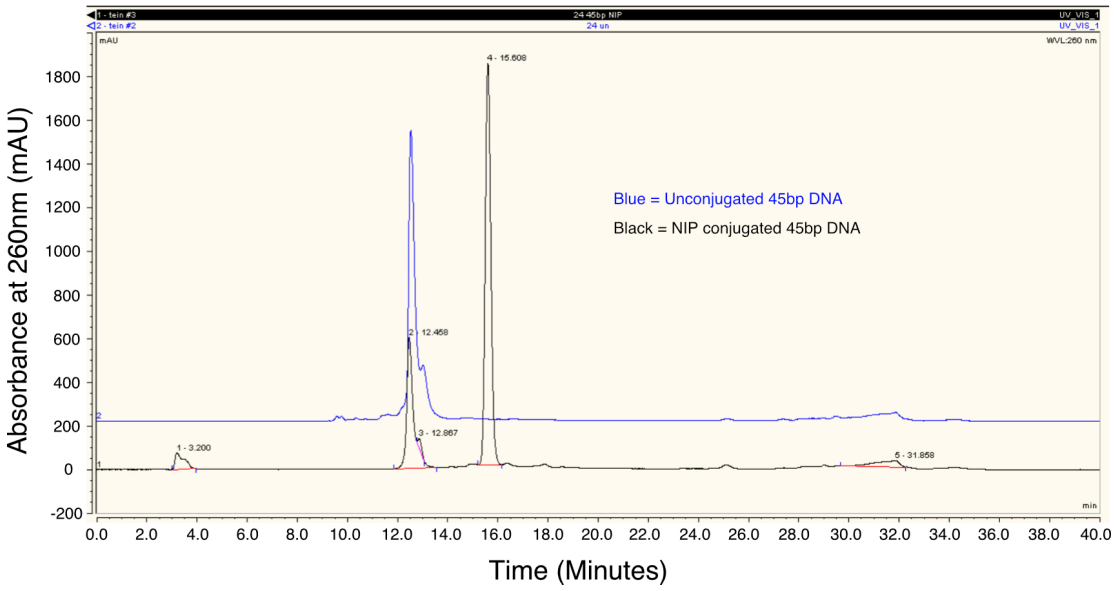

Figure 4.3: A comparison of HPLC elution profiles of unconjugated and NIP-conjugated 45bp DNA samples. Blue trace, unconjugated; black trace, NIP-conjugated.

Biotin DNA, 55bp NIP DNA and 55bp NIP Biotin DNA, was carried out. The elution profiles of each DNA sample purified using HPLC chromatography is shown in Figure 4.4. The results obtained for all DNA samples were very similar to that shown in Figure 4.3 where two major peaks were seen. The DNA fractions comprising the second peak were collected as the NIP-conjugated fraction. These samples were then dried and reconstituted in Millipore water. The concentration of the recovered NIP-conjugated DNA was around 14-16 nmol in each case, suggesting that around 75% of each initial DNA sample became conjugated with NIP hapten. Some minor peaks were also evident during the purification as shown in Figure 4.4. However, these were most likely degraded DNA fragments or other minor contaminations.

4.4.2 Formation of double stranded DNA

After formation of dsDNA, samples were analysed on 20% polyacrylamide gels

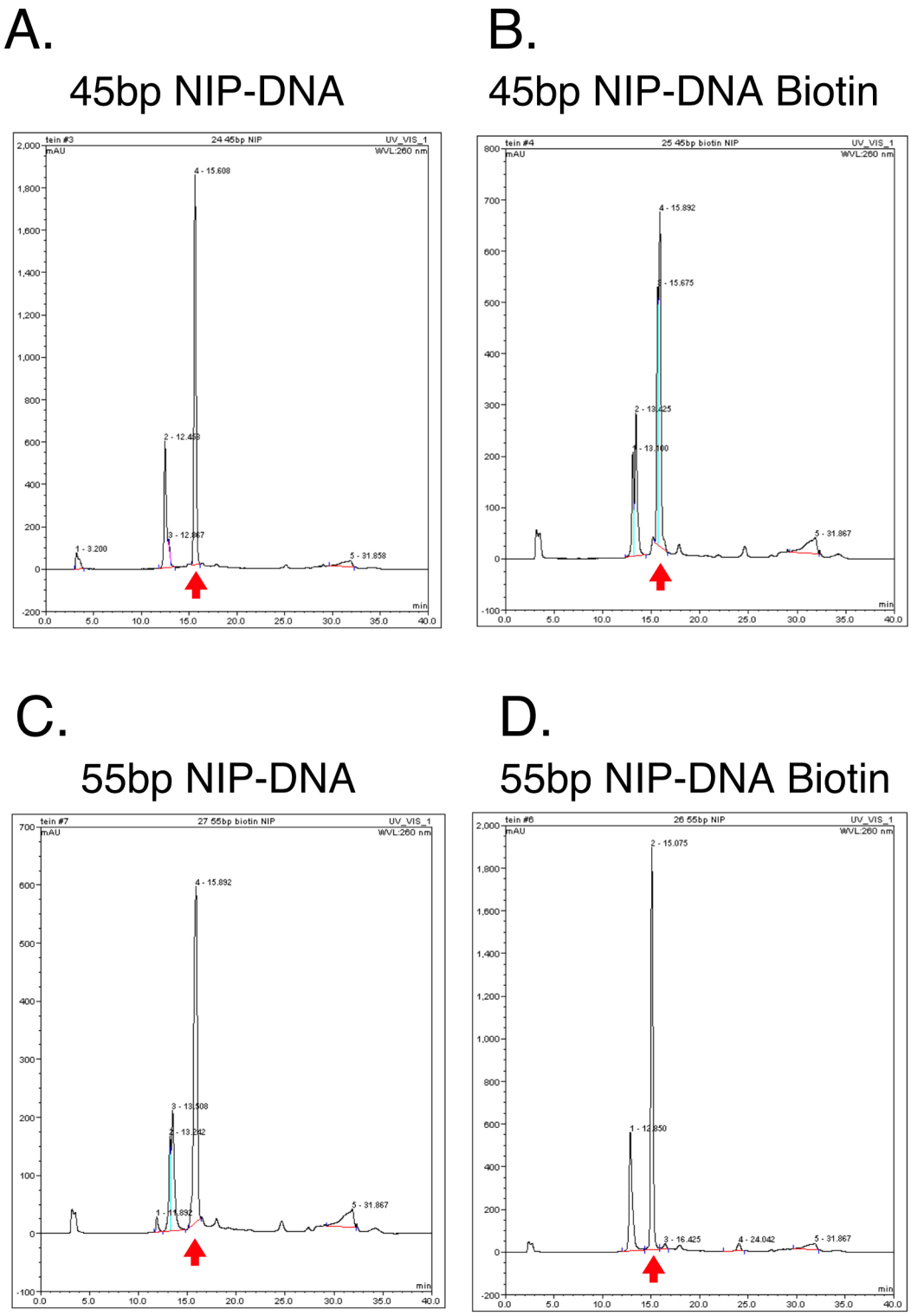

Figure 4.4: HPLC chromatography profiles of different DNA samples. Red arrow indicates the fractions that were purified. **A**) 45bp NIP-DNA. **B**) 45bp NIP-DNA Biotin. **C**) 55bp NIP-DNA. **D**) 55bp NIP-DNA Biotin.

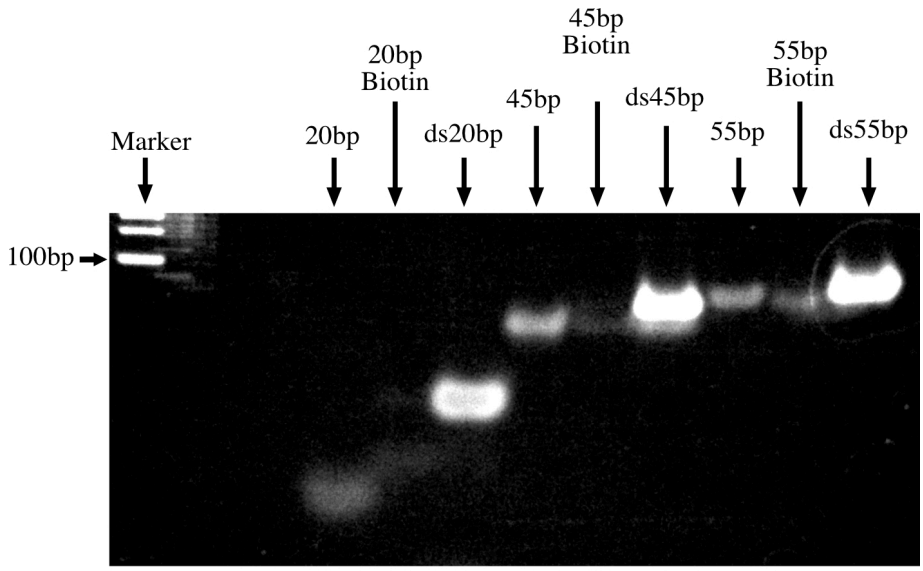

Figure 4.5: Polyacrylamide DNA electrophoresis. DNA was stained with SYBR Safe DNA Gel Stain. Marker; DNA molecular weight markers. 20bp, 20bp ssDNA; 20bp Biotin, biotinylated 20bp ssDNA; ds20bp, 20bp dsDNA; 45bp, 45bp ssDNA; 45bp Biotin, biotinylated 45bp ssDNA; ds45bp, 45bp dsDNA; 55bp, 55bp ssDNA; 55bp Biotin, biotinylated 55bp ssDNA; ds55bp, 55bp dsDNA.

(Figure 4.5). dsDNA of 20bp, 45bp and 55bp was seen to have been successfully generated as demonstrated by the products having significantly larger molecular weights than either of their respective parent ssDNAs. The difference in the molecular weight between the parent 55bp ssDNA and the product 55bp dsDNA, shown in Figure 4.5, was less marked but still apparent. A 14% polyacrylamide gel had been attempted to provide a more distinctive separation between these species. However, the result was not ideal as severe smearing was observed for both 45bp and 55bp dsDNA. Due to the limited amount of NIP-conjugated DNA further attempts were not attempted. In addition, the success of dsDNA formation was also supported by the fluorescent intensity of the dsDNA bands, shown in Figure 4.5 lane ds20bp, ds45bp and ds55bp, which were stronger than those of the corresponding ssDNA bands, since the staining reagent is reported by the manufacturer to exhibit higher binding to dsDNA than ssDNA. The result from Figure 4.5 also indicated that the DNA staining reagent bound less well to biotinylated ssDNA as shown by the

significantly weak fluorescent intensity, especially in lane 20bp Biotin which was barely visible. The reason for this may be due to the presence of biotin, positioned at the middle of the ssDNA, which might have caused some disturbance to the binding of the staining reagent. Nonetheless, the successful formation of dsDNA indicated that the generation of a bivalent molecular "ruler" could be achieved. The subsequent step would be to determine if the NIP conjugated to DNA could be recognised by anti-NIP antibodies.

4.4.3 The estimated length of each of the DNA fragment

The length of each DNA fragment was calculated based on the solved DNA structure where a single complete turn, consisting of 10 nucleotides, was determined to have a length of 34Å (3.4nm) (Watson and Crick, 1953) and the length of the 6 carbon linker chain based on a Carbon-Carbon bond length reported to be 1.54Å (0.154nm) (Pauling and Brockway, 1937) and the result is shown in Table 4.6. The overall estimated length of 20bp NIP-dsDNA was 7.57nm, 45bp NIP-dsDNA was 16.06nm and 55bp NIP-dsDNA was 19.47nm.

Table 4.6: Estimated length of each DNA fragment

Number of DNA base pairs	dsDNA length[A] (nm)	One 6 Carbon linker (C6) length[B] (nm)	Total estimated length (nm)
20	6.8	0.77	7.57
45	15.3	0.77	16.07
55	18.7	0.77	19.47

Note: [A] The estimated overall length of dsDNA not including C6 or NIP antigen, based on 0.34nm per nucleotide (Watson and Crick, 1953).

[B] The estimated length of the 6 carbon atom linker, based on a C-C distance of 0.154nm i.e. 5 x 0.154 (Pauling and Brockway, 1937).

4.4.4 NIP-dsDNA antigen recognition

In order for the NIP-dsDNA to be used as a molecular "ruler", the NIP antigens covalently conjugated to the DNA have to be able to be bound by an anti-NIP antibody. Generated 20bp NIP-dsDNA antigen recognition was analysed using ELISA and the result is shown in Figure 4.6. Anti-NIP wt hIgG1 appeared to be able to bind to NIP antigen conjugated to 20bp dsDNA that had formed a complex with Mono-Strep (NIP-dsDNA/Strep) as evidenced by the significant difference (almost two-fold) in absorbance level between sample wells coated with 0.5μM, 1.0μM and 2.0μM 20bp NIP-dsDNA/Strep and the control wells. The anti-NIP wt hIgG1 was specific for NIP antigen and had no or very little non-specific binding to monovalent streptavidin as shown by the low absorbance level of control wells coated with 1.0μM monovalent streptavidin alone. It was noticed that coating of different concentrations of 20bp NIP-dsDNA/Strep resulted in very similar absorbance levels, as seen in Figure 4.6. This finding suggested that the sample wells might have been saturated with 20bp NIP-dsDNA/Strep at all concentrations, limiting the amount of antibody able to bind. To resolve this issue, a similar ELISA analysis but with lower concentrations of 20bp NIP-dsDNA/Strep was carried out to check if a 'dose-response' curve could be achieved. The result of this analysis is shown in Figure 4.7. Surprisingly, a maximum absorbance level was achieved when coating 20bp NIP-dsDNA/Strep at a concentration of around 0.4μM, and increasing concentrations of coating material beyond this point did not appear to result in higher levels of anti-NIP antibody binding. This result suggested that the sample well may be saturated at a concentration of 0.4μM 20bp NIP-dsDNA/Strep and due to the limited availability of NIP antigen molecules (only two per complex) the corresponding low levels of anti-NIP antibody binding resulted in low absorbance levels. Nonetheless, the

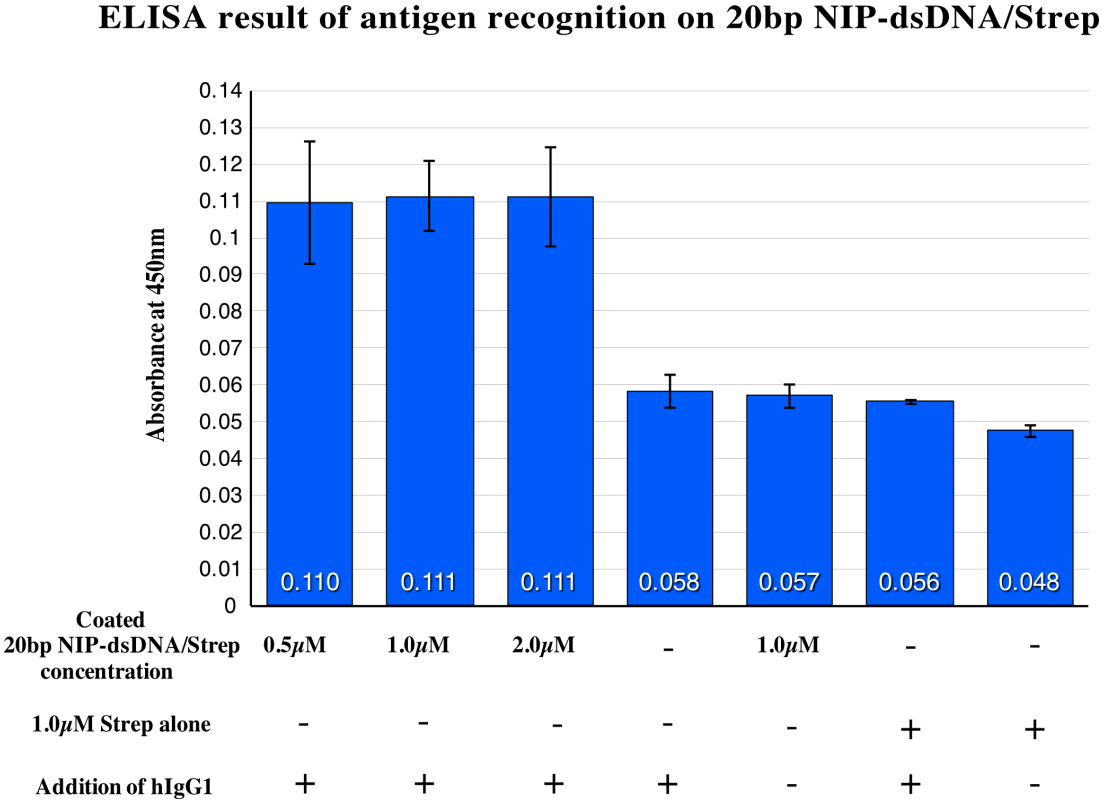

Figure 4.6: ELISA result of antigen recognition of 20bp NIP-dsDNA/Strep by anti-NIP wt hIgG1. Either different concentrations of 20bp NIP-dsDNA/Strep (0.5μM, 1.0μM and 2.0μM), 1.0 mM Strep alone, or buffer only were coated onto sample wells and 20μg/ml of anti-NIP wildtype hIgG1 was incubated to allow binding. Anti-mouse lambda light chain-HRP was used to detect antibody binding. +/- represented the addition or absence of particular protein. The results shown are the average of duplicate determinations, and the bars represent standard deviation measurements. A representative experiment of 3 is shown.

successful detection of bound anti-NIP wt hIgG1 confirmed that the recognition site of NIP antigen was not hindered by the structure of the dsDNA and Mono-Strep and that the generation of a molecular "ruler" for measuring an antibody bivalent antigenic distance had been successful.

4.5 DISCUSSION

As mentioned previously, the free movements of the Fab arms to conduct better positioning for antigen binding are mainly governed by the length and flexibility of the region between the end of the CH1 domain and the first inter-heavy chain disulphide bridge, i.e. the upper hinge region for IgG. Therefore, the maximum

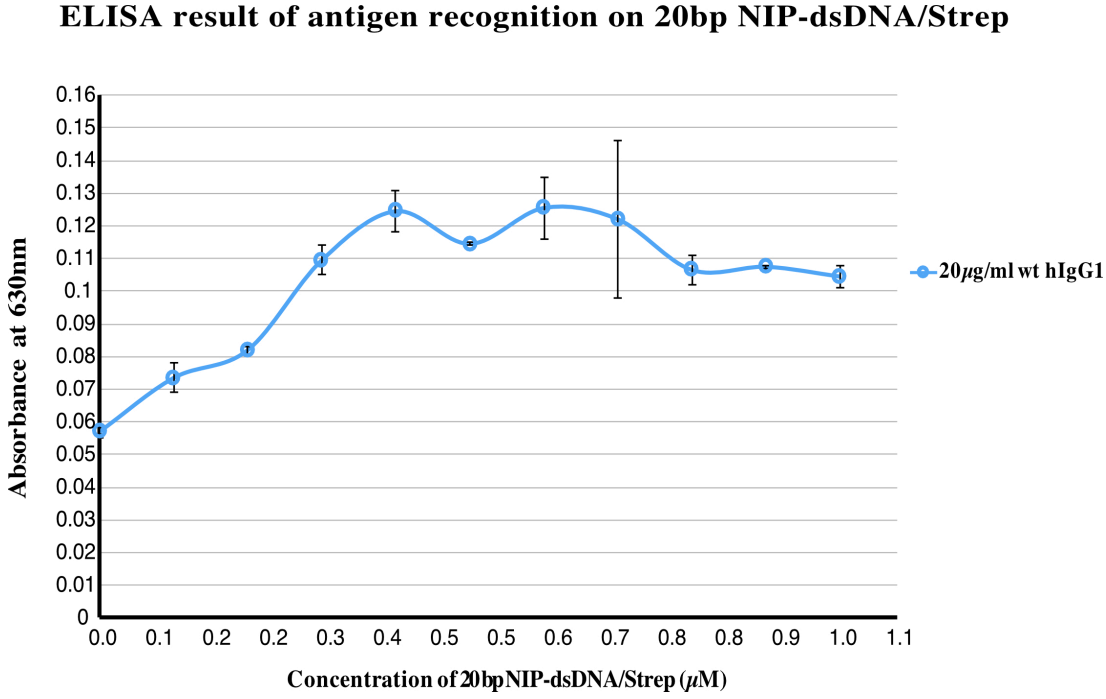

Figure 4.7: ELISA result of antigen recognition of 20bp NIP-dsDNA/Strep by anti-NIP wt hIgG1. Different concentrations of 20bp NIP-dsDNA/Strep (0.0-1.0μM) were coated onto sample wells and 20μg/ml of anti-NIP wildtype hIgG1 was incubated to allow binding. Anti-mouse lambda light chain-HRP was used to detect antibody binding. The results shown are the average of duplicate determinations, and the bars represent standard deviation measurements. A representative experiment of 3 is shown.

distance of antigen binding between two Fab arms of an IgG antibody would be expected to be dependent on the length and flexibility of the upper hinge region. It was hypothesised that the longer the upper hinge region of an IgG the further the Fab arms may be spaced away from the Fc region, thus granting a greater bivalent antigenic distance. To test this hypothesis, a molecular "ruler" is required in order to be able to accurately determine the bivalent antigenic distance of IgG antibodies with different upper hinge lengths. This chapter aimed to test whether dsDNA might serve as a suitable molecular "ruler" and has successfully confirmed that dsDNA is a reasonable choice for this role because the length of dsDNA can be easily manipulated and calculated and, more importantly, the target antigen can be conjugated to the 5′ ends of the dsDNA, thus, producing a bivalent ligand.

As mentioned in the Introduction (section 4.1), the Fab tip to tip distance of hIgA1 was reported to be 17nm (Boehm *et al*., 1999). This project has generated new mutant hIgG1 antibodies with either the whole or partial hIgA1 hinge region incorporated. Hence, the length of the molecular "rulers" had to be carefully designed in order to be suitable for sensing differences in the bivalent binding of these antibodies to antigen. This project produced three different dsDNA products with lengths of 20bp, 45bp and 55bp, each with NIP hapten covalently conjugated to the 5′ end of each strand. Given the double stranded nature of DNA, there should be two NIP haptens attached to each DNA product, representing a bivalent molecular "ruler". The overall estimated length of 20bp NIP-dsDNA was 7.57nm, that of 45bp NIP-dsDNA was 16.06nm, and that of 55bp NIP-dsDNA was 19.47nm. The lengths of all three dsDNA products were well below the reported dsDNA persistence length of 50nm (Smith *et al*., 1992; Hagerman, 1988). Therefore, all three should maintain a rigid linear structure, suitable for providing an accurate length measurement.

20bp NIP-dsDNA with an estimated length of 7.57nm was designed so that all the antibodies generated in this project, especially wt hIgG1 which has the shortest predicted hinge length, would be able to bind bivalently. In contrast, the longer NIP-dsDNAs were designed with the hope that they might serve to distinguish between the bivalent binding abilities of the different antibodies, such that we might encounter a condition where some of the antibodies were only able to bind monovalently. In particular, 55bp NIP-dsDNA (19.47nm) was designed with length surpassing the estimated bivalent antigenic distance of hIgA1 (~17nm) so that, at least wt hIgG1 antibody would not be able to bind bivalently to this ligand. This

allows an easier approach in the interpretation of monovalent binding in subsequent analyses.

Antibody binding to antigens conjugated to dsDNA had been reported in the past (Paar *et al*., 2002). Paar and colleagues generated several DNP-dsDNA molecules ranging from 3.1nm to 10.2nm in length and showed that bivalent DNP-dsDNA of length around 4.4-5.1nm were able to stimulate mast cell degranulation, via binding of anti-DNP human IgE. In constrast, bivalent ligands of length above 6.8nm were unable to do so (Paar *et al*., 2002). The NIP-dsDNA molecules generated in this chapter share similar features to the DNP-dsDNA mentioned in the previous investigation except for the differing antigens, the additional biotin incorporation and the Mono-Strep association. Fortunately, the NIP antigen conjugated to dsDNA was shown to be recognisable by anti-NIP wt hIgG1 after incorporation of the biotin molecule and complex formation with Mono-Strep. This finding paved the way for the usage of these NIP-dsDNA molecules for subsequent SPR analyses in Chapter 5.

One possible alternative approach to measure the bivalent antigenic distance of an antibody would be the use of molecular printing, which transfers molecules or materials to a suitable surface in molecular scale, ranging from sub-50-nm to μm (Braunschweig *et al*., 2009). The advance technology of molecular printing has allowed the transfer of DNA proteins, peptides, polymers, and metal ions onto many types of surfaces (Braunschweig *et al*., 2009; Torres *et al*., 2011). As a result, molecular printing might be able to "print" targeted antigen at defined distances to investigate the bivalent antigenic distance of an antibody. Orth and colleagues had used a molecular printing technique to generate a patterned lipid bilayer containing

2,4-dinitrophenyl (DNP) antigens, distanced from 1.5μm to 60μm apart, and showed that anti-DNP IgE could bind these patterned antigens through fluorescence imaging (Orth *et al*., 2003). One concern of using molecular imaging would be the cost of production and the availability of the involved machineries. In addition, whether the antigen could be printed at a distance of 5-20nm has to be confirmed as the bivalent antigenic distance of IgG would be expected to fall within this range. In contrast, the dsDNA used in this project is very cost-effective compared to the materials used in molecular printing and the distance between two adjacent antigens could start as short as 3.4nm, which is 10bp, up to 50nm, which is the limit of the reported DNA persistent length. Therefore, using DNA is definitely an ideal approach.

Another approach to tackle the measurement of the bivalent antigenic distance of an antibody would be to adapt the model used by Sosnick et al (1992) in which X-ray and neutron scattering was performed on antibodies that had formed a complex with deuterated antigens (Sosnick *et al*., 1992). Due to the differing neutron scattering length of hydrogen and deuterium, the bivalent antigenic distance of an antigen bound antibody could be determined (Sosnick *et al*., 1992). In this case, we could generate a similar dsDNA bivalent ligand of differing lengths with deuterated antigen covalently attached and subject the generated antigen-antibody complex to X-ray and neutron scattering analyses to determine the bivalent antigenic distance of the antibody. However, the dissociations of antibody from antigen has to be taken into consideration, but this obstacle might be overcome by using antigens with high binding affinity with specific antibodies to reduce overall dissociation rate. Another concern of this approach would be the generation of an antibody binding with two individual bivalent ligands or polymeric immune complexes consisting of multiple

antigen-antibody linked to each other. Both formations would cause the measurement to be inaccurate. Nonetheless, having alternative options is always advantageous as conducting different studies can help to strengthen the validity of a finding.

CHAPTER FIVE
FUNCTIONAL ANALYSES OF RECOMBINANT ANTIBODIES

CHAPTER 5. FUNCTIONAL ANALYSES OF RECOMBINANT ANTIBODIES

5.1 INTRODUCTION

The previous chapter described the role of NIP-dsDNA molecules as molecular "rulers" to estimate the bivalent antigenic distances of different antibodies. This chapter will describe utilisation of the generated dsDNA molecules for such measurement. The procedure involves the association of the generated NIP-dsDNA molecules with Mono-Strep, which had been previously immobilised onto sensor chips, to form a protein complex for surface plasmon resonance (SPR) analyses, which is capable of detecting real-time antibody-antigen association and dissociation (Nguyen *et al*., 2015; Torreri *et al*., 2005; Homola *et al*., 1999; Adamczyk *et al*., 2000; MacKenzie *et al*., 1996). As described previously, it was expected that an antibody molecule capable of binding bivalently to immobilised antigens should have a longer dissociation time compared to an antibody molecule bound monovalently to a single antigen molecule. Applying the same principle to NIP-dsDNA, it might be predicted that if the NIP-dsDNA was too long (i.e. the NIP molecules are spaced too far apart) for an antibody molecule to bind bivalently, the antibody molecule would tend to dissociate much more readily than when bound to a shorter NIP-dsDNA since it will be binding predominantly in a monovalent fashion. Therefore, by observing the association and dissociation of antibody binding to different lengths of NIP-dsDNA via SPR, estimates of the range of bivalent antigenic distance of each generated antibody may be determined. If the NIP-dsDNA molecular ruler model was proven to be successful, this would allow the determination of the range of bivalent antigenic distances of several different wildtype antibodies, such as IgM, IgE, IgA, IgD and IgG, in future investigations. In

addition, it should be possible to use similar antigen-dsDNA models to determine the optimal antigen binding distance to achieve maximum effector effect from bispecific antibodies and BiTE molecules, as described in Chapter 1, which interact with two different target antigens bound at close proximity.

Target cell-effector cell bridging by antibody molecules is likely to be exceptionally important for pathogen clearance. When invading pathogens are opsonised by antibodies they may be efficiently cleared by Fc-bearing effector cells, such as macrophages, natural killer cells and neutrophils, through ADCC (Schroeder Jr and Cavacini, 2010; Desjarlais and Lazar, 2011; Lazar *et al*., 2006; Tang *et al*., 2007). However, these antibody effector mechanisms required the Fc region of the antibody to interact with corresponding Fc receptors (Dilillo and Ravetch, 2015; Lazar *et al*., 2006; Lu *et al*., 2015; Schroeder Jr and Cavacini, 2010). As a result, having a better target cell-effector cell bridging efficiency would improve pathogen clearance by the immune system.

There were several Fcγ receptors expressed by immune cells, as described in Chapter 1. Each has its own antibody binding profile (Woof and Burton, 2004; Bruhns *et al*., 2009). For example, the relative binding affinity of human FcγRI for the human IgG subclasses is IgG1 = IgG3 > IgG4 >> IgG2 (Woof and Burton, 2004). Interestingly, Redpath and colleagues generated a mutant human IgG3 with a shortened hinge and showed that it had reduced binding to FcγRI compared to wt IgG3 (Redpath *et al*., 1998), which suggested that the length of the hinge region might play a role in enabling optimal FcγRI interaction. In addition, Goh and colleagues generated a matched set of human IgG antibodies of different subclasses and compared their

ability to induce phagocytosis by THP-1 cells (Goh *et al*., 2011). The authors reported that IgG3 elicited a higher bacterial uptake by phagocytosis after bacterial opsonisation than IgG1 (Goh *et al*., 2011). IgG3 has the longest hinge region among all human IgGs, therefore, it is possible that the extra hinge length allowed IgG3 to better adopt a favourable conformation for optimal FcγR binding to induce phagocytosis. However, the argument regarding the difference in the amino acid composition of the constant regions between the IgG subclasses remained valid. The constant regions of different IgG subclasses do not share identical amino acid sequences (Burton, 1987) and, more importantly, variable region structure and function has been reported to be affected by the constant domains of different IgG subclasses (Janda *et al*., 2012; Janda *et al*., 2016). Therefore, keeping identical constant regions of antibody might be crucial in certain structural investigations. The hinge mutants generated in this project have identical constant domains, therefore, it is reasonable to seek to determine whether the structural modification of upper hinge extension in IgG might have an effect on target cell-effector cell bridging. The approach in investigating target cell-effector cell bridging by antibody molecules will be further described below.

5.1.1 Surface plasmon resonance (SPR) analyses

SPR utilises an optical technique to measure the refractive index changes in the vicinity of a thin metal layer resulting from changes in the mass of molecules associated with the layer (Nguyen *et al*., 2015; Homola *et al*., 1999; Torreri *et al*., 2005). Therefore, when an association occurs any changes are immediately recorded. SPR had been used in a variety of applications to determine the interactions and binding affinities of different ligands and analytes including protein-protein, protein-

DNA, receptor-drug, and virus-protein interactions (Homola *et al*., 1999; Nguyen *et al*., 2015; Torreri *et al*., 2005). In this chapter, NIP-dsDNA could not be immobilised directly onto the sensor chip due to DNA and the sensor chip surface being highly negatively charged, thus, repulsion will occur. Therefore, Mono-Strep was firstly immobilised onto the CM5 sensor chip at a low density. NIP-dsDNA was then introduced to allow association with Mono-Strep via the incorporated biotin molecule. The rationale for immobilising Mono-Strep at a low density was to ensure that on average each Mono-Strep molecule is likely to be positioned at some distance away from each other so that the likelihood of an antibody molecules being able to bind to two adjacent immobilised NIP-dsDNA molecules could be kept very low. Such an incidence is illustrated in Figure 5.1. As mentioned previously, the length of each NIP-dsDNA molecule, at either 20bp, 45bp or 55bp, was designed according to the previously reported Fab tip to tip distances of immunoglobulins. In brief, 20bp NIP-dsDNA was designed in order to enable all the antibodies under test to bind bivalently, 45bp NIP-dsDNA was designed in order to enable antibodies with longer reach to bind bivalently, and 55bp NIP-dsDNA was designed such that none of the antibodies would be likely to bind bivalently. Monovalent binding and bivalent binding should be differentiated from SPR analysis by monitoring the dissociation curve. It was expected that bivalent binding would present a slower dissociation rate due to longer antigen association time, as mentioned earlier. In contrast, monovalent binding should present a faster dissociation rate compared to bivalent binding due to shorter antigen association time. Therefore, SPR should enable investigation of the bivalent antigenic distance of each antibody under test.

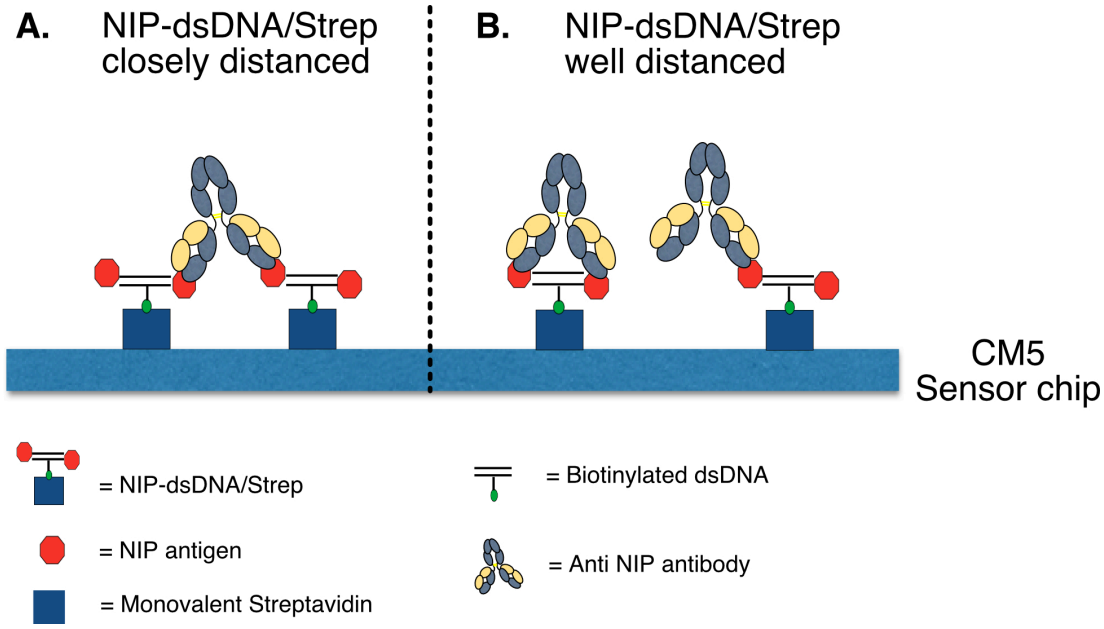

Figure 5.1: A schematic diagram of different scenarios following monovalent streptavidin immobilisation on a CM5 sensor chip. A. A scenario where monovalent streptavidin is immobilised at close proximity to each other (high density) allowing an anti-NIP antibody to bind to two adjacent NIP-dsDNA molecules. B. A scenario where monovalent streptavidin was immobilised at positions more distance to each other (low density), such that an anti-NIP antibody is able to bind to only one NIP-dsDNA molecule. Scenario B is that which the experimental approach was designed to achieve.

5.1.2 Rosette Test

This chapter hypothesised that an increase in the upper hinge length of IgG1 would tend to also increase the target cell-effector cell bridging efficiency of an IgG1 antibody due to the extra reach and possibly flexibility granted through the upper hinge extension. To investigate this hypothesis, a rosette test was performed. The surface of sheep red blood cells were derivatised with NIP-hapten and coated with different concentrations of anti-NIP antibodies before being incubated with THP-1, a human monocytic cell line, that expresses both FcγRI and FcγRII (Fleit and Kobasiuk, 1991) to generate rosettes. The association between sheep red blood cells and Fab arms, via NIP antigen binding, and between the Fc region and Fcγ receptors, expressed on the surface of THP-1, would hold both cells closely associated to

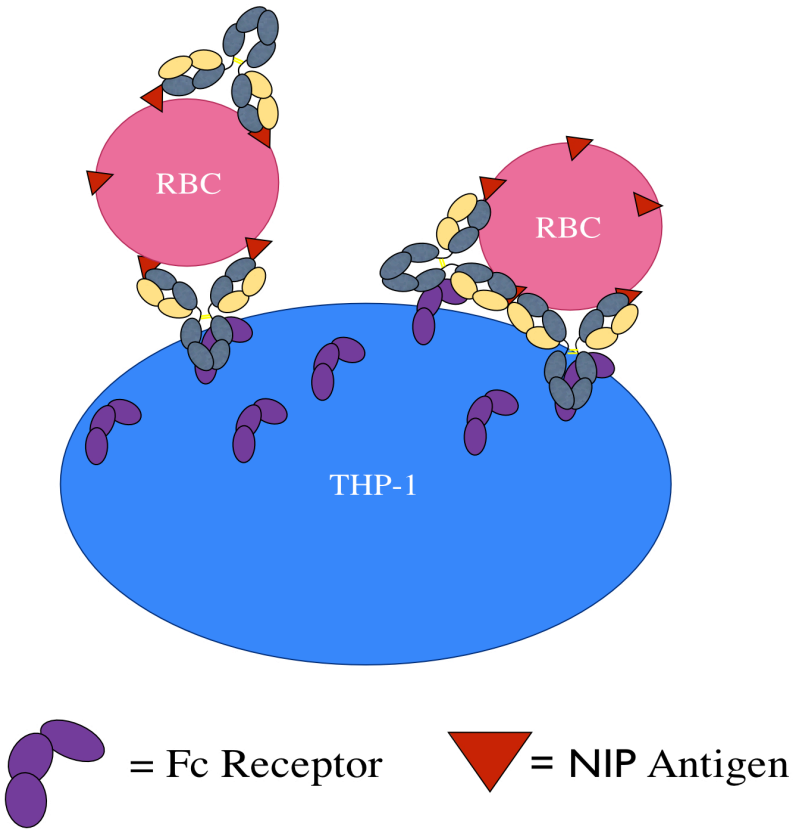

Figure 5.2: A schematic diagram illustrating the rosette formation. Sheep red blood cell (RBC) was derivatised with NIP antigen and incubated with anti-NIP IgG1 antibodies before being further incubated with effector cell, THP-1, which expresses Fcγ receptors. The taret cell-effector cell bridging is formed by the interactions between an antibody binding to target antigen on the surface of RBC via Fab arms and the Fc region associating with Fcγ receptor on the surface of THP-1.

each other, thus, generating a phenomenon known as rosettes, as indicated in Figure 5.2. This system creates a scenario resembling pathogen clearance in which red blood cells are considered as target cells and THP-1 cells as effector cells. Michel and colleagues used a rosette inhibition assay to determine the binding affinity of Fc receptors for the antibodies Dob and Lec (both were hinge-deleted hIgG1 mutants) compared to that of wt hIgG1. They showed that Dob and Lec displayed very reduced rosette formation capability with THP-1 cells (Klein *et al*., 1981). In a different scenario, Walker and colleagues generated a matched set of chimeric anti-NIP human IgG1, IgG2, IgG3 and IgG4 molecules and investigated their interactions with human FcγRI and FcγRII via a rosetting assay (Walker *et al*., 1989). The

authors showed that among all subclasses of hIgGs, hIgG1 and hIgG3 were the best performers in rosette assays with U937, K562 and Daudi cells (Walker *et al*., 1989). Based on these earlier successes, the rosetting assay was chosen as a suitable assay to allow comparison of the target cell-effector cell bridging efficiency of a matched set of IgG antibodies. An antibody displaying enhanced rosette formation would suggest improved performance at pathogen clearance, since it would model close interaction of the effector cells necessary for phagocytosis or other means of destroying pathogens.

5.2 AIMS

This chapter hypothesised that a longer upper hinge length would increase the bivalent antigenic distance and improve the overall antigenic reach of an antibody. In addition, this chapter also hypothesised that dsDNA might be a suitable "molecular ruler" to measure the bivalent antigenic distance of an antibody. As a result, the aims of this chapter were to

1) determine if upper hinge extension is able to increase the maximum bivalent antigenic distance of an IgG1 molecule.

2) determine if the NIP-dsDNA model would function as a suitable model for measuring the bivalent antigenic distance of an antibody.

3) investigate if upper hinge extension is able to increase the target cell-effector cell bridging efficiency of an IgG1 antibody.

5.3 MATERIALS AND METHODS

5.3.1 MATERIALS AND BUFFERS

CM4 and CM5 Sensor chips

CM4 and CM5 Sensor chips purchased from GE Healthcare Life Sciences were stored at 4ºC, and brought to room temperature before use.

HBS-EP Buffer

HBS-EP Buffer (0.01M HEPES pH 7.4, 0.15 M NaCl, 3 mM EDTA, 0.005% v/v Surfactant P20) purchased from GE Healthcare Life Sciences was stored at 4ºC and brought to room temperature before use.

Sheep red blood cells (RBC)

Sheep blood in Alsever's solution was purchased from TCS Bioscience Ltd. and stored at 4ºC.

Isotonic borate buffer

100mM boric acid, 25mM borax, 75mM NaCl was prepared in Millipore water and stored at 4ºC.

NIP hapten

NIP-caproic acid-OSuccinimide (NIP-cap-OSu) was purchased from Biosearch Technologies. An appropriate amount of NIP-cap-OSu was dissolved in dimethyl formamide to give a final concentration of 10mg/ml prior to use.

5.3.2 SURFACE PLASMON RESONANCE ANALYSIS

5.3.2.1 Immobilisation of NIP-dsDNA on CM4/CM5 sensor chip

Immobilisation of NIP-dsDNA on CM4/CM5 sensor chip was performed using the protocol described by Liu and Wilson (2010) with some modifications as described below. Due to lower degree of carboxylation, the immobilisation level of CM4 sensor chip is about 30% of CM5 sensor chip according to manufacturer guidance.

Immobilisation of monovalent streptavidin (Mono-Strep)

A CM4/CM5 sensor chip was inserted into a Biacore® X machine (GE Healthcare Life Sciences) and primed several times with HBS-EP buffer. A sensorgram was initiated and both flow cell 1 (FC1) and flow cell 2 (FC2) of the sensor chip was run at a flow rate of 5µl/min to allow the temperature to stabilise to room temperature. 100µl of 1µM Mono-Strep was prepared in 10mM Sodium Acetate pH4.5 (GE Healthcare Life Sciences) in a 1.5ml microfuge tube. At pH4.5, the overall net charge of Mono-Strep becomes positive, facilitating the association of Mono-Strep with the dextran of the sensor chips which is negatively charged. 50µl of 0.1M N-hydroxysuccinimide (NHS) and 50µl 0.4M 1-ethyl-3-(3-dimethylaminopropyl) carbodiimide hydrochloride (EDC) (both freshly prepared) were mix gently together in a microfuge tube. 50µl of NHS/EDC mixture were then injected to activate the sensor chip surface (for 10 minutes). Subsequently 100µl of 1µM of Mono-Strep was injected into the system. Using "Manual Injection", 25µl of 1µM of Mono-Strep was injected each time until the monitored Response Unit (RU) showed a reading of around 2500-3000RU for a CM4 sensor chip or 1500-2000RU for a CM5 sensor chip. When the desired RU reading was achieved, the injection procedure was

stopped and the sensor chip surface was deactivated with 50µl of ethanolamine-hydrochloride (10 minutes). The sensorgram was stopped and the sensor chip was then primed several times with HBS-EP buffer.

Immobilisation of NIP-dsDNA

After the immobilisation of Mono-Strep, a new sensorgram was initiated in which the flow was only over FC2 at a flow rate of 2µl/min. FC1 would serve as a control, thus, no NIP-dsDNA would be immobilised on it. On separate chips, 50µl of either 10µM 20bp NIP-dsDNA, 45bp NIP-dsDNA or 55bp NIP-dsDNA was prepared in HBS-EP buffer in a 0.5ml microfuge tube. 20µl of the particular NIP-dsDNA was injected into the system to allow binding to Mono-Strep on FC2 to occur (10 minutes). Subsequently the flow rate was increased to 10µl/ml and 10µl of 50mM sodium hydroxide (GE Healthcare Life Sciences) was injected to wash and remove any loosely bound NIP-dsDNA from the surface of the sensor chip (1 minute). The sensor chip was primed several times with HBS-EP buffer, and was then ready for investigations to proceed.

5.3.2.2 Determination of binding of anti-NIP antibodies to immobilized NIP-dsDNA

A CM4 sensor chip with an immobilisation level of approximately 2300RU of 20bp NIP-dsDNA was generated by the above procedure and inserted into the Biacore® X system. A sensorgram was initiated at a flow rate of 15µl/min over both FC1 and FC2. FC1 was the reference control. Anti-NIP wt hIgG1, 0.5HA, 1HA and ONeg antibodies at molar concentrations ranging from 2nM to 28nM were prepared in HBS-EP buffer. 20µl of each concentration was injected into the system to allow

antigen binding and held for 300 seconds with the same flow rate, 15µl/min, to resemble a washing process before the unchangeable programmed washing process, (high flow rate) was initiated. Subsequently the sensor chip surface was regenerated by injecting 10µl of 50mM sodium hydroxide (GE Healthcare Life Sciences) to remove all bound antibodies and enable subsequent analyses on the same chip. The same procedure was repeated with each concentration of the different antibodies.

5.3.2.3 Investigation of bivalent antigenic distance in SPR experiments

Different CM5 sensor chips on which either 20bp NIP-dsDNA, 45bp NIP-dsDNA and 55bp NIP-dsDNA was immobilised were generated in the above procedure.

Investigation using high antibody saturation level

For each different CM5 sensor chip, following insertion in the Biacore® X machine, a sensorgram was initiated at a flow rate of 10µl/min over both FC1 and FC2, and FC1 was selected as the reference control. Anti-NIP wt hIgG1, 0.5HA, 1HA and ONeg antibodies were each prepared at 20nM in HBS-EP buffer respectively. 30µl of antibody was injected into the system each time to allow antigen binding and held for 300 seconds before the washing process was initiated. Subsequently the sensor chip surface was regenerated by injecting 10µl of 50mM sodium hydroxide (GE Healthcare Life Sciences) to remove all bound antibody. The same procedure was repeated for the investigation of each of the different antibodies.

Investigation using low antibody saturation level (100RU)

For each different CM5 sensor chip, a sensorgram was initiated at a flow rate of 10µl/min over both FC1 and FC2, and FC1 was selected as the reference control.

Anti-NIP wt hIgG1, 0.5HA, 1HA and ONeg antibodies were each prepared at 2nM in HBS-EP buffer. Using "Manual injection", 100µl of antibody was injected into the system each time to allow antigen binding and the RU of the sensorgram was monitored. The injection was stopped when the antibody-antigen binding reached 100RU and held for 300 seconds before the washing process was initiated. Subsequently the sensor chip surface was regenerated by injecting 10µl of 50mM sodium hydroxide (GE Heathcare Life Sciences) for 60 seconds to remove all bound antibodies. The same procedure was repeated for the investigation of each of the different antibodies.

5.3.3 ROSETTING ASSAY

5.3.3.1 Analysis of Fcγ receptor expression on THP-1 cells using flow cytometry

Each test was done in duplicate and required 3 x 10^6 cells. An appropriate number of THP-1 cells were harvested as described in section 2.6.3 and resuspended in cold PBN buffer (0.1% (w/v) BSA, 0.01% NaN_3, in PBS) at a density of 3 x 10^6 cells/100µl. 100µl aliquots were pipetted into 1.5ml microfuge tube. For investigation of FcγRI expression, THP-1 cells were incubated with 100µl FITC-conjugated mouse anti-human CD64 antibody (Table 2.1 No.5) for 1 hour on ice, in the dark. For analysis of FcγRII expression, THP-1 cells were incubated with 100µl FITC-conjugated mouse anti-human CD32 antibody (Table 2.1 No.6) for 1 hour on ice and kept in the dark. When the incubations were completed, cells were washed three times with 500µl cold PBN buffer by centrifuging for 5 minutes at 250g. Cells were resuspended in 500µl of PBN buffer and transferred to 5ml polystyrene round-bottom tubes (BD Bioscience) for subsequent flow cytometry analyses. Cells were

analysed on a BD FACSCanto II machine (BD Biosciences).

5.3.3.2 Derivatisation of RBC with NIP

2ml sheep RBC was pipetted into a 30ml Universal tube. 8ml of isotonic borate buffer was added to wash the RBC before centrifuging for 5 minutes at 250g. The supernatant was discarded and the washing process was repeated twice. After the final wash, the cell pellet was resuspended in 5ml of isotonic borate buffer and centrifuged for 5 minutes at 300g to pack the RBC cell pellet. The supernatant was discarded and the volume of RBC cell pellet was measured using a 1ml pipette after 0.5ml resuspension of cell pellet with isotonic borate buffer. When the volume of RBC had been determined, an appropriate volume of isotonic borate buffer was added to the cells to make a 10% (v/v) RBC suspension. An appropriate volume of 10mg/ml NIP-cap-OSu (1µl for every ml of 10% RBC suspension) was added and incubated at room temperature for 1 hour on a roller. After the incubation period, the cells were washed 3 times with 5ml of PBS and centrifuging for 5 minutes at 250g each time. The supernatant was discarded and the cell pellet was resuspended in PBS to give a 10% (v/v) RBC suspension.

5.3.3.3 Coating of NIP-derivatised RBC with anti-NIP antibodies

wt hIgG1, 0.5HA, 1HA and ONeg anti NIP antibodies were each prepared at various concentrations up to14µg/ml in PBS. 6µl of each concentration was pipetted into a 1.5ml microfuge tube. 12µl 10% NIP-derivatised RBC was added to each microfuge tube and gently mixed. All tubes were incubated for 1 hour at 37ºC in an incubator. Subsequently the cells were washed 3 times with 100µl of PBS, centrifuging for 5 minutes at 250g each time. The supernatant was discarded and the cell pellet was

resuspended in 108µl PBS to make a 1% (v/v) RBC suspension.

5.3.3.4 Rosetting assay

Each test was done in duplicate and required 25µl effector cells at a density of 2 x 10^6 cells/ml. An appropriate number of THP-1 cells were harvested as described in section 2.6.3 and resuspended in PBS at 2 x 10^6 cells/ml. 25µl THP-1 cells were pipetted into each well of a 96 well U-bottom plate (Falcon®, Corning Inc.). 25µl of a 1% suspension of RBC coated with each antibody was pipetted into duplicate sample wells. 50µl PBS was then added to each well producing a final volume of 100µl in each well. The plate was allowed to stand at room temperature for 15 minutes before being centrifuged at 50g for 1 minute to enhance cell interaction. The plate was then transferred to an incubator at 37ºC for 90 minutes. After the incubation period, cells were briefly mixed by gently pipetting up and down. Cells were transferred to a haemocytometer to be examined under a microscope and the percentage rosette formation was determined. In this assay, a rosette was defined as an effector cell having three or more RBC attached. The minimum number of effector cells counted for each test was at least 100 cells. The average percentage rosette formation were determined for different antibodies and normalised against wt hIgG1 by setting the maximum rosette formation seen with the usage of 14µg/ml of wt hIgG1 as 100%.

5.4 RESULTS

5.4.1 The success of different immobilisations

Immobilisation of high levels of Mono-Strep onto CM4 sensor chips was found to be challenging. In some attempts, a Mono-Strep immobilisation level of less than

600RU was achieved, which was considered to be a very low level since it is reportedly possible to exceed 4000RU in immobilisations on CM4, according to the manufacturer's guidance. In an attempt to resolve this issue, the concentration of Mono-Strep was doubled to 2μM during the immobilisation step but the RU obtained was similar and failed to exceed 600RU. After introducing 20bp NIP-dsDNA to these CM4 sensor chips with low Mono-Strep immobilisation, the resultant binding lead to an increase of about 50-80RU. These low immobilisation CM4 sensor chips were then tested with anti-NIP wt hIgG1 but showed insignificant antibody binding. Therefore, it was concluded that these sensor chips were unsuitable for the proposed investigations.

Fortunately, there was one CM4 sensor chip that had an immobilisation level of Mono-Strep of around 2300RU. After the introduction of 20bp NIP-dsDNA, the overall RU increased to approximately 2500RU. The reason as to why one CM4 sensor chip could be immobilised up to 2300RU with 1μM of Mono-Strep but not the others was not known because the immobilising procedure was carried out identically. As a result of this seeming variability, CM5 sensor chips were selected as an alternative because they have a higher capacity for immobilisation than CM4 sensor chips (see section 5.3.2.1 for the difference between CM4 and CM5). All generated sensor chips used in this chapter are listed in Table 5.1. Although the immobilisation level of Mono-Strep on the CM5 sensor chip was still considered low, since immobilization can reportedly exceed 6000RU on CM5 sensor chips according to the manufacturer's guidance, it was sufficient for carrying out the planned investigations.

Table 5.1: Details of generated CM4/CM5 sensor chips

Type of sensor chip	Type of dsDNA	Final approximate RU
CM4	20bp NIP-dsDNA	2500 RU
CM5	20bp NIP-dsDNA	1900RU
CM5	45bp NIP-dsDNA	2000RU (High)
CM5	45bp NIP-dsDNA	1000RU (Low)
CM5	55bp NIP-dsDNA	1500RU

Note: There were two CM5 sensor chips on which 45bp dsDNA was immobilised, thus, they were designated either high or low, on the basis of their RU values.

5.4.2 Binding to NIP-dsDNA assessed by SPR analysis

All four antibodies tested, wt hIgG1, 0.5HA, 1HA and ONeg, were able to bind to the NIP antigen on 20bp NIP-dsDNA as shown in Figure 5.3**.** The maximum RU obtained by all antibodies were around 600RU which indicated that all the antibodies reached a similar saturation level**.** As presented in Figure 5.3, all the hinge mutants, 0.5HA, 1HA and ONeg, showed similar association and dissociation patterns to those of wt hIGg1, suggesting that hinge extension had no significant impact on antigen recognition when the antigens are interposed by a stretch of 20 bp of DNA. In addition, at low concentrations, for example 2nM - 6nM, all antibodies seemed to show very slow dissociation as seen in Figure 5.3, consistent with the relatively high binding affinity the anti-NIP antibody is known to have for NIP.

5.4.3 Estimation of the bivalent antigenic distance of the different antibodies

In this study the determination of the bivalent antigenic distances of different antibodies depends of their relative rates of dissociation from NIP antigen, as

A. SPR analysis of wt hIgG1 binding to 20bp NIP-dsDNA

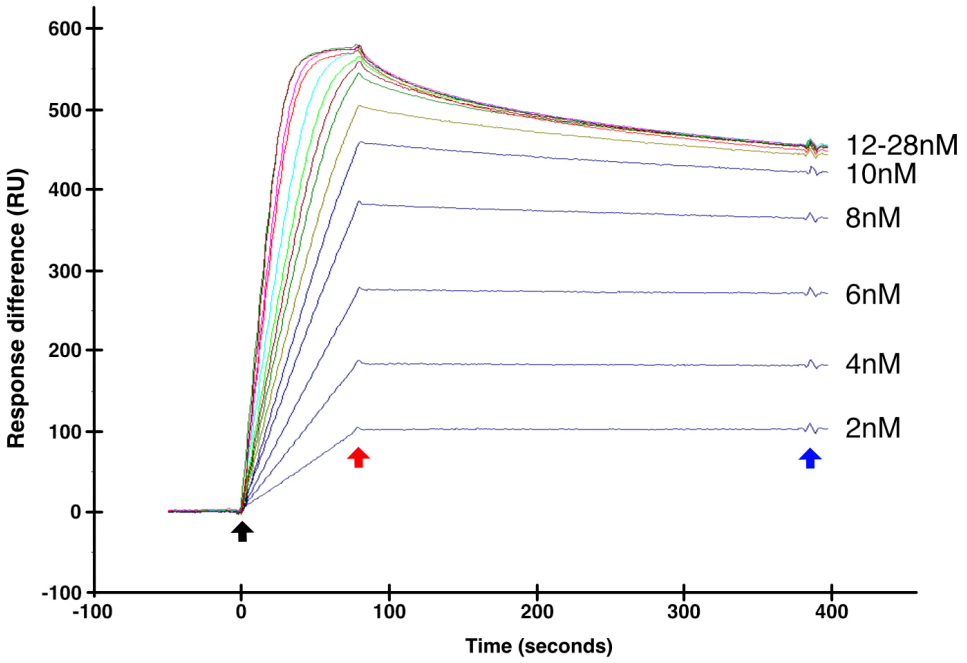

B. SPR analysis of 0.5HA binding to 20bp NIP-dsDNA

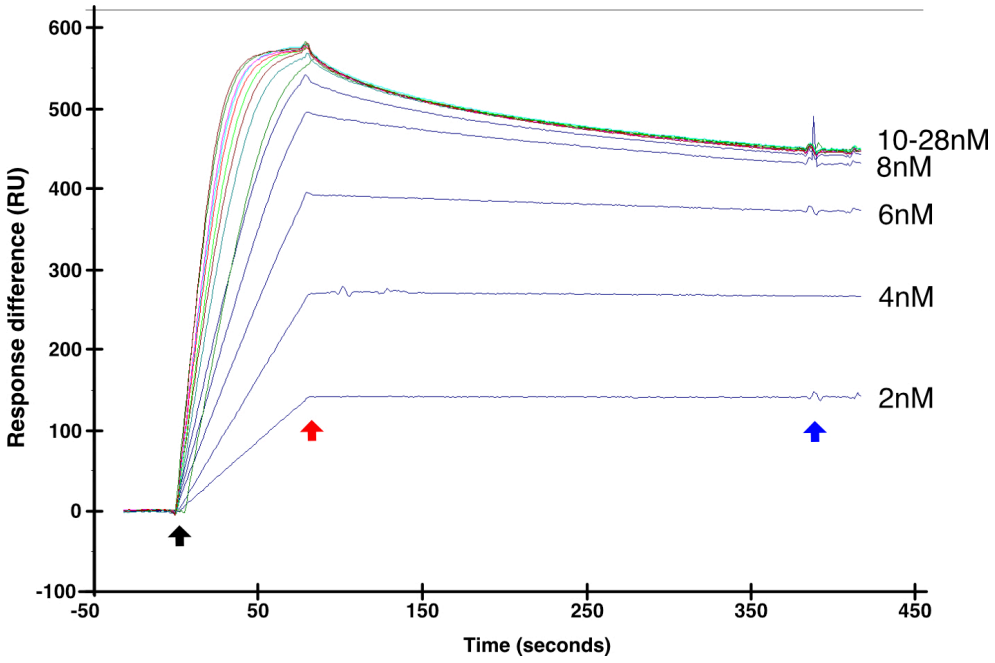

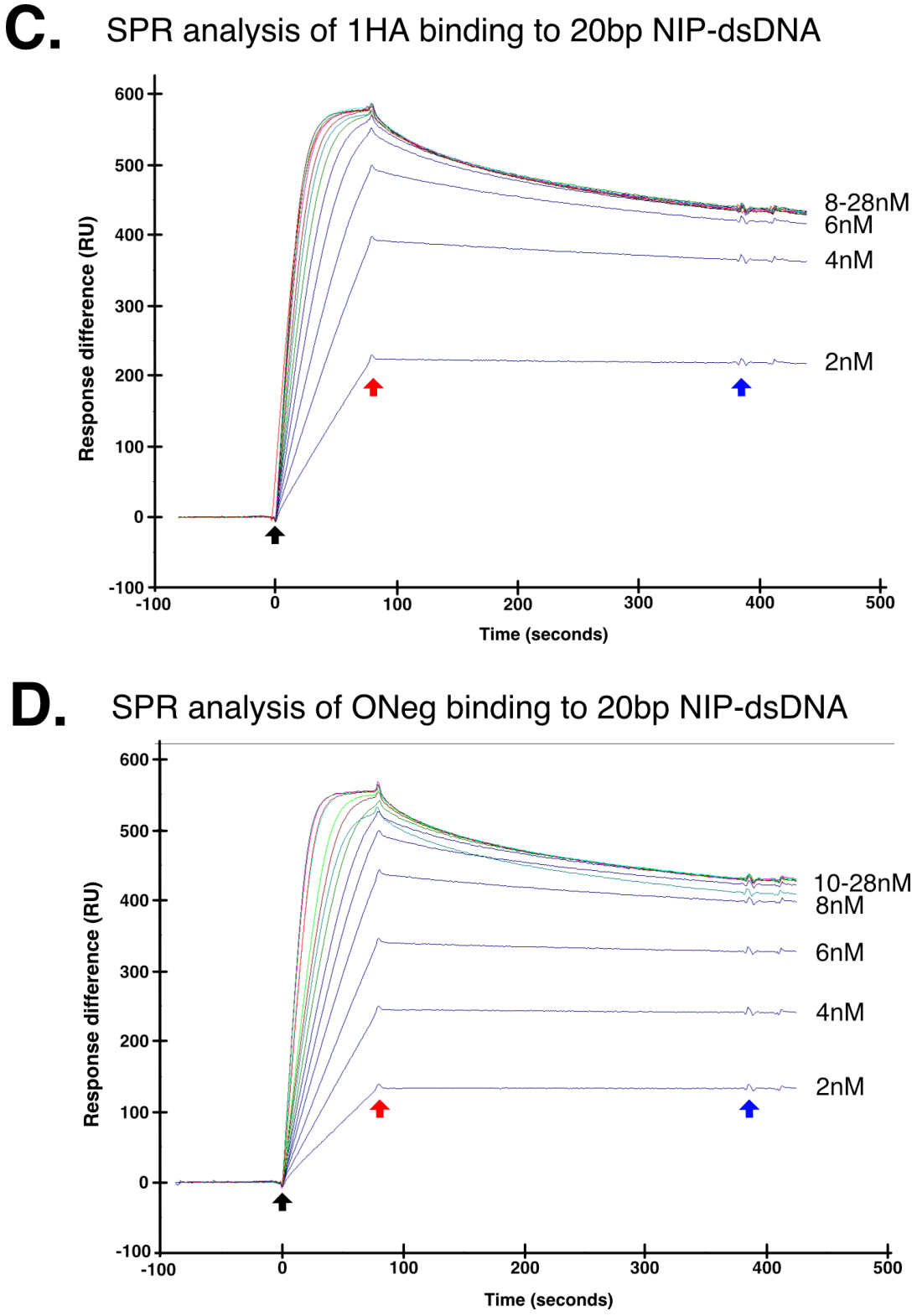

Figure 5.3: Results of SPR analyses of different anti-NIP IgG antibodies binding to 20bp NIP-dsDNA at different concentrations between 2nM and 28nM. **A**. wt hIgG1; **B**. 0.5HA; **C.** 1HA; **D**. ONeg. 20µl antibody was injected for every test at a flow rate of 15µl/min and continued for 300 seconds before washing. The starting point of antibody injection of all curves had been superimposed so that the RU value and time were identical for all curves. Different antibody concentration injections are represented by different colours. A representative experiment of two is shown.

discussed previously. Antibody molecules which have bound bivalently are expected to have a slower rate of dissociation when compared to antibody molecules which have only bound monovalently. Two different concentrations, 20nM and 2nM, of antibodies were used for this investigation. The 20nM option was used to estimate the maximum RU that could be obtained for each sensor chip and to confirm that all the antibodies were behaving similarly, as previously determined using the CM4 sensor chip. In addition, the 20nM option was used to study the monovalent/bivalent binding activity of each antibody at saturation. However, one limitation to the determination of monovalent/bivalent binding at 20nM was that at saturation level there is likely to be a mixture of antibody binding modes, with some molecules being bound monovalently and others bivalently to the target NIP antigen. Therefore, the interpretation of the results obtained requires care, and should be further verified. To further strengthen the findings from the studies using 20nM, a lower concentration of 2nM was used and the injection was stopped when the antigen binding had reached a value of 100RU. The reason for such a procedure was that using 2nM antibody gave a better control over the level of binding during antibody-antigen association and stopping the injections at 100RU would create a situation in which the amount of antibody injected into the system was insufficient to bind all available antigen. Thus, there would be no competition for antigen binding and the antibodies would be free to bind to their target antigen with minimal steric hindrance. As a result, the difference between monovalent and bivalent binding of an antibody may be more easily determined.

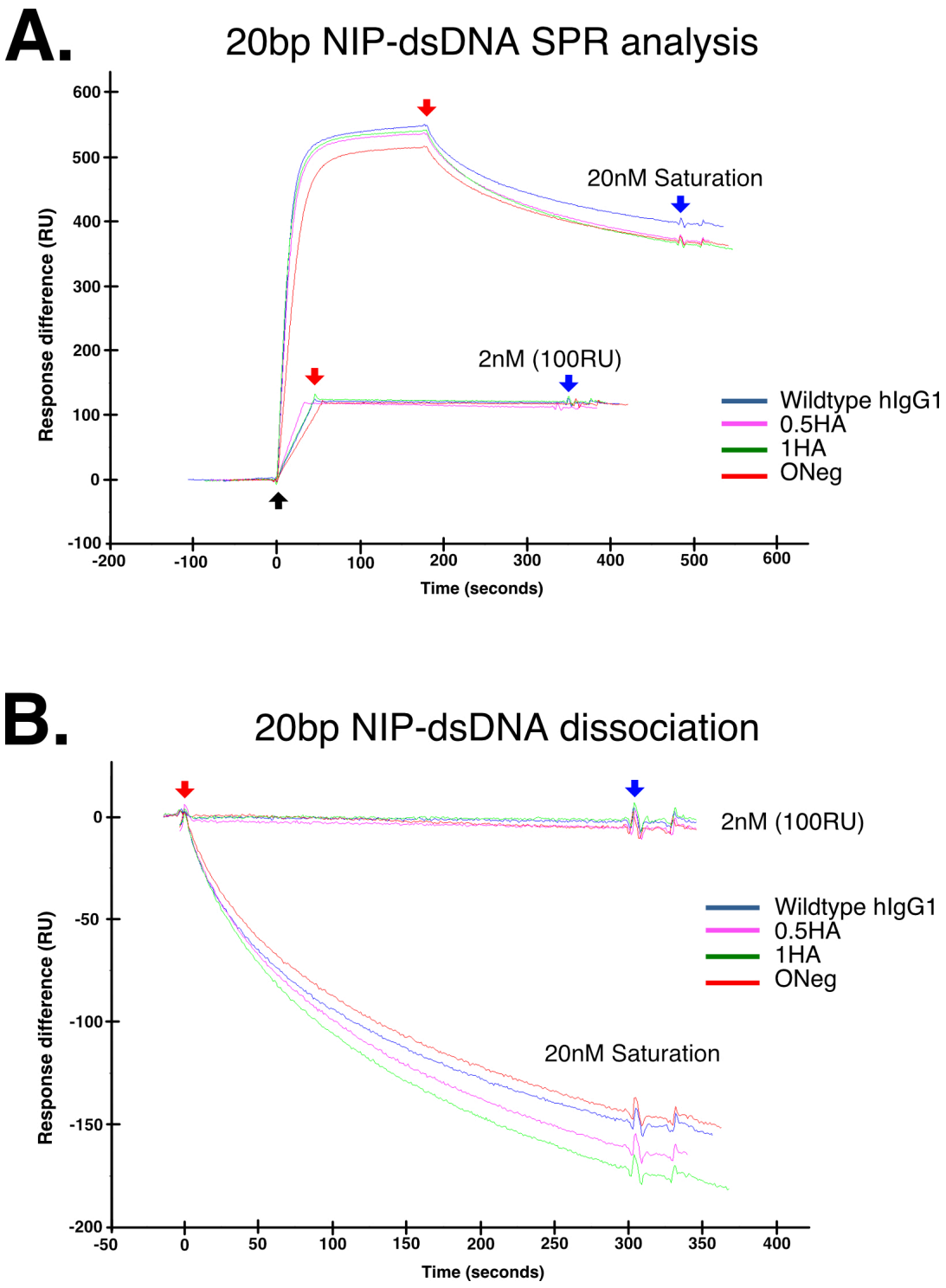

Figure 5.4: A comparison of SPR profiles of 20nM and 2nM concentrations of different antibodies binding to the 20bp NIP-dsDNA surface. **A**) SPR profile of different antibodies binding to 20bp NIP-dsDNA. **B**) Dissociation of different antibodies from the 20bp NIP-dsDNA surface. For 20nM, 30µl antibody was injected and continued for 300 seconds before washing whereas for 2nM 100µl of antibody was injected and the injection stopped when 100RU was reached. Each test was performed at a flow rate of 10µl/min. The starting point of antibody injection (**A**) or the end of antibody injection (**B**) of all curves had been superimposed so that the RU value and time were identical for all curves. Blue, wt hIgG1; Pink, 0.5HA; Green, 1HA; Red, ONeg. Black arrow, antibody injection; Red arrow, injection stopped; Blue arrow, washing began. A representative experiment of 2 is shown.

Association and dissociation with 20bp NIP-dsDNA

As presented in Figure 5.4, at a concentration of 20nM a similar pattern of antibody-antigen association and dissociation was observed when compared to the earlier results obtained from CM4 sensor chip, Figure 5.3. This result indicated that there were no significant differences in antigen binding activity between the 20bp NIP-dsDNA immobilised on CM5 and CM4 sensor chips. When a concentration of 20nM was used, all antibodies seems to reach saturation level approximately 45 seconds after injection and the maximum RU obtained were around 450-550RU. With a maximum RU of 450RU, it was reasoned that a reading of 100RU would be likely to reflect a situation where only about 20% of the available antigen molecules were bound. All the tested antibodies at 2nM concentration required around 20 seconds after injection to achieve 100RU, as indicated in Figure 5.4.

When the dissociation curves of each antibody at different concentrations were compared as shown in Figure 5.4 B, the dissociation curves of all antibodies at 2nM (100RU) were significantly different from those obtained at 20nM (saturated). Noticeably, at 2nM (100RU) the dissociation curve resembled a virtually linear trace whereas at 20nM (saturated) a clear dissociation curve was apparent. The reason for this phenomenon was predicted to be due to the difference between monovalent and bivalent binding. As mentioned previously, a concentration of 20nM would likely saturate the sensor chip, and thus there would be a mixture of monovalently bound and bivalently bound molecules. Monovalently bound antibodies would tend to dissociate at a faster rate than bivalently binding antibodies. Hence a faster decrease in RU would tend to result for the 20nM concentration than the 2nM one. In contrast, the almost linear dissociation trace observed with 2nM (100RU), Figure 5.4B,

strongly suggests the presence of mainly bivalently bound molecules resulting in a slower rate of dissociation. This reasoning was supported by the predicted length of 20bp NIP-dsDNA of 7.57nm which was well within the reported 14.5 nm Fab tip to tip distance from hIgG1 (Kol). Therefore, bivalent binding to the 20bp NIP-dsDNA was highly feasible for all the IgG variants.

As seen in Figure 5.4B, there were no significant differences in the rates of dissociation between the different antibodies at 2nM(100RU). However, at 20nM(saturated) the antibodies showed slight differences in their rates of dissociation. ONeg appeared to have the slowest dissociation rate followed by wt hIgG1, then 0.5HA and finally 1HA with the quickest dissociation rate. One possible explanation for this observation was that the combination of longer upper hinge and the absence of O-linked glycans at the hinge region of ONeg probably allowed a better positioning of the Fab arms of ONeg to conduct antigen binding, thus, allowing more efficient bivalent binding activity. Although 1HA has the same upper hinge length as ONeg (both have 21 amino acids), 1HA appears to have some O-linked glycans at the upper hinge region which arguably might tend to increase overall steric hindrance between the two Fab arms when they come close to together to bind the two NIP antigens of 20bp-dsDNA which is separated about 7.57nm away from each other. Thus, maintaining bivalent binding was less efficient for 1HA. 0.5HA has a shorter upper hinge length and presumably lesser O-linked glycans when compared to 1HA. Therefore, the overall steric hindrance may be lower than that of 1HA but higher than that of wt hIgG1, meaning that 0.5HA had a slower dissociation rate when compared to 1HA but a faster dissociation rate when compared to wt hIgG1, as observed in Figure 5.4B. These results suggested that the

upper hinge length and the presence of O-linked glycans at the upper hinge region may play some role in the overall positioning of the Fab arms of an antibody with regards to antigen binding.

In summary, the study using 20bp NIP-dsDNA showed that dsDNA has a high potential as molecular ruler as different antibodies are able to bind to the targeted antigen covalently attached to dsDNA in SPR analyses. The results using 2nM of antibodies demonstrated that bivalent binding produced a tight association between antibody and antigen in the context of NIP antigen recognition. Further analyses would be require to determine if there is a difference in the dissociation rate between bivalent and monovalent binding in the context of NIP antigen recognition in order to validate the potential of dsDNA as molecular ruler to measure the bivalent antigenic distance of an antibody.

Association and dissociation with 45bp NIP-dsDNA

As presented in Figure 5.5, at a concentration of 20nM (saturated) all tested antibodies appeared to reach saturation levels approximately 45 seconds after injection and the maximum RU obtained were around 150-200RU. When the dissociation curves for each antibody were compared, as shown in Figure 5.5B, ONeg appeared to have a slower dissociation rate than the other antibodies. This difference in dissociation rate was more noticeable at a concentration of 20nM (saturated) than at 2nM (100RU). Such a result suggests that ONeg may be more capable of binding bivalently to 45bp NIP-dsDNA molecules than the other antibodies tested. Although apparently binding bivalently, ONeg did not produce a similar tight association as seen with 20bp NIP-dsDNA at a concentration of 2nM in

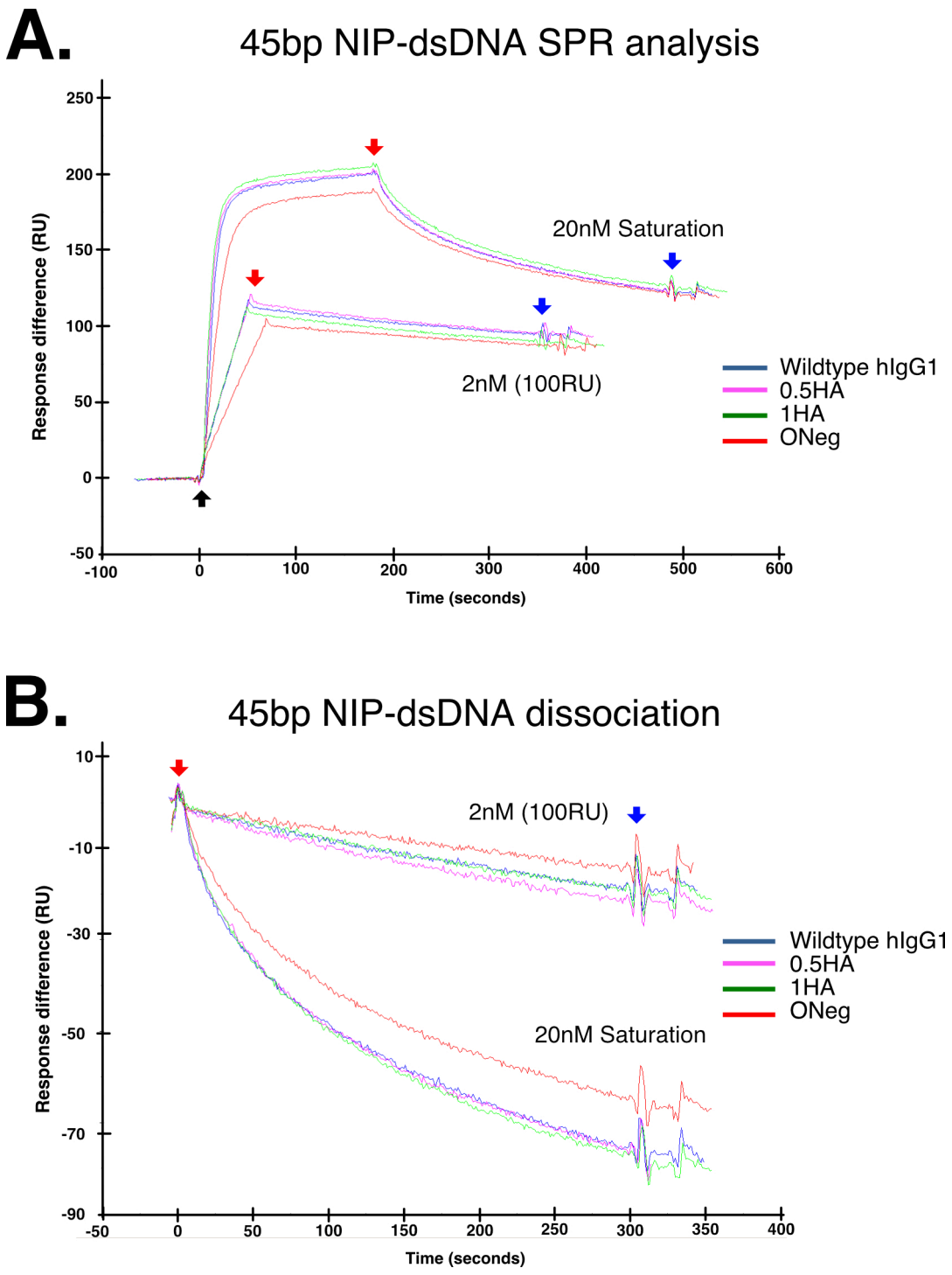

Figure 5.5: A comparison of SPR profiles of 20nM and 2nM concentrations of different antibodies binding to 45bp NIP-dsDNA surface. **A**) SPR analyses at 20nM and 2nM concentrations of different antibodies binding to 45bp NIP-dsDNA. **B**) Dissociation of different antibodies from the 45bp NIP-dsDNA surface. For 20 nm, 30µl antibody was injected whereas for 2nM 100µl was injected and the injection stopped when 100RU was reached. Each test was performed at a flow rate of 10µl/min and held for 300 seconds before washing. The starting point of antibody injection (**A.**) or the end of antibody injection (**B**.) of all curves had been superimposed so that the RU value and time were identical for all curves. Blue, wt hIgG1; Pink, 0.5HA; Green, 1HA; Red, ONeg. Black arrow, antibody injection; Red arrow, injection stopped; Blue arrow, washing began. A representative experiment of 2 is shown.

both occasions. With 20bp NIP-dsDNA (2nM), there was almost no significant changes in RU during the expected ONeg dissociation period, as seen in Figure 5.4B. However, with 45bp NIP-dsDNA (2nM) a decrease in RU was noticed during the expected ONeg dissociation period, as indicated in Figure 5.5B. One possible explanation for this finding is that the length of 45bp NIP-dsDNA at 16.07nm, was very close to the maximum bivalent antigenic distance of ONeg. Hence, although ONeg was perhaps capable of binding bivalently, the binding tension exerted on the Fab arms to do this was too great for ONeg to maintain bivalent binding for a long period of time. Thus, bivalent binding was abolished. This reasoning seems to be supported by the faster dissociation rate of 1HA, which had the same hinge length as ONeg, to 45bp NIP-dsDNA. Such behaviour may possibly be due to 1HA having O-linked glycans present at the hinge region resulting in an overall reduction in Fab arm reach or flexibility, thus, abolished the bivalent binding activity.

The result obtained from 45bp NIP-dsDNA strongly suggested that the combination of NIP-dsDNA and SPR could provide a platform to estimate the maximum bivalent antigenic distance of antibody. However, there was a concern that the results obtained in Figure 5.5B might be due to a phenomenon where ONeg was binding to two adjacent 45bp-NIP-dsDNA molecules as previously described in Figure 5.1. To minimise the likelihood of an antibody molecule binding to two adjacent 45bp NIP-dsDNA molecules, a different CM5 sensor chip was generated using a lower concentration of Mono-Strep in the immobilisation step (0.5μM instead of 1μM), to create a sensor chip with a lower density of 45bp NIP-dsDNA than the original sensor chip with readings of about 1000RU instead of 2000RU recorded at the immobilisation step. Interestingly, the results obtained from the new sensor chip

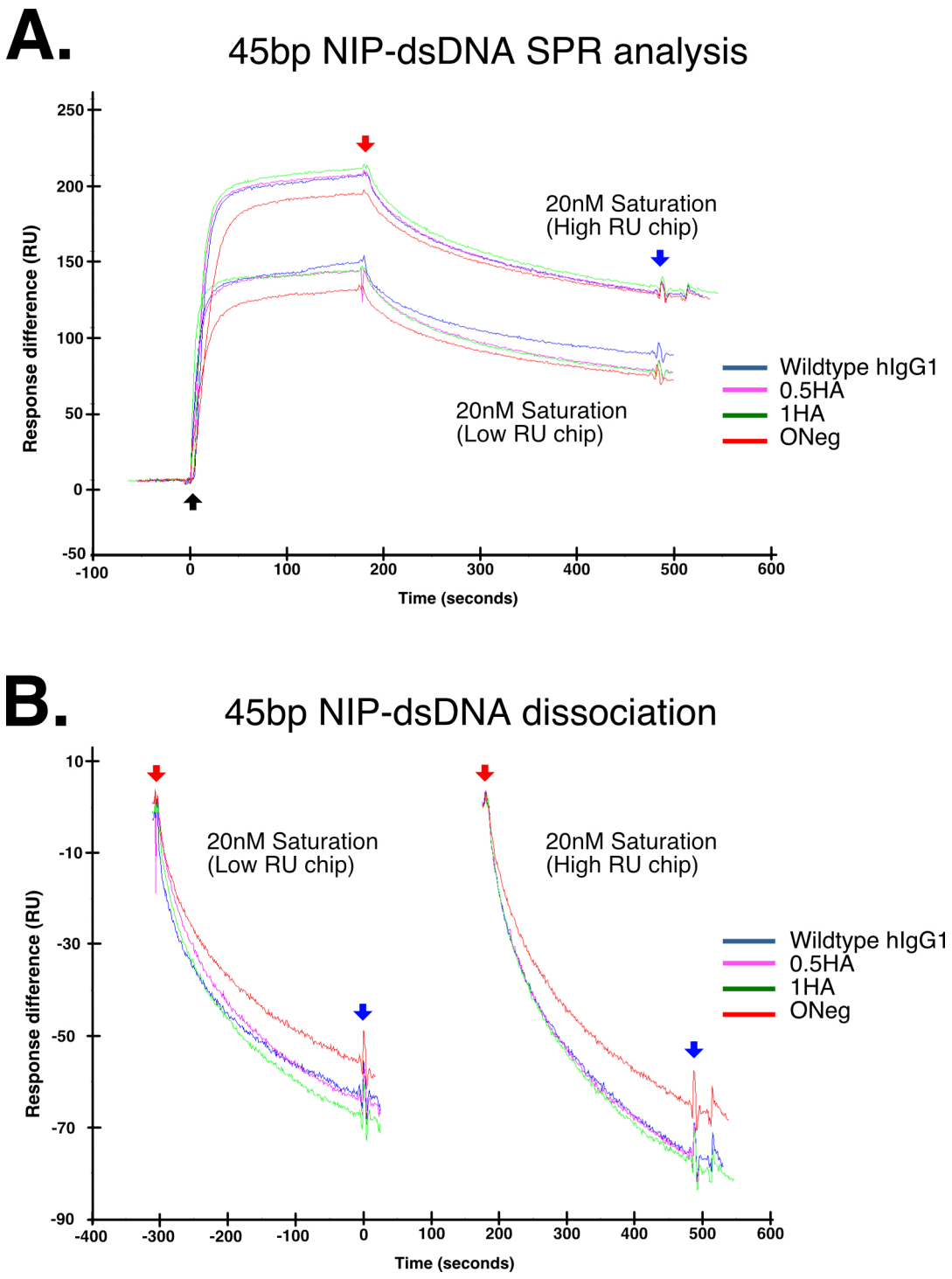

Figure 5.6: A comparison of SPR profiles of 20nM concentrations of different antibodies binding to different concentration of 45bp-dsDNA immobilised surface. **A)** SPR analyses of both 20nM and 2nM concentrations of different antibodies binding to 45bp NIP-dsDNA. **B**) Dissociation of different antibodies from 45bp NIP-dsDNA surfaces. For 20nm, 30µl antibody was injected whereas for 2 nM 100µl antibody injection was stopped when 100RU was reached. Each test was performed at a flow rate of 10µl/min and held for 300 seconds before washing. Blue, wt hIgG1; pink, 0.5HA; green, 1HA; red, ONeg. The starting point of antibody injection (**A.**) or the end of antibody injection (**B**.) of all curves had been superimposed so that the RU value and time were identical for all curves. Blue, wt hIgG1; Pink, 0.5HA; Green, 1HA; Red, ONeg. Black arrow, antibody injection; Red arrow, injection stopped; Blue arrow, washing began. A representative experiment of 2 is shown.

were very similar to the results obtained with the higher density chip, as shown in Figure 5.6. Again ONeg was shown to display the slowest dissociation rate when compared to wt hIgG1, 0.5HA and 1HA. Therefore, both results confirmed the slower dissociation rate of ONeg on 45bp NIP-dsDNA which was consistent with it possibly having a greater capability for bivalent binding to the 45 bp NIP-dsDNA. In summary, the results obtained from the study using 45bp NIP-dsDNA suggested that the bivalent antigenic distance could potentially be evaluated using the combination of dsDNA and SPR analyses as observed from the result of the binding activity of ONeg on 45bp-dsDNA. Furthermore, the results suggested that wt hIgG1, 0.5HA and 1HA may have bivalent antigenic distances less than 16.07nm whereas ONeg may have had a bivalent antigenic distance around 16.07nm or more.

Association and dissociation with 55bp NIP-dsDNA

As presented in Figure 5.7, at a concentration of 20nM (saturated) all antibodies seemed to reach saturation level approximately 45 seconds after injection and the maximum RU obtained were around 100-120RU. When the dissociation traces of each antibody were compared, as shown in Figure 5.7B, there seemed to be no significant difference between the dissociation rates from 55bp NIP-dsDNA. Due to the maximum RU of this sensor chip being around 100RU, the investigation using 2nM of each antibody was modified to stop when the reflective index reached 60RU instead of 100RU. The observation of similar dissociation curves for all antibodies at both 20nM (saturated) and 2nM (60RU) concentrations suggested that all antibodies had a similar binding pattern to 55bp NIP-dsDNA, which is most likely monovalent binding. It was noticed that in the investigation using at 2nM of 0.5HA, 0.5HA required a longer period of time to reach 60RU compared to other antibodies as seen

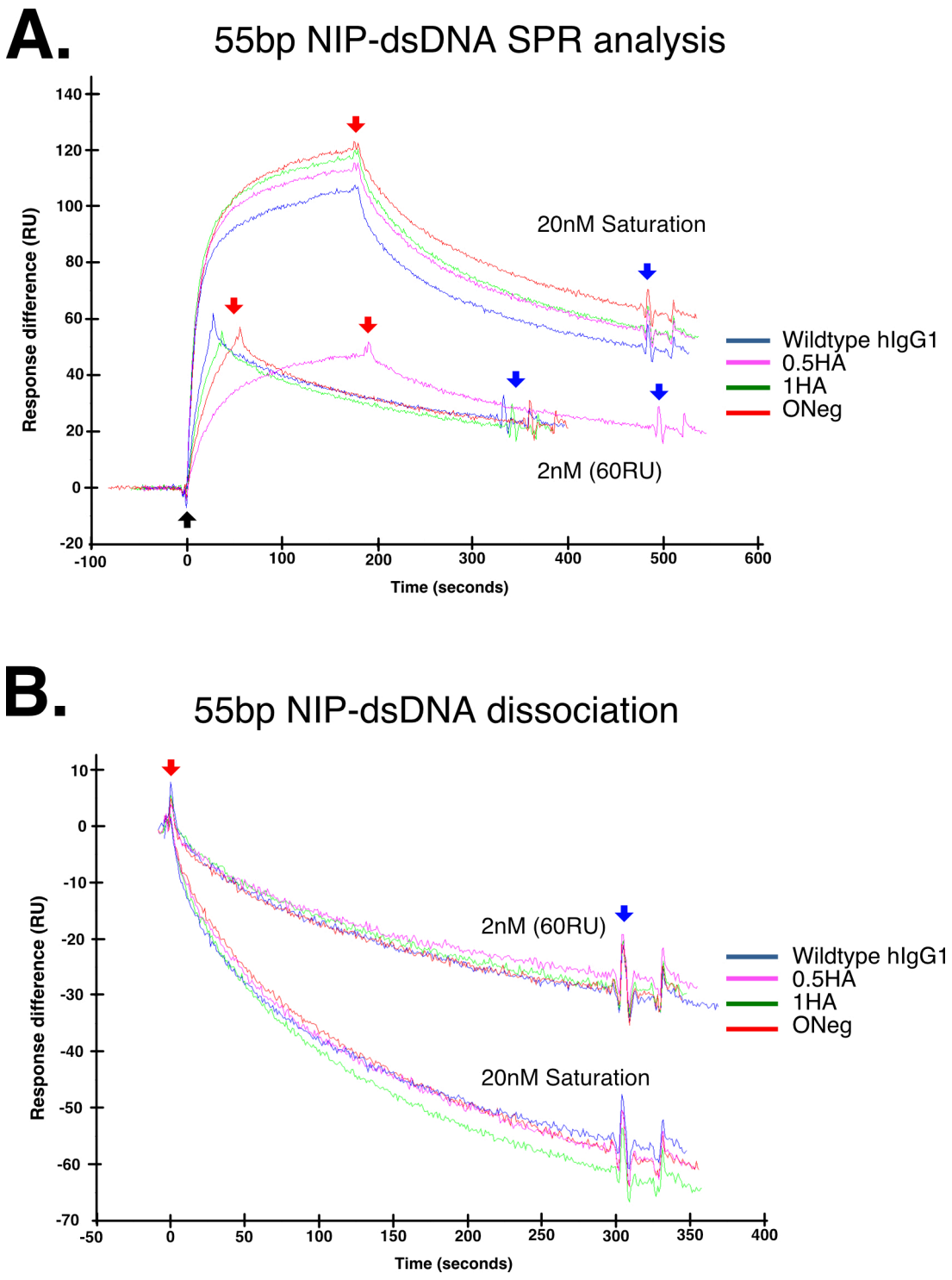

Figure 5.7: A comparison of SPR profiles of 20nM and 2nM concentrations of different antibodies binding to 55bp NIP-dsDNA surface. **A)** SPR analyses of 20nM and 2nM concentrations of different antibodies binding to 55bp NIP-dsDNA. **B**) Dissociation of different antibodies from the 55bp NIP-dsDNA surface. For 20 nm, 30µl antibody was injected whereas for 2 nM, 100µl antibody injection was stopped when 100RU was reached. Each test was performed at a flow rate of 10µl/min and held for 300 seconds before washing. Blue, wt hIgG1; pink, 0.5HA; green, 1HA; red, ONeg. The starting point of antibody injection (**A.**) or the end of antibody injection (**B**.) of all curves had been superimposed so that the RU value and time were identical for all curves. Blue, wt hIgG1; Pink, 0.5HA; Green, 1HA; Red, ONeg. Black arrow, antibody injection; Red arrow, injection stopped; Blue arrow, washing began. A representative experiment of 2 is shown.

in Figure 5.7 A. The exact reason for this phenomenon was not known, however, it was noticed that the maximum RU that the can be achieved by anti-NIP antibodies reduced slightly after each regeneration process which involved the use of 10µl of 50mM sodium hydroxide. Therefore, it was reasonable to suggest that the 0.5HA antigen binding phenomenon noticed in Figure 5.7 A might be due to the instability or the overall reduction in the amount of immobilised Mono-Strep/55bp NIP-dsDNA on the relevant sensor chip after several usages. Nonetheless, the results obtained indicated that 55bp-dsDNA, which had a predicted length of 19.47nm, may have exceeded the maximum bivalent antigenic distance of all the antibodies tested, including ONeg.

In summary, wt hIgG1, 0.5HA and 1HA appear to have a bivalent antigenic distance of less than 16.07nm. In contrast, ONeg may have a bivalent antigenic distance of between 16.07nm and 19.47nm, as indicated from the binding to 45bp NIP-dsDNA and 55bp NIP-dsDNA.

5.4.4 Determination of Fcγ receptor expression on THP-1 cells

To carry out target cell-effector cell bridging analysis, the expression of Fcγ receptors on the surface of the effector cells first had to be confirmed. In addition, the type of Fcγ receptors expressed should be identified because of their differing antibody binding affinity as described in Chapter 1, which might affect the interpretation of results obtained. As indicated in Figure 5.8, THP-1 cells expressed both FcγRI and FcγRII, as evidenced by the fluorescence observed in the flow cytometry analysis. This confirmation of Fcγ receptor expression allowed THP-1 to be used as the effector cell in subsequent rosetting assays.

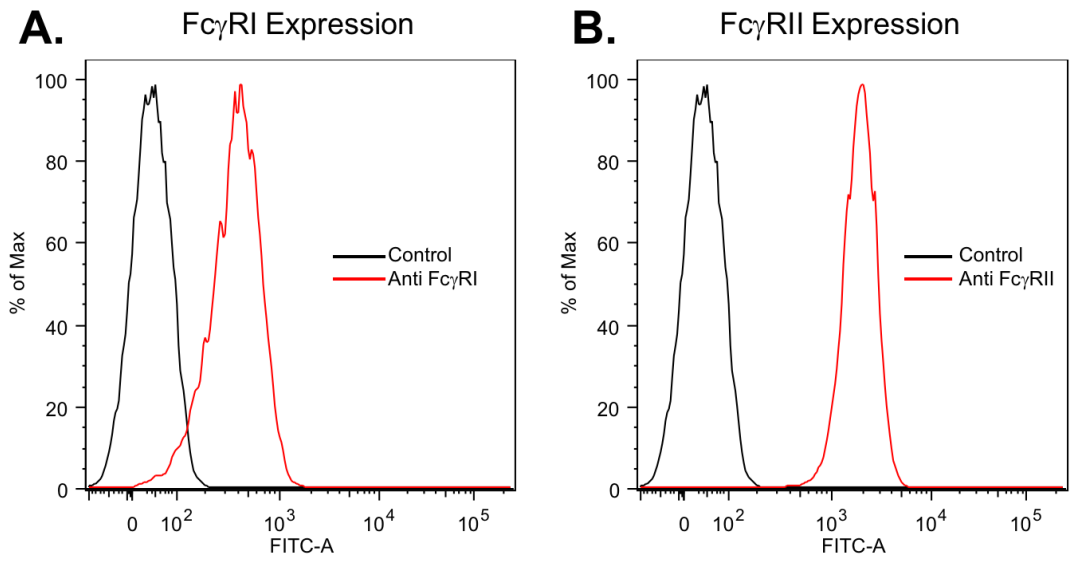

Figure 5.8: Result of flow cytometry analysis of FcγRI and FcγRII expression on THP-1 cells. **A.** Detection of FcγRI expression by probing THP-1 cells with anti-human CD64 FITC conjugated antibody. **B.** Detection of FcγRII expression by probing THP-1 cells with anti-human CD32 FITC conjugated antibody. In control, THP-1 was incubated with buffer only. Black line, control; red line, test with specific antibody. A representative experiment of 3 is shown.

5.4.4 Rosetting assay

A rosetting assay was performed to investigate whether upper hinge extension was able to impact on the target cell-effector cell bridging efficiency of an engineered IgG antibody. The results of rosette formation with each antibody is shown in Figure 5.9. Two hinge mutants, 0.5HA and 1HA, displayed very slightly increased levels of rosette formation compared to wt hIgG1. 0.5HA, which had half the hIgA1 hinge inserted, gave maximal rosette formation at the lowest concentrations, followed by 1HA which had the longest hinge insertion. One possible explanation for these minor differences is that both 1HA and 0.5HA have O-linked glycans within the hinge region which may impact to a small extent on the conformation of the hinge. Thus, it may be hypothesised that 0.5HA and 1HA may have a more open conformational structure, resulting in a slightly better reach to target antigens between target and

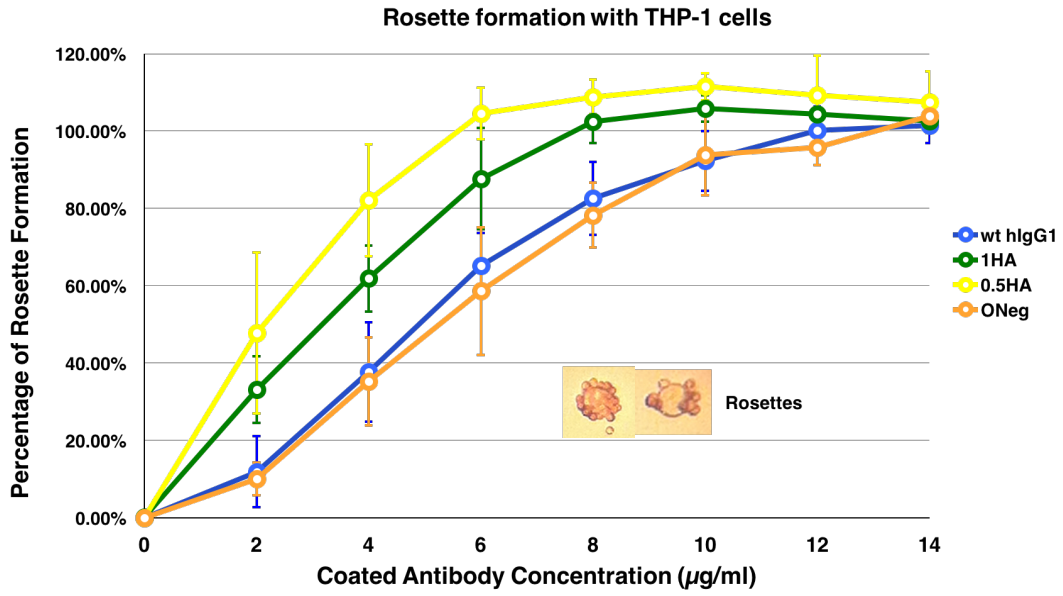

Figure 5.9: Formation of rosettes with THP-1 cells and NIP-derivatized red blood cells coated with different concentrations of anti-NIP antibodies. Results were normalised by setting the maximal rosette formation achieved with wildtype hIgG1 as 100%. Blue, wt hIgG; green, 1HA; yellow, 0.5HA; brown ONeg. Inset lower right shows the appearance of typical rosettes. The results shown are the amassed results of 3 experiments. The bars represent standard deviation measurements.

effector cell when compared to wt hIgG1 and ONeg, which both lack the O-linked glycans. It was perhaps surprising that ONeg behaved similarly to wt hIgG1 in rosette formation despite ONeg having a longer hinge and seemingly being able to bind bivalently to 45bp-dsDNA, whilst the other antibodies could not. The major difference between ONeg and 1HA is the presence of O-linked glycans within the hinge region. Therefore, the result in Figure 5.9 suggested that possibly a slightly more open conformational structure of antibody at the hinge region resulting from O-linked glycosylation may influence target cell-effector cell bridging efficiency to a small extent. However, further experimentation would be required to verify any differences in hinge conformation resulting from variation in glycosylation. Moreover, the differences observed are very minor indeed, since half-maximal rosette formation lies in all cases between 2 µg/ml and 6 µg/ml. The similar percentage rosette formation observed for ONeg and wt hIgG1 suggest that hinge

length may not be the only factor influencing target cell-effector cell bridging efficiency. Rather, a combination of hinge length and conformational structure, or other factors, may influence the outcome of rosetting assays to a small extent.

5.5 DISCUSSION

The structure of immunoglobulin molecules has been very well studied over the years. However, the functional bivalent antigenic distance between the antigen binding sites of the two Fab arms of different antibody molecules has not been fully determined to date. Previous studies had described attempts to estimate the Fab tip to tip distances based on the results from electron microscopy, neutron/X-ray scattering and crystallography of the antibodies. Using such techniques estimates of 120Å for rabbit IgGs (Valentine and Green, 1967), 117Å - 134Å for murine IgGs (Sosnick *et al*., 1992), 145Å for KOL (human IgG1) (Marquart *et al*., 1980) and 17nm (170Å) for human IgA1 (Boehm *et al*., 1999) have been reported. However, these reported calculations were estimations based on the conformational structure that the relevant antibodies adopted at the particular moment of analysis or crystallisation and were not the actual functional bivalent antigenic distance of the antibodies. In contrast, the model presented in this chapter utilised NIP-coupled dsDNA of different lengths as molecular rulers and the combination with SPR analysis as a means to estimate the bivalent antigenic distance. This approach was considered to be more accurate as it required the antibody to actually bind to target antigens that were spaced at different distances apart. The determination of the bivalent antigenic distance of an antibody was based on the theory regarding the difference in the rate of dissociation from antigen of monovalently bound antibody molecules and bivalently bound antibody molecules.

This project had hypothesised that upper hinge extension might increase the bivalent antigenic distance of an IgG1 antibody and in this chapter evidence has been presented in support of this hypothesis. Of particular note is the apparent bivalent binding activity of ONeg to 45bp NIP-dsDNA. In summary, three different NIP-dsDNA molecules, 20bp NIP-dsDNA, 45bp NIP-dsDNA and 55bp NIP-dsDNA, which differed in overall estimated length were generated for the investigation. The estimated length of 20bp NIP-dsDNA at 7.57nm, was well within the reported Fab tip to tip distance of Kol (145Å) (Marquart *et al*., 1980). Therefore, it was expected that all the tested antibodies would be able to bind bivalently to 20bp NIP-dsDNA. Indeed, this expectation was validated by the observed low dissociation rates of all antibodies at 2nM (100RU) from 20bp NIP-dsDNA, which suggested that the mode of binding was chiefly bivalent in nature. Subsequently, the hypothesis was supported by the binding of the generated antibodies to 45bp NIP-dsDNA. With an estimated length of 16.06nm, 45bp NIP-dsDNA was designed to differentiate the monovalent and bivalent binding capabilities of the matched set of anti-NIP antibodies. The slower rate of dissociation of ONeg from 45bp NIP-dsDNA, compared to those of wt hIgG1, 0.5HA and 1HA, suggested that ONeg was the only recombinant antibody tested to be more capable of bind bivalently to 45bp NIP-dsDNA. Finally, 55bp NIP-dsDNA with an estimated length of 19.47nm was designed to exceed the reported Fab tip to tip distance of hIgA1, estimated to be 17nm (Boehm *et al*., 1999), with the expectation that no bivalent binding activity would be possible for the antibodies tested. Indeed, all antibodies showed similar rates of dissociation, suggesting that all could only bind monovalently to 55bp NIP-dsDNA. The proposed binding activity of each different antibody to 20bp NIP-dsDNA, 45bp NIP-dsDNA and 55bp NIP-dsDNA is summarised in Figure 5.10.

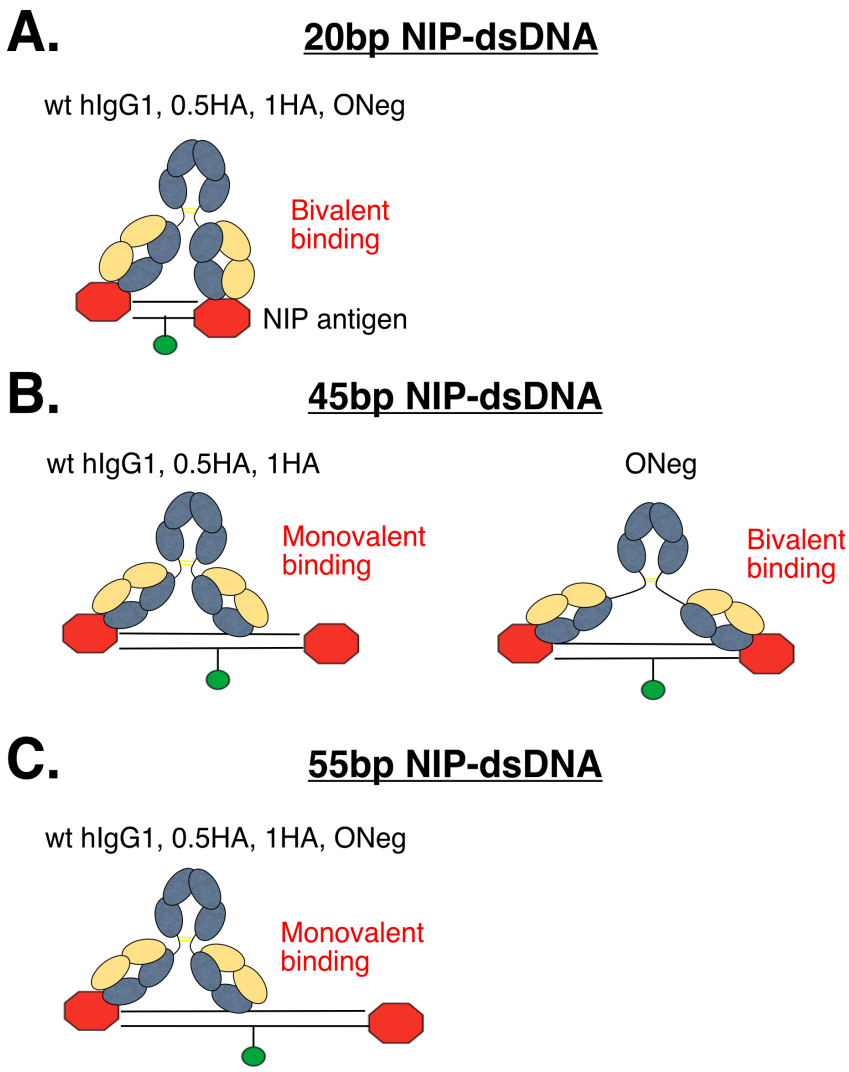

Figure 5.10: A diagram illustrating the proposed binding activity of different anti-NIP hinge mutant antibodies (wt hIgG1, 0.5HA, 1HA and ONeg) to different NIP-dsDNA bivalent ligands. **A**) All antibodies appear to bind bivalently to 20bp NIP-dsDNA which was predicted to be 7.57nm. **B**) wt hIgG1, 0.5HA and 1HA appeared to be less capable or unable to bind bivalently to 45bp NIP-dsDNA, which was predicted to be 16.07nm, whilst ONeg demonstarted some potential of bivalent binding. **C**) All antibodies appeared to bind monovalently to 55bp NIP-dsDNA which was predicted to be 19.4nm. wt hIgG1, wild type human IgG1; 0.5HA, half hinge hIgG1 mutant; 1HA full hinge hIgG1 mutant; ONeg, O-linked glycosylation negative full hinge hIgG1 mutant.

The results from the SPR analyses have shown that the NIP-dsDNA/SPR measurement model to be a feasible model for such determinations. More importantly, 1HA which has an insertion of the same number of amino acids as ONeg was less capable to bind bivalently to 45bp NIP-dsDNA unlike ONeg. This finding suggested that this measuring model may be highly sensitive and suitable to

accurately determine the bivalent antigenic distance of an antibody. In the future, this measuring model should allow the determination of the bivalent antigenic distance of other anti-NIP antibodies, such as wildtype IgG (of any subclass), IgA (of either subclass), IgM, IgE, and IgD. Moreover, bispecific antibodies and also other antibody formats like BiTE, might be amenable to future investigation by such means. Since the dsDNA bivalent ligand is formed by the association of two independent ssDNA, it should be possible to covalently conjugate different antigens to each ssDNA respectively in order to generate a dsDNA bivalent ligand consisting of two different antigens for the bivalent antigenic distance investigation of bispecific antibodies.

This project also hypothesised that an increase in upper hinge length would increase the target cell-effector cell bridging efficiency of an IgG antibody by improving the overall antigenic reach of Fab arms. This chapter took advantage of a rosetting assay as a model to compare the target cell-effector cell bridging efficiency of the different antibodies under test. An earlier study had demonstrated that THP-1 expressed both FcγRI and FcγRII (Fleit and Kobasiuk, 1991) and our findings confirmed this result. Due to the presence of FcγRI, which has the highest affinity for IgG and is able to bind monomer IgG at high affinity (Woof and Burton, 2004; Bruhns *et al*., 2009; Kiyoshi *et al*., 2015), it was predicted that majority of the target cell-effector cell bridging during rosetting would be mediated through FcγRI, although FcγRII may contribute to some extent. In a previous study, Walker and colleagues treated U937 and Daudi cell with bromelin which cleaved surface glycoproteins and reduced the net surface charge of cells and demonstrated an increase in rosette formation with both U937 and Daudi when hIgG1 and hIgG3 was used to coat RBCs (Walker *et al*.,

1989). More importantly, Daudi cells which expressed FcγRII but not FcγRI displayed better rosette formation after such treatment (Walker *et al*., 1989), suggesting that overcoming the repulsion forces between cells aided antibody bridging. With that reasoning, an increase in hinge length would be beneficial as it would extend the Fab arms of an antibody, allowing bridges to form between target cell and effector cell without such close approach, thereby avoiding mutual repulsion and resulting in more efficient binding. This reasoning was in agreement with the observation that the hinge mutants 0.5HA and 1HA elicited very slightly higher levels of rosette formation that wt hIgG1 when used at the same coating concentration. However, the slightly lower rosette formation of ONeg despite having a longer hinge than wt hIgG1 suggested that an increase in hinge length may not be the only factor in target cell-effector cell bridging efficiency. As a result, it was hypothesised that an open conformational structure of the hinge region may also be necessary. The main difference between ONeg and other hinge mutants is the absence of O-linked glycosylation. As described in Chapter 3, both 0.5HA and 1HA were proposed to adopt a more open hinge conformation due to the presence of O-linked glycosylation at the incorporated hinge region of hIgA1. It is possible that the presence of O-linked glycans help to maintain an open hinge conformation in 0.5HA and 1HA and maintain the Fab arms away from Fc region, thus, keeping the repulsion forces, mentioned above, to a minimum.

Finally, target cell-effector cell bridging is likely to also depend on the availability and geometry of the targeted antigen. In the context of the NIP antigen rosetting assay, NIP antigen was used in an excessive amount which would derivatise all available reactive sites of the surface of RBC. However, in reality, the availability of

target antigen on the surface of a pathogen may vary extensively and might be separated by significant distances from neighbouring molecules. In addition, the geometry of the targeted antigen might be a factor in governing the accessibility of the targeted epitope to Fab arms. Recently, Giuntini and colleagues compared the bactericidal activity, via complement activation, of chimeric IgG antibodies against two outer membrane meningococcal vaccine antigens and reported that IgG1 was the best performer in CDC activation against PorA (an abundant antigen) but IgG3 was better against FHbp (a limited and variably distributed antigen) (Giuntini *et al*., 2016). The superior performance of IgG3 against sparse antigens was most likely due to a longer and probably better flexibility of the upper hinge region which allowed the Fab arms to gain a better reach against target antigen. Such findings would further support the idea of upper hinge extension of IgG antibody contributing to a longer bivalent antigenic distance as well as better flexibility to bind to hidden or inaccessible epitopes.

Previously, Redpath and colleagues had generated a hIgG3 hinge deleted mutant, hIgG3m15, consisting of only 15 amino acids at the hinge region rather than the usual 63 amino acids, and showed that when compared to wt hIgG3, hIgG3m15 had a comparable binding to FcγRI but reduced binding to FcγRIIa. However, hIgG3m15 was more potent in mediating ADCC (Redpath *et al*., 1998). On the other hand, Tan and colleagues generated several hIgG3 hinge mutants, by duplication or removal of hIgG3 hinge exons, with different hinge lengths ranging from 17-107 amino acids and compared their proficiency in complement activation (Tan *et al*., 1990). Due to a similar complement binding and activation level exhibited by different antibodies, except hIgG3 mutant with a hinge length of 107 amino acids that showed reduced

complement fixing, the authors reported that the hinge length of hIgG3 is not sufficient to affect complement binding and activation. The exact reason for the reduced complement fixation by the mutant hIgG3 with the longest hinge length, 107 amino acids, was not known (Tan *et al*., 1990). However, these findings were not in agreement with the findings reported by Norderhaug and colleagues (1991). Norderhaug and colleagues similarly generated several hIgG3 hinge mutants with shortened hinge lengths (around 15 amino acids) and a hIgG3 mutant that carried the hinge region of hIgG4 to investigate the role of hinge length in complement activation (Norderhaug *et al*., 1991). The authors reported that hIgG3s with reduced hinge length were more efficient at complement activation than wt hIgG3. Unfortunately, this project did not manage to study both the ADCC and complement activation of the generated hIgG1 hinge mutants, therefore, it is not possible to comment on the role of upper hinge length of IgG1 in ADCC and complement activation. However, such studies are worth investigating to improve our understanding of the impact of structural features on antibody functionality.

In summary, the NIP-dsDNA model coupled with SPR analysis would be useful in determining the bivalent antigenic distance of different antibodies including bispecific antibodies. In addition, upper hinge extension was shown to most likely improve the reach of the Fab arms and increase the maximum bivalent antigenic distance of an IgG antibody. Finally, to improve overall target cell-effector cell bridging efficiency of IgG, it is suggested that upper hinge extension should be accompanied by certain requirements which could contribute to the maintenance of an open conformational structure of the antibody at the upper hinge region.

CHAPTER SIX
GENERATION OF Fc FUSION PROTEIN EXPRESSION PLASMIDS

CHAPTER 6. GENERATION OF Fc FUSION PROTEIN EXPRESSION PLASMIDS

6.1 INTRODUCTION

Fc fusion proteins are an expanding class of proteins in which a variety of proteins are fused with the Fc region of an immunoglobulin in order to impart novel function. Some of them, such as etanercept, aflibercept, rilonacept, belatacept and abatacept, are used in clinical therapies (Czajkowsky *et al*., 2012). For example, etanercept is a Fc fusion protein that was engineered to comprise tumour necrosis factor receptor (TNFR) fused to the Fc region of human IgG1, in order to function as a TNF inhibitor by acting as a decoy receptor (Haraoui and Bykerk, 2007). The creation of etanercept greatly benefited the treatment of several inflammatory diseases especially rheumatoid arthritis (RA) (Haraoui and Bykerk, 2007).

One of the major advantages of the Fc fusion protein format is the ability to utilise the long plasma half-life of immunoglobulins which is regulated by interaction with a unique Fc receptor called FcRn (Roopenian and Akilesh, 2007). FcRn binds specifically to the Fc region of IgG, however, it only interacts with IgG Fc at acidic pH 4.5-6.5 but not at physiological pH 7.4 (Roopenian and Akilesh, 2007). As described in Chapter 1 Figure 1.7B, when an IgG monomer is phagocytosed by a phagocytic cell through interaction with FcγR, the resultant phagocytic vacuole fuses with an endosome which contains FcRn, and is gradually acidified. When the vacuole reaches pH 4.5-6.5, FcRn is able to bind to the Fc region of the IgG and prevent the antibody from entering the degradation pathway. The IgG may then be recycled back to the extracellular environment and on reaching the extracellular

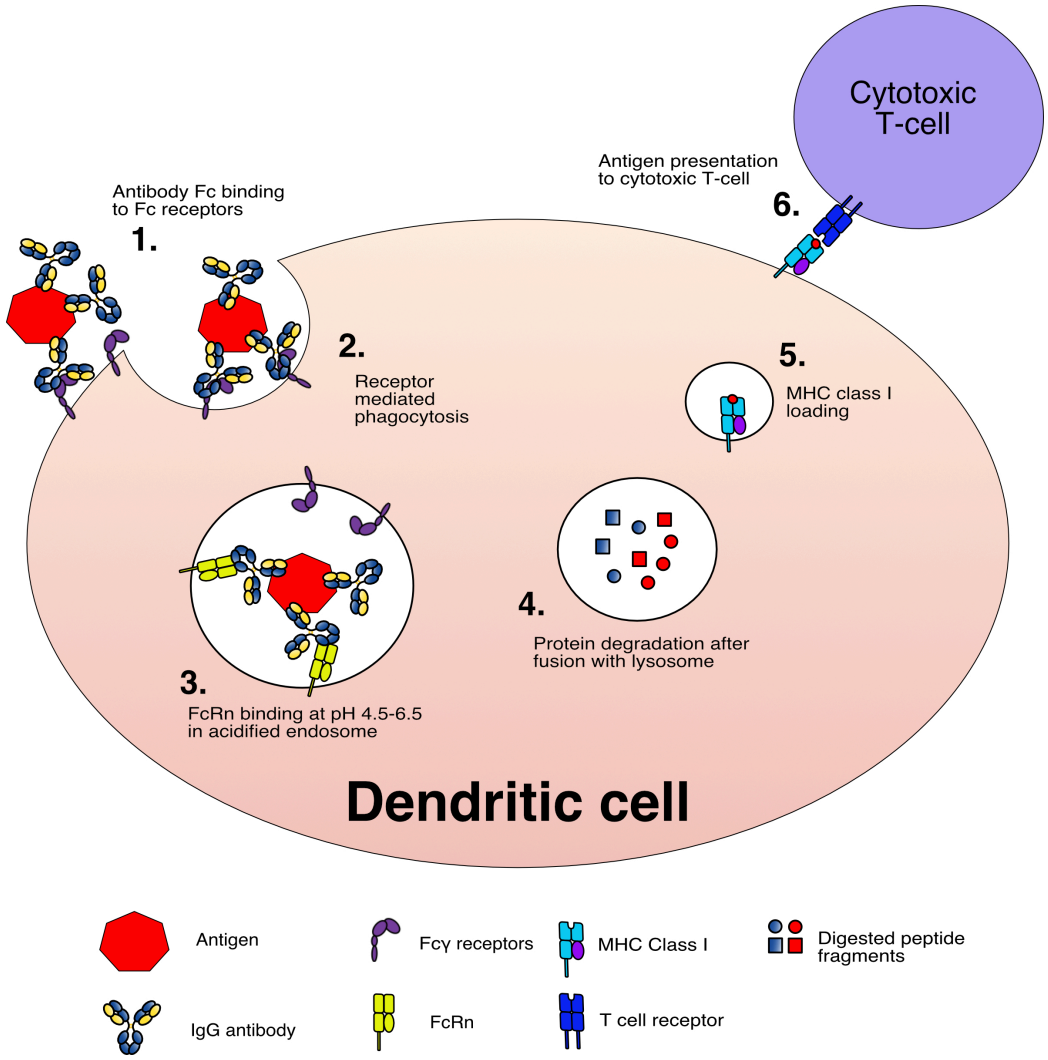

Figure 6.1: A schematic diagram illustrating the process of antigen cross presentation mediated by FcRn in a dendritic cell. **1**) Antigen immune complex bound to Fcγ receptors. **2**) Fcγ receptor activation induces phagocytosis of the immune complex. **3**) FcRn binding to Fc region of IgG antibodies in acidified endosome. **4**, **5** and **6**) Antigen is digested into small peptides and loaded onto MHC class I for antigen presentation to activate cytotoxic T cells.

space with a pH of 7.4, the IgG will dissociate form FcRn and be released to carry out its immunological function again (Roopenian and Akilesh, 2007). More recently, FcRn was shown to be capable of promoting antigen cross presentation in dendritic cells, which resulted in presentation of digested exogenous antigens on MHC-I molecules and subsequent activation of cytotoxic T cells (Liu *et al*., 2011; Baker *et al*., 2011). The process of antigen cross presentation is briefly described in Figure 6.1.

Baker and colleagues showed that dendritic cells that expressed FcRn were able to initiate a cytotoxic T cell response with a 100-fold lower antigen concentration than that required for dendritic cells that did not express FcRn (Baker *et al*., 2011). In addition, the authors also showed that a mutant hIgG1, known as IHH-IgG, which was unable to bind to FcRn provided a confirmatory result. Thus, immune complexes formed by IHH-IgG were unable to effectively activate a cytotoxic T cells response (Baker *et al*., 2011). In a further study, Baker and colleagues used adoptive transfer of wildtype dendritic cells into $Fcgrt^{-/-}$ mice (i.e. mice lacking FcRn expression) that were suffering from induced colorectal cancer. They found that transfer of the wildtype FcRn-positive dendritic cells greatly improved the infiltration of cytotoxic T cells into the tumour environment and provided protective immunity to the mice that lacked FcRn expression, whereas transfer of DC lacking FcRn expression did not (Baker *et al*., 2013). An interpretation of these findings is that the enhanced T cell cytotoxic response was due to antigen cross presentation that occurred within newly transferred dendritic cells that expressed FcRn. As a result, the engagement of antibodies with FcRn seems to be crucial for the induction of antigen cross presentation to obtained an enhanced cytotoxic T cell activity against exogenous antigens. In a different study, Ye and colleagues fused the herpes simplex virus type-2 (HSV-2) glycoprotein gD to the Fc region of murine IgG2a and vaccinated both wt mouse expressing FcRn and $Fcgrt^{-/-}$ mouse with the generated Fc fusion protein before subjecting them to HSV challenge (Ye *et al*., 2011). The authors reported that the wt mice displayed complete protection against the viral challenge and had stronger T cell and antibody responses when compared to the FcRn knockout mice (Ye *et al*., 2011). Again, this result supports the idea that FcRn is capable of promoting antigen cross presentation by dendritic cells. These findings in antigen

cross presentation studies raise the possibility of using FcRn antigen presentation as a means to induce effective anti-tumour immune responses. It can be hypothesised that one might generate a potential cancer vaccine by fusing a protein which is highly expressed by cancer cells to the Fc region of IgG. Such a vaccine might induce effective antigen cross presentation of the fused protein and thereby activate relevant cytotoxic T cells to kill cancer cells.

One major obstacle in this Fc-fusion protein approach is the selection of a suitable protein to be fused with the Fc region of wt hIgG1, since the majority of proteins expressed by cancer cells are also found in normal cells. T cells and B cells undergo selection in the thymus and bone marrow respectively, whereby self-epitopes are presented to naïve T cells and B cells and any self-reactive cells are eliminated. Therefore, this defensive mechanism should prevent any immune response against self-expressed proteins. As a result, the selection of a protein expressed by cancer cells but not on normal cells has proven to be difficult. Fortunately, a group of proteins known as cancer testis antigens (CTA) have been shown to be expressed only by cancer cells but not normal cells other than testis, ovary and placenta (Scanlan *et al*., 2002). This CTA appear suitable as candidate proteins for Fc-fusion cancer vaccines. Although CTA are expressed in testis, ovary and placenta, these sites are immune privileged sites in which the activation of an immune response is greatly reduced or well tolerated (Hong and Van Kaer, 1999; Li *et al*., 2012). Therefore, if an immune response was initiated against cancer cells by an CTA-Fc fusion vaccine it might be expected that no severe damage would occur to CTA-expressing normal tissues, such as testis, ovary and placenta, in the body. With such reasoning, CTA proteins may serve as suitable candidates to be fused to the Fc

region of wt hIgG1 to generate potential cancer vaccines. By fusing CTA protein to the Fc region of IgG, the resultant Fc fusion protein would benefit from long plasma half-life due to FcRn binding, thus, increasing the chances of the Fc fusion protein to elicit host antibodies directed against CTA protein and form immune complexes via antigen binding. As a result, this could induce antigen cross presentation of the CTA protein to activate cytotoxic T cells which might serve to eliminate CTA expressing cancer cells. The concept of using such vaccine will be further described below.

6.1.1 Melanoma-associated antigen (MAGE) A protein family

As mentioned above, CTA are a unique class of proteins that were highly expressed by cancer cells but expression on normal tissues is restricted to testis, ovary and placenta (Scanlan *et al*., 2002). Several protein classes have been categorised as CTA over the years, including melanoma-associated antigens (MAGE), NY-ESO-1, and synovial sarcoma X (SSX) antigens (Scanlan *et al*., 2002). Amongst these protein classes, MAGE have been well studied and found to be expressed by a wide range of different cancers, such as those of ovary, lung, breast and bladder (Müller-Richter *et al*., 2009; Figueiredo *et al*., 2011; Schultz-Thater *et al*., 2011; Meek and Marcar, 2012). MAGE-1 (now renamed to MAGE-A1) was the first member to be identified after isolating the corresponding cytotoxic T cell from an autologous melanoma patient (van der Bruggen *et al*., 1991). Many more family members had been identified subsequently and currently MAGE were categorised into three subfamilies known as MAGE-A, MAGE-B and MAGE-C (Meek and Marcar, 2012; Sang *et al*., 2011). MAGE-A have been well studied and consists of twelve family members, named MAGE-A1 to MAGE-A12 (Meek and Marcar, 2012; Sang *et al*., 2011). The actual function of each MAGE-A proteins is still unknown but it was identified that

Figure 6.2: A schematic diagram illustrating the MAGE-A protein family members aligned based on the MAGE Homology Domain (MHD) (purple). MAGE-A7 is a pseudo-gene therefore not shown. The numbering above each protein family member represents amino acid residues. Image adapted from (Meek and Marcar, 2012).

all MAGE-A proteins share a conserved domain consisting of around 165-171 amino acids termed MAGE Homology Domain (MHD), as shown in Figure 6.2 (Sang *et al*., 2011). MAGE A proteins have been reported to be expressed by a variety of different cancers (Müller-Richter *et al*., 2009; Figueiredo *et al*., 2011; Schultz-Thater *et al*., 2011; Meek and Marcar, 2012). Figueiredo and colleagues reported the expression of MAGE-A1, -A3 and -A4 in patients suffering from laryngeal

squamous cell carcinoma based on an immunohistochemistry technique (Figueiredo *et al*., 2011). On the other hand, Müller-Richter and colleagues reported the expression of MAGE-A2, -A3, -A4, -A6 and -A10 in five oral squamous cell carcinoma cell lines (Müller-Richter *et al*., 2009). In a more detailed investigation, Schultz-Thater and colleagues generated a monoclonal antibody against MAGE-A10 and investigated the expression of MAGE-A10 in a variety of cancers (Schultz-Thater *et al*., 2011). The authors reported that MAGE-A10 was highly expressed in breast, oesophagus, lung and skin cancers (Schultz-Thater *et al*., 2011). MAGE-A proteins are highly expressed in various cancer diseases as mentioned above. More importantly, all MAGE-A proteins share a conserved MAGE Homology Domain (MHD). Therefore, if a cytotoxic T cell immune response is initiated against an epitope belonging to the MHD it may be expected that the relevant cytotoxic T cell immune response would be effective against all cancer cells that express MAGE-A proteins.

In this study, MAGE-A2 was selected as the protein to be fused with the Fc region of wt hIgG1 to generate a potential cancer vaccine. The exact role of MAGE-A2 is as yet unknown. However, investigations have shown that MAGE-A2 can directly bind to p53 core and recruit transcription repressors to repress p53 activity (Monte *et al*., 2006). Such activity might be expected to result in the initiation of an uncontrollable cell proliferation thus causing the development of cancer. In an immunotherapeutic view, Graff-Dubois and colleagues had identified a few HLA-A*0201 restricted MAGE-A peptides which were able to stimulate specific cytotoxic T cells to kill human cancer cells that expressed different MAGE-A proteins, including MAGE-A2 (Graff-Dubois *et al*., 2002). In addition, Tanzarella and colleagues identified a HLA-

B*3701 restricted MAGE-A peptide, which was expressed by MAGE-1, -2, -3 and -6 (MAGE-A1, -A2, -A3, -A6), that could induce a cytotoxic T cell immune response against COS-7 cells which were co-transfected with HLA-B*3701 and MAGE-1, -2, -3 and -6 respectively (Tanzarella *et al*., 1999). Based on such findings, MAGE-A2 was considered a reasonable candidate for a generation of an Fc-fusion protein vaccine.

6.1.2 Fusion of MAGE-A2 with IgG1 Fc

The antigen cross presentation assays carried out in previous studies involved the activation of Fcγ receptors on the surface of dendritic cells to induce phagocytosis of immune complexes (Baker *et al*., 2013; Baker *et al*., 2011). It is not known if a monomeric MAGE-A2-Fc (MFc) molecule would induce antigen cross presentation by itself. Therefore, as a precaution the binding site for Fcγ receptors on any MFc should not be disturbed to examine the characteristic of monomeric MFc. The binding site on IgG for Fcγ receptors has been localised to the lower hinge region (Woof and Burton, 2004). In addition, the crystal structure of MAGE-A2 protein has not been solved. Therefore, it is not known if the structure of the MAGE-A2 protein would be likely to cause any steric hindrance to the Fc region. As a result, it was decided that a 13 amino acid peptide linker, GSSGGGSSGGSSS, should be introduced to the C-terminal of the MAGE-A2 protein and fused to the N-terminal of the hinge region of IgG. It was hoped that the linker might help to keep the MAGE-A2 protein distanced apart from IgG Fc region and minimise any possible steric hindrance. By keeping the hinge region of the IgG intact, the cysteine residues that were responsible for interchain disulphide bonding would be undisturbed. Therefore, it was expected that two MFc polypeptide chains would associate and link together

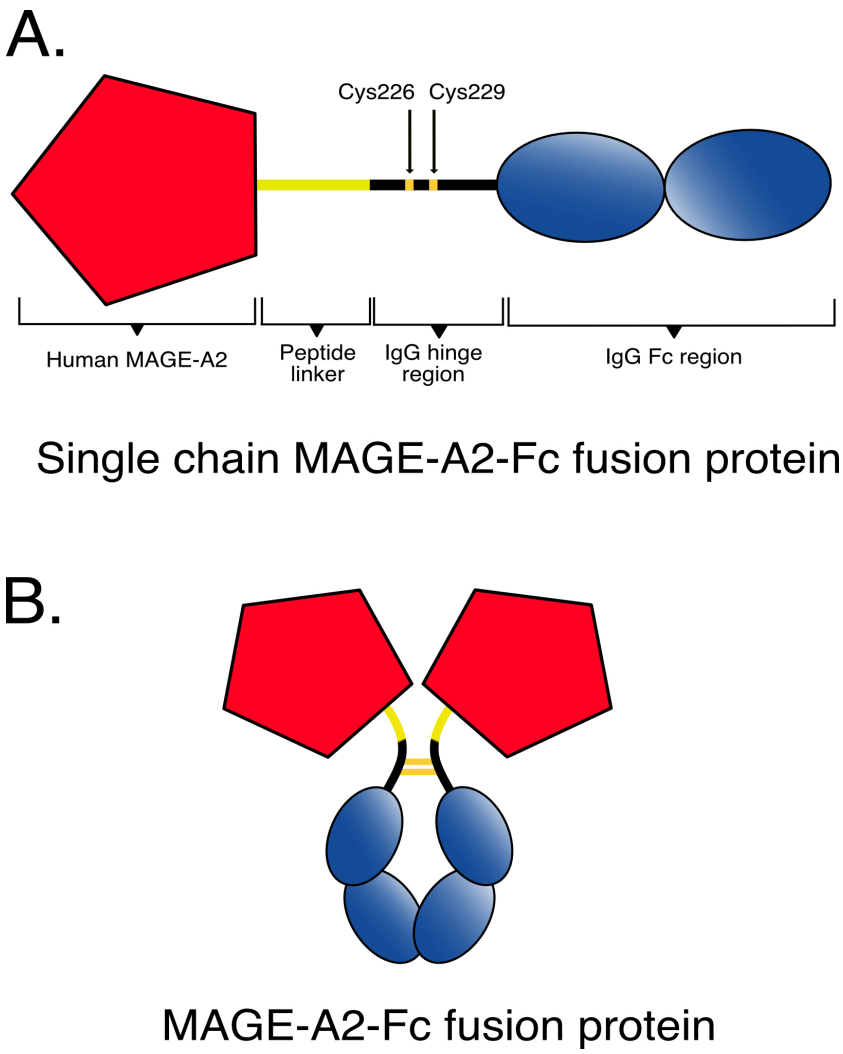

Figure 6.3: A schematic diagram illustrating the general structure of MAGE-A2-Fc fusion protein (MFc). **A**) The expected general structure of a MFc polypeptide which consists of the IgG Fc region, IgG hinge region, peptide linker and human MAGE-A2 protein. Cys226 and Cys229 (EU numbering) form the interchain disulphide bond with another single chain MFc. **B**) The predicted general structure of MFc protein in which interchain disulphide bonding had been formed between two MFc polypeptides.

just as in an immunoglobulin molecule. A diagram illustrating the expected general structure of MFc is shown in Figure 6.3.

6.1.3 The role of FcRn in the concept of MAGE-A2-Fc (MFc) fusion protein as cancer vaccine

MAGE-A2-Fc fusion cancer vaccine protein (MFc) was designed with the aim of utilising the antigen cross presentation ability of FcRn to induce a suitable cytotoxic

T cell immune response against cancer cells. In addition, the inclusion of the Fc region of IgG in MFc was designed to take advantage of the long plasma half-life of associated with FcRn engagement. The concept of MFc as a potential cancer vaccine is illustrated in Figure 6.4. In brief, when MFc is injected into the patient, MFc would encounter host antibodies that would specifically recognise MAGE-A2 as foreign protein thereby forming immune complexes. Subsequently these immune complexes would be taken up by phagocytic cells, in particular dendritic cells, via FcγR engagement. The phagocytic vacuole would fuse with endosomes, which contained FcRn, and become gradually acidified to initiate protein degradation. When the pH of the endosome reached pH 4.5-6.5, the histidine residues of the Fc region would be protonated and association with FcRn would occur (Roopenian and Akilesh, 2007). The late endosomes would fuse with lysosomes and MFc would be degraded and digested into appropriate short peptides to be loaded onto MHC class I and MHC class II molecules. Baker and colleagues had demonstrated that IgG immune complexes remain bound to FcRn within the intracellular compartment after 60 minutes whereas IHH-IgG immune complexes were not found after internalisation beyond 60 minutes (Baker *et al*., 2011). The authors suggested that the longer period of time that immune complexes were retained by FcRn allowed for proper digestion of antigens in order to be presented on MHC class I molecules (Baker *et al*., 2011). The exact mechanism of antigen cross presentation to MHC class I molecules was still unknown and remains under investigation. However, antigen presentation on MHC class I molecules would activate corresponding cytotoxic T cells to induce an immune response against cancer cells that expressed MAGE-A2 or other MAGE-A proteins that contained similar peptide sequences. In a different scenario, it was also possible that MFc would encounter FcγR-expressing

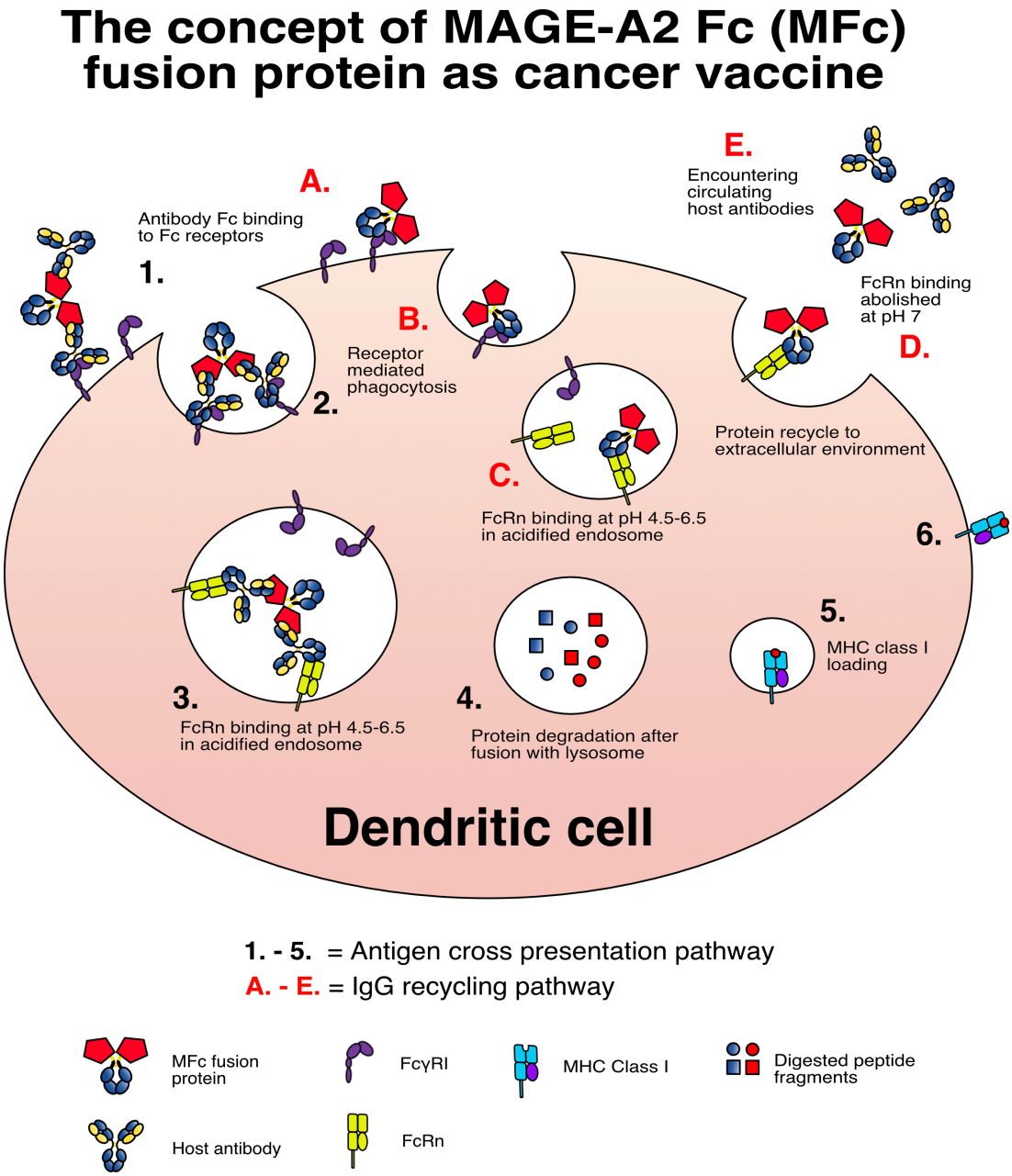

Figure 6.4: A schematic diagram illustrating the concept of MAGE-A2-Fc (MFc) fusion protein as a cancer vaccine. **1, 2, 3, 4, and 5** highlight the key mechanisms of antigen cross presentation pathway and **A, B, C, D, E** highlight the key mechanisms of the recycling pathway. **1** and **A**) MFc immune complex or monomer bound to FcγRI. **2** and **B**) FcγRI activation induced phagocytosis of MFc. **3** and **C**) FcRn binding to MFc in acidified endosome. **4**, **5** and **6**) MFc is digested into small peptides and loaded onto MHC class I for antigen presentation to activate cytotoxic T cells. **D and E**) FcRn-bound MFc is transported to the extracellular space and released at pH 7 to encounter host antibodies.

cells before an immune complex was formed. The Fc region of MFc was derived from wt hIgG1, thus, it would have a high affinity for FcγRI and could bind to FcγRI as a monomer. In such cases, upon FcγRI engagement MFc might be expected to be internalised via FcγRI binding and the resultant vacuole would fuse with an endosome that contained FcRn. The endosome would be gradually acidified and when the pH reached pH 4.5-6.5 FcRn would bind to the Fc region of MFc, therefore, protecting MFc from protein degradation. Ward and colleagues had demonstrated that IgG molecules that are unable to bind to FcRn proceed into the lysosomal pathway in which are degraded whereas IgG that are able to bind FcRn are recycled back to the extracellular space (Ward *et al*., 2003). As a result, MFc might be expected to be recycled back to the extracellular environment and the association with FcRn would be abolished at pH 7, thus, resulting in the release of MFc back into the blood stream, allowing MFc to encounter circulating host antibodies.

6.2 AIMS

This chapter hypothesised that a potential cancer vaccine could be generated by fusing human MAGE-A2 to the Fc region of IgG antibody to stimulate a strong cytotoxic T cells immune response against MAGE-A2 expressing cancer cells. As a result, the aim of this chapter was to generate MFc fusion proteins using both murine IgG2a or wt hIgG1 Fc regions. This chapter also aimed to investigate whether such MFc fusion proteins could be successfully produced in mammalian cells using recombinant antibody technology.

6.3 MATERIALS AND METHODS

6.3.1 PLASMIDS

pMAGE-A2

A plasmid, pMAGE-A2, encoding wildtype human MAGE-A2 was a gift from Bianca Ihrig and Dr David Meek (University of Dundee).

pFUSEN-mG2AFc

A plasmid, pFUSEN-mG2AFc, encoding the hinge region and the CH2 and CH3 constant domains of the murine IgG2a heavy chain, was purchased from InvivoGen.

pHCCR

The pHCCR plasmid encoding the majority of the constant region of the heavy chain of wildtype human IgG1 (wt hIgG1) was described in Chapter 2.

6.3.2 CONSTRUCTION OF Kz-hMFc AND Kz-mMFc PLASMIDS

6.3.2.1 Generation of hMFc (MAGE-A2 fused with wt hIgG1 Fc) expression plasmid

The procedure for fusing sequence encoding human MAGE-A2 to that encoding the Fc region of wt hIgG1 is illustrated in Figure 6.5.

A. MAGE-A2 amplification

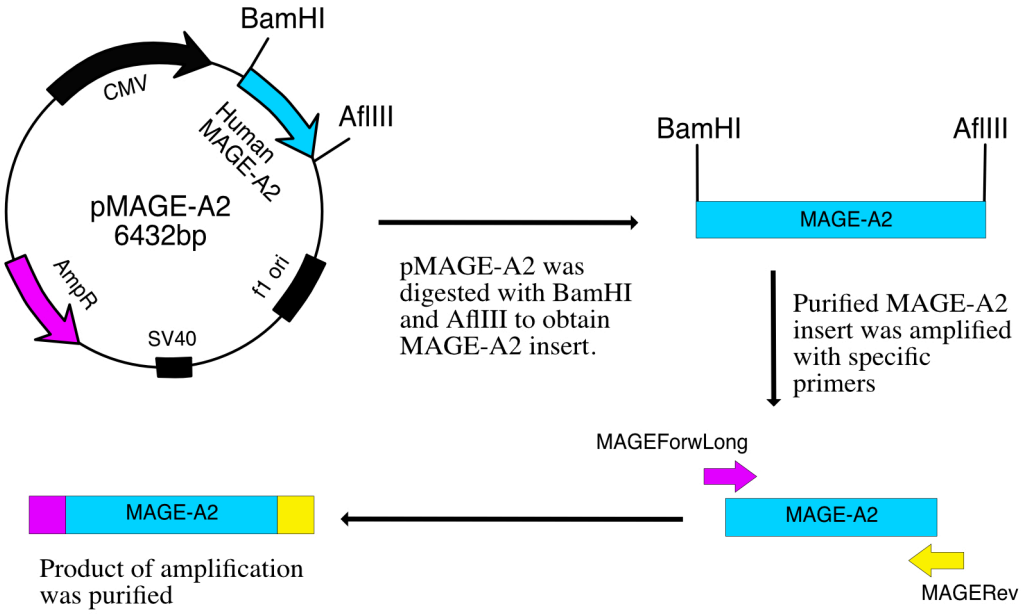

B. hIgG1 Fc amplification

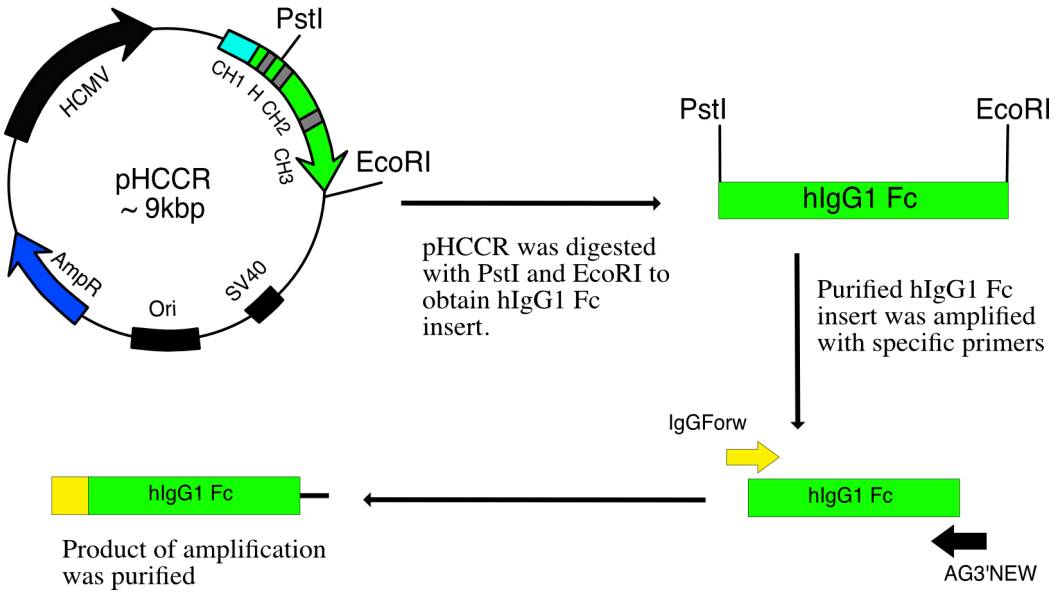

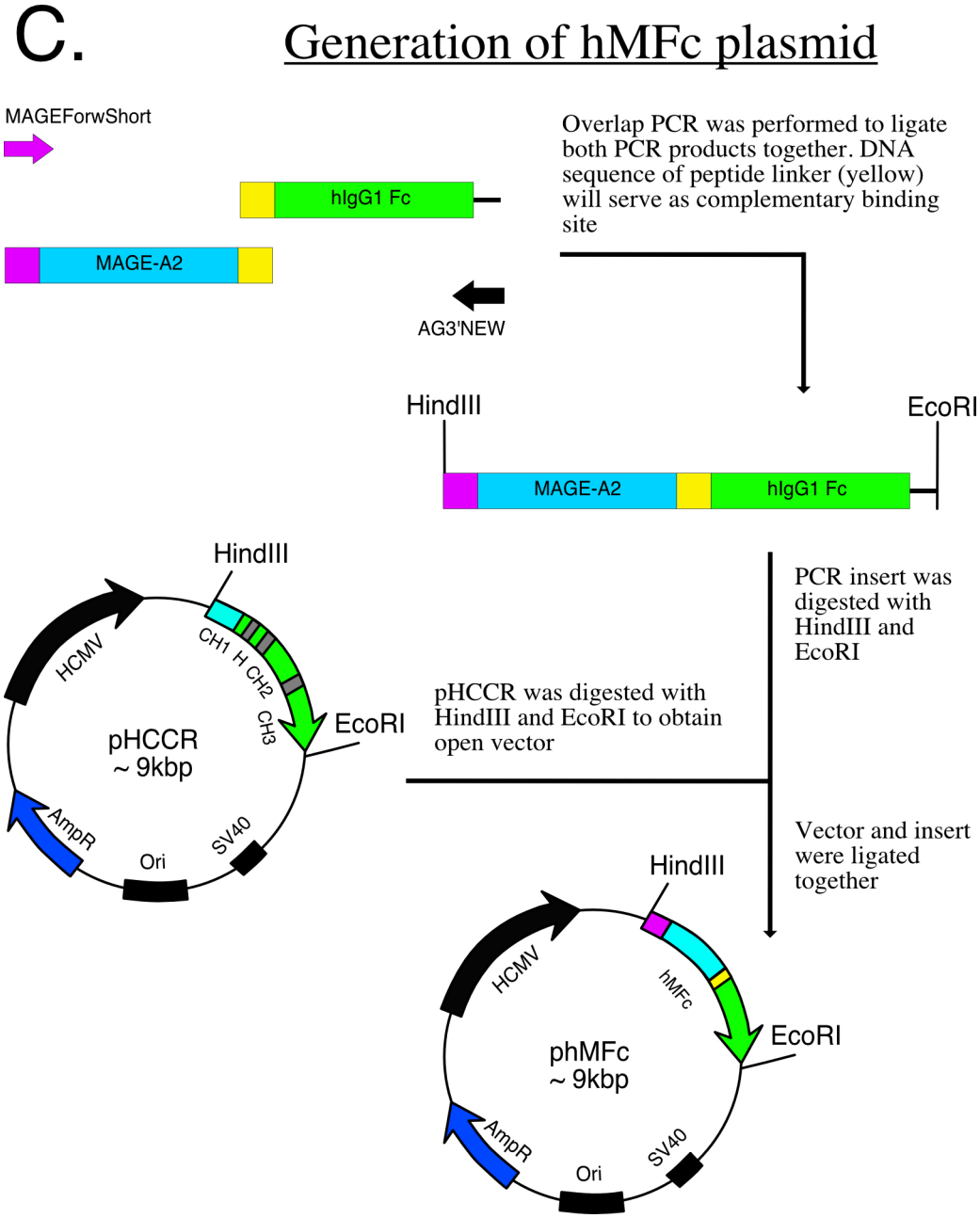

Figure 6.5: A schematic diagram illustrating the generation of the MAGE-A2-hFc expression vector. **A**) MAGE-A2 amplification procedure. pMAGE-A2 was digested with BamHI and AflIII to obtain the insert containing MAGE-A2 DNA sequence which was amplified with specific primers to introduce sequence encoding an immunoglobulin secretion signal peptide (purple) at the 5´ end and one encoding a linker peptide (yellow) at the 3´ end. **B**) hIgG1 Fc amplification procedure. pHCCR was digested with PstI and EcoRI to obtain the insert containing hIgG1 Fc DNA sequence which was amplified with specific primers to introduce sequence encoding a linker peptide (yellow) at the 5´ end. **C**) Generation of hMFc expression vector. An overlap PCR was performed to fuse the PCR products from **A** and **B** together using specific primers and the final product was digested with HindIII and EcoRI. pHCCR was digested with HindIII and EcoRI to obtain an open vector to ligate with the previously digested insert.

Amplification of sequence encoding MAGE-A2

pMAGE-A2 was digested with restriction enzymes Afl III and BamHI at 37ºC for 1 hour as described in section 2.4.1. Gel electrophoresis and DNA gel extraction were performed to purify digested a DNA fragment of about 965bp, containing the DNA sequence of MAGE-A2 (insert). Primers MAGEForwLong and MAGERev (Table 2.2, No. 9 & 8) were used at an annealing temperature of 50ºC to amplify the purified DNA insert to obtain a DNA product of approximately 1050bp, which contained a HindIII site at the 5' end. Primers MAGEForwLong and MAGERev were designed to introduce sequence encoding an immunoglobulin secretion signal peptide, MGWSCIILFLVATATGVHS, at the 5´ end and sequence encoding a 13 amino acid peptide linker, GSSGGGSSGGSSS, at the 3´ end of the amplified MAGE-A2 DNA sequence. PCR products were run on a DNA agarose gel as described in section 2.4.4 and DNA bands of the correct sizes were extracted as described in section 2.4.5.

Amplification of sequence encoding wt hIgG1 Fc region

pHCCR was digested with restriction enzymes EcoRI and PstI at 37ºC for 1 hour as described in section 2.4.1. Gel electrophoresis and DNA gel extraction were performed to purify a digested DNA fragment of about 1031bp, containing sequence encoding the Fc region of wt hIgG1 (insert). Primers IgGForw and AG3´NEW (Table 2.2, No. 10 & 4) were used at an annealing temperature of 40ºC to amplify the purified DNA insert to obtain a DNA product of approximately 1034bp, which contained an EcoRI site at the 3´ end. PCR products were run on a DNA agarose gel as described in section 2.4.4 and DNA bands of the correct sizes were extracted as described in section 2.4.5.

Fusion of MAGE-A2 with wt hIgG1 Fc region and generation of plasmid construct

Using a PCR procedure described in section 2.4.3, an overlap PCR extension was performed by using a mix of 2µl of extracted MAGE-A2 and 2µl of extracted wt hIgG1 Fc DNA fragments as templates and MAGEForwShort and AG3´NEW as primers (Table 2.2, No. 7 & 4) at an annealing temperature of 50ºC, to produce a final DNA product of approximately 2056bp. Gel electrophoresis and DNA gel extraction were carried out subsequently. Purified DNA fragment and plasmid pHCCR were then digested with restriction enzymes HindIII and EcoRI as described in section 2.4.1. Gel electrophoresis and DNA gel extraction were performed to purify the digested DNA fragment of 2044bp (insert) and digested pHCCR of about 8000bp (vector). Both purified DNA fragments were then ligated as described in section 2.4.6 and transformed into competent DH5α *E. coli* as described in section 2.4.7. After purifying the plasmids from positive clones as described in section 2.4.9, DNA sequencing was carried out (section 2.4.11) to ensure that sequence encoding MAGE-A2 had been correctly fused with that encoding the Fc region of wt hIgG1. A plasmid with the correct DNA sequence was named as phMFc.

6.3.2.2 Generation of Kz-hMFc expression plasmid

It was later realised that the phMFc expression vector did not contain the Kozak consensus sequence which is important for efficient protein expression (Lida and Masuda, 1996). Therefore, incorporation of the required Kozak sequence was carried out. The process for introduction of the Kozak consensus sequence is illustrated in Figure 6.6. phMFc was digested with restriction enzymes HindIII and EcoRI as described in section 2.4.1. Gel electrophoresis and DNA gel extraction were

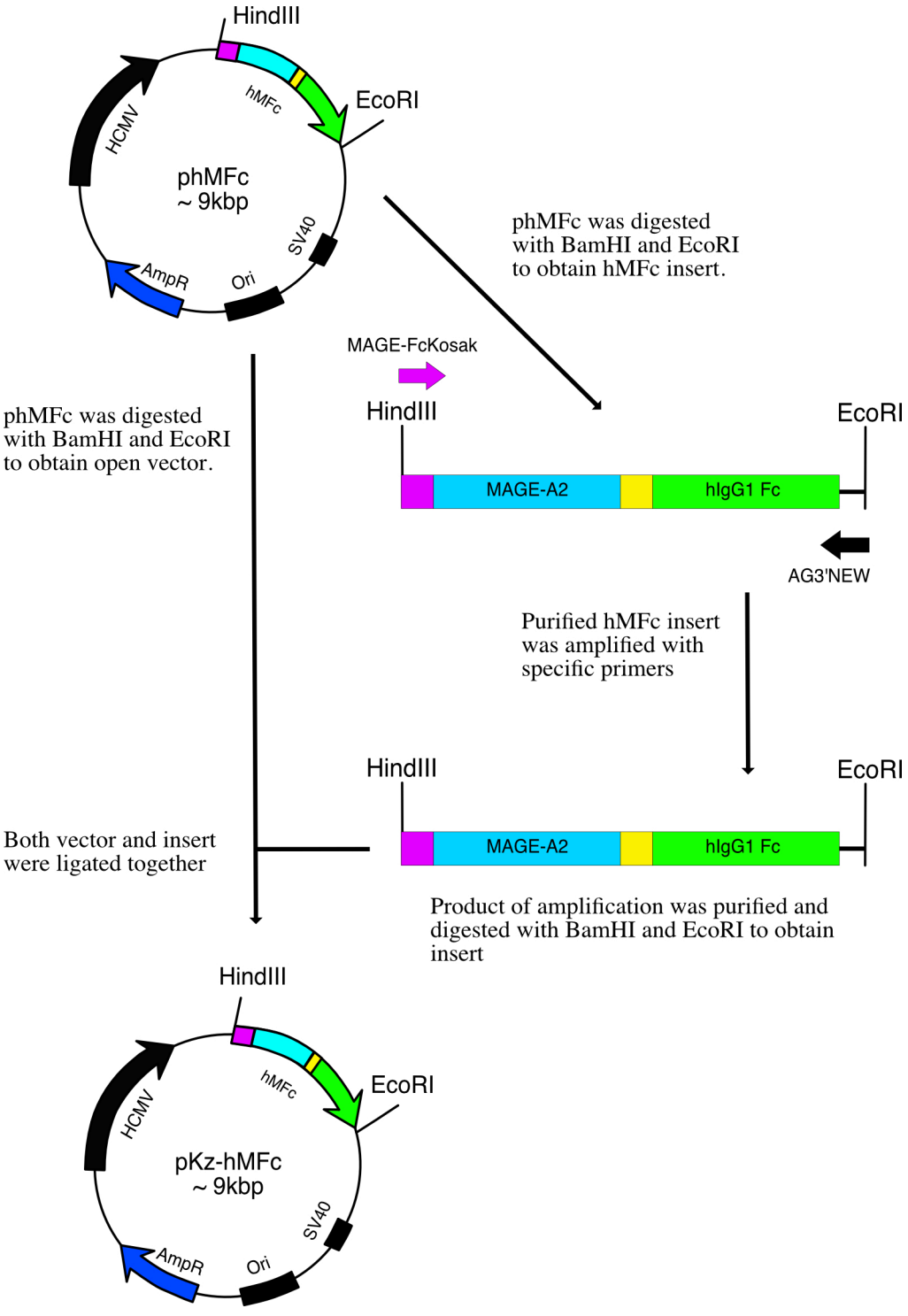

Figure 6.6: A schematic diagram illustrating the incorporation of the Kozak consensus sequence into the hMFc expression vector. phMFc was digested with HindIII and EcoRI to obtain the insert containing hMFc DNA sequence and an open vector. The hMFc insert was amplified with specific primers to introduce the Kozak consensus sequence and ligated with the purified vector.

performed to purify a digested DNA fragment of about 2044bp, containing the DNA sequence of hMFc. Primers MAGE-FcKosak and AG3´NEW (Table 2.2, No. 11 & 4) were used at an annealing temperature of 60ºC to amplify the purified DNA insert to obtain a DNA product of approximately 2061bp, which contained sequence encoding a HindIII site at the 5´ end and an EcoRI site at the 3´ end. Gel electrophoresis and DNA gel extraction were carried out subsequently. Purified DNA fragment and plasmid pHCCR were then digested with restriction enzymes HindIII and EcoRI as described in section 2.4.1. Gel electrophoresis and DNA gel extraction were performed to purify the digested DNA fragment of 2049bp (insert) and digested pHCCR of about 8000bp (vector). Both purified DNA fragments were then ligated as described in section 2.4.6 and transformed into competent DH5α *E. coli* as described in section 2.4.7. After purifying the plasmids from positive clones as described in section 2.4.9, DNA sequencing was carried out (section 2.4.11) to ensure that the Kozak consensus sequence had been incorporated. A plasmid with the correct DNA sequence was named as pKz-hMFc.

6.3.2.3 Amplification of sequence encoding the murine IgG2a Fc region

The procedure for fusing sequence encoding human MAGE-A2 to that encoding the Fc region of murine IgG2a is illustrated in Figure 6.7.

Amplification of sequence encoding murine IgG2a Fc region

pFUSEN-mG2AFc was digested with restriction enzymes EcoRI and HpaI at 37ºC for 1 hour as described in section 2.4.1. Gel electrophoresis and DNA gel extraction were performed to purify a digested DNA fragment at about 1031bp, containing sequence encoding the Fc region of murine IgG2a (insert). Primers MouseFcForw

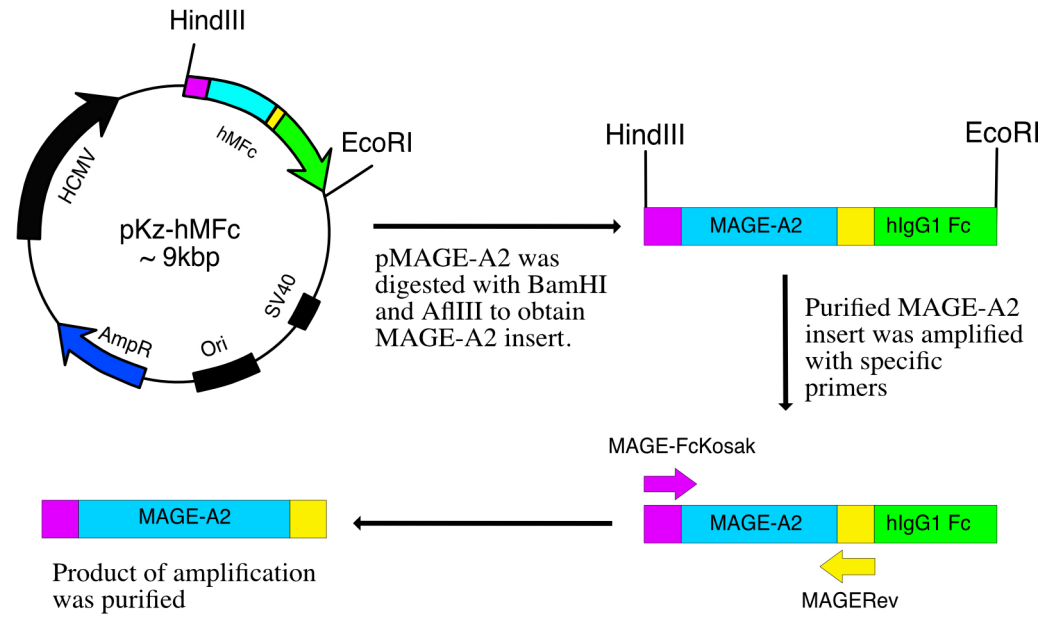
A.
MAGE-A2 amplification
HindIII
EcoRI
hMFc
HCMV
pKz-hMFc
~ 9kbp
SV40
AmpR
Ori
pMAGE-A2 was digested with BamHI and AflIII to obtain MAGE-A2 insert.
HindIII
EcoRI
MAGE-A2
hIgG1 Fc
Purified MAGE-A2 insert was amplified with specific primers
MAGE-FcKosak
MAGE-A2
hIgG1 Fc
MAGERev
MAGE-A2
Product of amplification was purified

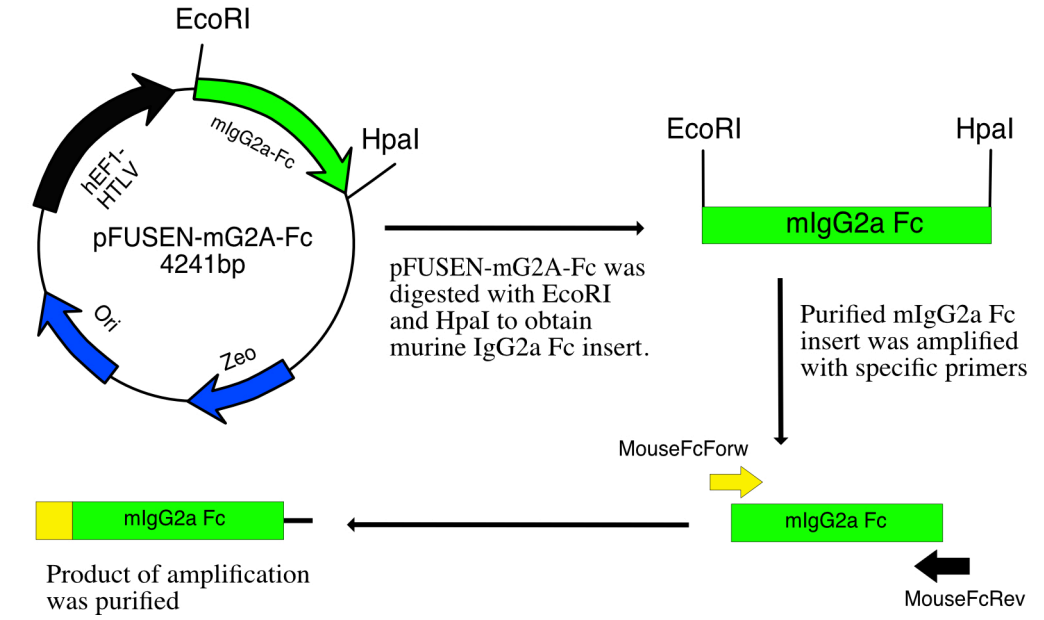
B.
Murine IgG2a Fc amplification
EcoRI
mIgG2a-Fc
HpaI
hEF1-HTLV
pFUSEN-mG2A-Fc
4241bp
Ori
Zeo
pFUSEN-mG2A-Fc was digested with EcoRI and HpaI to obtain murine IgG2a Fc insert.
EcoRI
HpaI
mIgG2a Fc
Purified mIgG2a Fc insert was amplified with specific primers
MouseFcForw
mIgG2a Fc
MouseFcRev
mIgG2a Fc
Product of amplification was purified

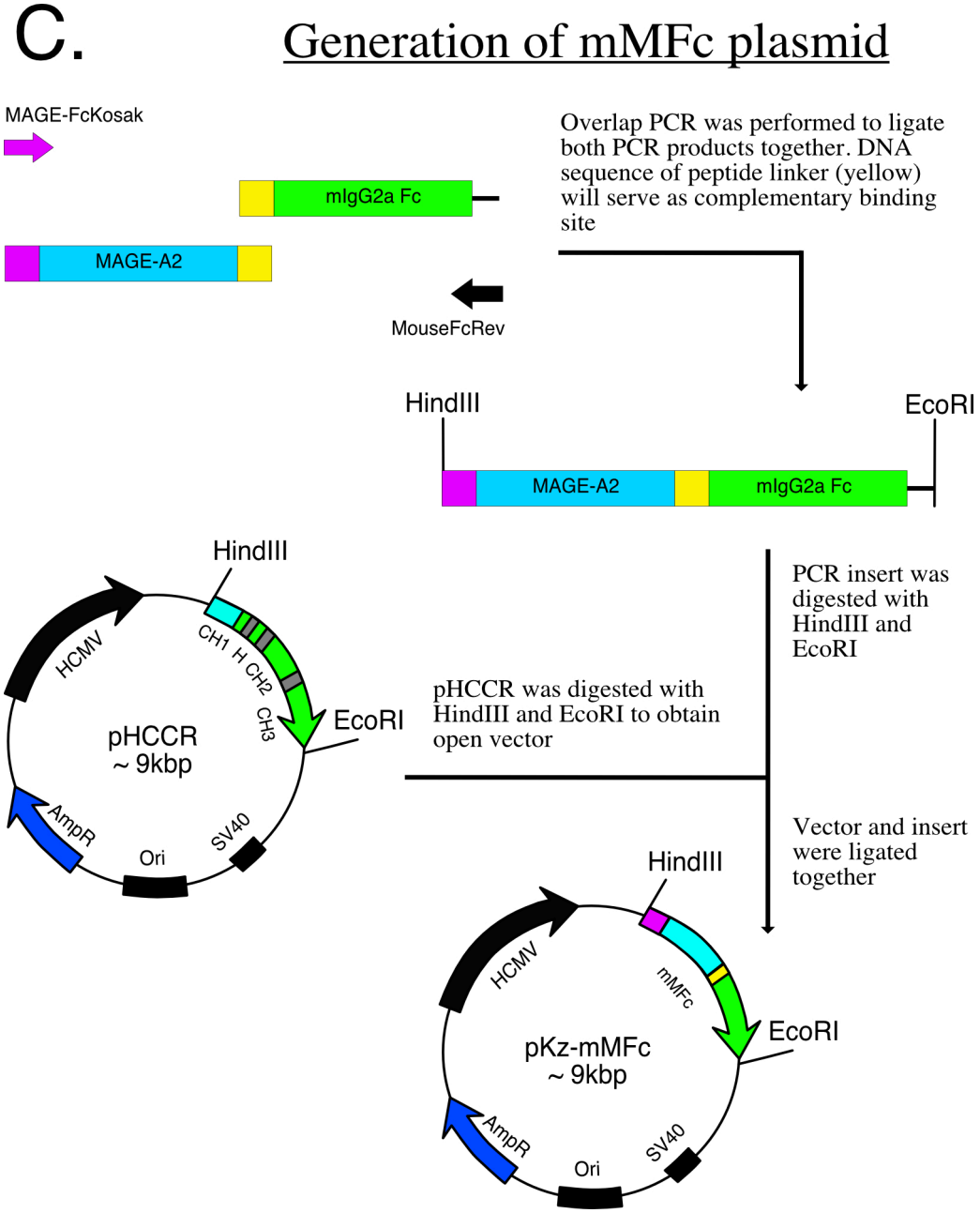

Figure 6.7: A schematic diagram illustrating the generation of MAGE-A2-mFc Fc-fusion protein expression vector. **A**) MAGE-A2 amplification procedure. pKz-hMFc was digested with HindIII and EcoRI to obtain the insert containing MAGE-A2-hFc DNA sequence which was amplified with specific primers to obtain a suitable MAGE-A2 insert. **B**) Murine IgG2a Fc amplification procedure. pFUSEN-mG2A-Fc was digested with EcoRI and HpaI to obtain the insert containing mIgG2a Fc DNA sequence which was amplified with specific primers to introduce sequence encoding a linker peptide (yellow) at the 5´ end. **C**) Generation of mMFc expression vector. An overlap PCR was performed to fuse the PCR products from **A** and **B** together using specific primers and the final product was digested with HindIII and EcoRI. pHCCR was digested with HindIII and EcoRI to obtain an open vector to ligate with the previously digested insert.

and MouseFcRev (Table 2.2, No.12 & 13) were used at an annealing temperature of 62ºC to amplify the purified DNA insert to obtain a DNA product of approximately 717bp, which contained an EcoRI site at the 3´ end. PCR products were run on a DNA agarose gel as described in section 2.4.4 and DNA bands of the correct sizes were extracted as described in section 2.4.5.

Amplification of sequence encoding MAGE-A2

pKz-hMFc was digested with restriction enzymes HindIII and EcoRI as described in section 2.4.1. Gel electrophoresis and DNA gel extraction were performed to purify a digested DNA fragment at about 2044bp, containing the DNA sequence of hMFc. Primers MAGE-FcKosak and MAGERev (Table 2.2, No. 11 & 8) were used at an annealing temperature of 66ºC to amplify the purified DNA insert to obtain a DNA product of approximately 1055bp, which contained a HindIII site at the 5´ end.

Fusion of MAGE-A2 with murine IgG2a Fc region and generation of plasmid construct

Using a PCR procedure described in section 2.4.3, an overlap PCR extension was performed by using a mix of 2µl of extracted MAGE-A2 and 2µl of extracted murine IgG2a Fc DNA fragments as templates and MAGE-FcKosak and MouseFcRev as primers (Table 2.2, No. 11 & 13) at an annealing temperature of 55ºC, to produce a final DNA product of approximately 1687bp. Gel electrophoresis and DNA gel extraction were carried out subsequently. Purified DNA fragment and plasmid pHCCR were then digested with restriction enzymes HindIII and EcoRI as described in section 2.4.1. Gel electrophoresis and DNA gel extraction were performed to purify the digested DNA fragment of 1675bp (insert) and digested pHCCR of about

8000bp (vector). Both purified DNA fragments were then ligated as described in section 2.4.6 and transformed into competent DH5α *E. coli* as described in section 2.4.7. After purifying the plasmids from positive clones as described in section 2.4.9, DNA sequencing was carried out (section 2.4.11) to ensure that sequence encoding MAGE-A2 had been correctly fused with that encoding the Fc region of murine IgG2a. A plasmid with the correct DNA sequence was named as pKz-mMFc.

6.3.3 PRODUCTION AND CHARACTERISATION OF hMFc AND mMFc

6.3.3.1 hMFc and mMFc production and purification from FreeStyle 293-F cells

Frozen FreeStyle 293-F cells were thawed and maintained in appropriate growth conditions as shown in section 2.6.2. Before the day of transfection, each flask of cells was split and seeded at 5 x 10^5 cells/ml in an Erlenmeyer flask in a total volume of 25ml, so that on the day of transfection the cells were at 1 x 10^6 cells/ml with a viability of 90% or above. For transfection, 293Fectin (Invitrogen) and Opti-MEM (1X) (Gibco Life Technologies) were brought to room temperature. For a single transfection, aliquots of 0.833ml of Opti-MEM (1X) were pipetted into two 30ml Universal tubes. In one tube, the DNA listed in Table 6.1 was added and mixed gently. In the other tube, 33.25µl of 293Fectin was added and allowed to incubate for exactly 5 minutes at room temperature before the addition of the DNA mixture prepared earlier. Once the DNA mixture was added, the solution was gently mixed and allowed to incubate for 20-30 minutes at room temperature. When completed, the solution was added to the FreeStyle 293-F cells and incubated on a shaker in an incubator in 8% CO_2 at 37ºC. Fusion protein was ready to be harvested and purified after 4 days as described in section 2.8.

Table 6.1: Amount of DNA required for FreeStyle 293-F cells transfection

Type of DNA expression vector	Amount of DNA
pKz-hMFc or pKz-mMFc	4.17μg
pAdvantage vector (Promega)	4.17μg

Note: The ratio of fusion plasmid to pAdvantage is 1:1.

6.3.3.2 Characterisation of hMFc and mMFc

Fc fusion protein purifications were carried out as described in section 2.8. Purified Fc fusion proteins were subjected to SDS-PAGE as described in section 2.8.6. Protein gels were stained with Coomassie as described in section 2.8.8 to determine the purity of the Fc fusion proteins generated. To further analyse the purified proteins, they were subjected to western blotting as described in section 2.8.7. After the blocking and washing procedure, the membranes were incubated with the detecting antibodies shown below. All membranes were washed and developed with appropriate substrate.

Antibodies for hMFc detection

To detect hMFc, the following antibodies were used: polyclonal rabbit anti-human IgG HRP conjugated (Table 2.1, No.2), monoclonal mouse anti-human MAGE-A2 (6C1) (Table 2.1, No.18), monoclonal mouse anti-human MAGE-A2 (1H4) (Table 2.1, No.17) and polyclonal goat anti mouse kappa light HRP conjugated (Table 2.1, No.19).

Antibodies for mMFc detection

To detect mMFc, the following antibodies were used: polyclonal goat anti-mouse IgG HRP conjugated (Table No.20), monoclonal mouse anti-human MAGE-A2 (6C1) (Table 2.1, No.18), monoclonal mouse anti-human MAGE-A2 (1H4) (Table 2.1, No.17) and polyclonal goat anti mouse kappa light HRP conjugated (Table 2.1, No.19).

6.3.3.3 Prediction of the unstructured region of hMFc

Due to the observation that both hMFc and mMFc proteins tended to form aggregates (described in Results), the stability of the protein structure of MAGE-A2 was questioned, with the existence of unstructured regions being a possibility. Since the crystal structure of MAGE-A2 has not been solved, software (http://iupred.enzim.hu) which could predict the unstructured regions of a protein was used to investigate if MAGE-A2 might have any unstructured regions (Dosztányi *et al*., 2005). The amino acid sequence of hMFc was uploaded to the webpage and the option of "structured regions" was selected.

6.4 RESULTS

6.4.1 Generation of hMFc expression plasmid

Using the primer combinations of MAGEForwLong and MAGERev to amplify the digested human MAGE-A2 insert from pMAGE-A2, and IgGForw and AG3´NEW to amplify the digested wt hIgG1 Fc insert from pHCCR, DNA amplified fragments of the correct sizes of 1050bp and 1034bp respectively were obtained as shown in Figure 6.8 A and B. Primer MAGEForwLong was designed to introduce sequence

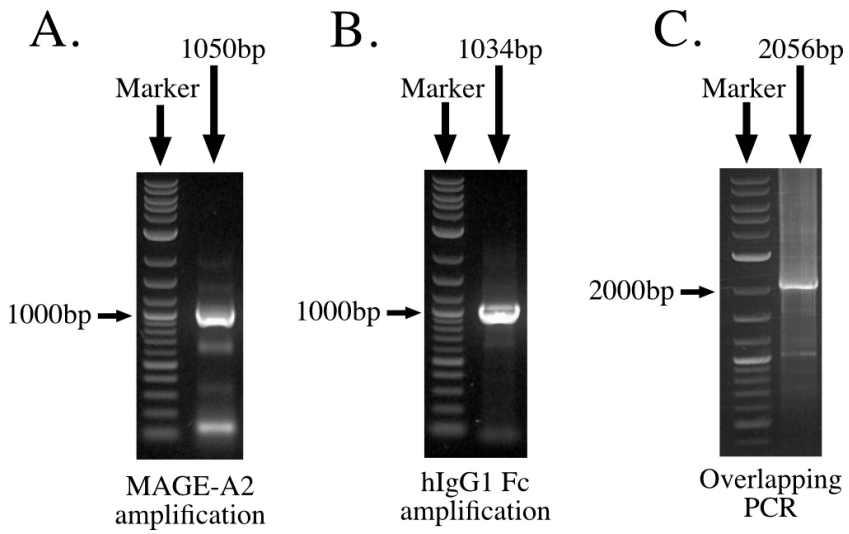

Figure 6.8: Results of molecular cloning for the generation of the hMFc expression plasmid. **A)** MAGE-A2 amplification. Lane 1050bp shows PCR amplification using MAGEForwLong and MAGERev to obtain a DNA fragment of 1050bp. **B**) wt hIgG1 Fc amplification. Lane 1034bp shows PCR amplification using IgGForw and AG3'NEW to obtain a DNA fragment of 1034bp. **C**) Overlapping PCR amplification. Complementary DNA fragments of 1050bp and 1034bp from **A** and **B** were amplified using MAGEForwShort and AG3´NEW to produce a fragment of 2056bp.

encoding an immunoglobulin secretion signal peptide, MGWSCIILFLVATATGVHS, to the 5´ end of the MAGE-A2 gene sequence to allow MFc to be secreted to the extracellular compartment for easier purification. On the other hand, primer MAGERev was designed to incorporate sequence encoding a 13 amino acids peptide linker, GSSGGGSSGGSSS, at the 3´ end of MAGE-A2 gene sequence. The DNA sequence of the peptide linker served as a complementary region, shown in yellow in Figure 6.5, to aid the fusion of MAGE-A2 sequence with that of wt hIgG1 Fc region via overlapping PCR. The result of the subsequent overlapping PCR procedure, using the primer combinations of MAGEForwShort and AG3´NEW, is shown in Figure 6.8 C. The band obtained of approximately 2000bp indicated that the 1050bp and 1034bp DNA fragments had annealed through their complementary regions leading to successful amplification. The purified PCR product and pHCCR vector were ligated together after digestion with restriction

enzymes HindIII and EcoRI. After transforming the plasmids into *E.coli*, DNA plasmids were purified from positive clones and subsequent DNA sequencing confirmed that sequences encoding the immunoglobulin secretion signal, peptide linker had been incorporated and that fusion of sequences encoding MAGE-A2 and wt hIgG1 Fc had been successful, as shown in the final hMFc DNA and translated protein sequences in Figure 6.9. The correct plasmid was named as phMFc.

6.4.2 Introduction of Kozak consensus sequence into the hMFc expression plasmid

phMFc and pAdvantage were used to transfect FreeStyle 293-F cells and the hMFc protein was purified using Protein G-Sepharose. SDS-PAGE and western blotting were carried out. However, it was discovered that the expression of hMFc protein were very low and hardly detectable (data not shown). It was realised that the expression plasmid phMFc was lacking the Kozak consensus sequence which promotes high protein expression. To resolve this, primer combinations of MAGE-FcKosak, which contained the Kozak consensus sequence, and AG3´NEW were used to amplify the hMFc insert, which was first purified from the digestion of phMFc with restriction enzymes HindIII and EcoRI. The purified PCR product and phMFc vector were ligated together after digestion with restriction enzymes HindIII and EcoRI (data not shown). After transforming the plasmids into *E.coli*, DNA plasmids were purified from positive clones and subsequent DNA sequencing confirmed that introduction of Kozak consensus sequence prior to the start codon of hMFc encoding sequence had been successful, as indicated in the final mMFc DNA and translated protein sequences in Figure 6.9. The correct plasmid was named as pKz-hMFc.

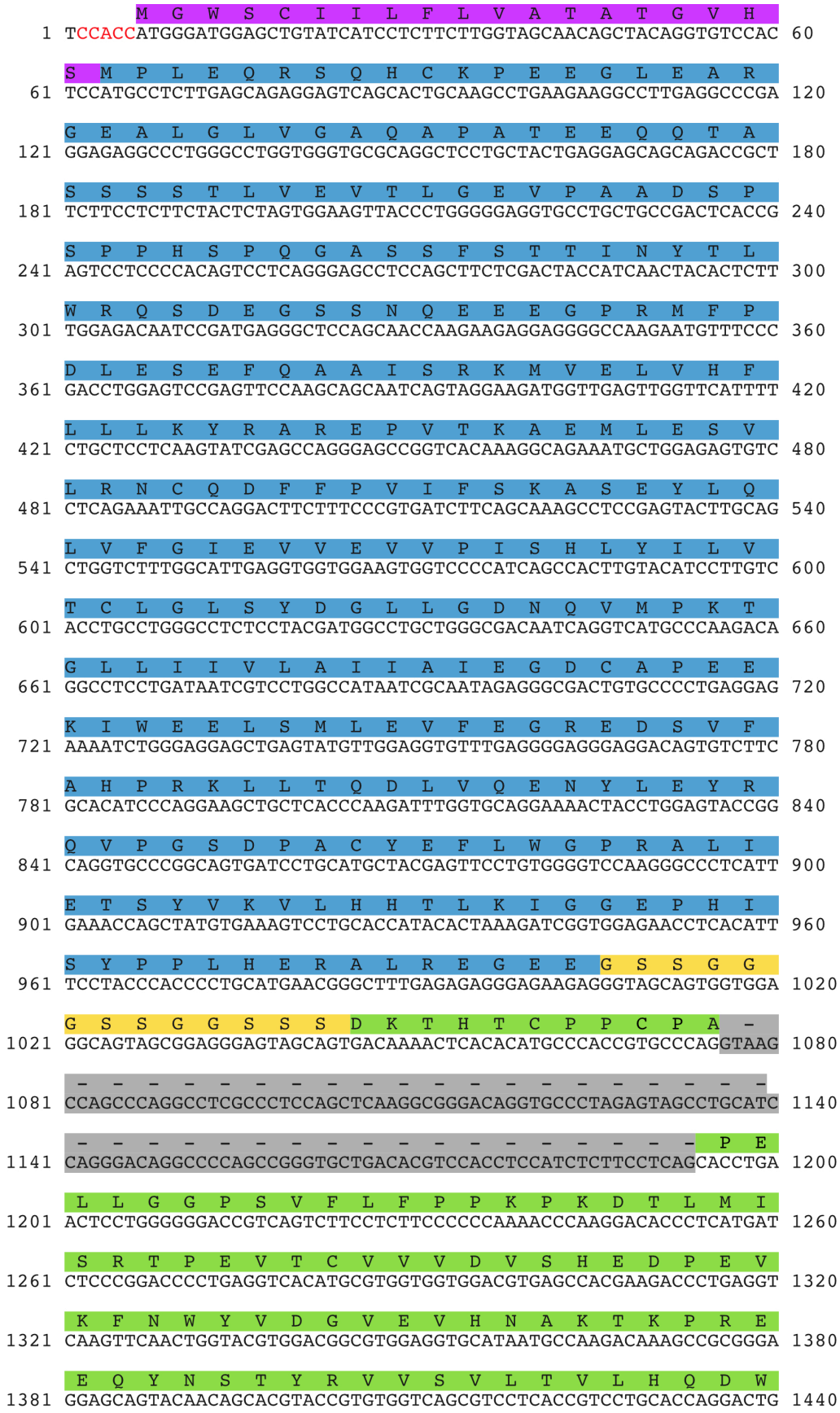
M G W S C I I L F L V A T A T G V H
1 TCCACCATGGGATGGAGCTGTATCATCCTCTTCTTGGTAGCAACAGCTACAGGTGTCCAC 60
S M P L E Q R S Q H C K P E E G L E A R
61 TCCATGCCTCTTGAGCAGAGGAGTCAGCACTGCAAGCCTGAAGAAGGCCTTGAGGCCCGA 120
G E A L G L V G A Q A P A T E E Q Q T A
121 GGAGAGGCCCTGGGCCTGGTGGGTGCGCAGGCTCCTGCTACTGAGGAGCAGCAGACCGCT 180
S S S S T L V E V T L G E V P A A D S P
181 TCTTCCTCTTCTACTCTAGTGGAAGTTACCCTGGGGGAGGTGCCTGCTGCCGACTCACCG 240
S P P H S P Q G A S S F S T T I N Y T L
241 AGTCCTCCCCACAGTCCTCAGGGAGCCTCCAGCTTCTCGACTACCATCAACTACACTCTT 300
W R Q S D E G S S N Q E E E G P R M F P
301 TGGAGACAATCCGATGAGGGCTCCAGCAACCAAGAAGAGGAGGGGCCAAGAATGTTTCCC 360
D L E S E F Q A A I S R K M V E L V H F
361 GACCTGGAGTCCGAGTTCCAAGCAGCAATCAGTAGGAAGATGGTTGAGTTGGTTCATTTT 420
L L L K Y R A R E P V T K A E M L E S V
421 CTGCTCCTCAAGTATCGAGCCAGGGAGCCGGTCACAAAGGCAGAAATGCTGGAGAGTGTC 480
L R N C Q D F F P V I F S K A S E Y L Q
481 CTCAGAAATTGCCAGGACTTCTTTCCCGTGATCTTCAGCAAAGCCTCCGAGTACTTGCAG 540
L V F G I E V V E V V P I S H L Y I L V
541 CTGGTCTTTGGCATTGAGGTGGTGGAAGTGGTCCCCATCAGCCACTTGTACATCCTTGTC 600
T C L G L S Y D G L L G D N Q V M P K T
601 ACCTGCCTGGGCCTCTCCTACGATGGCCTGCTGGGCGACAATCAGGTCATGCCCAAGACA 660
G L L I I V L A I I A I E G D C A P E E
661 GGCCTCCTGATAATCGTCCTGGCCATAATCGCAATAGAGGGCGACTGTGCCCCTGAGGAG 720
K I W E E L S M L E V F E G R E D S V F
721 AAAATCTGGGAGGAGCTGAGTATGTTGGAGGTGTTTGAGGGGAGGGAGGACAGTGTCTTC 780
A H P R K L L T Q D L V Q E N Y L E Y R
781 GCACATCCCAGGAAGCTGCTCACCCAAGATTTGGTGCAGGAAAACTACCTGGAGTACCGG 840
Q V P G S D P A C Y E F L W G P R A L I
841 CAGGTGCCCGGCAGTGATCCTGCATGCTACGAGTTCCTGTGGGGTCCAAGGGCCCTCATT 900
E T S Y V K V L H H T L K I G G E P H I
901 GAAACCAGCTATGTGAAAGTCCTGCACCATACACTAAAGATCGGTGGAGAACCTCACATT 960
S Y P P L H E R A L R E G E E G S S G G
961 TCCTACCCACCCCTGCATGAACGGGCTTTGAGAGAGGGAGAAGAGGGTAGCAGTGGTGGA 1020
G S S G G S S S D K T H T C P P C P A -
1021 GGCAGTAGCGGAGGGAGTAGCAGTGACAAAACTCACACATGCCCACCGTGCCCAGGTAAG 1080
- -
1081 CCAGCCCAGGCCTCGCCCTCCAGCTCAAGGCGGGACAGGTGCCCTAGAGTAGCCTGCATC 1140
- P E
1141 CAGGGACAGGCCCCAGCCGGGTGCTGACACGTCCACCTCCATCTCTTCCTCAGCACCTGA 1200
L L G G P S V F L F P P K P K D T L M I
1201 ACTCCTGGGGGGACCGTCAGTCTTCCTCTTCCCCCCAAAACCCAAGGACACCCTCATGAT 1260
S R T P E V T C V V V D V S H E D P E V
1261 CTCCCGGACCCCTGAGGTCACATGCGTGGTGGTGGACGTGAGCCACGAAGACCCTGAGGT 1320
K F N W Y V D G V E V H N A K T K P R E
1321 CAAGTTCAACTGGTACGTGGACGGCGTGGAGGTGCATAATGCCAAGACAAAGCCGCGGGA 1380
E Q Y N S T Y R V V S V L T V L H Q D W
1381 GGAGCAGTACAACAGCACGTACCGTGTGGTCAGCGTCCTCACCGTCCTGCACCAGGACTG 1440

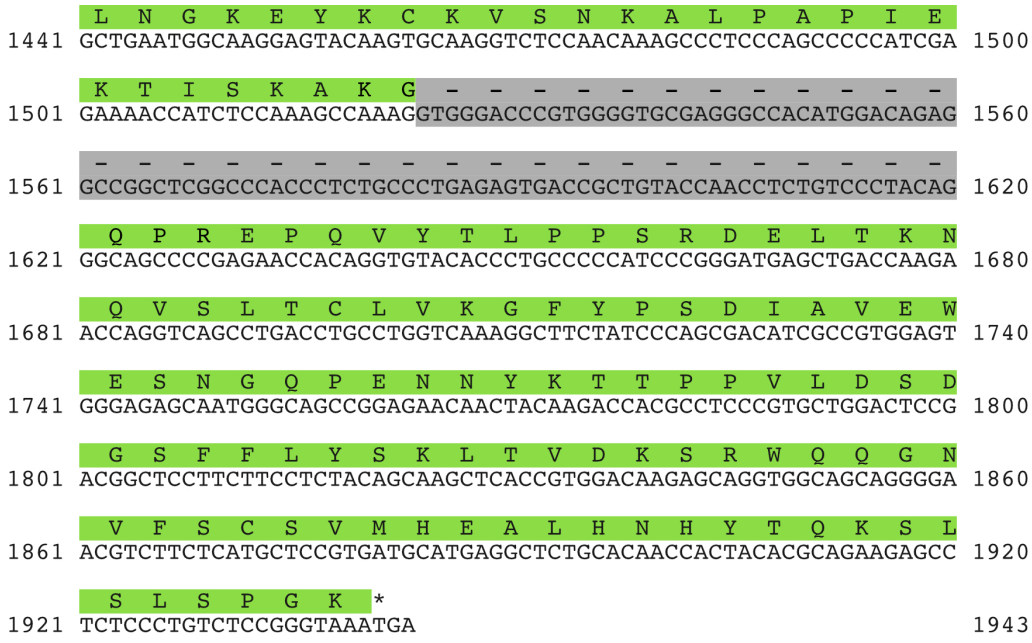

Figure 6.9: The DNA sequence encoding hMFc and corresponding translated protein sequences. Red, Kozak consensus sequence; Purple, protein sequence of immunoglobulin secretion signal peptide; Blue, protein sequence of full length human MAGE-A2 protein; Yellow, protein sequence of the 13 amino acid peptide linker; Green, protein sequence of wt hIgG1 Fc region; Grey, intron segments; *, stop codon.

6.4.3 Generation of mMFc expression plasmid

Using the primer combinations of MAGE-FcKosak and MAGERev to amplify the digested human MAGE-A2 insert from pKz-hMFc, and MouseFcForw and MouseFcRev to amplify the digested mIgG2a Fc insert from pFUSEN-mG2AFc, DNA amplified fragments of the correct sizes of 1055bp and 717bp respectively were obtained as shown in Figures 6.10A and 6.10B. Similar to the previous generation of hMFc, the DNA sequence of the peptide linker served as a complementary region, shown in yellow in Figure 6.10, to aid the fusion of sequences encoding MAGE-A2 and mIgG2a Fc via overlapping PCR. The result of the subsequent overlapping PCR procedure, using the primer combinations of MAGE-FcKosak and MouseFcRev, is shown in Figure 6.10C. The band obtained of

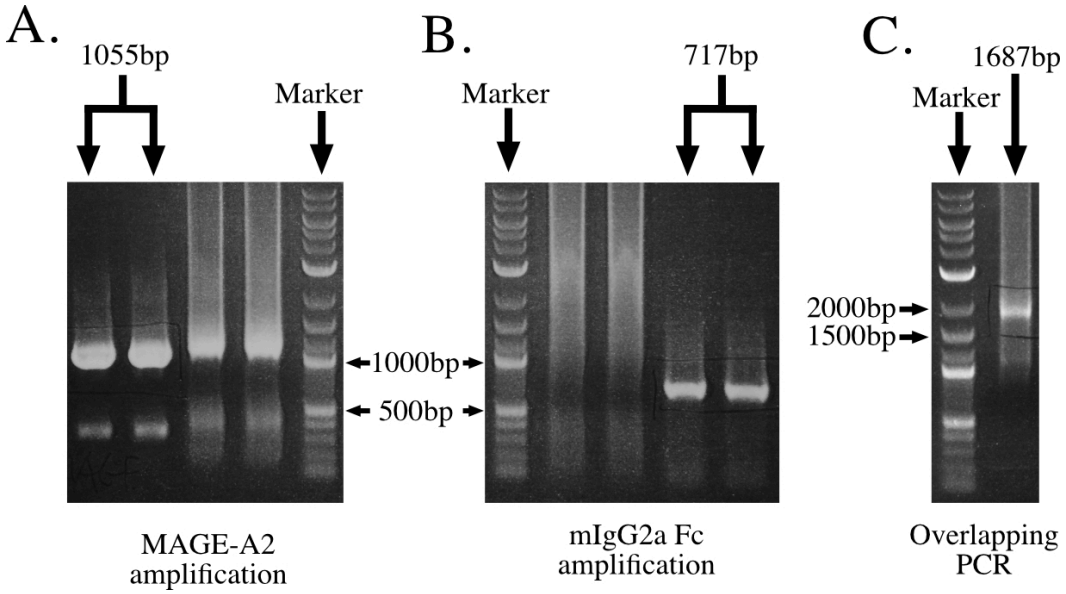

Figure 6.10: Results of molecular cloning for the generation of mMFc expression plasmid. **A)** MAGE-A2 amplification. Lane 1055bp shows PCR amplification using MAGE-FcKosak and MAGERev to obtain DNA fragment at 1055bp. **B**) mIgG2a Fc amplification. Lane 717bp shows PCR amplification using MouseFcForw and MouseFcRev to obtain DNA fragment at 717bp. **C**) Overlapping PCR amplification. Complementary DNA fragments of 1055bp and 717bp from **A** and **B** were amplified using MAGE-FcKosak and MouseFcRev to produce a fragment of 1687bp.

approximately 1687bp indicated that the 1055bp and 717bp DNA fragments had annealed through their complementary regions leading to successful amplification. The purified PCR product and pHCCR vector were ligated together after digestion with restriction enzymes HindIII and EcoRI. After transforming the plasmids into *E.coli*, DNA plasmids were purified from positive clones and subsequent DNA sequencing confirmed that the fusion of sequences encoding MAGE-A2 and mIgG2a Fc had been successful (data not shown). The correct plasmid was named as pKz-mMFc. The final mMFc DNA and translated protein sequences is shown in Figure 6.11.

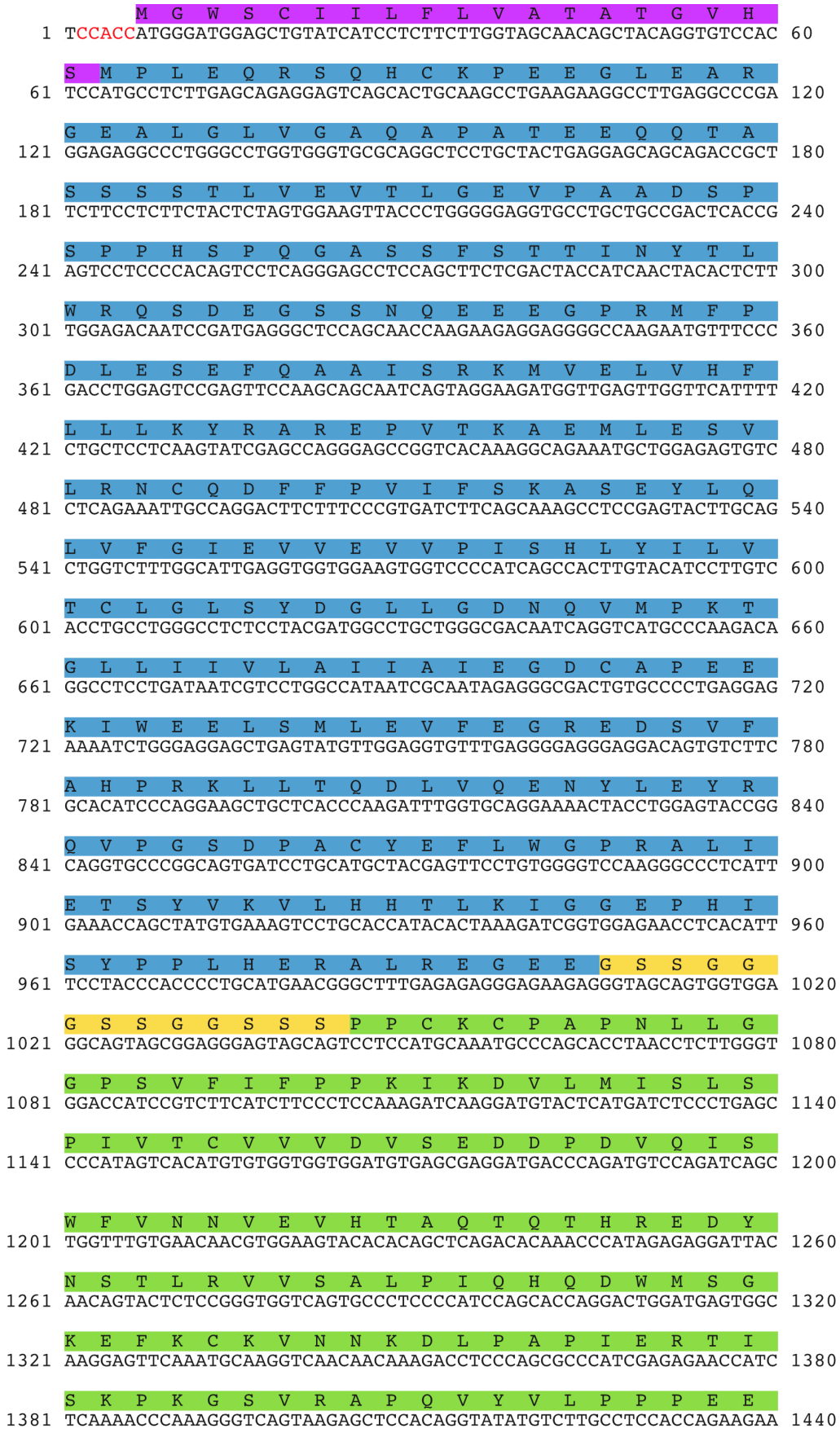
M G W S C I I L F L V A T A T G V H
1 TCCACCATGGGATGGAGCTGTATCATCCTCTTCTTGGTAGCAACAGCTACAGGTGTCCAC 60
S M P L E Q R S Q H C K P E E G L E A R
61 TCCATGCCTCTTGAGCAGAGGAGTCAGCACTGCAAGCCTGAAGAAGGCCTTGAGGCCCGA 120
G E A L G L V G A Q A P A T E E Q Q T A
121 GGAGAGGCCCTGGGCCTGGTGGGTGCGCAGGCTCCTGCTACTGAGGAGCAGCAGACCGCT 180
S S S S T L V E V T L G E V P A A D S P
181 TCTTCCTCTTCTACTCTAGTGGAAGTTACCCTGGGGGAGGTGCCTGCTGCCGACTCACCG 240
S P P H S P Q G A S S F S T T I N Y T L
241 AGTCCTCCCCACAGTCCTCAGGGAGCCTCCAGCTTCTCGACTACCATCAACTACACTCTT 300
W R Q S D E G S S N Q E E E G P R M F P
301 TGGAGACAATCCGATGAGGGCTCCAGCAACCAAGAAGAGGAGGGGCCAAGAATGTTTCCC 360
D L E S E F Q A A I S R K M V E L V H F
361 GACCTGGAGTCCGAGTTCCAAGCAGCAATCAGTAGGAAGATGGTTGAGTTGGTTCATTTT 420
L L L K Y R A R E P V T K A E M L E S V
421 CTGCTCCTCAAGTATCGAGCCAGGGAGCCGGTCACAAAGGCAGAAATGCTGGAGAGTGTC 480
L R N C Q D F F P V I F S K A S E Y L Q
481 CTCAGAAATTGCCAGGACTTCTTTCCCGTGATCTTCAGCAAAGCCTCCGAGTACTTGCAG 540
L V F G I E V V E V V P I S H L Y I L V
541 CTGGTCTTTGGCATTGAGGTGGTGGAAGTGGTCCCCATCAGCCACTTGTACATCCTTGTC 600
T C L G L S Y D G L L G D N Q V M P K T
601 ACCTGCCTGGGCCTCTCCTACGATGGCCTGCTGGGCGACAATCAGGTCATGCCCAAGACA 660
G L L I I V L A I I A I E G D C A P E E
661 GGCCTCCTGATAATCGTCCTGGCCATAATCGCAATAGAGGGCGACTGTGCCCCTGAGGAG 720
K I W E E L S M L E V F E G R E D S V F
721 AAAATCTGGGAGGAGCTGAGTATGTTGGAGGTGTTTGAGGGGAGGGAGGACAGTGTCTTC 780
A H P R K L L T Q D L V Q E N Y L E Y R
781 GCACATCCCAGGAAGCTGCTCACCCAAGATTTGGTGCAGGAAAACTACCTGGAGTACCGG 840
Q V P G S D P A C Y E F L W G P R A L I
841 CAGGTGCCCGGCAGTGATCCTGCATGCTACGAGTTCCTGTGGGGTCCAAGGGCCCTCATT 900
E T S Y V K V L H H T L K I G G E P H I
901 GAAACCAGCTATGTGAAAGTCCTGCACCATACACTAAAGATCGGTGGAGAACCTCACATT 960
S Y P P L H E R A L R E G E E G S S G G
961 TCCTACCCACCCCTGCATGAACGGGCTTTGAGAGAGGGAGAAGAGGGTAGCAGTGGTGGA 1020
G S S G G G S S S P P C K C P A P N L L G
1021 GGCAGTAGCGGAGGGAGTAGCAGTCCTCCATGCAAATGCCCAGCACCTAACCTCTTGGGT 1080
G P S V F I F P P K I K D V L M I S L S
1081 GGACCATCCGTCTTCATCTTCCCTCCAAAGATCAAGGATGTACTCATGATCTCCCTGAGC 1140
P I V T C V V V D V S E D D P D V Q I S
1141 CCCATAGTCACATGTGTGGTGGTGGATGTGAGCGAGGATGACCCAGATGTCCAGATCAGC 1200
W F V N N V E V H T A Q T Q T H R E D Y
1201 TGGTTTGTGAACAACGTGGAAGTACACACAGCTCAGACACAAACCCATAGAGAGGATTAC 1260
N S T L R V V S A L P I Q H Q D W M S G
1261 AACAGTACTCTCCGGGTGGTCAGTGCCCTCCCCATCCAGCACCAGGACTGGATGAGTGGC 1320
K E F K C K V N N K D L P A P I E R T I
1321 AAGGAGTTCAAATGCAAGGTCAACAACAAAGACCTCCCAGCGCCCATCGAGAGAACCATC 1380
S K P K G S V R A P Q V Y V L P P P E E
1381 TCAAAACCCAAAGGGTCAGTAAGAGCTCCACAGGTATATGTCTTGCCTCCACCAGAAGAA 1440

```
     E  M  T  K  K  Q  V  T  L  T  C  M  V  T  D  F  M  P  E  D
1441 GAGATGACTAAGAAACAGGTCACTCTGACCTGCATGGTCACAGACTTCATGCCTGAAGAC 1500

     I  Y  V  E  W  T  N  N  G  K  T  E  L  N  Y  K  N  T  E  P
1501 ATTTACGTGGAGTGGACCAACAACGGGAAAACAGAGCTAAACTACAAGAACACTGAACCA 1560

     V  L  D  S  D  G  S  Y  F  M  Y  S  K  L  R  V  E  K  K  N
1561 GTCCTGGACTCTGATGGTTCTTACTTCATGTACAGCAAGCTGAGAGTGGAAAAGAAGAAC 1620

     W  V  E  R  N  S  Y  S  C  S  V  V  H  E  G  L  H  N  H  H
1621 TGGGTGGAAAGAAATAGCTACTCCTGTTCAGTGGTCCACGAGGGTCTGCACAATCACCAC 1680

     T  T  K  S  F  S  R  T  P  G  K  *
1681 ACGACTAAGAGCTTCTCCCGGACTCCGGGTAAATGA                          1716
```

Figure 6.11: The DNA sequence encoding mMFc and corresponding translated protein sequences. Red, Kozak consensus sequence; Purple, protein sequence of immunoglobulin secretion signal peptide; Blue, protein sequence of full length human MAGE-A2 protein; Yellow, protein sequence of the 13 amino acid peptide linker; Green, protein sequence of wt mIgG2a Fc region; *, stop codon.

6.4.4 Production and characterisation of Fc fusion proteins

Two Fc fusion expression plasmids, pKz-hMFc and pKz-mMFc, were each transfected together with pAdvantage into FreeStyle 293-F cells. After 4 days, supernatants of the cell cultures were harvested and incubated with Protein G-Sepharose, and the expressed Fc fusion proteins purified. The success of Fc fusion protein purification from the supernatants of the cell cultures indicated that the introduction of the immunoglobulin secretion signal peptide was successful and that the Fc fusion proteins were being secreted into the extracellular space. More importantly, the success of Fc fusion protein purification using Protein G-Sepharose indicated that, at least, the Fc region of the Fc fusion proteins had folded up correctly, since recognition of Fc by protein G is dependent on IgG Fc having its correct three-dimensional conformation. In addition, the results also suggested that the fusion of human MAGE-A2 did not cause major steric hindrance to the Fc region. It was presumed that the introduction of the 13 amino acid peptide linker kept MAGE-A2 and the Fc region apart from each other, thus, allowing the Fc region to bind

efficiently to Protein G-Sepharose. The amount of Fc fusion protein obtained from a single 25ml transfection was around 80-120μg for both Fc fusion proteins.

Purified fusion proteins were subjected to SDS-PAGE, as described in Section 2.8.6. Figure 6.12A shows the results of Coomassie staining of purified Fc fusion proteins after SDS-PAGE under both non-reducing and reducing conditions. Figure 6.12B shows the western blotting results obtained for purified Fc fusion proteins after probing with anti-human IgG heavy chain HRP or anti-mouse IgG heavy chain HRP or with the different monoclonal anti-human MAGE-A2 antibodies (6C1 or 1H4). The results from Coomassie staining of both MFc proteins, Figure 6.12A, suggest that there were major protein aggregations. Neither protein appeared to enter the stacking gel of SDS-PAGE, as seen in the lanes run under non-reduced conditions. However, both Fc fusion proteins entered the protein gel under reducing conditions, suggesting that the aggregates were held together, at least in part, by disulphide bridges. It was noticed that several protein bands were detected under Coomassie staining, Figure 6.12A, and the positions of these protein bands were identical for both hMFc and mMFc. This suggests that either there were other proteins binding to the MFc proteins which were co-purified during Protein G-Sepharose step or the MFc proteins were undergoing protein degradation.

To further understand the situation of the Fc fusion proteins, western blotting was carried out. Using antibodies targeting against the human MAGE-A2 and human or murine IgG heavy chain, several protein bands were detected as shown in Figure 6.12 B. Human MAGE-A2 protein was predicted to have a mass of around 35kDa

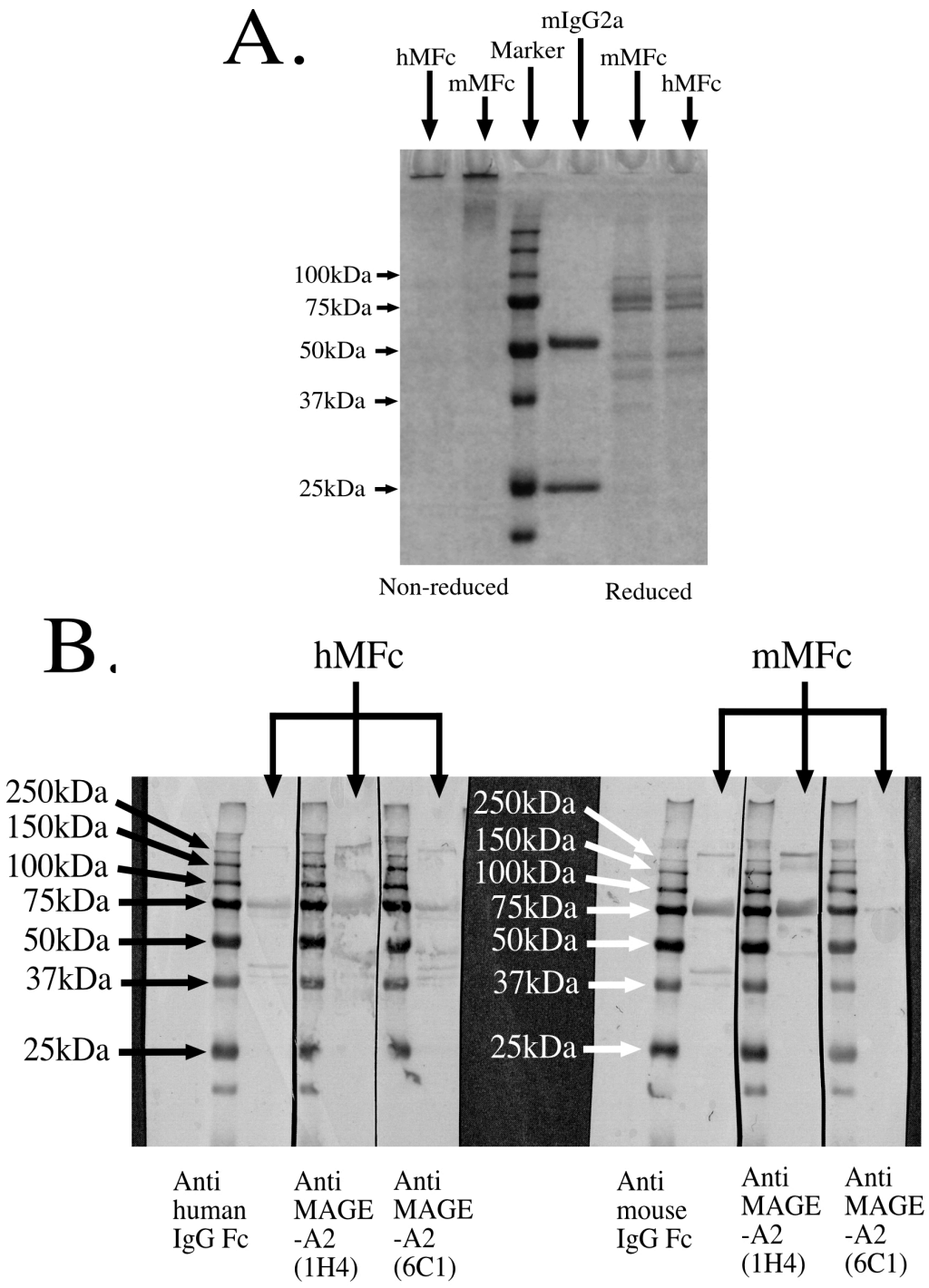

Figure 6.12: Coomassie and western blot staining of purified hMFc (human MAGE-A2 fused with wt hIgG1 Fc region) and mMFc (human MAGE-A2 fused with murine IgG2a Fc region) after SDS-PAGE and western blotting. **A)** Coomassie staining of purified hMFc and mMFc under both non-reducing and reducing conditions. mIgG2a was loaded as a molecular weight indicator control. Molecular weight markers were run in the middle lane. **B)** Western blotting of purified hMFc and mMFc under reducing condition. Molecular weight markers were run in the left hand lane in all cases. Detecting antibodies are shown below the relevant part of each blot.

(with the assumption that there were no posttranslational modifications) and the IgG Fc region for both human IgG1 and murine IgG2a were around 25-30kDa. As a result, the molecular weight for a single full length MFc polypeptide under reduced condition would be expected to be around 65kDa. Bands that gave the strongest detection signal and which were consistently detected in all investigations were located at around 75kDa, which was quite close to the estimated molecular weight of MFc. This suggests that the major band detected around 75kDa is most likely full length MFc. The identity of a band, located at above 250kDa, that was detected in all western blotting investigations, is most likely to be aggregates of MFc that are not fully reduced. By comparing the protein bands observed between Coomassie staining and western blotting, it was also found that a noticeable protein band located between 75kDa-100kDa was seen in Coomassie staining but not in western blotting. This indicates that there were contaminations of other proteins during protein purification and most likely these proteins were bound to MAGE-A2 rather than IgG Fc because previous antibody purification (Chapter 3) had shown no such contamination. In addition, there were also multiple minor protein bands detected below 75kDa which might also be contaminating proteins. However, these smaller molecular weight proteins were recognised by anti-human/mouse IgG Fc and anti-human MAGE-A2 antibodies. Thus, the results suggest that the MFc proteins might be suffering from some level of degradation.

6.4.5 Unstructured region of hMFc

Due to the observation that MAGE-A2 fusion proteins were forming aggregates, it was hypothesised that MAGE-A2 protein might be relatively unstable and might contain unstructured regions which might drive undesired aggregation. Software

A.

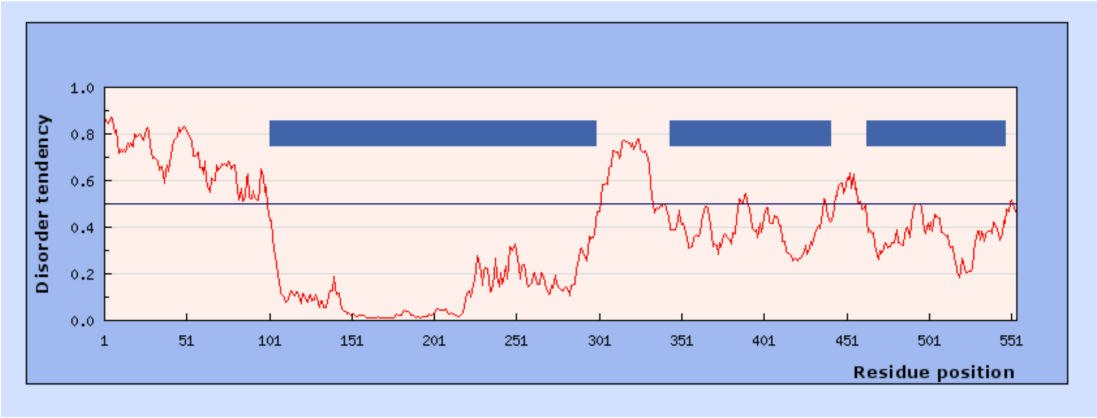

B.

MPLEQRSQHCKPEEGLEARGEALGLVGAQAPATEEQQTASSSSTLV
EVTLGEVPAADSPSPPHSPQGASSFSTTINYTLWRQSDEGSSNQEEEG
PRMFPDLESEFQAAISRKMVELVHFLLLKYRAREPVTKAEMLESVLR
NCQDFFPVIFSKASEYLQLVFGIEVVEVVPISHLYILVTCLGLSYDGLL
GDNQVMPKTGLLIIVLAIIAIEGDCAPEEKIWEELSMLEVFEGREDSV
FAHPRKLLTQDLVQENYLEYRQVPGSDPACYEFLWGPRALIETSYV
KVLHHTLKIGGEPHISYPPLHERALREGEEGSSGGGSSGGSSSDKTHT
CPPCPAPELLGGPSVFLFPPKPKDTLMISRTPEVTCVVVDVSHEDPEV
KFNWYVDGVEVHNAKTKPREEQYNSTYRVVSVLTVLHQDWLNGK
EYKCKVSNKALPAPIEKTISKAKGQPREPQVYTLPPSRDELTKNQVS
LTCLVKGFYPSDIAVEWESNGQPENNYKTTPPVLDSDGSFFLYSKLT
VDKSRWQQGNVFSCSVMHEALHNHYTQKSLSLSPGK

Figure 6.13: Result of prediction of unstructured regions in hMFc. **A**) The protein sequence of hMFc was uploaded to a webpage capable of predicting unstructured regions of a protein. The graph represents disorder frequency of amino acids of the uploaded protein in which the higher the disorder frequency (above 0.5), the more likely the involved region is unstructured. The blue bars indicate structured regions. **B**) The protein sequence of the uploaded hMFc corresponding to the result of prediction. Protein sequence in red represents the predicted unstructured regions. Highlighted protein sequence represents different region of the hMFc, Blue, full length human MAGE-A2 protein; Yellow, 13 amino acid peptide linker; Green, wt hIgG1 Fc region.

which could help in predicting unstructured regions of a protein was utilised to predict unstructured regions in hMFc. The result of the prediction was shown in Figure 6.13, and indicates that the first N-terminal 100 amino acids of MAGE-A2 may be unstructured. More importantly, there was a cysteine residue within this predicted unstructured region, which, if easily accessible, might be factor in

promoting protein aggregation through disulphide bonding. In addition, the last 15 amino acids located at the C-terminus of MAGE-A2, the 13 amino acid peptide linker, and the first 16 amino acids located of wt hIgG1 Fc region (hinge region) were also predicted to be unstructured. However, the unstructured state of the peptide linker and the hinge region of hIgG1 were within our expectation because the peptide linker was designed to provide flexibility to keep MAGE-A2 and the IgG Fc region separated by some distance. These two sites are expected to be flexible rather than unstructured. As a result, the unstructured region of the N-terminal of MAGE-A2 might be responsible for the protein aggregation of MFc, however, further investigations were required to confirm this hypothesis.

6.5 DISCUSSION

This chapter aimed to fuse human MAGE-A2 protein, which is a member of the CTA class of proteins, to the Fc region of either wt hIgG1 and murine IgG2a using recombinant antibody technology. MAGE-A2 protein is not a secretory protein. Therefore, in order for the Fc fusion protein to be secreted to the extracellular environment, a secretory signal peptide had to be introduced to the N-terminus of MFc. By directing the protein to the extracellular environment, the purification of the protein would be a lot easier as there is no requirement to break open the cells, thus, this approach should greatly reduce the contamination of other proteins. In addition, MAGE-A2 had been reported to be able to repress the activity of p53 which is a major cell proliferation regulator (Monte *et al*., 2006). As a result, directing MAGE-A2 protein away from the intracellular environment of a cell would be the best option to prevent any potential effector mechanism of MAGE-A2. The procedures described in this chapter utilised a natural secretory signal peptide of

immunoglobulin to drive secretion of MFc into the extracellular environment. The production of the Fc fusion proteins was successful and the Fc fusion proteins could be purified using Protein G-Sepharose from the supernatant of the transfected cells. However, it was noticed that the amount of Fc fusion proteins being expressed and purified were quite low compared to earlier antibody production and purification in Chapter 3. The amount of Fc fusion protein obtained was around 80-120μg per 25 ml transfection whereas the amount of antibody obtained in Chapter 3 was around 200-250μg per 25 ml transfection. Thus, there was more than 50% reduction in the amount of purified Fc fusion proteins obtained compared to antibodies. Attempts to improve expression levels were made, in which the amount of DNA for Fc fusion protein expression vector used during transfection was increased up to 3 times. However, no significant increase in the amount of purified Fc fusion protein resulted. Hence, the exact reason for the low level of protein recovery was not known. It might be that the transfection procedure requires further optimisation, or MFc proteins might be suffering from protein degradation as the earlier result suggests.

The molecular weight of a single monomeric full length MFc polypeptide chain under reducing condition was expected to be around 65kDa (35kDa for MAGE-A2 and 25-30kDa for IgG Fc). However, the result from western blotting indicated that the molecular weight of MFc was around 75kDa which suggests that MAGE-A2 might contain other post-translational modifications, apart from the expected N-linked glycosylation at Asn297 of the IgG Fc region (Burmeister *et al*., 1994; Burton, 1987; Davies *et al*., 1975; Dekkers *et al*., 2016; Jefferis, 2005). Previous work had reported that MAGE-A2 could bind to the core of p53 resulting in the repression of p53 transcriptional activity (Monte *et al*., 2006). p53 is a major protein that governs

cell proliferation and is highly regulated. Therefore, there is a high possibility that the activity of MAGE-A2 is dependent on post-translational modification to control its activity on p53. However, whether post-translational modification exists in the secreted MAGE-A2 form requires further investigation. It is well known that the IgG Fc does not contain post-translational modifications other than the N-linked glycosylation that occurs at Asn297. Therefore, one approach to determine the post-translation modification of MAGE-A2 would be to mutate Asn297 to alanine to abolish the N-linked glycosylation at IgG Fc. As a result, any other post-translational modifications detected from further investigations would suggest that MAGE-A2 is being post-translationally modified. As mentioned above, it is expected that Asn297 located at the CH2 domain of IgG will be glycosylated. However, no investigation was carried out in this project to confirm this hypothesis. One approach to confirm the presence of the N-linked glycosylation at Asn297 would be the use of Concanavalin A (Con A), which binds specifically to α-D-mannosyl and α-D-glucosyl groups that are found present at the N-linked glycosylation of IgG (Huang *et al*., 2016; Dekkers *et al*., 2016), to detect the presence of N-linked glycans at Asn 297. Since it is not known if MAGE-A2 would also contain any glycans that could associate with Con A, therefore, it is best to cleave MAGE-A2 prior to Con A detection by using the enzyme papain because the cleavage site of papain, indicated in Figure 1.11B, is still retained within hMFc, as shown in Figure 6.9 above. As mentioned in Section 6.1.2, MFc was expected to form a homodimer like an immunoglobulin via disulphide bonds within the hinge region. However, no protein bands were detected around 150kDa (2 x 65kDa), which was the molecular weight of full length MFc. Notably, a strong protein band was visible above 250kDa and was reactive against antibodies which could recognise both human or mouse IgG Fc and

human MAGE-A2 via western blotting. Due to the molecular weight being much greater than the expected molecular weight of 150kDa, the identity of this protein being MFc assembled into homodimers is quite unlikely. Therefore, further experiments are required to determine the precise assembly of MFc protein.

The Coomassie staining of purified Fc fusion proteins under non-reducing conditions suggests that the Fc fusion proteins were forming protein aggregates which most likely involved disulphide bond formation because all non-covalent interactions should be abolished under non-reducing conditions. More importantly, the protein sequence of MAGE-A2 indicates that there were five cysteine residues within MAGE-A2. The structure of MAGE-A2 is still unsolved, but if all cysteine residues within MAGE-A2 are assumed to form intrachain disulphide bonds there will still be one remaining free cysteine which could react with other free cysteines of other proteins if it is located at an exposed position. More importantly, it was predicted that the first 100 amino acids of MAGE-A2 may be an unstructured region and within these 100 amino acids there is a cysteine residue. If the above reasoning is true, then this cysteine-10 might be responsible for protein aggregation via disulphide bonding.

In addition, the existence of single soluble MFc polypeptide chains should not be neglected. Normally, the heavy chain of an immunoglobulin is retained within the endoplasmic reticulum (ER) by the binding of a protein known as heavy chain binding protein (BiP) to the CH1 domain of the heavy chain until the heavy chain assembles with the light chain (Hendershot *et al*., 1987). Hendershot and colleagues had shown that light chain negative cell lines that expressed mutant IgG with CH1

domain deletion were able to secrete free heavy chains, including monomeric heavy chain, which highlighted the role of CH1 domain in immunoglobulin assembly (Hendershot *et al*., 1987). In the case of MAGE-A2 fusion protein, the CH1 domain of IgG had been removed to allow the fusion of MAGE-A2. There is a possibility that monomeric MFc may be secreted into the extracellular environment. More importantly, these monomeric MFcs would contain two free cysteines at the hinge region. With the addition of the 13 amino acid peptide linker at the N terminus of the hinge region, the free cysteine residues may be quite exposed to participate in an interaction with other proteins, including other monomeric MFcs. Whether the protein aggregation was formed due to interchain disulphide bonding with other proteins after secretion or after SDS denaturing is yet unknown. However, the presence of other proteins which were not detected by either anti human/mouse IgG Fc and anti human MAGE-A2 antibodies suggests that may be other proteins associating with MFc and mostly likely the interaction is via interchain disulphide bonding. Therefore, the aggregation of MFc has to be solved in order ensure that MFc could carry out its intended function as anticipated.

On the other hand, under reducing conditions there was evidence of several protein bands with molecular weights smaller than the full length 75kDa MFc, which contained IgG Fc epitopes and MAGE-A2 epitopes detectable during western blot analyses. It is possible that MFc might be suffering from protein degradation. In this case, it is very likely that the MAGE-A2 protein of MFc was subjected to protein degradation alone because the Fc region has to be intact in order to bind to Protein G-Sepharose. More importantly, there were no protein bands detected at 25kDa or below in both Coomassie staining and western blotting, suggesting that the Fc region

of the MFc remained intact. Secreted proteins are usually protected from protein degradation as they are removed from the intracellular proteolysis system in mammalian cell culture. If MFc is indeed being degraded, it is possible that proteases were secreted into the extracellular environment by cells during culture or were released to the extracellular environment upon cell death. Protein degradation of MAGE-A2 may be initiated due to the predicted unstructured region located at the N-terminus of MAGE-A2. Clincke and colleagues showed that protease activity existed in human recombinant interferon-γ (IFN-γ) expressing CHO cell cultures and such protease activity could be minimised with the addition of iron citrate during cell culture (Clincke *et al*., 2011). Therefore, it may of interest in future experiments to test whether addition of iron citrate to the culture medium might prevent MFc degradation.

One possible approach to overcome the protein aggregation and protein stability issue of MFc would be to use a stable domain of MAGE-A2 to fuse with Fc region of IgG rather than the full length MAGE-A2 protein. Although the crystal structure of MAGE-A2 protein has not been solved, Newman and colleagues have determined the crystal structures of the MAGE Homology Domain (MHD) and the C terminal structure of MAGE-A3 and -A4 (Newman *et al*., 2016). The authors described that the structure of the MHD were very similar for both MAGE-A3 and MAGE-A4 (Newman *et al*., 2016). In addition, MHD is a highly conserved region within MAGE-A family proteins and is found in the majority of the MAGE-A proteins, including MAGE-A2, as shown in Figure 6.2. Indeed, the aligned MHD protein sequences of MAGE-A2, -A3 and -A4 as illustrated in Figure 6.14 show that the

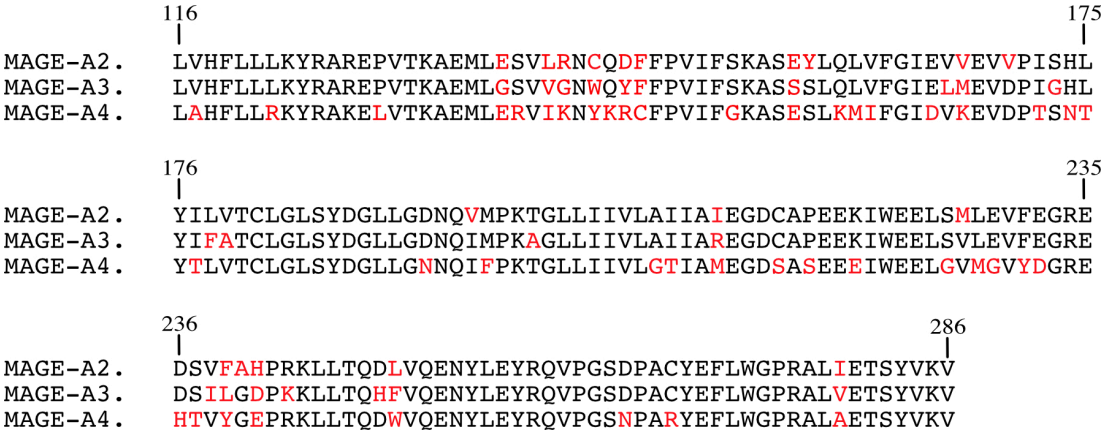

Figure 6.14: A diagram illustrating the aligned sequences of the Mage Homology Domain (MHD) of MAGE-A2,-A3 and -A4. Red coloured letters represent mismatches. Accession code for MAGE-A2 is P43356. Protein sequence of MAGE-A3 and -A4 was obtained from the crystal structure of MAGE-A3 (4V0P) and MAGE-A4 (2WA0).

MHD of MAGE-A2 has a similarity of up to 84.8% with MAGE-A3 and 71.9% with MAGE-A4. There is a high possibility that the same MHD structure would be adopted by the MAGE-A2. The success in crytallizing the MHD of MAGE-A3 and A4 proteins suggests that MHD might be a stable domain. Therefore, MFc could be reengineered to consist only of the MHD of MAGE-A2 fused directly to the Fc region of IgG in the hope of reducing the overall protein aggregation and increasing protein stability.

Finally, MAGE-A3 has been used as cancer vaccine in the past. GlaxoSmithKline Biologicals generated a cancer vaccine by fusing a lapidated protein D derived from *H. influenzae* to the N-terminus of human MAGE-A3 (Marchand *et al.*, 2003). With the combination of immunological adjuvant, this MAGE-A3 vaccine was first tested on MAGE-A3 positive patients by Marchand and colleagues (Marchand *et al.*, 2003). The authors reported that a few patients showed signs of tumour regression and the vaccine was generally well tolerated (Marchand *et al.*, 2003). The MAGE-A3

vaccine managed to enter a phase III clinical trial over the past few years, but the clinical trial was halted when the vaccine was found to be unable to improve overall survival of patients (Vansteenkiste *et al*., 2016). However, it was reported by the authors that ~100% (921/925) patients had shown expression of anti-MAGE-A3 IgG antibodies after four treatment doses when compared to 9% (42/491) in the placebo group (Vansteenkiste *et al*., 2016). The finding of anti-MAGE-A3 IgG antibody production was in agreement with our reasoning that MAGE-A proteins would be recognised as foreign proteins when being vaccinated. The major difference between the MAGE-A3 vaccine mentioned above and our MAGE-A2 Fc fusion protein was the incorporation of the IgG Fc region rather than a bacterial protein. It is expected that the MAGE-A2 Fc fusion protein described in this project would perform better than the MAGE-A3 vaccine mentioned above due to an increase in plasma half-life, which should stimulate extensive host antibody production, and the better association with FcRn to induce antigen cross presentation. However, more investigations are required to confirm this expectation.

In summary, MFc can be produced from FreeStyle 293-F transfected cell culture and purified using Protein G-Sepharose. However, more studies are required to determine if the MAGE-A2 protein is stable in secreted form as MAGE-A2 protein seems to have a possibility of being degraded. Investigation into the association of MAGE-A2 with other soluble proteins needs to be carried out as well due to the observation of strong protein aggregations because the association of other proteins with MAGE-A2 would possibly reduce exposure of MAGE-A2 epitopes to host antibodies which would in return reduce the formation of MFc immune complexes that is required for antigen cross presentation initiation.

CHAPTER SEVEN

ANALYSIS OF ANTIGEN CROSS PRESENTATION ELICITED BY Fc FUSION PROTEIN

CHAPTER 7 ANALYSIS OF ANTIGEN CROSS PRESENTATION ELICITED BY Fc FUSION PROTEIN

7.1 INTRODUCTION

Exogenous antigens are usually taken up by phagocytes or antigen presenting cells (APC) via pinocytosis or phagocytosis and undergo proteolysis before digested peptides are presented in complex with MHC Class II molecules. However, studies have shown that exogenous antigens can be presented in complex with MHC Class I molecules by a process known as antigen cross presentation, described previously in Figure 6.1. The exact mechanism mediating antigen cross presentation is yet unclear and remains under investigation.

Several APC, such as macrophages and B cells, are capable of antigen cross presentation (Hon *et al*., 2005; Delamarre *et al*., 2005). However, dendritic cells (DC) had been identified as the most efficient APC for antigen cross presentation *in vivo* (Amigorena and Savina, 2010; Delamarre *et al*., 2005). Recently, Liu and colleagues reported that after IgG-IC phagocytosis the pH within the phagosome of macrophages reduced rapidly to a pH below 6. In contrast, the pH of the phagosome of DC following IgG-IC phagocytosis remained neutral (Liu *et al*., 2011). The authors suggested that the difference in pH might have an effect on the initiation of different proteases and that full proteolysis is required for antigen cross presentation to enrich the digested peptide pool for both MHC Class I and II presentation (Liu *et al*., 2011). Acidification relies on the activity of the ATP-dependent vacuolar pump (V-ATPase) which controls the transport of protons. Trombetta and colleagues reported that DC in different stages of maturation exhibit different efficiency in the

assembly of V-ATPase in lysosomes, which in turn results in a difference in the pH regulation of dendritic cell lysosomes (Trombetta *et al*., 2003). In addition, Delamarre and colleagues reported that DC have a lower expression of most lysosomal proteases when compared to macrophages (Delamarre *et al*., 2005). Differences in DC lysosome pH and protease levels might be responsible for differing antigen cross presentation efficiency because both may impact on the time required for the antigen proteolysis necessary to generate digested peptides suitable for presentation on MHC Class I molecules.

Although DC perform most effectively in regards to antigen cross presentation, the efficiency of antigen cross presentation varies within different subsets of DC. It is now believed that the murine $CD8^+$ DC subset (counterparts of human BDCA-3^+ DC) is the most competent antigen cross presenting cell when compared to other subsets (Baker *et al*., 2014; Joffre *et al*., 2012). However, Baker and colleagues showed that $CD8^-CD11b^+$ DC were able to cross present in a FcRn-dependent manner when incubated with a 10-fold lower antigen concentration compared to $CD8^+CD11b^-$ DC (Baker *et al*., 2011). The functional specialisations of different murine DC subsets is reviewed in (Joffre *et al*., 2012). The intracellular mechanisms mediating antigen cross presentation are believed to involve two different pathways termed the "cytosolic" and "vacuolar" pathways (Joffre *et al*., 2012). The main difference between the two is the location where the antigen is degraded. The cytosolic pathway is sensitive to proteasome inhibitors and involves antigen being exported out of the phagosome into the cytosol and subjected to proteasomal degradation. The digested peptides are suggested to be transported into the endoplasmic reticulum or phagosome and loaded onto MHC-Class I molecules with the assistance of

transporter associated with antigen processing 1 (TAP1) and TAP2 (Joffre *et al*., 2012). On the other hand, the vacuolar pathway can be inhibited by lysosomal proteolysis inhibitors and involves the antigen being degraded within the phagosome after lysosomal fusion. The digested peptide is then loaded onto MHC Class I molecule with the assistance of TAP1 and TAP2 without the involvement of the endoplasmic reticulum (Joffre *et al*., 2012). It has been noted that components of the MHC Class I loading machinery such as TAP have been detected within the phagosome as well as MHC Class I molecules themselves (Amigorena and Savina, 2010). However, the regulation of antigens into different pathways is still unknown and remains under investigation.

As mentioned in Chapter 6, the rationale behind development of the MAGE-A2 Fc fusion protein (MFc) was to utilise FcRn antigen cross presentation ability in DC to initiate a cytotoxic T cell response against MAGE-A2-expressing cancer cells. To investigate if MFc could be phagocytosed by DC and cross presented on MHC Class I molecules to activate cytotoxic T cells, an antigen cross presentation system (explained below), involving an eight amino acid peptide, SIINFEKL, and a cytotoxic T cell cell line known as B3Z was utilised. In the past, Moore and colleagues immunised mice of different strains with transfected cells which produced chicken ovalbumin (OVA) endogenously and demonstrated that only the mouse strain C57BL/6 expressing the murine MHC Class I allele, H-2K^{b}, was capable of inducing a cytotoxic T cell immune response against transfected cells (Moore *et al*., 1988). More importantly, the authors cultured the reactive T cells and showed that a similar T cell immune response was not induced with cells incubated with soluble OVA for up to 24 hours when compared with transfected OVA-producing cells.

Thus, effective presentation of the digested OVA peptide was highly restricted to MHC Class I rather than MHC Class II (Moore *et al*., 1988). It was later discovered by Falk and colleagues that the H-2K^{b} restricted OVA peptide sequence was SIINFEKL, also known as $OVA_{257-264}$ (Falk *et al*., 1991). Taking this further, Karttunen and colleagues utilised a NFAT-*lac*Z reporter construct and transfected the murine cytotoxic T cell which was capable of recognising the MHC Class I, H-2K^{b}, when loaded with SIINFEKL peptide, to generate a cell line known as B3Z that is capable of producing β-galactosidase enzyme upon activation via the recognition of SIINFEKL peptide (Karttunen *et al*., 1992). As a result, a system to study antigen cross presentation using OVA or proteins with SIINFEKL incorporation was developed. Schuurhuis and colleagues incubated OVA IC with DC and showed that they could efficiently activate B3Z T cells but a similar activation was not possible with soluble OVA (Schuurhuis *et al*., 2002). On the other hand, Gil-Torregrosa and colleagues incubated DC of different maturation stages with OVA IC and fixed the cells after 3 hours. This enabled them to study the antigen cross presentation efficiency of DC at different maturation stages by analysing the activation of corresponding B3Z T cells (Gil-Torregrosa *et al*., 2004). In a different scenario, Shaw and Starnbach fused the SIINFEKL peptide to the N-terminus of diphtheria toxin and showed that diphtheria toxin receptor-expressing DC from transgenic mice was capable of activating B3Z T cells. This finding suggested that SIINFEKL-diphtheria toxin was cross presented to MHC Class I molecules (Shaw and Starnbach, 2006). Based on these results, it was proposed that investigation of the antigen cross presentation of MFc might be possible by incorporating the eight amino acid SIINFEKL sequence into the MAGE-A2 protein. The rationale was that when MFc was digested after phagocytosis by DC, the SIINFEKL peptide would be loaded onto

MHC Class I molecules resulting in the activation of corresponding B3Z T cells, thereby providing a useful *in vitro* indicator of antigen cross presentation of MFc.

7.1.1 Formation of MFc immune complexes (IC)

As mentioned earlier, in the tests described above soluble OVA was unable to activate a cytotoxic T cell response unlike OVA IC (Moore *et al*., 1988). Therefore, the formation of IC seems to be an important factor in antigen cross presentation. It was considered that the ideal situation would be to generate polyclonal mouse anti-human MAGE-A2 antibodies and used the antibodies to form IC with hMFc. However, due to time constraints this approach was not carried out. Fortunately, Ober and colleagues when investigating the binding of IgGs of different species to human or mouse FcRn showed that mouse FcRn displays binding to IgG from a wider range of species than human FcRn (Ober *et al*., 2001). In this chapter, rabbit anti-mouse IgG antibodies were used to form IC with mMFc proteins. Rabbit IgG is one of the few immunoglobulin species capable of binding to both human and mouse FcRn (Ober *et al*., 2001). Schuurhuis and colleagues used OVA-specific rabbit IgG to form IC with OVA in order to study antigen cross presentation with mouse DC (Schuurhuis *et al*., 2002). Similarly, Rafiq and colleagues used OVA-specific rabbit IgG to form IC with OVA to 'immunise' DC in order to demonstrate tumour immunity in mouse models (Rafiq *et al*., 2002). As a result, rabbit IgG was considered a suitable antibody to be used in this chapter as a means to generate IC with mMFc for antigen cross presentation analyses.

7.1.2 B3Z T cells

B3Z T cells are murine cytotoxic T cells that was capable of recognising SIINFEKL

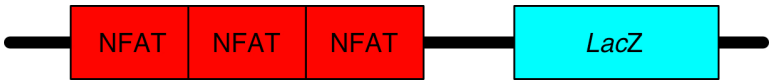

Figure 7.1: A schematic diagram illustrating the NFAT-*lac*Z reporter construct. Transcription of the *lac*Z gene is regulated by three NFAT binding sites. It was expected that all three NFAT binding sites had to be bound to initiate transcription of the *lac*Z gene.

peptide loaded onto H-2K^{b} MHC Class I molecules (Karttunen *et al*., 1992). More importantly, B3Z T cells produce β-galactosidase upon activation due to having been transfected with a NFAT-*lac*Z reporter construct (Karttunen *et al*., 1992). The basics of the NFAT-*lac*Z reporter construct are illustrated in Figure 7.1.

During an immune response, a cytotoxic T cell only produces interleukin-2 (IL-2) when activated (Fiering *et al*., 1990). The reason for this is that IL-2 is highly regulated and it requires the binding of several transcription factors to induce IL-2 gene transcription. One of these transcription factors was identified to be nuclear factor of activated T cells (NFAT) (Fiering *et al*., 1990). Fiering and colleagues reported that NFAT binding activity was only found in activated T cells, and therefore they utilised the NFAT binding site to create a NFAT driven *lac*Z reporter construct (Fiering *et al*., 1990), shown in Figure 7.1. The authors reported that the NFAT-*lac*Z reporter construct required the concentration of NFAT to reach a certain threshold in order to initiate the transcription of the *lac*Z gene. This requirement was suggested to be due to the transcription being governed by three NFAT binding sites (Fiering *et al*., 1990). It was expected that all three NFAT binding sites had to be bound in order to initiate transcription (Fiering *et al*., 1990). As a result, β-galactosidase would only be produced upon activation of T cells.

7.2 AIMS

This chapter hypothesised that SIIN-MFc proteins in IC formation would be phagocytosed by dendritic cells and digested in order to generate the SIINFEKL peptide to be cross presented on MHC Class I molecule. As a result, this chapter aimed to determine if SIIN-MFc protein could be taken up by DC and enter the antigen cross presentation pathway in order to activate corresponding cytotoxic T cell. The digested peptide SIINFEKL of SIIN-MFc protein was expected to be presented on MHC Class I molecules and activate correspondent B3Z T-cells if the antigen cross presentation pathway was successfully engaged.

7.3 MATERIALS AND METHODS

7.3.1 MATERIALS AND BUFFER

Mice

All mice were wildtype C57BL/6 (gift from Prof. Colin Watts' group, University of Dundee).

Red blood cell (RBC) lysis buffer

Red blood cell lysis buffer (155mM ammonium chloride, 12mM sodium bicarbonate, 0.1mM EDTA, pH 7.3) was prepared and stored at 4ºC. Buffer was warmed to 37ºC prior to use.

Complete RPMI medium (cRPMI)

Supplements listed in Table 7.1 were added to RPMI-1640 and stored at 4ºC. Medium was warmed to 37ºC prior to use.

Table 7.1: Supplement details to make complete RPMI medium

Supplements	Final concentration
Sodium pyruvate	1X
Non essential amino acids	1X
Kanamycin	1X
L-Glutamine	1X
β-mercaptoethanol	50μM
Foetal calf serum (low endotoxin)	10%

Note: 1X Kanamycin = 100 μg/ml Kanamycin
1X Sodium Pyruvate = 1mM Sodium Pyruvate
1X Non-Essential Amino Acids = A mixture of 7 amino acids, 0.1mM of each amino acid
1X L-Glutamine = 2mM L-Glutamine

Murine bone marrow dendritic cell medium (BMDC-Medium)

200ml of cRPMI was filter sterilised through a 0.22μm pore size polyethersulfone membrane unit (Corning Inc.) to remove any potential pathogens which could activate dendritic cells during cell culture. Recombinant murine granulocyte-macrophage colony-stimulating factor (GM-CSF) (PeproTech) was then added to the medium to a final concentration of 10ng/ml. Completed medium was stored at 4ºC and was warmed to 37ºC prior to use.

Murine splenic dendritic cell medium (SDC-Medium)

200ml of cRPMI was filter sterilised through a 0.22μm pore size polyethersulfone membrane unit (Corning Inc.) to remove any potential pathogens which could activate dendritic cells during cell culture. Recombinant murine GM-CSF

(PeproTech) and recombinant human transforming growth factor beta 1 (TGF-β1) (R&D Systems Europe, Ltd.) were then added to the medium to a final concentration of 10ng/ml and 1ng/ml respectively. Completed medium was stored at 4ºC and was warmed to 37ºC prior to use.

CPRG Buffer

0.15mM chlorophenolred-β-D-galactopyranoside (CPRG) (Calbiochem®, Merck Millipore), 0.5% (v/v) Nonidet P-40 (Sigma) was prepared in PBS. The solution was stored at 4ºC prior to use.

PBN Buffer

0.5% (w/v) BSA (Sigma), 0.1%(w/v) NaN_3 was prepared in PBS. The solution was stored at 4ºC and kept on ice during usage.

RIPA Buffer

50mM Tris-HCl, pH 7.4
1% (v/v) Nonidet P-40
0.5% (w/v) sodium deoxycholate
0.1% (w/v) SDS
150mM NaCl
2mM EDTA
50mM NaF

Solution with the above content was prepared in Milli-Q water and stored at room temperature. Halt™ Protease Inhibitor Cocktail EDTA-free (Thermo Fisher Scientific) (final concentration 1X) was added to the buffer prior to use.

7.3.2 PLASMIDS

pKz-mMFc

A plasmid, pKz-mMFc, encoding a Fc fusion protein of human MAGE-A2 fused to the Fc region of mouse IgG2a which was derived previously in Chapter 6, Figure 6.7.

7.3.3 INCORPORATION OF SIINFEKL PEPTIDE TO MFc

7.3.3.1 Insertion of SIINFEKL peptide DNA encoding sequence to mMFc expression plasmid

Within the DNA sequence of MAGE-A2, there is a unique ApaI restriction site suitable for digestion, shown in Figure 7.2. Primer Siinfekl1 (Table 2.2, No.14) was designed to utilise this restriction site to incorporate sequence encoding SIINFEKL peptide into MAGE-A2 as shown in Figure 7.2. Unfortunately, this approach was unable to proceed due to unsuccessful digestion with ApaI enzyme. As a result, a different approach was carried out which involved multiple PCR amplification steps. This procedure was described in Figure 7.3.

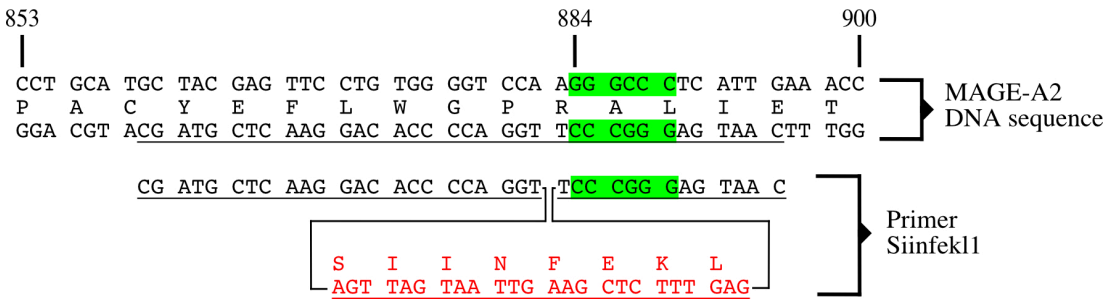

Figure 7.2: A diagram illustrating the ApaI site within MAGE-A2 DNA sequence and the design of primer Siinfekl1 for the incorporation of SIINFEKL peptide.

First step

pKz-mMFc was digested with restriction enzymes HindIII and EcoRI at 37ºC for 1 hour as described in section 2.4.1. Gel electrophoresis and DNA gel extraction were performed to purify a DNA fragment at about 1732bp, containing the sequence of mMFc (insert). Primers MAGE-FcKosak, and Siinfekl1 (Table 2.2, No.11 & 14) were used at an annealing temperature of 65ºC with the purified DNA insert as template to amplify a DNA product of approximately 930bp, which contained a N-terminal HindIII site and C-terminal ApaI site. PCR products were run on a DNA agarose gel as described in section 2.4.4 and DNA bands of the correct sizes were extracted as described in section 2.4.5.

Second step

Purified mMFc (insert) from pKz-mMFc restriction enzyme digest was used as DNA template and amplified using a primer combination of the purified PCR product from step 1 and MAGERev (Table 2.2, No. 8) at an annealing temperature of 65ºC to obtain a DNA product of approximately 1079bp. PCR products were run on a DNA agarose gel as described in section 2.4.4 and a DNA band of the correct size was extracted as described in section 2.4.5. Purified PCR product would be used as a primer in the subsequent PCR amplification.

Third step

Purified mMFc (insert) from pKz-mMFC digestion was used as DNA template and amplified using a primer combination of purified PCR product from step two and primer MouseFcRev (Table 2.2, No. 13) at an annealing temperature of 65ºC to

A. Incorporation of SIINFEKL

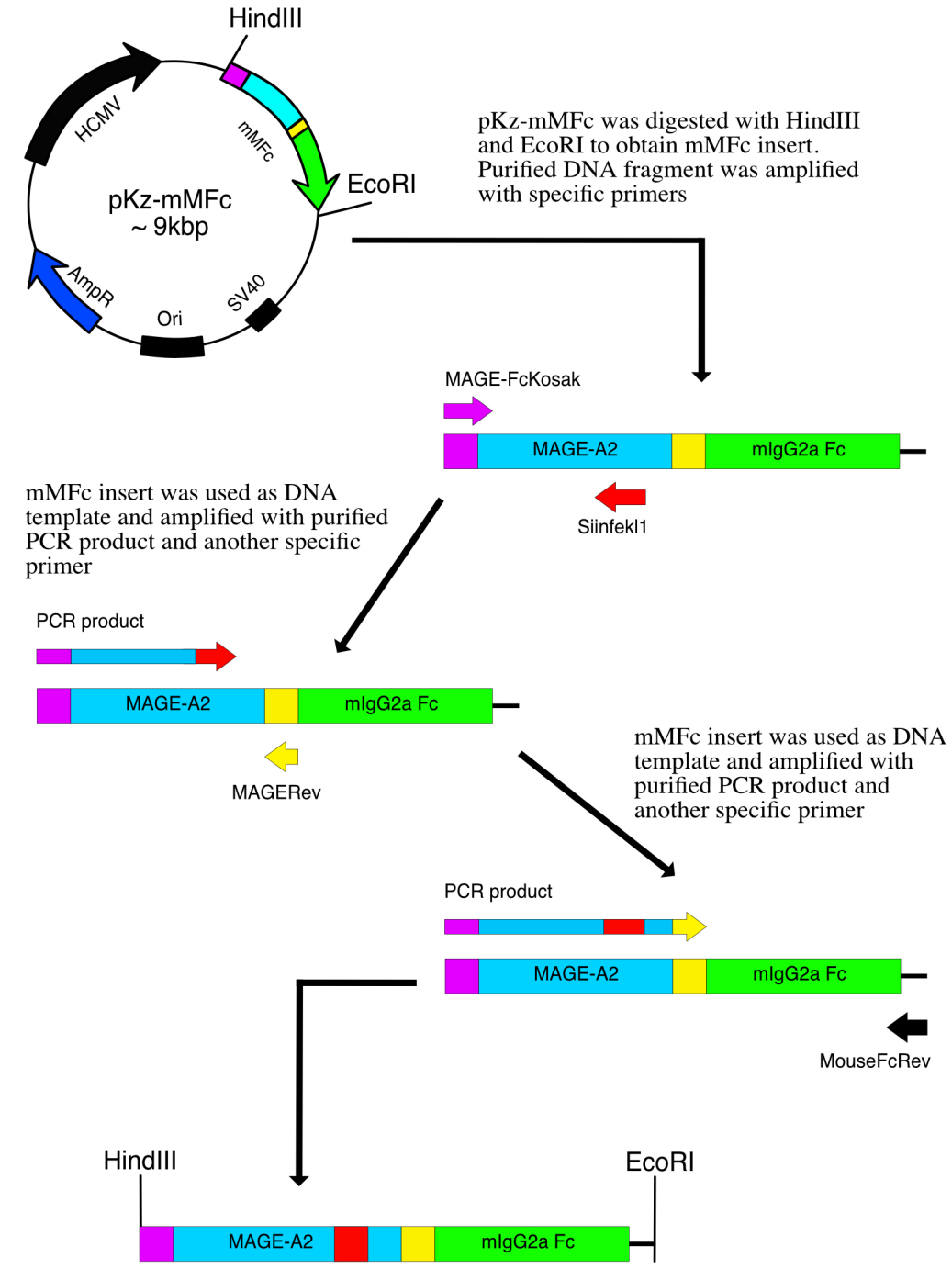

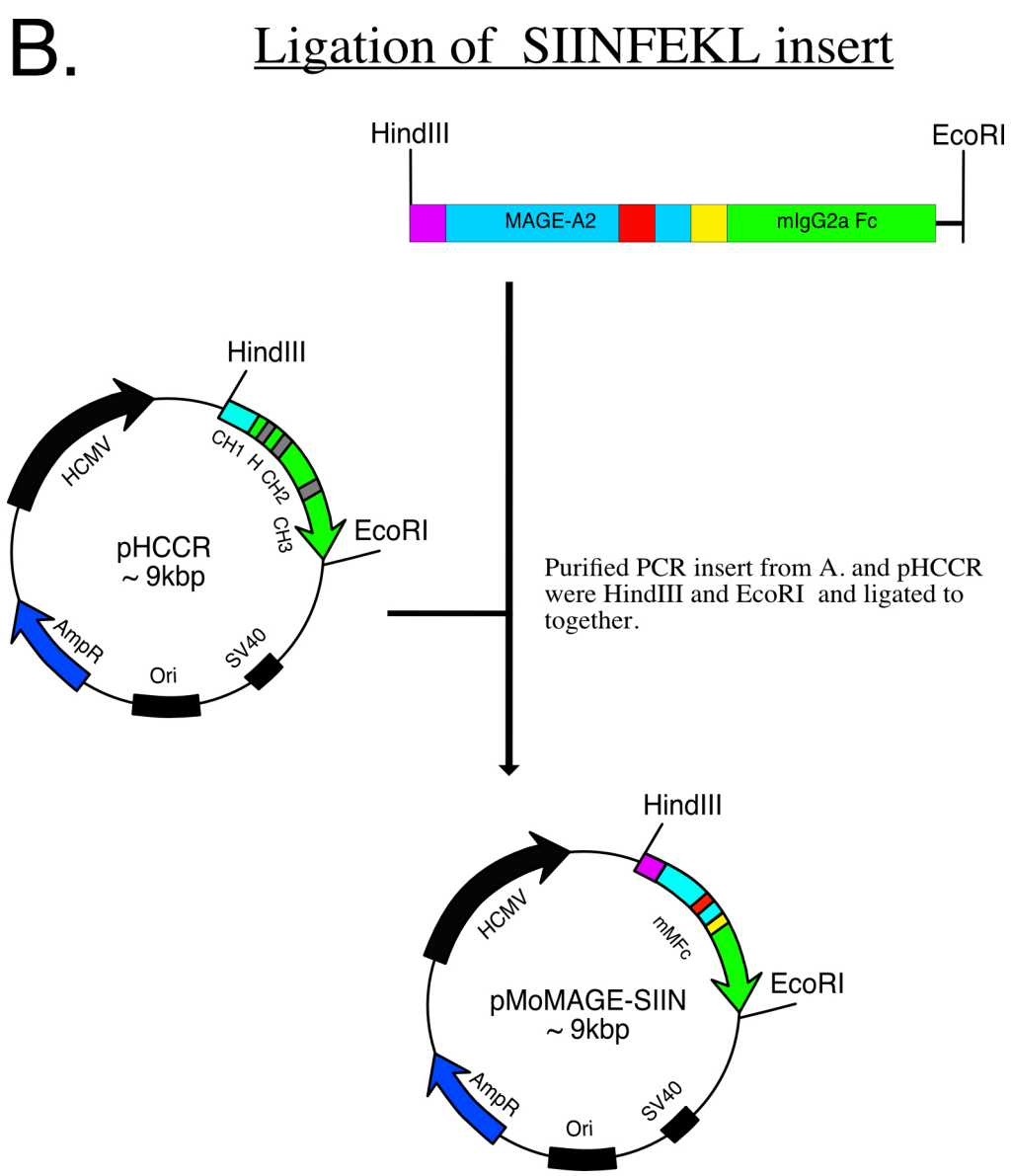

Figure 7.3: A schematic diagram illustrating the incorporation of sequence encoding the SIINFEKL peptide into MAGE-A2 and the generation of an expression vector. **A**) Incorporation of sequence encoding SIINFEKL peptide into MAGE-A. pKz-mMFC was digested with HindIII and EcoRI to obtain the insert containing mMFc DNA sequence (insert), and this was used as template in an amplification with specific primers to introduce SIINFEKL sequence (red). The PCR product was purified and further amplified with a specific primerMFC. Finally, the second PCR product was purified and again further amplified with another specific primerMFC. **B**) Generation of an expression vector. Final PCR product from **A** was digested with HindIII and EcoRI. pHCCR was digested with HindIII and EcoRI to obtain a cut vector to ligate with the previously digested insert.

obtain a DNA product of approximately 1762bp. Gel electrophoresis and DNA gel extraction were carried out subsequently. Purified DNA fragment and plasmid pHCCR were then digested with restriction enzymes HindIII and EcoRI as described in section 2.4.1. Gel electrophoresis and DNA gel extraction were performed to purify the digested DNA fragment of 1750bp (insert) and digested pHCCR of about 8000bp (vector). Both purified DNA fragments were then ligated as described in section 2.4.6 and transformed into competent DH5α *E. coli* as described in section 2.4.7. After purifying the plasmids from positive clones as described in section 2.4.9, DNA sequencing was carried out (section 2.4.11) to ensure that the desired mutations had been incorporated, and that no errors had been introduced. A plasmid with correct DNA sequence was named as pMoMAGE-SIIN.

7.3.4 PRODUCTION AND CHARACTERISATION OF SIIN-mMFc

7.3.4.1 SIIN-mMFc production and purification from FreeStyle 293-F cells

FreeStyle 293-F cells were thawed from liquid nitrogen and maintained in appropriate growth conditions as shown in section 2.6.2. On the day before transfection, each flask of cells was passaged and used to seed 5 x 10^5 cells/ml in an Erlenmeyer flask in a total volume of 25ml, so that on the day of transfection cells were at 1 x 10^6 cells/ml with a viability of 90% or above. For transfection, 293Fectin (Invitrogen) and Opti-MEM (1X) (Gibco Life Technologies) were brought to room temperature. For a single transfection, two aliquots of 0.833ml of Opti-MEM (1X) were pipetted into two 30ml Universal tubes. In one tube, the amount of DNA listed in Table 7.2 was added and mixed gently. In the other tube, 33.25µl of 293Fectin was added and allowed to incubate for exactly 5 minutes at room temperature before

Table 7.2: Amount of DNA required for FreeStyle 293-F cells transfection

Type of DNA expression vector	Amount of DNA
pMoMAGE-SIIN	4.17μg
pAdvantage vector (Promega)	4.17μg

the addition of the DNA mixture. Once the DNA mixture was added, the solution was gently mixed and allowed to incubate for 20-30 minutes at room temperature. When completed, the solution was added to the FreeStyle 293-F cells and incubated on a shaker in an incubator in 8% CO_2 at 37ºC. SIIN-mMFc was ready to be harvested and purified after 4 days as described in section 2.8.

7.3.4.2 Characterisation of SIIN-mMFc

SIIN-mMFc purifications were carried out as described in section 2.8. Purified SIIN-mMFc were subjected to SDS-PAGE as described in section 2.8.6. Protein gels were stained with Coomassie as described in section 2.8.8 to determine the purity of the Fc fusion protein generated. To further analyse the purified protein, SIIN-mMFc was subjected to western blotting as described in section 2.8.7. After the blocking and washing procedure, the membranes were incubated with polyclonal goat anti-mouse IgG HRP conjugated (Table No.20) and monoclonal mouse anti-human MAGE-A2 (6C1) (Table 2.1, No.18) or monoclonal mouse anti-human MAGE-A2 (1H4) (Table 2.1, No.17). Both monoclonal antibodies were detected with polyclonal goat anti mouse kappa light HRP conjugated (Table 2.1, No.19). All membranes were washed and developed with appropriate substrate.

7.3.5 GENERATION OF BONE MARROW DERIVED DENDRITIC CELLS AND SPLENIC DERIVED DENDRITIC CELLS

7.3.5.1 Bone marrow dendritic cell (BMDC) isolation and culture

A sacrificed mouse was sterilised with 70% (v/v) ethanol. Tibia and femur from both hind legs were extracted with minimal flesh attached. All bones were sterilised using 70% (v/v) ethanol and washed with cRPMI. Both ends of the bones were cut using a bone cutter to expose the bone marrow. All bone marrow was flushed out with cRPMI using a 10ml syringe and a 25G needle onto a 70µm pore size EASYstrainer (Greiner Bio-One) that was placed on top of a 50ml polypropylene tube (Greiner Bio-One). The strainer was washed with 10ml cRPMI and the collected cells were centrifuged for 5 minutes at 250g. The supernatant was discarded and the cell pellet was resuspended in 1ml RBC lysis buffer. The mixture was allowed to stand for 1 minute before being washed twice with 20ml cRPMI and centrifuged for 5 minutes at 250g each time. The supernatant was discarded and the cells were resuspended in BMDC-Medium at 10^6 cells/ml. 2ml bone marrow cells were added to each well of a Costar® 6 well plate - Ultra low attachment surface (Corning Inc.) and incubated for 5-7 days in an incubator at 37ºC, 5% CO_2. The medium was changed whenever required until BMDC had been generated.

7.3.5.2 Splenic dendritic cell (SDC) isolation and culture

A sacrificed mouse was sterilised with 70% (v/v) ethanol. The spleen of the mouse was isolated and washed briefly in 10ml cRPMI in a 50ml polypropylene tube. The spleen was then squashed through a 70µm pore size EASYstrainer into a 50ml polypropylene tube using a plunger of a 10ml syringe to homogenise the spleen cells.

The strainer was washed with 10ml cRPMI and the collected cells were centrifuged for 5 minutes at 250g. The supernatant was discarded and the cell pellet was washed twice with 20ml cRPMI and centrifuged for 5 minutes at 250g each time. The supernatant was discarded and the cells were resuspended in 30ml of SDC-Medium. 5ml splenic cells were added to each well of a Costar® 6 well plate - Ultra low attachment surface and incubated for 14-20 days in an incubator at 37ºC, 5% CO_2. The medium was changed whenever required until SDC had been generated.

7.3.5.3 Harvesting BMDC and SDC

BMDC were ready to be used at day 5-7 while SDC was ready at day 14-20. BMDC and SDC were pipetted into separate 50ml polypropylene tubes. 5ml BMDC or SDC medium were used to wash the wells to collect any remaining DC and added to their respective tubes. Cells were centrifuged for 5 minutes at 250g before being washed 3 times with 20ml cRPMI and centrifuged for 5 minutes at 250g each time. BMDC and SDC were resuspended in cRPMI at 1 x 10^6 cells/ml.

7.3.6 ANTIGEN PRESENTATION ASSAY

7.3.6.1 Formation of IC

mMFc (without SIINFEKL) and SIIN-mMFc (with SIINFEKL) were each incubated with rabbit anti-mouse IgG (Table 2.1, No.16) and mouse anti-human MAGE-A2 (1H4) (Table 2.1, No.17) in cRPMI at a concentration ratio of 1:2.5:2.5 for 1 hour at room temperature. The final concentration of each component was 10µg/ml mMFc or SIIN-mMFc, and 25µg/ml of each antibody respectively.

Chicken ovalbumin (OVA) (Sigma) was incubated with rabbit anti-ovalbumin antibody (Table 2.1, No.15) in cRPMI at a concentration ratio of 1:2.5 for 1 hour at room temperature. The final concentration of each component was 10μg/ml OVA and 25μg/ml antibody.

7.3.6.2 B3Z antigen presentation assay

100μl of 10μg/ml mMFc or SIIN-mMFc was prepared in cRPMI in either monomeric or IC format were pipetted into a 96 well U-bottom plate (Falcon®, Corning Inc.). Serial dilution was performed resulting in a final volume of 50μl of protein in each well with a descending concentration gradient across the assay plate. 50μl BMDC or SDC at 1 x 10^6 cells/ml in cRPMI were then added to each well and incubated for 4 hours at 37ºC in an incubator, to allow protein uptake and digestion to occur. When the incubation had completed, 50μl B3Z T cells at 1 x 10^6 cells/ml in cRPMI were added to each well and incubated overnight at 37ºC in an incubator, to allow sufficient time for antigen presentation and β-galactosidase enzyme to be produced. Chicken ovalbumin in soluble format (5mg/ml) or IC format (10μg/ml) and 1μM of SIINFEKL peptide (InvivoGen) was was prepared in cRPMI and added to BMDC as a positive control. cRPMI was added to BMDC as a negative control.

To analyse antigen presentation efficiency, after the above incubations cells were centrifuged for 5 minutes at 250g. The supernatant was discarded and the cells were washed twice with 200μl PBS and centrifuged for 5 minutes at 300g each time. Cells were lysed with 200μl of CPRG buffer and allowed to develop for 6 hours or 24 hours at 37ºC in an incubator. Absorbance at 595nm was measured after either 6 hours or 24 hours using a UV spectrophotometer (Ultrospec 2000, Pharmaia Biotech).

7.3.7 INVESTIGATION OF THE EXPRESSION LEVEL OF DIFFERENT Fc RECEPTORS

7.3.7.1 Flow cytometry analysis

2 x 10^6 cells were required for a single flow cytometry test. B3Z T cells, BMDC and SDC were harvested as described earlier using cold PBN buffer as the washing buffer. After the final wash, cells were resuspended in 100µl human anti-mouse CD64 PE (Table 2.1, No.7) in PBN buffer to detect murine FcγRI expression or 100µl goat anti-mouse CD32/CD16/FcγRIIB (Table 2.1, No.8) in PBN buffer to detect murine FcγRII and FcγRIII expression. 100µl goat anti-human IgA (Table 2.1, No.12) was used as the primary control antibody for the latter test. Cells were then kept in the dark and incubated on ice for 1 hour. After the primary incubation, cells were washed with 500µl cold PBN buffer and centrifuged for 5 minutes at 300g each time for 3 times. After washing, cells that were for detection of the expression of murine FcγRI were resuspended in 500µl cold PBN buffer and were transferred to a 5ml polystyrene round-bottom tube (BD Bioscience) for flow cytometry analysis. Cells that were for detection of the expression of murine FcγRII and FcγRIII were resuspended in 100µl of anti-sheep/goat IgG FITC (Table 2.1, No.11) in PBN buffer and kept in the dark and incubated on ice for 1 hour. Cells were then washed with 500µl cold PBN buffer and centrifuged for 5 minutes at 300g each time for 3 times before resuspending in 500µl cold PBN buffer for flow cytometry analysis.

7.3.7.2 Preparation of cell lysate and whole liver lysate

5 x 10^6 - 7 x 10^6 BMDC, SDC or bone marrow derived macrophages (BMDM) (gift from Dr. Kathleen Reyskens, University of Dundee) were harvested in 1.5ml

microfuge tubes. Cells were washed with 500µl PBS and centrifuged for 5 minutes at 300g each time for 3 times. After the final wash, cells were resuspended in 100µl RIPA buffer. Cells were then sonicated for 10 seconds using an Ultrasonic Processor, Model CV33 to fully lyse the cells. Cell lysate was centrifuged for 10 minutes at 16000g and the supernatant was transferred into a 1.5ml microfuge tube and stored at -20ºC prior to use.

The liver of a wildtype C57BL/6 mouse (gift from Dr. Sarah Thomson, University of Dundee) was squashed through a 70µm pore size EASYstrainer the into a 50ml polypropylene tube using a plunger of a 10ml syringe to homogenise the liver cells. The strainer was washed with 10ml PBS and the collected cells were centrifuged for 5 minutes at 250g. The supernatant was discarded and the cell pellet was resuspended with 5ml RBC lysis buffer. The mixture was allowed to stand for 1 minute before being washed 3 times with 20ml PBS and centrifuged for 5 minutes at 250g each time. After the final wash, the cell pellet was resuspended in 2ml RIPA buffer. Cells were then sonicated for 10 seconds using an Ultrasonic Processor, Model CV33 to fully lyse the cells. Cell lysate was centrifuged for 10 minutes at 16000g and the supernatant was aliquoted into 1.5ml microfuge tubes and stored at -20ºC prior to use. Protein concentrations of all cell lysates were determined using BCA assay analysis (Section 2.8.5.2).

7.3.7.3 Western blotting

Protein molecular weight markers (section 2.7.3) and 10µg protein of each cell lysate was loaded to sample wells of a SDS-PAGE gel and SDS-PAGE electrophoresis was performed. Proteins were then transferred to nitrocellulose membrane and the

membrane was blocked with 5% non-fat milk. Membrane was incubated with 5ml of rabbit anti-mouse FcRn (Table 2.1, No.9) in PBS-T overnight at 4ºC on a roller. After primary incubation, the membrane was washed 3 times with PBS-T and incubated with 5ml goat anti-rabbit IgG-HRP conjugate (Table 2.1, No.14) in PBS-T for another hour at room temperature on a roller. After secondary incubation, the membrane was washed 3 times with PBS-T and developed using Pierce® ECL Western Blotting Substrate (Thermo Fisher Scientific). Protein bands were visualised on a LI-COR Odyssey Fc (LI-COR Bioscience UK Ltd). After visualisation of desired protein bands, the membrane was washed 3 times with PBS-T and incubated in rabbit anti-actin (Table 2.1, No.13) in PBS-T for 1 hour at room temperature on a roller. Membrane was then washed 3 times with PBS-T before being incubated with 5ml goat anti-rabbit IgG-HRP conjugate (Table 2.1, No.14) in PBS-T for another hour at room temperature on a roller. The membrane was then developed using the same substrate and visualised after a similar washing process.

7.4 RESULTS

7.4.1 Incorporation of SIINFEKL peptide into MAGE-A2

Using the primer combinations of MAGE-FcKosak and Siinfekl1 to amplify the digested mMFc insert from pKz-mMFc, an amplified fragment of the correct size of 930bp was obtained as shown in Figure 7.4A. After the introduction of SIINFEKL coding sequence into the DNA sequence of MAGE-A2, the purified PCR product was used as a primer for further amplification along with primer MAGERev using mMFc insert as template. An amplified fragment of the correct size of 1079bp was obtained as shown in Figure 7.4B. Finally, the purified product from the second PCR

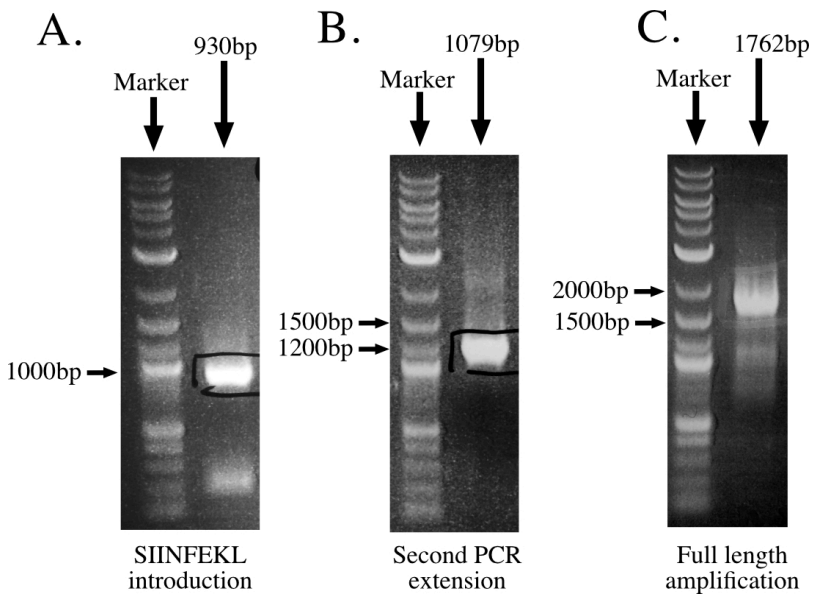

Figure 7.4: Results of molecular cloning for the incorporation of SIINFEKL peptide into mMFc. **A)** SIINFEKL coding sequence introduction into MAGE-A2. Lane 930bp shows PCR amplification using MAGE-FcKosak and Siinfekl1 to obtain DNA fragment at 930bp. **B**) PCR product extension. Lane 1079bp shows PCR amplification using PCR product from A. and primer MAGERev to obtain DNA fragment at 1079bp. **C**) Full length SIINFEKL containing mMFc amplification. Lane 1762bp shows PCR amplification using PCR product from B. and primer MouseFcRev to obtain DNA fragment at 1762bp.

was used as a primer for further amplification along with primer MouseFcRev using mMFc insert as DNA template to generate the full length DNA sequence for SIINFEKL containing mMFc (SIIN-mMFc). An amplified fragment of the correct size of 1762bp was obtained as shown in Figure 7.4C. The purified DNA fragment and pHCCR was digested with restriction enzymes HindIII and EcoRI and ligated together to generate the expression vector for SIIN-mMFc. The incorporation of the SIINFEKL encoding sequence was verified by DNA sequencing, as indicated in Figure 7.5.

7.4.2 Production and characterisation of SIIN-mMFc

The SIIN-mMFc expression plasmid, pMoMAGE-SIIN, was transfected into FreeStyle 293-F cells. After 4 days, supernatants of the cell cultures were incubated with Protein G-Sepharose and SIIN-mMFc proteins were efficiently purified. The

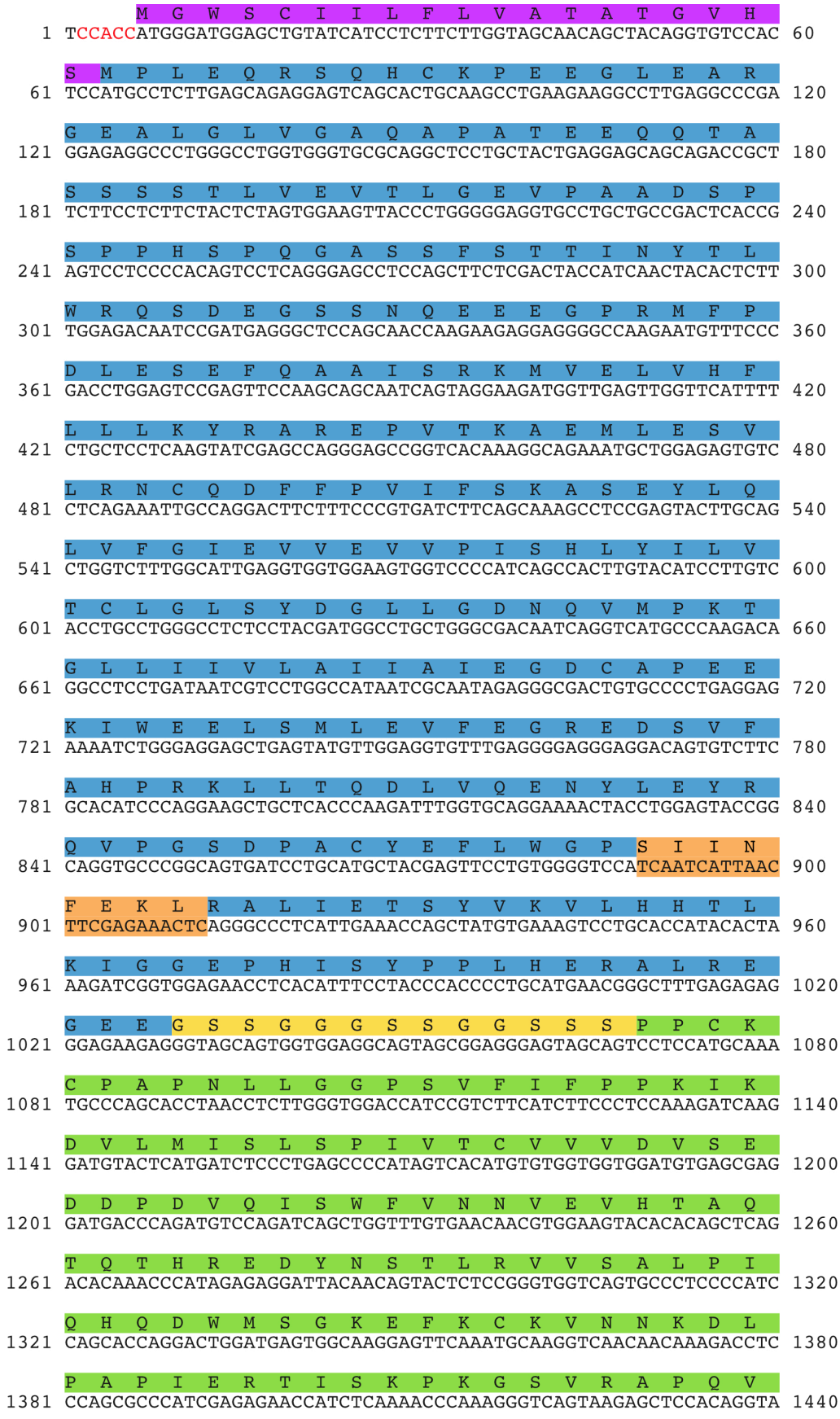
M G W S C I I L F L V A T A T G V H
1 TCCACCATGGGATGGAGCTGTATCATCCTCTTCTTGGTAGCAACAGCTACAGGTGTCCAC 60
S M P L E Q R S Q H C K P E E G L E A R
61 TCCATGCCTCTTGAGCAGAGGAGTCAGCACTGCAAGCCTGAAGAAGGCCTTGAGGCCCGA 120
G E A L G L V G A Q A P A T E E Q Q T A
121 GGAGAGGCCCTGGGCCTGGTGGGTGCGCAGGCTCCTGCTACTGAGGAGCAGCAGACCGCT 180
S S S S T L V E V T L G E V P A A D S P
181 TCTTCCTCTTCTACTCTAGTGGAAGTTACCCTGGGGGAGGTGCCTGCTGCCGACTCACCG 240
S P P H S P Q G A S S F S T T I N Y T L
241 AGTCCTCCCCACAGTCCTCAGGGAGCCTCCAGCTTCTCGACTACCATCAACTACACTCTT 300
W R Q S D E G S S N Q E E E G P R M F P
301 TGGAGACAATCCGATGAGGGCTCCAGCAACCAAGAAGAGGAGGGGCCAAGAATGTTTCCC 360
D L E S E F Q A A I S R K M V E L V H F
361 GACCTGGAGTCCGAGTTCCAAGCAGCAATCAGTAGGAAGATGGTTGAGTTGGTTCATTTT 420
L L L K Y R A R E P V T K A E M L E S V
421 CTGCTCCTCAAGTATCGAGCCAGGGAGCCGGTCACAAAGGCAGAAATGCTGGAGAGTGTC 480
L R N C Q D F F P V I F S K A S E Y L Q
481 CTCAGAAATTGCCAGGACTTCTTTCCCGTGATCTTCAGCAAAGCCTCCGAGTACTTGCAG 540
L V F G I E V V E V V P I S H L Y I L V
541 CTGGTCTTTGGCATTGAGGTGGTGGAAGTGGTCCCCATCAGCCACTTGTACATCCTTGTC 600
T C L G L S Y D G L L G D N Q V M P K T
601 ACCTGCCTGGGCCTCTCCTACGATGGCCTGCTGGGCGACAATCAGGTCATGCCCAAGACA 660
G L L I I V L A I I A I E G D C A P E E
661 GGCCTCCTGATAATCGTCCTGGCCATAATCGCAATAGAGGGCGACTGTGCCCCTGAGGAG 720
K I W E E L S M L E V F E G R E D S V F
721 AAAATCTGGGAGGAGCTGAGTATGTTGGAGGTGTTTGAGGGGAGGGAGGACAGTGTCTTC 780
A H P R K L L T Q D L V Q E N Y L E Y R
781 GCACATCCCAGGAAGCTGCTCACCCAAGATTTGGTGCAGGAAAACTACCTGGAGTACCGG 840
Q V P G S D P A C Y E F L W G P S I I N
841 CAGGTGCCCGGCAGTGATCCTGCATGCTACGAGTTCCTGTGGGGTCCATCAATCATTAAC 900
F E K L R A L I E T S Y V K V L H H T L
901 TTCGAGAAACTCAGGGCCCTCATTGAAACCAGCTATGTGAAAGTCCTGCACCATACACTA 960
K I G G E P H I S Y P P L H E R A L R E
961 AAGATCGGTGGAGAACCTCACATTTCCTACCCACCCCTGCATGAACGGGCTTTGAGAGAG 1020
G E E G S S G G G S S G G S S S P P C K
1021 GGAGAAGAGGGTAGCAGTGGTGGAGGCAGTAGCGGAGGGAGTAGCAGTCCTCCATGCAAA 1080
C P A P N L L G G P S V F I F P P K I K
1081 TGCCCAGCACCTAACCTCTTGGGTGGACCATCCGTCTTCATCTTCCCTCCAAAGATCAAG 1140
D V L M I S L S P I V T C V V V D V S E
1141 GATGTACTCATGATCTCCCTGAGCCCCATAGTCACATGTGTGGTGGTGGATGTGAGCGAG 1200
D D P D V Q I S W F V N N V E V H T A Q
1201 GATGACCCAGATGTCCAGATCAGCTGGTTTGTGAACAACGTGGAAGTACACACAGCTCAG 1260
T Q T H R E D Y N S T L R V V S A L P I
1261 ACACAAACCCATAGAGAGGATTACAACAGTACTCTCCGGGTGGTCAGTGCCCTCCCCATC 1320
Q H Q D W M S G K E F K C K V N N K D L
1321 CAGCACCAGGACTGGATGAGTGGCAAGGAGTTCAAATGCAAGGTCAACAACAAAGACCTC 1380
P A P I E R T I S K P K G S V R A P Q V
1381 CCAGCGCCCATCGAGAGAACCATCTCAAAACCCAAAGGGTCAGTAAGAGCTCCACAGGTA 1440

```
     Y  V  L  P  P  P  E  E  E  M  T  K  K  Q  V  T  L  T  C  M
1441 TATGTCTTGCCTCCACCAGAAGAAGAGATGACTAAGAAACAGGTCACTCTGACCTGCATG 1500

     V  T  D  F  M  P  E  D  I  Y  V  E  W  T  N  N  G  K  T  E
1501 GTCACAGACTTCATGCCTGAAGACATTTACGTGGAGTGGACCAACAACGGGAAAACAGAG 1560

     L  N  Y  K  N  T  E  P  V  L  D  S  D  G  S  Y  F  M  Y  S
1561 CTAAACTACAAGAACACTGAACCAGTCCTGGACTCTGATGGTTCTTACTTCATGTACAGC 1620

     K  L  R  V  E  K  K  N  W  V  E  R  N  S  Y  S  C  S  V  V
1621 AAGCTGAGAGTGGAAAAGAAGAACTGGGTGGAAAGAAATAGCTACTCCTGTTCAGTGGTC 1680

     H  E  G  L  H  N  H  H  T  T  K  S  F  S  R  T  P  G  K  *
1681 CACGAGGGTCTGCACAATCACCACACGACTAAGAGCTTCTCCCGGACTCCGGGTAAATGA 1740
```

Figure 7.5: The DNA sequence encoding SIIN-mMFc and corresponding translated protein sequences. Red, Kozak consensus sequence; Purple, protein sequence of immunoglobulin secretion signal peptide; Blue, protein sequence of full length human MAGE-A2 protein; Orange, SIINFEKL peptide; Yellow, protein sequence of the 13 amino acid peptide linker; Green, protein sequence of wt mIgG2a Fc region; *, stop codon.

amount of SIIN-mMFc obtained from a single 25ml transfection was around 80-120μg, which was very similar to the amount of protein obtained for both hMFc and mMFc in Chapter 6. This suggests that incorporation of the SIINFEKL sequence into MAGE-A2 protein did not have any significant impact on the production and expression of SIIN-mMFc in FreeStyle 293-F cells.

Purified SIIN-mMFc protein was subjected to SDS-PAGE, as described in Section 2.8.6. Figure 7.6A shows the results of Coomassie staining of purified SIIN-mMFc and mMFc proteins after SDS-PAGE under both non-reducing and reducing conditions, and Figure 7.6B shows the western blotting results obtained for purified SIIN-mMFc and mMFc proteins after probing with anti-mouse IgG heavy chain HRP or with the different monoclonal anti-human MAGE-A2 antibodies (6C1 or 1H4) followed by anti-mouse kappa-HRP antibody. The SIINFEKL sequence was not added at the N- nor C- termini of mMFc but incorporated within the mMFc protein sequence. The success in producing and purifying SIIN-mMFc indicates that incorporation of SIINFEKL sequence into mMFc did not affect the expression of the

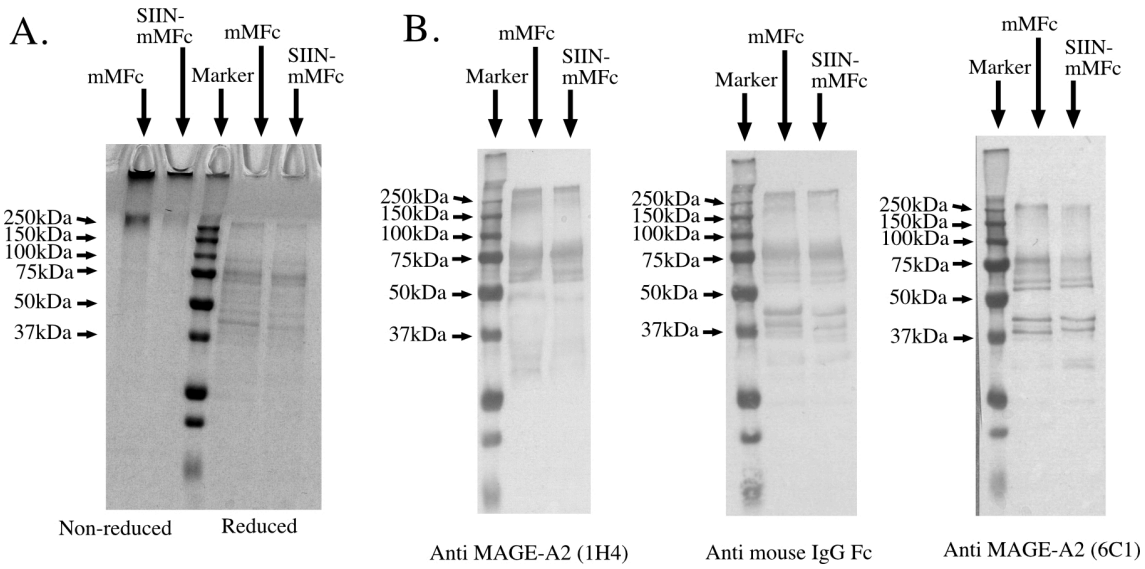

Figure 7.6: Coomassie staining and western blot of purified SIIN-mMFc (human MAGE-A2 with SIINFEKL incorporation fused with murine IgG2a Fc region) and mMFc (human MAGE-A2 fused with murine IgG2a Fc region) after SDS-PAGE and western blotting. **A)** Coomassie staining of purified SIIN-mMFc and mMFc under both non-reducing and reducing conditions. Molecular weight markers were run in the middle lane. **B)** Western blotting of purified SIIN-mMFc and mMFc under reducing conditions. Molecular weight markers were run in the left hand lane in all cases. Blot on left was probed with anti MAGE-A2 (1H4) detecting antibody. Blot in middle was probed with anti-mouse IgG heavy chain detecting antibody. Blot on right was probed with anti MAGE-A2 (6C1) detecting antibody.

protein. It was noticed that after both Coomassie staining and western blotting investigations, similar protein bands for both SIIN-mMFc and mMFc were obtained, as shown in Figure 7.6. Thus, it suggests that both SIIN-mMFc and mMFc were suffering from similar protein aggregations and that the incorporation of SIINFEKL peptide probably did not have any major effect on the overall protein conformational structure.

7.4.3 Antigen presentation assay

Both mMFc and SIIN-mMFc in both soluble and IC forms were used to carry out antigen presentation assays. mMFc was used as negative control as mMFc did not contain the SIINFEKL peptide necessary to activate B3Z T cells when presented on MHC-Class I. On the other hand, soluble OVA, OVA IC and SIINFEKL peptide

were used as positive controls. The results of antigen presentation assays using BMDC are shown in Figure 7.7 and using SDC in Figure 7.8. Under the conditions of the assay, it was found that incubation of SIIN-mMFc at 5μg/ml for 4 hours with either BMDC and SDC did not activate B3Z T cells. In addition, incubation of 5mg/ml soluble OVA or 5μg/ml OVA IC with either BMDC and SDC were also found unable to activate B3Z T cells.

Three major factors might be considered as contributing to the disappointing failure of B3Z T cell activation by all antigens other than SIINFEKL peptide. The first factor which may account for this failure is improper antigen digestion. However, this factor does not seem to be true because the antigens used as positive controls in this assay, OVA and OVA IC, were also found to be unable to activate B3Z T cells. OVA was the original antigen used to generate B3Z T cells, and therefore, it was expected that OVA would efficiently activate B3Z T cells when incubated with DC. As a result, the failure of OVA and OVA IC to activate B3Z T cells suggests that antigen digestion was not responsible for the failure of B3Z T cell activation. The second factor was reasoned to be due to the malfunction of B3Z T cells to produce β-galactosidase enzyme upon recognition of SIINFEKL peptide presented on MHC Class I molecule. However, this possibility could be excluded because incubation of 0.175-1μM of SIINFEKL peptide with both BMDC and SDC was found to efficiently activate B3Z T cells. With such findings, it was concluded that the B3Z T cell was not responsible for the failure of OVA and SIIN-mMFc in the antigen presentation assay. The third factor, which was reasoned to be the malfunction of the dendritic cells in antigen cross presentation, was therefore considered to be the most likely reason for the unsuccessful activation of B3Z T cells by both SIIN-mMFc and

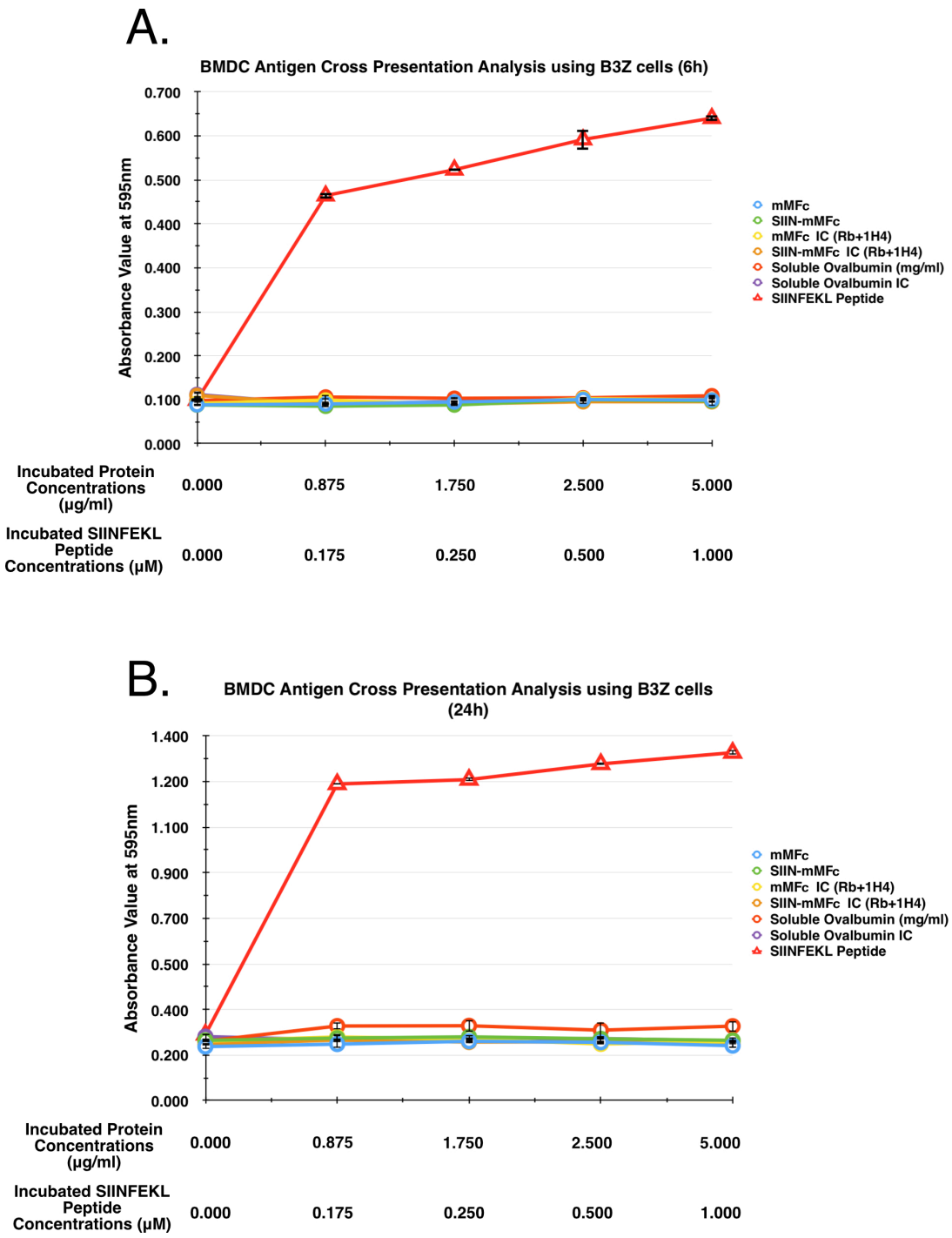

Figure 7.7: β-galactosidase enzyme activity of B3Z T cells following MAGE-A2 Fc fusion protein antigen cross presentation by BMDC. BMDC were incubated with SIIN-mMFc, mMFc or chicken ovalbumin in either soluble or immune complex form for 4 hours before incubation with B3Z T cells. β-galactosidase enzyme activity was assayed 6 hours (**A**) and 24 hours (**B**) after the introduction of B3Z T cells. 1µM SIINFEKL peptide was used as positive control. The results shown are the average of two determinations, and the bars represent standard error. A representative experiment of three is shown.

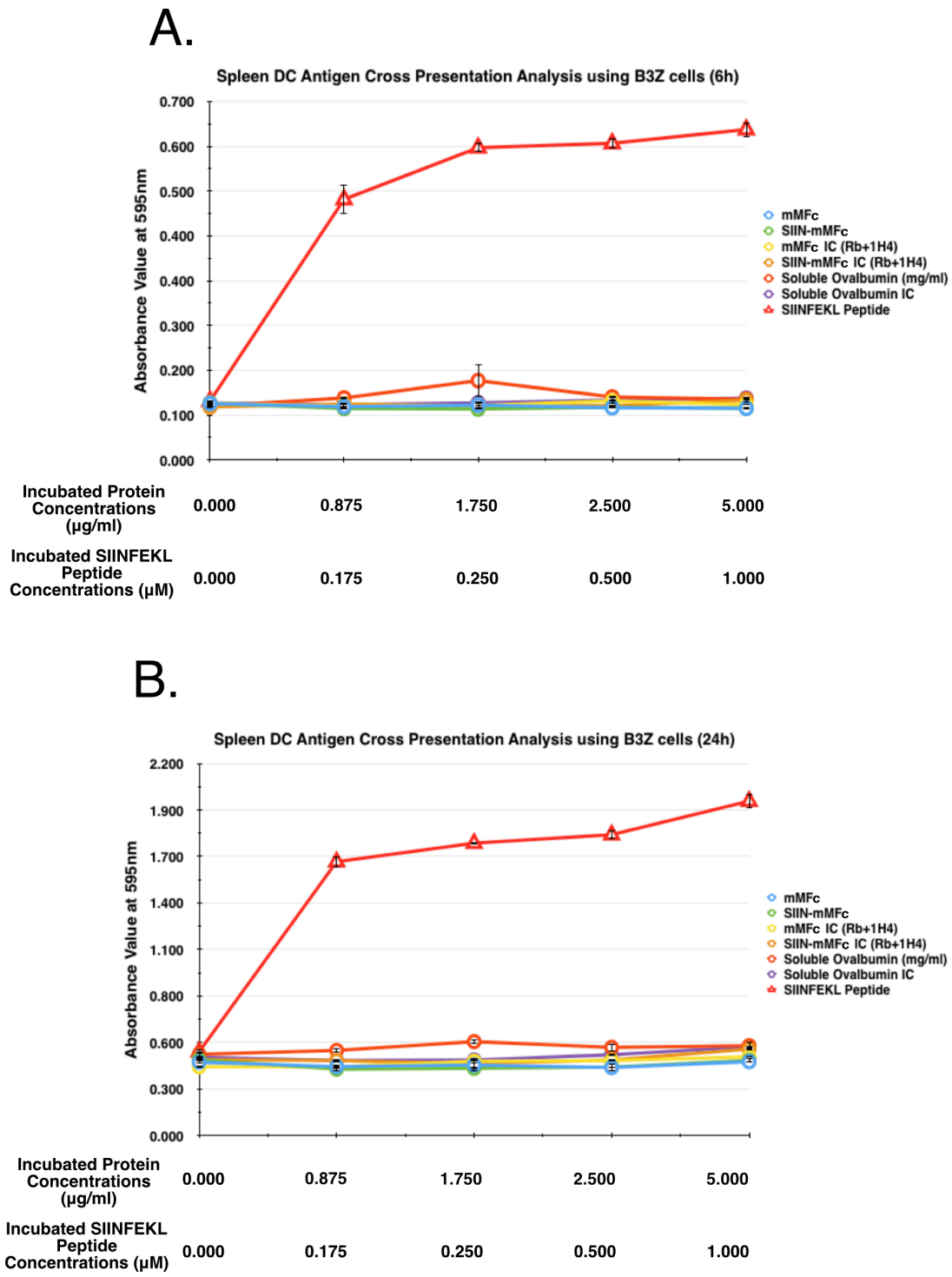

Figure 7.8: β-galactosidase enzyme activity of B3Z T cells following MAGE-A2 Fc fusion protein antigen cross presentation by SDC. SDC were incubated with SIIN-mMFc, mMFc or chicken ovalbumin in either soluble or immune complex form for 4 hours before incubation with B3Z T cells. β-galactosidase enzyme activity was assayed 6 hours (**A**) or 24 hours (**B**) after the introduction of B3Z T cells. 1µM SIINFEKL peptide was used as positive control. The results shown are the average of two determinations, and the bars represent standard error. A representative experiment of three is shown.

OVA antigens.

7.4.4 Investigation on the expression level of different Fc receptors in DC

Due to the reasoning that the unsuccessful activation of B3Z T cells in antigen cross presentation assay might be due to the malfunction of dendritic cells, an investigation into the expression level of Fcγ receptors and FcRn was carried out. Fcγ receptors are required for the internalisation of antigen IC via receptor mediated phagocytosis. Thus, the expression of Fcγ receptors on the surface of dendritic cells is crucial for efficient and successful cross presentation of antigen IC. The results of assays to determine the expression levels of FcγRI and FcγRII via flow cytometry are shown in Figure 7.9. Both BMDC and SDC exhibited strong expression of both FcγRI and FcγRII as indicated by the fluorescent intensity shift in the flow cytometry analysis graph in Figure 7.9. With such findings, it is believed that both SIIN-mMFc IC and OVA IC should not have any problems in triggering antigen phagocytosis via association with both FcγRI and FcγRII on the surface of dendritic cells. On the other hand, FcRn is required for the effective induction of antigen cross presentation of antigen IC. Therefore, the expression level of FcRn is also very important for efficient antigen cross presentation. The expression level of FcRn on both BMDC and SDC was determined via western blotting is shown in Figure 7.10. B3Z T cells were used as a negative control, whereas BMDM and whole liver cell lysate were used as positive controls for FcRn expression. The molecular weight of mouse FcRn was previously reported to be 55kDa (Neuber *et al*., 2014). As a result, the strong visible protein band detected in the lane loaded with liver lysate at around 50kDa, shown in Figure 7.10, is expected to be mouse FcRn. Interestingly, it was found that both SDC and BMDC had a very low FcRn expression level compared to BMDM.

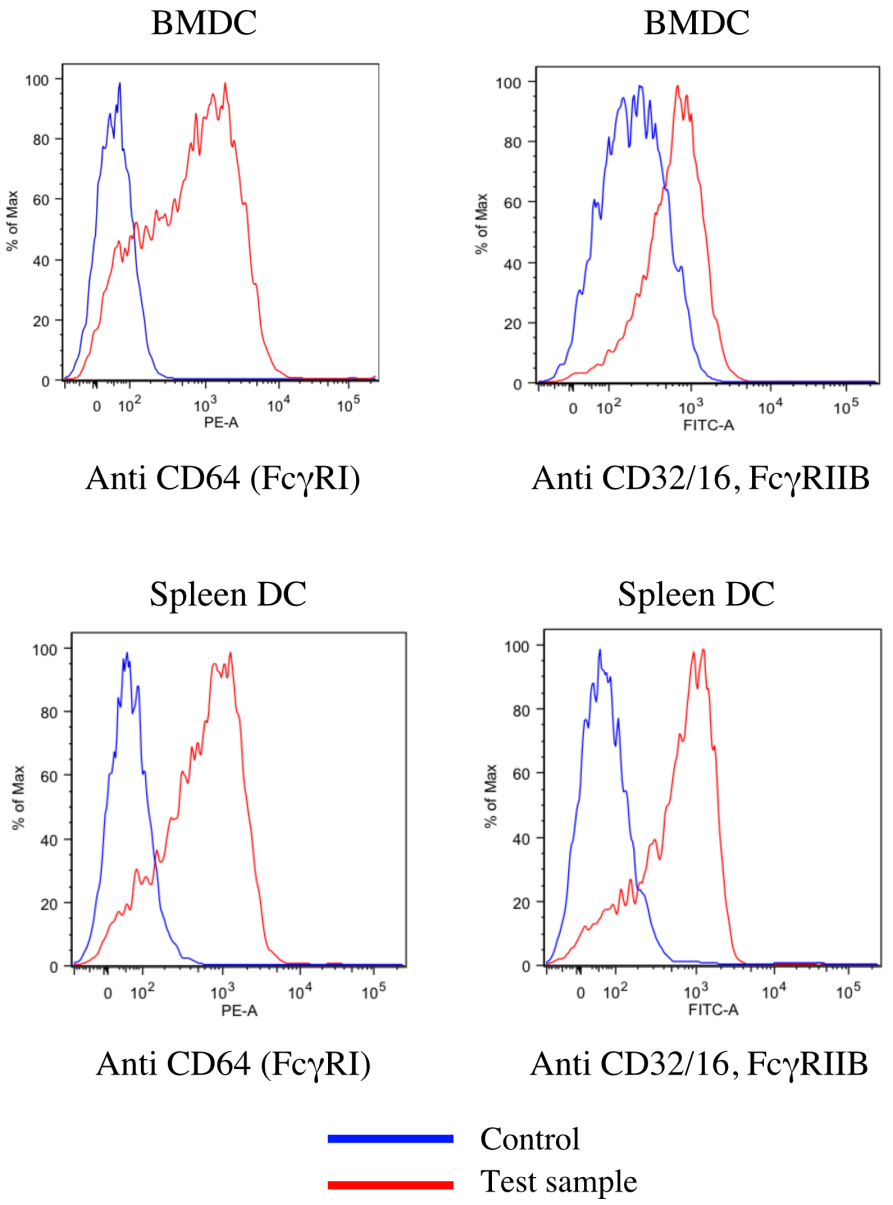

Figure 7.9: Flow cytometry analyses of the expression level of different Fcγ receptors on the surface of bone-marrow derived dendritic cells (BMDC) and spleen derived dendritic cells (Spleen DC). Cells were probed using anti-mouse CD64 antibody or anti-CD32/16, FcγRIIB antibody. Cells incubated with buffer alone were used as control. A representative experiment of three is shown.

The expression level of FcRn in BMDC appeared especially low, with the FcRn protein band being hardly noticeable. This finding suggests that the low expression level of FcRn in both SDC and BMDC might be the factor leading to non-activation of B3Z T cells because there were probably insufficient of FcRn available to bind

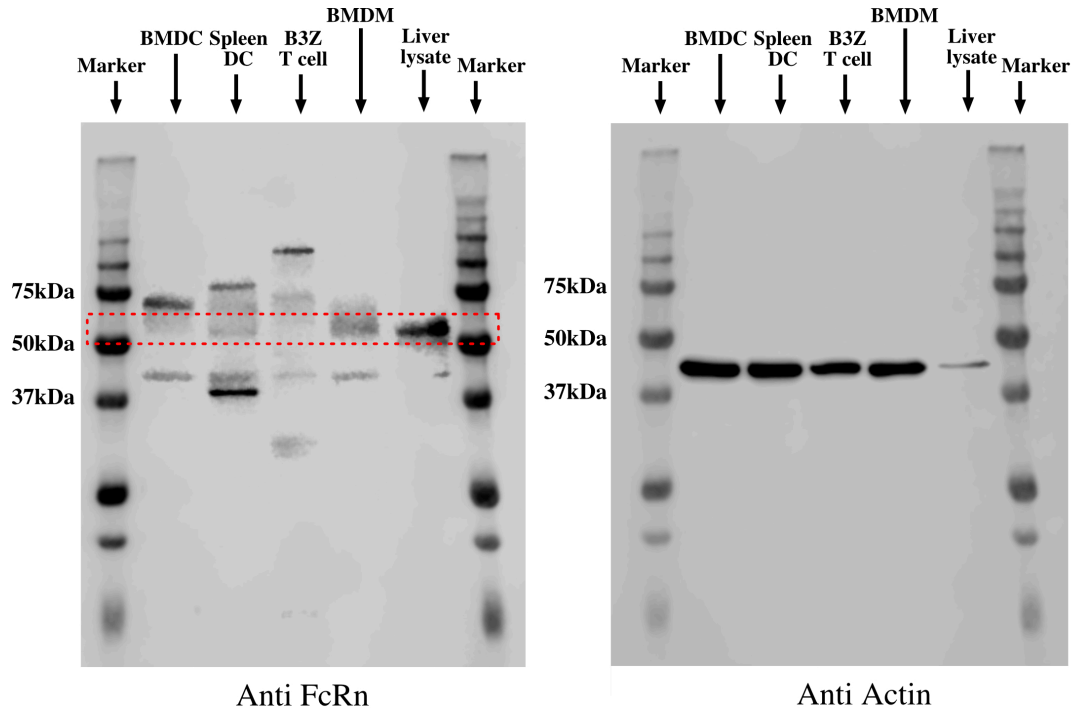

Figure 7.10: Western blotting for the detection of FcRn expression. DC were lysed with RIPA buffer and sonicated. The position of FcRn protein band is expected to lie in the region bounded by the red dotted line. Marker, protein molecular weight markers. From left to right the cells shown were: BMDC (bone marrow derived dendritic cells), Spleen DC (spleen derived dendritic cell), B3Z T cells (cytotoxic T cell), BMDM (bone marrow derived macrophage), Liver lysate (whole liver cell lysate). B3Z T cells were used as a negative control and BMDM and liver cell lysate were used as positive controls for FcRn expression. Expression of actin was detected as a loading control.

to antigen IC in order to induce an efficient antigen cross presentation. However, it must not be neglected that the soluble OVA antigen was not able to induce an activation in B3Z T cells either. The concentration of soluble OVA, 5mg/ml, used to incubate with dendritic cells was 10-fold higher than the OVA IC form and at such high concentration soluble OVA does not require the formation of antigen IC to induce antigen cross presentation. As a result, the failure of soluble OVA to activate B3Z T cells suggests that the low expression level of FcRn might not be the sole factor in causing the unsuccessful attempt at antigen cross presentation assay.

7.0 DISCUSSION

In this chapter, an antigen presentation assay was carried out to determine if MFc

protein would be taken up by dendritic cells via phagocytosis and cross presented on MHC Class I molecule after protein digestion to activate corresponding cytotoxic T cells. The antigen presentation assay using SIIN-mMFc was unable to activate the corresponding cytotoxic B3Z T cell. The result from western blotting suggests that both BMDC and SDC have low expression levels of FcRn and this might be one of the possible factors contributing to the unsuccessful antigen cross presentation. As mentioned in Chapter 6, the association of FcRn is important for the induction of antigen cross presentation. In experiments conducted by others, FcRn-expressing DC were able to activate cytotoxic T cells when a 100-fold lower antigen concentration was used when compared to DC that did not express FcRn (Baker *et al*., 2011). The authors also showed that the association of FcRn with IgG retained that IgG IC within an intracellular compartment whereas IHH-IgG IC were not retained (Baker *et al*., 2011). In addition, Baker and colleagues utilised an induced colorectal cancer system and showed that the adoptive transfer of wildtype DC to $Fcgrt^{-/-}$ mice greatly improved the activation of cytotoxic T cells and improved the protective immunity in such mice (Baker *et al*., 2013). As a result, the low expression level of FcRn detected in both BMDC and SDC described here might have cause a reduced association of antigen IC with FcRn. If the association with FcRn is required to achieve a certain signaling threshold to retain antigen IC in an intracellular compartment for antigen cross presentation induction, the low expression level of FcRn might abolish such signaling activity, thereby leading to inefficient antigen cross presentation. Having said that, the actual binding capability of SIIN-mMFc to FcRn has not been confirmed in this chapter. It was expected that SIIN-mMFc would be able to bind to FcRn due to the successful purification of SIIN-mMFc using Protein G-Sepharose. Both protein G and FcRn binds to a similar but distinct region at the CH2-CH3

interface of IgG Fc region. The binding of SIIN-mMFc to Protein G-Sepharose indicated that the CH2-CH3 domain of the IgG Fc region is most likely in an intact conformational structure, suggesting it should not have any problem in binding to FcRn. Nonetheless, due to the FcRn binding site being different from that for Protein G, it would be important to investigate whether SIIN-mMFC can actually associate with FcRn in a future investigation. SPR analysis would be a good choice for determining the binding activity of MFc to different Fc receptors such as Fcγ receptors and FcRn and would allow comparison to the binding of wild type IgG. Such an approach would allow investigation of whether there is any significant difference between the two.

Another point to consider is that proteolysis of endogenous proteins usually involves the ubiquitination system and the digested peptides are presented on MHC Class I molecules. Hence, in future experiments SIIN-mMFc could be transfected into MHC Class I H-2K^{b} expressing cells (cells from mouse strain C57BL/6 are suitable), and the ability of such transfected cells to activate B3Z T cells could be investigated. This experiment would confirm whether SIIN-mMFc can be properly digested to produce SIINFEKL peptide during the antigen cross presentation mechanism.

The rationale behind the use of MFc protein in this project was to utilise the IgG Fc region to achieve long plasma half life via association with FcRn in order to stimulate production of anti-MAGE-A2 host antibodies and induce efficient formation of MFc IC, which in turn might promote induction of antigen cross presentation through FcRn engagement. Although the association of IgG IC with FcRn was shown to play a crucial role in antigen cross presentation in previous studies (Baker *et al*., 2011; Baker *et al*., 2013), there are other ways of achieving

antigen cross presentation other than the formation of IgG IC. Lasarte and colleagues fused the extra domain A (EDA) from fibronectin with SIINFEKL peptide or OVA protein. Upon incubation of these fusion proteins with BMDC, the authors showed that the SIINFEKL peptide from both proteins was presented on the MHC Class I molecule and activated B3Z T cells (Lasarte *et al*., 2007). EDA is an endogenous ligand for Toll-like Receptor 4 (TLR4) which is expressed on the surface of DC (Lasarte *et al*., 2007). The authors reported that the binding of the fusion proteins to TLR4 facilitated entry of the fusion protein into the MHC Class I cytosolic pathway, which resulted in antigen cross presentation, and such activity was blocked when a monoclonal antibody against TLR4 was used (Lasarte *et al*., 2007). Based on this approach, MAGE-A2 might be fused with EDA as an alternative option to achieve a similar cancer vaccine effect. However, due to the absence of IgG Fc region, MAGE-A2-EDA might be compromised in terms of a low plasma half-life.

In a different scenario, Fayolle and colleagues fused a known MHC Class I viral peptide originating from lymphocytic choriomeningitis virus (LCMV) to the catalytic domain of adenylate cyclase toxin (CyaA) of *B. pertussis* and immunised mice with the resultant toxin (Fayolle *et al*., 1996). The authors showed that cytotoxic T cells isolated from immunised mice were able to lyse cells that were coated with immunised viral peptide (Fayolle *et al*., 1996). It is believed that the toxin penetrated the membrane of cells and delivered the LCMV peptide into the cytosolic compartment before being subjected to MHC Class I cytosolic pathway (Fayolle *et al*., 1996). The findings from the studies suggested another alternative option in promoting antigen cross presentation activity in which MAGE-A2 protein could be utilised. However, there are several limitations regarding the approach of

using CyaA as the carrier protein. First, it might not be feasible to fuse full length MAGE-A2 protein to CyaA since it might disturb the invasive activity of CyaA. As a result, the restricted MHC Class I peptide of MAGE-A2 would first need to be identified and fused with CyaA. This approach will restrict the corresponding cytotoxic T cell recognition to the fused peptide after immunisation which limits the activation of different cytotoxic T cell clones. On the other hand, use of MAGE-A2 Fc fusion protein should allow digestion of the full length MAGE-A2 protein, thus, generating different peptides that might associate with MHC Class I leading to a higher possibility of activating multiple cytotoxic T cell clones and inducing a stronger immune response. The second limitation is the identity of the CyaA target. It was reported that CyaA is capable of penetrating directly into different types of cells through the plasma membrane and does not require any specific receptors for its invasive activity (Fayolle *et al*., 1996). The activation of cytotoxic T cells requires the specific stimulation from antigen presenting cells such as macrophages and dendritic cells. It is expected that specific targeting of DC by CyaA would be problematic unless DC were isolated from the patient and reintroduced back to the patient after treatment with the toxin.

In summary, efforts to demonstrate presentation of peptides derived from MFc-based antigens were unsuccessful. However, the SIIN-mMFc does not seem to be responsible for the failure because the positive controls were unsuccessful also. Further investigations are required to identify the problem and to confirm that MFc protein can undergo the antigen cross presentation mechanism. Nonetheless, some of the alternative options which might induce antigen cross presentation of MAGE-A2 have also been discussed.

CHAPTER EIGHT
CONCLUDING REMARKS

CHAPTER 8: CONCLUDING REMARKS

The work detailed in this thesis took advantage of protein engineering techniques and recombinant antibody technology to generate novel IgG hinge mutants and potential cancer vaccines in the format of Fc-fusion proteins, to further extend the understanding of antibody biology and function.

Many recent antibody studies have been focusing on identifying new potential targets and improving the binding affinity to Fc receptors as a mean to diversify different antigen targets as well as improving effector function. However, there are still many areas concerning the antibody molecule itself that are worthy of investigation. The hinge region has long been believed to provide flexibility to the antibody. In this study, it has been demonstrated that the upper hinge length of IgG may have the capacity to modulate the bivalent binding activity of IgG to enhance overall avidity. In addition, the importance of the presence of glycans at the hinge region was also highlighted by the reduced rosette formation noted for different IgG hinge mutants. Although some of modifications may not contribute to a significant enhancement in antibody functionality, a combination of several modifications may, in fact, help to significantly improve antibody functionality. As a result, all antibody engineering techniques which could improve antigen binding or effector function are highly valuable and any future investigations aimed at improving the understanding of antibody biology are highly encouraged. A better performing antibody would reduce the overall required dosage in therapeutic applications, which, in return, would reduce the overall cost of the drug.

This study has used a novel approach to calculate the bivalent antigenic distance of an antibody. The combination of surface plasmon resonance and the molecular ruler, NIP-dsDNA, has proven useful in investigation of the molecular distance involved. The NIP-dsDNA measuring model is expected to be much more accurate when compared to conventional approaches, such as protein crystallography, X-ray or neutron scattering techniques, because the length of dsDNA can be easily calculated, and, more importantly, the measurement is the actual functional antigen binding distance of the antibody. In addition, DNA production and DNA conjugation is relatively cost-effective and easy. As a result, this measuring model will be useful for other proteins if the related protein-protein binding distance is of interest.

Finally, this study has attempted to generate a potential cancer vaccine by fusing human MAGE-A2 to IgG Fc. Unfortunately, a strong protein aggregation was encountered and the generated Fc-fusion protein was unable to stimulate a corresponding cytotoxic T cell response. The outcome of protein aggregation highlighted the importance of fully understanding protein characteristics. MAGE-A2 is not very well studied and information regarding the protein is rather scarce. As a result, it is difficult to pinpoint the exact reason for protein aggregation. More importantly, the crystal structure of MAGE-A2 is not available. Thus, it is hard to predict the events that might happen after fusion to IgG Fc. In the event of the continuation of MAGE-A2-Fc protein production, studies on the characteristics of MAGE-A2 or, at the very least, the structural conformation of MAGE-A2 ought to be carried out. Although the generated Fc-fusion protein was unable to activate cytotoxic T cells during the antigen cross presentation assay, it was shown that the failure is expected to be due to the incompetence of the dendritic cells. As a result,

the hope that MAGE-A2 Fc-fusion protein could be a potential cancer vaccine should not be abandoned. More investigations are required to further confirm the significance of MAGE-A2 Fc-fusion as a cancer vaccine.

8.1 Future perspectives

The understanding and rewards concerning the IgG hinge mutants, dsDNA measuring model and MAGE-A2-Fc fusion protein have not been fully discovered and are worth continuing. Some of the future directions which could be taken for each of the study compoents are described below.

1. Unfortunately, an ADCC assay was not performed using the IgG hinge mutants. It would be valuable to determine if the extension in hinge length or the presence of glycans at the hinge region have any effect on ADCC activity. With regard to antibody effector function, efficiency in complement fixation is also worth investigating as CDC is one of the main immune defensive mechanisms.

2. Now that the dsDNA measuring model is established, it would be worthwhile to determine the bivalent antigenic distance of each of the naturally occurring antibody classes and subclasses.

3. With regard to the MAGE-A2-Fc fusion proteins, some of the possible experiments have been previously discussed in Chapters 6 and 7. For example, fusion of just the MAGE MHD domain, rather than full length MAGE-A2, to IgG Fc might be attempted in order to tackle the problem of

protein aggregation. SIINFEKL incorporated MAGE-A2 Fc fusion protein could be expressed intracellularly to determine if the fusion protein might be properly digested to yield the correct sequence of SIINFEKL peptide.

Antibodies are some of the most fascinating protein molecules due to their high specificity in antigen targeting and low immunogenicity in inducing an unwanted immune response. More importantly, the antibody format has been diversified immensely and different functionalities have been achieved to provide better therapeutic purposes. Antibody therapy is likely to remain an active and exciting area for research for a very long time.

REFERENCES

REFERENCES

ADAMCZYK, M., MOORE, J. A. & YU, Z. 2000. Application of surface plasmon resonance toward studies of low-molecular-weight antigen–antibody binding interactions. *Methods,* **20,** 319-328.

AMIGORENA, S. & SAVINA, A. 2010. Intracellular mechanisms of antigen cross presentation in dendritic cells. *Curr. Opin. Immunol.,* **22,** 109-117.

ANTHONY, R. M., WERMELING, F. & RAVETCH, J. V. 2012. Novel roles for the IgG Fc glycan. *Ann. N.Y. Acad. Sci.,* **1253,** 170-180.

ARNOLD, J. N., WORMALD, M. R., SIM, R. B., RUDD, P. M. & DWEK, R. A. 2007. The impact of glycosylation on the biological function and structure of human immunoglobulins. *Annu. Rev. Immunol.,* **25,** 21-50.

BACKLIWAL, G., HILDINGER, M., CHENUET, S., WULHFARD, S., DE JESUS, M. & WURM, F. M. 2008. Rational vector design and multi-pathway modulation of HEK 293E cells yield recombinant antibody titers exceeding 1 g/l by transient transfection under serum-free conditions. *Nucl. Acids Res.,* **36,** e96-e96.

BAENZIGER, J. & KORNFELD, S. 1974. Structure of the carbohydrate units of IgA1 immunoglobulin: II. Structure of the O-glycosidically linked oligosaccharide units. *J. Bio. Chem.,* **249,** 7270-7281.

BAICI, A., KNÖPFEL, M. & FEHR, K. 1982. Cleavage of the four human IgG subclasses with Cathepsin G. *Scand. J. Immunol.,* **16,** 487-498.

BAKER, K., QIAO, S. W., KUO, T. T., AVESON, V. G., PLATZER, B., ANDERSEN, J. T., SANDLIE, I., CHEN, Z., DE HAAR, C., LENCER, W. I., FIEBIGER, E. & BLUMBERG, R. S. 2011. Neonatal Fc receptor for IgG (FcRn) regulates cross-presentation of IgG immune complexes by CD8−CD11b+ dendritic cells. *Proc. Natl Acad. Sci. USA,* **108,** 9927-9932.

BAKER, K., RATH, T., FLAK, M. B., ARTHUR, J. C., CHEN, Z., GLICKMAN, J. N., ZLOBEC, I., KARAMITOPOULOU, E., STACHLER, M. D., ODZE, R. D., LENCER, W. I., JOBIN, C. & BLUMBERG, R. S. 2013. Neonatal Fc receptor expression in dendritic cells mediates protective immunity against colorectal cancer. *Immunity,* **39,** 1095-1107.

BAKER, K., RATH, T., PYZIK, M. & BLUMBERG, R. S. 2014. The role of FcRn in antigen presentation. *Front. Immunol.,* **5,** 408.

BEHR, T. M., BLUMENTHAL, R. D., MEMTSOUDIS, S., SHARKEY, R. M., GRATZ, S., BECKER, W. & GOLDENBERG, D. M. 2000. Cure of metastatic human colonic cancer in mice with radiolabeled monoclonal antibody fragments. *Clin. Cancer Res.,* **6,** 4900-4907.

BINDON, C. I., HALE, G., BRÜGGEMANN, M. & WALDMANN, H. 1988. Human monoclonal IgG isotypes differ in complement activating function at the level of C4 as well as C1q. *J. Exp. Med.,* **168,** 127-142.

BOEHM, M. K., WOOF, J. M., KERR, M. A. & PERKINS, S. J. 1999. The Fab and Fc fragments of IgA1 exhibit a different arrangement from that in IgG: a study by X-ray and neutron solution scattering and homology modelling. *J. Mol. Biol.,* **286,** 1421-1447.

BONNER, A., FURTADO, P. B., ALMOGREN, A., KERR, M. A. & PERKINS, S. J. 2008. Implications of the near-planar solution structure of human myeloma dimeric IgA1 for mucosal immunity and IgA1 nephropathy. *J. Immunol.,* **180,** 1008-1018.

BOROSS, P., VAN DE POEL, K., VAN DE WINKEL, J. G. J. & LEUSEN, J. H. W. 2008. Fc Receptors. *In: eLS*. John Wiley & Sons, Ltd. DOI: 10.1002/9780470015902.a0000916.pub2

BRAUNSCHWEIG, A. B., HUO, F. & MIRKIN, C. A. 2009. Molecular printing. *Nat. Chem.,* **1,** 353-358.

BREKKE, O. H. & SANDLIE, I. 2003. Therapeutic antibodies for human diseases at the dawn of the twenty-first century. *Nat. Rev. Drug. Discov.,* **2,** 52-62.

BREZSKI, R. J. & JORDAN, R. E. 2010. Cleavage of IgGs by proteases associated with invasive diseases: An evasion tactic against host immunity? *mAbs,* **2,** 212-220.

BRUHNS, P., IANNASCOLI, B., ENGLAND, P., MANCARDI, D. A., FERNANDEZ, N., JORIEUX, S. & DAËRON, M. 2009. Specificity and affinity of human Fcγ receptors and their polymorphic variants for human IgG subclasses. *Blood,* **113,** 3716-3725.

BUCHMAN, A. R. & BERG, P. 1988. Comparison of intron-dependent and intron-independent gene expression. *Mol. Cell. Biol.,* **8,** 4395-4405.

BURMEISTER, W. P., HUBER, A. H. & BJORKMAN, P. J. 1994. Crystal structure of the complex of rat neonatal Fc receptor with Fc. *Nature,* **372,** 379-383.

BURTON, D. R. 1987. Structure and function of antibodies. *In: Molecular Genetics of Immunoglobulin*. CALABI, F. & NEUBERGER, M. S. eds. 1-50. Elsevier Amsterdam

BUTLER, M. & SPEARMAN, M. 2014. The choice of mammalian cell host and possibilities for glycosylation engineering. *Curr. Opin. Biotechnol.,* **30,** 107-112.

CARAYANNOPOULOS, L., HEXHAM, J. M. & CAPRA, J. D. 1996. Localization of the binding site for the monocyte immunoglobulin (Ig) A-Fc receptor (CD89) to the domain boundary between Cα2 and Cα3 in human IgA1. *J. Exp. Med. ,* **183,** 1579-1589.

CARTER, P., PRESTA, L., GORMAN, C. M., RIDGWAY, J. B., HENNER, D., WONG, W. L., ROWLAND, A. M., KOTTS, C., CARVER, M. E. & SHEPARD, H. M. 1992. Humanization of an anti-p185HER2 antibody for human cancer therapy. *Proc. Natl Acad. Sci. USA,* **89,** 4285-4289.

CHAMES, P., VAN REGENMORTEL, M., WEISS, E. & BATY, D. 2009. Therapeutic antibodies: successes, limitations and hopes for the future. *Br. J. Pharmacol,* **157,** 220-233.

CHINTALACHARUVU, K. R., CHUANG, P. D., DRAGOMAN, A., FERNANDEZ, C. Z., QIU, J., PLAUT, A. G., TRINH, K. R., GALA, F. A. & MORRISON, S. L. 2003. Cleavage of the human immunoglobulin A1 (IgA1) hinge region by IgA1 proteases requires structures in the Fc region of IgA. *Infect. Immun.,* **71,** 2563-2570.

CHINTALACHARUVU, K. R. & MORRISON, S. L. 1996. Residues critical for H-L disulfide bond formation in human IgA1 and IgA2. *J. Immunol.,* **157,** 3443-3449.

CHINTALACHARUVU, K. R., YU, L. J., BHOLA, N., KOBAYASHI, K., FERNANDEZ, C. Z. & MORRISON, S. L. 2002. Cysteine residues required for the attachment of the light chain in human IgA2. *J. Immunol.,* **169,** 5072-5077.

CLANCY, S. 2008. RNA splicing: Introns, exons and spliceosome. *Nature Education,* **1**:31.

CLINCKE, M.-F., GUEDON, E., YEN, F. T., OGIER, V. & GOERGEN, J.-L. 2011. Characterization of metalloprotease and serine protease activities in batch CHO cell cultures: control of human recombinant IFN-γ proteolysis by addition of iron citrate. *BMC Proc.,* **5,** p115.

COOLEY, C. B., RYNO, L. M., PLATE, L., MORGAN, G. J., HULLEMAN, J. D., KELLY, J. W. & WISEMAN, R. L. 2014. Unfolded protein response activation reduces secretion and extracellular aggregation of amyloidogenic immunoglobulin light chain. *Proc. Natl Acad. Sci. USA,* **111,** 13046-13051.

CZAJKOWSKY, D. M., HU, J., SHAO, Z. & PLEASS, R. J. 2012. Fc-fusion proteins: new developments and future perspectives. *EMBO Mol. Med.,* **4,** 1015-1028.

DAËRON, M. 1997. Fc receptor biology. *Annu. Rev. Immunol. ,* **15,** 203-234.

DAVIES, D. R., PADLAN, E. A. & SEGAL, D. M. 1975. Three-Dimensional Structure of Immunoglobulins. *Annu. Rev. Biochem.,* **44,** 639-667.

DEKKERS, G., PLOMP, R., KOELEMAN, C. A. M., VISSER, R., VON HORSTEN, H. H., SANDIG, V., RISPENS, T., WUHRER, M. & VIDARSSON, G. 2016. Multi-level glyco-engineering techniques to generate IgG with defined Fc-glycans. *Sci. Rep.,* **6,** 36964.

DEL POZO-YAUNER, L., BECERRIL, B., OCHOA-LEYVA, A., RODRÍGUEZ-AMBRIZ, S. L., CARRIÓN, J. I. P., ZAVALA-PADILLA, G., SÁNCHEZ-LÓPEZ, R. & VELASCO, D. A. F. 2015. The structural determinants of the immunoglobulin light chain amyloid aggregation. *In: Physical Biology of Proteins and Peptides: Theory, Experiment, and Simulation*. OLIVARES-

QUIROZ, L., GUZMÁN-LÓPEZ, O. & JARDÓN-VALADEZ, H. E. eds. 1-28. Springer International Publishing Cham

DELAMARRE, L., PACK, M., CHANG, H., MELLMAN, I. & TROMBETTA, E. S. 2005. Differential lysosomal proteolysis in antigen-presenting cells determines antigen fate. *Science,* **307,** 1630-1634.

DEMPSEY, P. W., VAIDYA, S. A. & CHENG, G. 2003. The art of war: Innate and adaptive immune responses. *Cell Mol. Life Sci.,* **60,** 2604-2621.

DENG, G., ZHENG, X., ZHOU, J., WEI, H., TIAN, Z. & SUN, R. 2015. Generation and preclinical characterization of an NKp80-Fc Fusion protein for redirected cytolysis of natural killer (NK) cells against leukemia. *J. Biol. Chem.,* **290,** 22474-22484.

DESJARLAIS, J. R. & LAZAR, G. A. 2011. Modulation of antibody effector function. *Exp. Cell. Res.,* **317,** 1278-1285.

DICKINSON, B. L., BADIZADEGAN, K., WU, Z., AHOUSE, J. C., ZHU, X., SIMISTER, N. E., BLUMBERG, R. S. & LENCER, W. I. 1999. Bidirectional FcRn-dependent IgG transport in a polarized human intestinal epithelial cell line. *J. Clin. Invest.,* **104,** 903-911.

DIEBOLDER, C. A., BEURSKENS, F. J., DE JONG, R. N., KONING, R. I., STRUMANE, K., LINDORFER, M. A., VOORHORST, M., UGURLAR, D., ROSATI, S., HECK, A. J. R., VAN DE WINKEL, J. G. J., WILSON, I. A., KOSTER, A. J., TAYLOR, R. P., SAPHIRE, E. O., BURTON, D. R., SCHUURMAN, J., GROS, P. & PARREN, P. W. H. I. 2014. Complement is activated by IgG hexamers assembled at the cell surface. *Science,* **343,** 1260-1263.

DILILLO, D. J. & RAVETCH, J. V. 2015. Fc-receptor interactions regulate both cytotoxic and immunomodulatory therapeutic antibody effector functions. *Cancer Immunol. Res.,* **3,** 704-713.

DOSZTÁNYI, Z., CSIZMOK, V., TOMPA, P. & SIMON, I. 2005. IUPred: web server for the prediction of intrinsically unstructured regions of proteins based on estimated energy content. *Bioinformatics,* **21,** 3433-3434.

DRINKWATER, N., COSSINS, B. P., KEEBLE, A. H., WRIGHT, M., CAIN, K., HAILU, H., OXBROW, A., DELGADO, J., SHUTTLEWORTH, L. K., KAO, M. W. P., MCDONNELL, J. M., BEAVIL, A. J., HENRY, A. J. & SUTTON, B. J. 2014. Human immunoglobulin E flexes between acutely bent and extended conformations. *Nat. Struct. Mol. Biol.,* **21,** 397-404.

DUNCAN, A. R. & WINTER, G. 1988. The binding site for C1q on IgG. *Nature,* **332,** 738-740.

DUNCAN, A. R., WOOF, J. M., PARTRIDGE, L. J., BURTON, D. R. & WINTER, G. 1988. Localization of the binding site for the human high-affinity Fc receptor on IgG. *Nature,* **332,** 563-564.

EDELMAN, G. M., CUNNINGHAM, B. A., GALL, W. E., GOTTLIEB, P. D., RUTISHAUSER, U. & WAXDAL, M. J. 1969. The covalent structure of an entire γG immunoglobulin molecule. *Proc. Natl Acad. Sci. USA,* **63,** 78-85.

FALK, K., ROTZSCHKE, O., STEVANOVIE, S., JUNG, G. & RAMMENSEE, H.-G. 1991. Allele-specific motifs revealed by sequencing of self-peptides eluted from MHC molecules. *Nature,* **351,** 290-296.

FALKENBURG, W. J. J., VAN SCHAARDENBURG, D., OOIJEVAAR-DE HEER, P., TSANG-A-SJOE, M. W. P., BULTINK, I. E. M., VOSKUYL, A. E., BENTLAGE, A. E. H., VIDARSSON, G., WOLBINK, G. & RISPENS, T. 2016. Anti-hinge antibodies recognize IgG subclass– and protease-restricted neoepitopes. *J. Immunol.,* **198,** 82-93.

FALKENBURG, W. J. J., VAN SCHAARDENBURG, D., OOIJEVAAR-DE HEER, P., TSANG-A-SJOE, M. W. P., BULTINK, I. E. M., VOSKUYL, A. E., BENTLAGE, A. E. H., VIDARSSON, G., WOLBINK, G. & RISPENS, T. 2017. Anti-hinge antibodies recognize IgG subclass– and protease-restricted neoepitopes. *J. Immunol.,* **198,** 82-93.

FAYOLLE, C., SEBO, P., LADANT, D., ULLMANN, A. & LECLERC, C. 1996. In vivo induction of CTL responses by recombinant adenylate cyclase of Bordetella pertussis carrying viral CD8+ T cell epitopes. *Eur. J. Immunol.,* **156,** 4697-4706.

FEINSTEIN, A. & MUNN, E. A. 1969. Conformation of the free and antigen-bound igm antibody molecules. *Nature,* **224,** 1307-1309.

FIERING, S., NORTHROP, J. P., NOLAN, G. P., MATTILA, P. S., CRABTREE, G. R. & HERZENBERG, L. A. 1990. Single cell assay of a transcription factor reveals a threshold in transcription activated by signals emanating from the T-cell antigen receptor. *Genes Dev.,* **4,** 1823-1834.

FIGUEIREDO, D. L. A., MAMEDE, R. C. M., SPAGNOLI, G. C., SILVA, W. A., ZAGO, M., NEDER, L., JUNGBLUTH, A. A. & SAGGIORO, F. P. 2011. High expression of cancer testis antigens MAGE-A, MAGE-C1/CT7, MAGE-C2/CT10, NY-ESO-1, and gage in advanced squamous cell carcinoma of the larynx. *Head & Neck,* **33,** 702-707.

FLEIT, H. B. & KOBASIUK, C. D. 1991. The human monocyte-like cell line THP-1 expresses Fc gamma RI and Fc gamma RII. *J. Leukoc. Biol,* **49,** 556-65.

FORTHAL, D. N., GACH, J. S., LANDUCCI, G., JEZ, J., STRASSER, R., KUNERT, R. & STEINKELLNER, H. 2010. Fc-glycosylation influences Fcγ receptor binding and cell-mediated anti-HIV activity of monoclonal antibody 2G12. *J. Immunol.,* **185,** 6876-6882.

FRENZEL, A., HUST, M. & SCHIRRMANN, T. 2013. Expression of recombinant antibodies. *Front Immunol.,* **4,** 217.

FUMIA, S., GOEDE, J. S., FISCHLER, M., LUGINBÜHL, A., FRICK, S., FODOR, P. & LUTZ, H. U. 2008. Human F(ab′)$_2$-containing immune complexes together with anti-hinge natural antibodies stimulate complement amplification *in vitro* and *in vivo*. *Mol. Immunol.,* **45,** 2951-2961.

GALA, F. A. & MORRISON, S. L. 2002. The role of constant region carbohydrate in the assembly and secretion of human IgD and IgA1. *J. Biol. Chem.,* **277,** 29005-29011.

GARRED, P., MICHAELSEN, T. E. & AASE, A. 1989. The IgG subclass pattern of complement activation depends on epitope density and antibody and complement concentration. *Scand. J. Immunol.,* **30,** 379-382.

GETTS, D. R., GETTS, M. T., MCCARTHY, D. P., CHASTAIN, E. M. L. & MILLER, S. D. 2010. Have we overestimated the benefit of human(ized) antibodies? *mAbs,* **2,** 682-694.

GIL-TORREGROSA, B. C., LENNON-DUMÉNIL, A. M., KESSLER, B., GUERMONPREZ, P., PLOEGH, H. L., FRUCI, D., ENDERT, P. V. & AMIGORENA, S. 2004. Control of cross-presentation during dendritic cell maturation. *Eur. J. Immunol.,* **34,** 398-407.

GIUNTINI, S., GRANOFF, D. M., BEERNINK, P. T., IHLE, O., BRATLIE, D. & MICHAELSEN, T. E. 2016. Human IgG1, IgG3 and IgG3 hinge truncated mutants show different protection capability against meningococci depending on the target antigen and epitope specificity. *Clin. Vaccine Immunol.,* **23,** 698–706.

GOH, Y. S., GRANT, A. J., RESTIF, O., MCKINLEY, T. J., ARMOUR, K. L., CLARK, M. R. & MASTROENI, P. 2011. Human IgG isotypes and activating Fcγ receptors in the interaction of *Salmonella enterica* serovar Typhimurium with phagocytic cells. *Immunology,* **133,** 74-83.

GOULD, H. J., SUTTON, B., J., BEAVIL, A., J., BEAVIL, R., L., MCCLOSKEY, N., COKER, H., A., FEAR, D. & SMURTHWAITE, L. 2003. The biology of IgE and the basis of allergic disease. *Annu. Rev. Immunol.,* **21,** 579-628.

GRAFF-DUBOIS, S., FAURE, O., GROSS, D.-A., ALVES, P., SCARDINO, A., CHOUAIB, S., LEMONNIER, F. A. & KOSMATOPOULOS, K. 2002. Generation of CTL recognizing an HLA-A*0201-restricted epitope shared by MAGE-A1, -A2, -A3, -A4, -A6, -A10, and -A12 tumor antigens: Implication in a broad-spectrum tumor immunotherapy. *J. Immunol.,* **169,** 575-580.

GUDDAT, L. W., HERRON, J. N. & EDMUNDSON, A. B. 1993. Three-dimensional structure of a human immunoglobulin with a hinge deletion. *Proc. Natl Acad. Sci.,* **90,** 4271-4275.

GUILLIAMS, M., BRUHNS, P., SAEYS, Y., HAMMAD, H. & LAMBRECHT, B. N. 2014. The function of Fc[gamma] receptors in dendritic cells and macrophages. *Nat. Rev. Immunol.,* **14,** 94-108.

HAGERMAN, P. J. 1988. Flexibility of DNA. *Annu. Rev. Biophys. Biophys. Chem.,* **17,** 265-286.

HARAOUI, B. & BYKERK, V. 2007. Etanercept in the treatment of rheumatoid arthritis. *Ther. Clin. Risk Manag.,* **3,** 99-105.

HARDING, F. A., STICKLER, M. M., RAZO, J. & DUBRIDGE, R. B. 2010. The immunogenicity of humanized and fully human antibodies: Residual immunogenicity resides in the CDR regions. *mAbs,* **2,** 256-265.

HENDERSHOT, L., BOLE, D., KOHLER, G. & KEARNEY, J. E. 1987. Assembly and secretion of heavy chains that do not associate posttranslationally with immunoglobulin heavy chain-binding protein. *J. Cell. Biol.,* **104,** 761-767.

HERR, A. B., BALLISTER, E. R. & BJORKMAN, P. J. 2003. Insights into IgA-mediated immune responses from the crystal structures of human FcαRI and its complex with IgA1-Fc. *Nature,* **423,** 614-620.

HIGEL, F., SEIDL, A., SÖRGEL, F. & FRIESS, W. 2016. N-glycosylation heterogeneity and the influence on structure, function and pharmacokinetics of monoclonal antibodies and Fc fusion proteins. *Eur. J. Pharm. Biopharm.,* **100,** 94-100.

HOMOLA, J., YEE, S. S. & GAUGLITZ, G. 1999. Surface plasmon resonance sensors: review. *Sens. Actuators B Chem.,* **54,** 3-15.

HON, H., ORAN, A., BROCKER, T. & JACOB, J. 2005. B lymphocytes participate in cross-presentation of antigen following gene gun vaccination. *J. Immunol.,* **174,** 5233-5242.

HONG, S. & VAN KAER, L. 1999. Immune privilege: Keeping an eye on natural killer T cells. *J. Exp. Med.,* **190,** 1197-1200.

HORGAN, C., BROWN, K. & PINCUS, S. H. 1993. Studies on antigen binding by intact and hinge-deleted chimeric antibodies. *J. Immunol.,* **150,** 5400-7.

HOSSLER, P. & KHATTAK, S. F. 2009. Optimal and consistent protein glycosylation in mammalian cell culture. *Glycobiology,* **19,** 936-949.

HOWARTH, M., CHINNAPEN, D. J. F., GERROW, K., DORRESTEIN, P. C., GRANDY, M. R., KELLEHER, N. L., EL-HUSSEINI, A. & TING, A. Y. 2006. A monovalent streptavidin with a single femtomolar biotin binding site. *Nat. Methods,* **3,** 267-273.

HUANG, T., CHEN, X., GU, H., ZHAO, C., LIU, X., YAN, M., DENG, X., ZHANG, Z. & GU, J. 2016. Fractionation of Fab glycosylated immunoglobulin G with concanavalin A chromatography unveils new structural properties of the molecule. *Oncotarget,* **7,** 31166-31176.

HUBER, R., DEISENHOFER, J., COLMAN, P. M., MATSUSHIMA, M. & PALM, W. 1976. Crystallographic structure studies of an IgG molecule and an Fc fragment. *Nature,* **264,** 415-420.

HUEHLS, A. M., COUPET, T. A. & SENTMAN, C. L. 2015. Bispecific T cell engagers for cancer immunotherapy. *Immunol. Cell Biol.,* **93,** 290-296.

IDUSOGIE, E. E., PRESTA, L. G., GAZZANO-SANTORO, H., TOTPAL, K., WONG, P. Y., ULTSCH, M., MENG, Y. G. & MULKERRIN, M. G. 2000. Mapping of the C1q binding site on Rituxan, a chimeric antibody with a human IgG1 Fc. *J. Immunol.,* **164,** 4178-4184.

INBAR, D., HOCHMAN, J. & GIVOL, D. 1972. Localization of Antibody-Combining Sites within the Variable Portions of Heavy and Light Chains. *Proc. Natl Acad. Sci. USA,* **69,** 2659-2662.

JANDA, A., BOWEN, A., GREENSPAN, N. S. & CASADEVALL, A. 2016. Ig constant region effects on variable region structure and function. *Front. Microbiol.,* **7,** 22.

JANDA, A., ERYILMAZ, E., NAKOUZI, A., COWBURN, D. & CASADEVALL, A. 2012. Variable region identical immunoglobulins differing in isotype express different paratopes. *J. Biol. Chem.,* **287,** 35409-35417.

JANEWAY, C. J., TRAVERS, P. & WALPORT, M. 2001a. The complement system and innate immunity. *In: Immunobiology: The Immune System in Health and Disease*. 5th ed. Garland Science New York

JANEWAY, C. J., TRAVERS, P. & WALPORT, M. 2001b. The generation of diversity in immunoglobulins. *In: Immunobiology: The Immune System in Health and Disease*. 5th ed. Garland Science New York

JANEWAY, C. J., TRAVERS, P. & WALPORT, M. 2001c. Principles of innate and adaptive immunity. *In: Immunobiology: The Immune System in Health and Disease*. 5th ed. Garland Science New York

JANEWAY, C. J., TRAVERS, P. & WALPORT, M. 2001d. Structural variation in immunoglobulin constant regions. *In: Immunobiology: The Immune System in Health and Disease*. 5th ed. Garland Science New York

JANEWAY, C. J., TRAVERS, P. & WALPORT, M. 2001e. The structure of a typical antibody molecule. *In: Immunobiology: The Immune System in Health and Disease*. 5th ed. Garland Science New York

JEFFERIS, R. 2005. Glycosylation of recombinant antibody therapeutics. *Biotechnol. Progress,* **21,** 11-16.

JOFFRE, O. P., SEGURA, E., SAVINA, A. & AMIGORENA, S. 2012. Cross-presentation by dendritic cells. *Nat. Rev. Immunol.,* **12,** 557-569.

KABIR, S. 1998. Jacalin: a jackfruit (Artocarpus heterophyllus) seed-derived lectin of versatile applications in immunobiological research. *J. Immunol. Meth.,* **212,** 193-211.

KARTTUNEN, J., SANDERSON, S. & SHASTRI, N. 1992. Detection of rare antigen-presenting cells by the lacZ T-cell activation assay suggests an

expression cloning strategy for T-cell antigens. *Proc. Natl Acad. Sci. USA,* **89,** 6020-6024.

KARU, A. E., BELL, W. C. & CHIN, T. E. 1995. Recombinant antibody technology. *ILAR J.,* **37,** 132-141.

KILÁR, F., SIMON, I., LAKATOS, S., VONDERVISZT, F., MEDGYESI, G. A. & ZÁVODSZKY, P. 1985. Conformation of human IgG subclasses in solution. *Eur. J. Biochem.,* **147,** 17-25.

KIYOSHI, M., CAAVEIRO, J. M. M., KAWAI, T., TASHIRO, S., IDE, T., ASAOKA, Y., HATAYAMA, K. & TSUMOTO, K. 2015. Structural basis for binding of human IgG1 to its high-affinity human receptor FcγRI. *Nat. Commun.,* **6,** 6866.

KLEIN, J. S., JIANG, S., GALIMIDI, R. P., KEEFFE, J. R. & BJORKMAN, P. J. 2014. Design and characterization of structured protein linkers with differing flexibilities. *Protein Eng. Des. Sel.,* **27,** 325-330.

KLEIN, M., HAEFFNER-CAVAILLON, N., ISENMAN, D. E., RIVAT, C., NAVIA, M. A., DAVIES, D. R. & DORRINGTON, K. J. 1981. Expression of biological effector functions by immunoglobulin G molecules lacking the hinge region. *Proc. Natl Acad. Sci. USA,* **78,** 524-528.

KOHLER, G. & MILSTEIN, C. 1975. Continuous cultures of fused cells secreting antibody of predefined specificity. *Nature,* **256,** 495-497.

KONTERMANN, R. E. 2011. Strategies for extended serum half-life of protein therapeutics. *Curr. Opin. Biotechnol.,* **22,** 868-876.

KUMAGAI, I. & TSUMOTO, K. 2002. Antigen–antibody binding. *In: eLS.* John Wiley & Sons, Ltd. DOI: 10.1038/npg.els.0001117

LABRIJN, A. F., MEESTERS, J. I., DE GOEIJ, B. E. C. G., VAN DEN BREMER, E. T. J., NEIJSSEN, J., VAN KAMPEN, M. D., STRUMANE, K., VERPLOEGEN, S., KUNDU, A., GRAMER, M. J., VAN BERKEL, P. H. C., VAN DE WINKEL, J. G. J., SCHUURMAN, J. & PARREN, P. W. H. I. 2013. Efficient generation of stable bispecific IgG1 by controlled Fab-arm exchange. *Proc. Natl Acad. Sci. USA,* **110,** 5145-5150.

LASARTE, J. J., CASARES, N., GORRAIZ, M., HERVÁS-STUBBS, S., ARRIBILLAGA, L., MANSILLA, C., DURANTEZ, M., LLOPIZ, D., SAROBE, P., BORRÁS-CUESTA, F., PRIETO, J. & LECLERC, C. 2007. The extra domain A from fibronectin targets antigens to TLR4-expressing cells and induces cytotoxic t cell responses *in vivo*. *J. Immunol.,* **178,** 748-756.

LAZAR, G. A., DANG, W., KARKI, S., VAFA, O., PENG, J. S., HYUN, L., CHAN, C., CHUNG, H. S., EIVAZI, A., YODER, S. C., VIELMETTER, J., CARMICHAEL, D. F., HAYES, R. J. & DAHIYAT, B. I. 2006. Engineered antibody Fc variants with enhanced effector function. *Proc. Natl Acad. Sci. USA,* **103,** 4005-4010.

LEATHERBARROW, R. J., RADEMACHER, T. W., DWEK, R. A., WOOF, J. M., CLARK, A., BURTON, D. R., RICHARDSON, N. & FEINSTEIN, A. 1985. Effector functions of a monoclonal aglycosylated mouse IgG2a: Binding and activation of complement component C1 and interaction with human monocyte Fc receptor. *Mol. Immunol.,* **22,** 407-415.

LEE, E. C., LIANG, Q., ALI, H., BAYLISS, L., BEASLEY, A., BLOOMFIELD-GERDES, T., BONOLI, L., BROWN, R., CAMPBELL, J., CARPENTER, A., CHALK, S., DAVIS, A., ENGLAND, N., FANE-DREMUCHEVA, A., FRANZ, B., GERMASCHEWSKI, V., HOLMES, H., HOLMES, S., KIRBY, I., KOSMAC, M., LEGENT, A., LUI, H., MANIN, A., O'LEARY, S., PATERSON, J., SCIARRILLO, R., SPEAK, A., SPENSBERGER, D., TUFFERY, L., WADDELL, N., WANG, W., WELLS, S., WONG, V., WOOD, A., OWEN, M. J., FRIEDRICH, G. A. & BRADLEY, A. 2014. Complete humanization of the mouse immunoglobulin loci enables efficient therapeutic antibody discovery. *Nat. Biotechnol.,* **32,** 356-363.

LI, N., WANG, T. & HAN, D. 2012. Structural, cellular and molecular aspects of immune privilege in the testis. *Front. Immunol.,* **3,** 152.

LI, T., DILILLO, D. J., BOURNAZOS, S., GIDDENS, J. P., RAVETCH, J. V. & WANG, L.-X. 2017. Modulating IgG effector function by Fc glycan engineering. *Proc. Natl Acad. Sci.,* **114,** 3485-3490.

LIDA, Y. & MASUDA, T. 1996. Strength of translation initiation signal sequence of mRNA as studied by quantification method: Effect of nucleotide substitutions upon translation efficiency in rat preproinsulin mRNA. *Nucleic Acids Res.,* **24,** 3313-3316.

LINDHOFER, H., HESS, J. & RUF, P. 2011. Trifunctional Triomab® Antibodies for Cancer Therapy. *In: Bispecific Antibodies*. KONTERMANN, R. E. ed., 289-312. Springer Berlin Heidelberg

LINDHOFER, H., MOCIKAT, R., STEIPE, B. & THIERFELDER, S. 1995. Preferential species-restricted heavy/light chain pairing in rat/mouse quadromas. Implications for a single-step purification of bispecific antibodies. *J. Immunol.,* **155,** 219-225.

LIU, H. & MAY, K. 2012. Disulfide bond structures of IgG molecules: Structural variations, chemical modifications and possible impacts to stability and biological function. *mAbs,* **4,** 17-23.

LIU, X., LU, L., YANG, Z., PALANIYANDI, S., ZENG, R., GAO, L.-Y., MOSSER, D. M., ROOPENIAN, D. C. & ZHU, X. 2011. The neonatal FcR-mediated presentation of immune-complexed antigen is associated with endosomal and phagosomal pH and antigen stability in macrophages and dendritic cells. *J. Immunol.,* **186,** 4674-4686.

LIU, Y. & WILSON, W. D. 2010. Quantitative analysis of small molecule–nucleic acid interactions with a biosensor surface and surface plasmon resonance

detection. *In: Drug-DNA Interaction Protocols*. FOX, K. R. ed., 1-23. Humana Press Totowa, NJ

LORENZO, C. D., ARCIELLO, A., COZZOLINO, R., PALMER, D. B., LACCETTI, P., PICCOLI, R. & D'ALESSIO, G. 2004. A fully human antitumor immunornase selective for ErbB-2-positive carcinomas. *Cancer Res.,* **64,** 4870-4874.

LU, J., CHU, J., ZOU, Z., HAMACHER, N. B., RIXON, M. W. & SUN, P. D. 2015. Structure of FcγRI in complex with Fc reveals the importance of glycan recognition for high-affinity IgG binding. *Proc. Natl Acad. Sci. USA,* **112,** 833-838.

LUCISANO VALIM, Y. M. & LACHMANN, P. J. 1991. The effect of antibody isotype and antigenic epitope density on the complement-fixing activity of immune complexes: a systematic study using chimaeric anti-NIP antibodies with human Fc regions. *Clin. Exp. Immunol.,* **84,** 1-8.

LUND, J., TOSHIYUKI, T., NORIKO, T., SARMAY, G., YOJI, A. & JEFFERIS, R. 1990. A protein structural change in aglycosylated IgG3 correlates with loss of huFcγRI and huFcγRIII binding and/or activation. *Mol. Immunol.,* **27,** 1145-1153.

LUTZ, H. U. & FUMIA, S. 2008. Therapeutic cleavage of IgG is dangerous in humans. *Trends Immunol.,* **29,** 353-354.

MACKENZIE, C. R., HIRAMA, T., DENG, S.-J., BUNDLE, D. R., NARANG, S. A. & YOUNG, N. M. 1996. Analysis by surface plasmon resonance of the influence of valence on the ligand binding affinity and kinetics of an anti-carbohydrate antibody. *J. Biol. Chem.,* **271,** 1527-1533.

MANTIS, N. J., ROL, N. & CORTHÉSY, B. 2011. Secretory IgA's complex roles in immunity and mucosal homeostasis in the gut. *Mucosal Immunol.,* **4,** 603-611.

MARCHAND, M., PUNT, C. J. A., AAMDAL, S., ESCUDIER, B., KRUIT, W. H. J., KEILHOLZ, U., HÅKANSSON, L., VAN BAREN, N., HUMBLET, Y., MULDERS, P., AVRIL, M. F., EGGERMONT, A. M. M., SCHEIBENBOGEN, C., UITERS, J., WANDERS, J., DELIRE, M., BOON, T. & STOTER, G. 2003. Immunisation of metastatic cancer patients with MAGE-3 protein combined with adjuvant SBAS-2: a clinical report. *Eur. J. Cancer,* **39,** 70-77.

MARQUART, M., DEISENHOFER, J., HUBER, R. & PALM, W. 1980. Crystallographic refinement and atomic models of the intact immunoglobulin molecule Kol and its antigen-binding fragment at 3.0 Å and 1.0 Å resolution. *J. Mol. Bio.,* **141,** 369-391.

MATTU, T. S., PLEASS, R. J., WILLIS, A. C., KILIAN, M., WORMALD, M. R., LELLOUCH, A. C., RUDD, P. M., WOOF, J. M. & DWEK, R. A. 1998. The glycosylation and structure of human serum IgA1, Fab, and Fc Regions and

the role of N-glycosylation on Fcα receptor interactions. *J. Biol. Chem.,* **273,** 2260-2272.

MAZOR, Y., VAN BLARCOM, T., MABRY, R., IVERSON, B. L. & GEORGIOU, G. 2007. Isolation of engineered, full-length antibodies from libraries expressed in *Escherichia coli*. *Nat. Biotech.,* **25,** 563-565.

MEEK, D. W. & MARCAR, L. 2012. MAGE-A antigens as targets in tumour therapy. *Cancer Letters,* **324,** 126-132.

MEKHAIEL, D. N. A., CZAJKOWSKY, D. M., ANDERSEN, J. T., SHI, J., EL-FAHAM, M., DOENHOFF, M., MCINTOSH, R. S., SANDLIE, I., HE, J., HU, J., SHAO, Z. & PLEASS, R. J. 2011. Polymeric human Fc-fusion proteins with modified effector functions. *Sci. Rep.,* **1,** 124-134.

MICHAELSEN, T. E., AASE, A., NORDERHAUG, L. & SANDLIE, I. 1992. Antibody dependent cell-mediated cytotoxicity induced by chimeric mouse-human IgG subclasses and IgG3 antibodies with altered hinge region. *Mol. Immunol.,* **29,** 319-326.

MISTRY, D. & STOCKLEY, R. 2011. The cleavage specificity of an IgA1 protease from *Haemophilus influenzae*. *Virulence,* **2,** 103-110.

MOHLER, K. M., TORRANCE, D. S., SMITH, C. A., GOODWIN, R. G., STREMLER, K. E., FUNG, V. P., MADANI, H. & WIDMER, M. B. 1993. Soluble tumor necrosis factor (TNF) receptors are effective therapeutic agents in lethal endotoxemia and function simultaneously as both TNF carriers and TNF antagonists. *J. Immunol.,* **151,** 1548-1561.

MONTE, M., SIMONATTO, M., PECHE, L. Y., BUBLIK, D. R., GOBESSI, S., PIEROTTI, M. A., RODOLFO, M. & SCHNEIDER, C. 2006. MAGE-A tumor antigens target p53 transactivation function through histone deacetylase recruitment and confer resistance to chemotherapeutic agents. *Proc. Natl Acad. Sci. USA,* **103,** 11160-11165.

MOORE, M. W., CARBONE, F. R. & BEVAN, M. J. 1988. Introduction of soluble protein into the class I pathway of antigen processing and presentation. *Cell,* **54,** 777-785.

MORELL, A., TERRY, W. D. & WALDMANN, T. A. 1970. Metabolic properties of IgG subclasses in man. *J. Clin. Invest.,* **49,** 673-680.

MÜLLER-RICHTER, U. D. A., DOWEJKO, A., REUTHER, T., KLEINHEINZ, J., REICHERT, T. E. & DRIEMEL, O. 2009. Analysis of expression profiles of MAGE-A antigens in oral squamous cell carcinoma cell lines. *Head Face Med.,* **5,** 10-10.

NAGASHIMA, H., KANEKO, K., YAMANOI, A., MOTOI, S., KONAKAHARA, S., KOHROKI, J. & MASUHO, Y. 2011. TNF receptor II fusion protein with tandemly repeated Fc domains. *J. Biochem.,* **149,** 337-346.

NEUBER, T., FRESE, K., JAEHRLING, J., JÄGER, S., DAUBERT, D., FELDERER, K., LINNEMANN, M., HÖHNE, A., KADEN, S., KÖLLN, J., TILLER, T., BROCKS, B., OSTENDORP, R. & PABST, S. 2014. Characterization and screening of IgG binding to the neonatal Fc receptor. *mAbs,* **6,** 928-942.

NEWMAN, J. A., COOPER, C. D. O., ROOS, A. K., AITKENHEAD, H., OPPERMANN, U. C. T., CHO, H. J., OSMAN, R. & GILEADI, O. 2016. Structures of two melanoma-associated antigens suggest allosteric regulation of effector binding. *PLoS ONE,* **11,** e0148762.

NGUYEN, H. H., PARK, J., KANG, S. & KIM, M. 2015. Surface plasmon resonance: A versatile technique for biosensor applications. *Sensors (Basel),* **15,** 10481-10510.

NIMMERJAHN, F. & RAVETCH, J. V. 2008. Fc[gamma] receptors as regulators of immune responses. *Nat. Rev. Immunol.,* **8,** 34-47.

NORDERHAUG, L., BREKKE, O., BREMNES, B., SANDIN, R., AASE, A., MICHAELSEN, T. E. & SANDLIE, I. 1991. Chimeric mouse human IgG3 antibodies with an IgG4-like hinge region induce complement-mediated lysis more efficiently than IgG3 with normal hinge. *Eur. J. Immunol.,* **21,** 2379-2384.

NOTT, A., MEISLIN, S. H. & MOORE, M. J. 2003. A quantitative analysis of intron effects on mammalian gene expression. *RNA,* **9,** 607-617.

NOVAK, J., TOMANA, M., KILIAN, M., COWARD, L., KULHAVY, R., BARNES, S. & MESTECKY, J. 2000. Heterogeneity of O-glycosylation in the hinge region of human IgA1. *Mol. Immunol.,* **37,** 1047-1056.

OBER, R. J., RADU, C. G., GHETIE, V. & WARD, E. S. 2001. Differences in promiscuity for antibody–FcRn interactions across species: implications for therapeutic antibodies. *Int. Immunol.,* **13,** 1551-1559.

ORTH, R. N., WU, M., HOLOWKA, D. A., CRAIGHEAD, H. G. & BAIRD, B. A. 2003. Mast cell activation on patterned lipid bilayers of subcellular dimensions. *Langmuir,* **19,** 1599-1605.

PAAR, J. M., HARRIS, N. T., HOLOWKA, D. & BAIRD, B. 2002. Bivalent ligands with rigid double-stranded DNA spacers reveal structural constraints on signaling by FcεRI. *J. Immunol.,* **169,** 856-864.

PAULING, L. & BROCKWAY, L. O. 1937. Carbon—carbon bond distances. The electron diffraction investigation of ethane, propane, isobutane, neopentane, cyclopropane, cyclopentane, cyclohexane, allene, ethylene, isobutene, tetramethylethylene, mesitylene, and hexamethylbenzene. Revised values of covalent radii. *J. Am. Chem. Soc,* **59,** 1223-1236.

PERUSSIA, B., DAYTON, E. T., LAZARUS, R., FANNING, V. & TRINCHIERI, G. 1983. Immune interferon induces the receptor for monomeric IgG1 on human monocytic and myeloid cells. *J. Exp. Med.,* **158,** 1092-1113.

PETRUŠIĆ, V., ŽIVKOVIĆ, I., STOJANOVIĆ, M., STOJIĆEVIĆ, I., MARINKOVIĆ, E. & DIMITRIJEVIĆ, L. 2011. Hexameric immunoglobulin M in humans: Desired or unwanted? *Med. Hypotheses,* **77,** 959-961.

PLEASS, R. J., DUNLOP, J. I., ANDERSON, C. M. & WOOF, J. M. 1999. Identification of residues in the CH2/CH3 domain interface of IgA essential for interaction with the human Fcα receptor (FcαR) CD89. *J. Biol. Chem.,* **274,** 23508-23514.

PRZEPIORKA, D., KO, C.-W., DEISSEROTH, A., YANCEY, C. L., CANDAU-CHACON, R., CHIU, H.-J., GEHRKE, B. J., GOMEZ-BROUGHTON, C., KANE, R. C., KIRSHNER, S., MEHROTRA, N., RICKS, T. K., SCHMIEL, D., SONG, P., ZHAO, P., ZHOU, Q., FARRELL, A. T. & PAZDUR, R. 2015. FDA approval: Blinatumomab. *Clin. Cancer Res.,* **21,** 4035-4039.

PUTNAM, F. W., LIU, Y. S. & LOW, T. L. 1979. Primary structure of a human IgA1 immunoglobulin. IV. Streptococcal IgA1 protease, digestion, Fab and Fc fragments, and the complete amino acid sequence of the alpha 1 heavy chain. *J. Biol. Chem.,* **254,** 2865-2874.

PYZIK, M., RATH, T., LENCER, W. I., BAKER, K. & BLUMBERG, R. S. 2015. FcRn: The architect behind the immune and nonimmune functions of IgG and albumin. *J. Immunol.,* **194,** 4595-4603.

QUEEN, C., SCHNEIDER, W. P., SELICK, H. E., PAYNE, P. W., LANDOLFI, N. F., DUNCAN, J. F., AVDALOVIC, N. M., LEVITT, M., JUNGHANS, R. P. & WALDMANN, T. A. 1989. A humanized antibody that binds to the interleukin 2 receptor. *Proc. Natl Acad. Sci. USA,* **86,** 10029-10033.

RADAEV, S., MOTYKA, S., FRIDMAN, W.-H., SAUTES-FRIDMAN, C. & SUN, P. D. 2001. The structure of a human type III Fcγ receptor in complex with Fc. *J. Biol. Chem.,* **276,** 16469-16477.

RADAEV, S. & SUN, P. D. 2001. Recognition of IgG by Fcγ Receptor: The role of Fc glycosylation and the binding of peptide inhibitors. *J. Biol. Chem.,* **276,** 16478-16483.

RAFIQ, K., BERGTOLD, A. & CLYNES, R. 2002. Immune complex–mediated antigen presentation induces tumor immunity. *J. Clin. Invest.,* **110,** 71-79.

RAJU, T. S. 2008. Terminal sugars of Fc glycans influence antibody effector functions of IgGs. *Curr. Opin. Immunol.,* **20,** 471-478.

RAMSLAND, P. A., FARRUGIA, W., BRADFORD, T. M., TAN SARDJONO, C., ESPARON, S., TRIST, H. M., POWELL, M. S., SZEE TAN, P., CENDRON, A. C., WINES, B. D., SCOTT, A. M. & HOGARTH, P. M. 2011. Structural basis for FcγRIIa recognition of human IgG and formation of inflammatory signaling complexes. *J. Immunol.,* **187,** 3208-3217.

RAVETCH, J. V. & PERUSSIA, B. 1989. Alternative membrane forms of FcγRIII(CD16) on human natural killer cells and neutrophils. Cell type-

specific expression of two genes that differ in single nucleotide substitutions. *J. Exp. Med.,* **170,** 481-497.

REDPATH, S., MICHAELSEN, T. E., SANDLIE, I. & CLARK, M. R. 1998. The influence of the hinge region length in binding of human IgG to human Fcγ receptors. *Hum. Immunol.,* **59,** 720-727.

RETH, M., HÄMMERLING, G. J. & RAJEWSKY, K. 1978. Analysis of the repertoire of anti-NP antibodies in C57BL/6 mice by cell fusion. I. Characterization of antibody families in the primary and hyperimmune response. *Eur. J. Immunol.,* **8,** 393-400.

RIDGWAY, J. B., PRESTA, L. G. & CARTER, P. 1996. 'Knobs-into-holes' engineering of antibody CH3 domains for heavy chain heterodimerization. *Protein Eng.,* **9,** 617-621.

RIVAT, C., RIVAT, L., ROPARTZ, C., SCHIFF, C. & FOUGEREAU, M. 1976. Deletion of hinge region of human myeloma lgG1 molecule (protein LEC) associated with nonexpression of G1m(3) and Km(1,2) allotypes. A possible genetic explanation at the DNA level. *Eur. J. Immunol.,* **6,** 545-551.

ROOPENIAN, D. C. & AKILESH, S. 2007. FcRn: the neonatal Fc receptor comes of age. *Nat. Rev. Immunol.,* **7,** 715-725.

ROUX, K. H., STRELETS, L., BREKKE, O. H., SANDLIE, I. & MICHAELSEN, T. E. 1998. Comparisons of the ability of human IgG3 hinge mutants, IgM, IgE, and IgA2, to form small immune complexes: A role for flexibility and geometry. *J. Immunol.,* **161,** 4083-4090.

ROUX, K. H., STRELETS, L. & MICHAELSEN, T. E. 1997a. Flexibility of human IgG subclasses. *J. Immunol.,* **159,** 3372-3382.

ROUX, K. H., STRELETS, L. & MICHAELSEN, T. E. 1997b. Flexibility of human IgG subclasses. *J. Immunol.,* 159**,** 3372-82.

ROYLE, L., ROOS, A., HARVEY, D. J., WORMALD, M. R., VAN GIJLSWIJK-JANSSEN, D., REDWAN, E.-R. M., WILSON, I. A., DAHA, M. R., DWEK, R. A. & RUDD, P. M. 2003. Secretory IgA N- and O-glycans provide a link between the innate and adaptive immune systems. *J. Biol. Chem.,* **278,** 20140-20153.

RYAN, M. H., PETRONE, D., NEMETH, J. F., BARNATHAN, E., BJÖRCK, L. & JORDAN, R. E. 2008. Proteolysis of purified IgGs by human and bacterial enzymes in vitro and the detection of specific proteolytic fragments of endogenous IgG in rheumatoid synovial fluid. *Mol. Immunol.,* **45,** 1837-1846.

SANDIN, S., ÖFVERSTEDT, L.-G., WIKSTRÖM, A.-C., WRANGE, Ö. & SKOGLUND, U. 2004. Structure and flexibility of individual immunoglobulin G molecules in solution. *Structure,* **12,** 409-415.

SANDLIE, I., AASE, A., WESTBY, C. & MICHAELSEN, T. E. 1989. C1q binding to chimeric monoclonal IgG3 antibodies consisting of mouse variable regions

and human constant regions with shortened hinge containing 15 to 47 amino acids. *Eur. J. Immunol.,* **19,** 1599-1603.

SANDSTRÖM, K., HAYLOCK, A. K., SPIEGELBERG, D., QVARNSTRÖM, F., WESTER, K. & NESTOR, M. 2012. A novel CD44v6 targeting antibody fragment with improved tumor-to-blood ratio. *Int. J. Oncol.,* **40,** 1525-1532.

SANG, M., LIAN, Y., ZHOU, X. & SHAN, B. 2011. MAGE-A family: Attractive targets for cancer immunotherapy. *Vaccine,* **29,** 8496-8500.

SAPHIRE, E. O., PARREN, P. W. H. I., PANTOPHLET, R., ZWICK, M. B., MORRIS, G. M., RUDD, P. M., DWEK, R. A., STANFIELD, R. L., BURTON, D. R. & WILSON, I. A. 2001. Crystal structure of a neutralizing human IgG against HIV-1: A template for vaccine design. *Science,* **293,** 1155-1159.

SAPHIRE, E. O., STANFIELD, R. L., MAX CRISPIN, M. D., PARREN, P. W. H. I., RUDD, P. M., DWEK, R. A., BURTON, D. R. & WILSON, I. A. 2002. Contrasting IgG structures reveal extreme asymmetry and flexibility. *J. Mol. Biol.,* **319,** 9-18.

SCANLAN, M. J., GURE, A. O., JUNGBLUTH, A. A., OLD, L. J. & CHEN, Y.-T. 2002. Cancer/testis antigens: an expanding family of targets for cancer immunotherapy. *Immunol. Rev.,* **188,** 22-32.

SCHNEIDER, S. & ZACHARIAS, M. 2012. Atomic resolution model of the antibody Fc interaction with the complement C1q component. *Mol. Immunol.,* **51,** 66-72.

SCHROEDER JR, H. W. & CAVACINI, L. 2010. Structure and function of immunoglobulins. *J. Allergy. Clin. Immunol.,* **125,** S41-S52.

SCHULTZ-THATER, E., PISCUOGLIO, S., IEZZI, G., LE MAGNEN, C., ZAJAC, P., CARAFA, V., TERRACCIANO, L., TORNILLO, L. & SPAGNOLI, G. C. 2011. MAGE-A10 is a nuclear protein frequently expressed in high percentages of tumor cells in lung, skin and urothelial malignancies. *Int. J. Cancer,* **129,** 1137-1148.

SCHUURHUIS, D. H., IOAN-FACSINAY, A., NAGELKERKEN, B., VAN SCHIP, J. J., SEDLIK, C., MELIEF, C. J. M., VERBEEK, J. S. & OSSENDORP, F. 2002. Antigen-antibody immune complexes empower dendritic cells to efficiently prime specific CD8 CTL responses *in vivo*. *J. Immunol.,* **168,** 2240.

SENIOR, B. W., DUNLOP, J. I., BATTEN, M. R., KILIAN, M. & WOOF, J. M. 2000. Cleavage of a recombinant human immunoglobulin A2 (IgA2)-IgA1 hybrid antibody by certain bacterial IgA1 proteases. *Infect. Immunol.,* **68,** 463-469.

SENIOR, B. W. & WOOF, J. M. 2005. The influences of hinge length and composition on the susceptibility of human IgA to cleavage by diverse bacterial IgA1 proteases. *J. Immunol.,* **174,** 7792-7799.

SENIOR, B. W. & WOOF, J. M. 2006. Sites in the CH3 domain of human IgA1 that influence sensitivity to bacterial IgA1 proteases. *J. Immunol.,* **177,** 3913-3919.

SHAW, C. A. & STARNBACH, M. N. 2006. Stimulation of CD8(+) T Cells following diphtheria toxin-mediated antigen delivery into dendritic cells. *Infect. Immunol.,* **74,** 1001-1008.

SHIELDS, R. L., NAMENUK, A. K., HONG, K., MENG, Y. G., RAE, J., BRIGGS, J., XIE, D., LAI, J., STADLEN, A., LI, B., FOX, J. A. & PRESTA, L. G. 2001. High resolution mapping of the binding site on human IgG1 for FcγRI, FcγRII, FcγRIII, and FcRn and design of IgG1 variants with improved binding to the FcγR. *J. Biol. Chem.,* **276,** 6591-6604.

SHOHET, J. M., PEMBERTON, P. & CARROLL, M. C. 1993. Identification of a major binding site for complement C3 on the IgG1 heavy chain. *J. Biol. Chem.,* **268,** 5866-5871.

SILVERTON, E. W., NAVIA, M. A. & DAVIES, D. R. 1977. Three-dimensional structure of an intact human immunoglobulin. *Proc. Natl Acad. Sci. USA,* **74,** 5140-5144.

SIMMONS, L. C., REILLY, D., KLIMOWSKI, L., SHANTHA RAJU, T., MENG, G., SIMS, P., HONG, K., SHIELDS, R. L., DAMICO, L. A., RANCATORE, P. & YANSURA, D. G. 2002. Expression of full-length immunoglobulins in *Escherichia coli*: rapid and efficient production of aglycosylated antibodies. *J. Immunol. Methods.,* **263,** 133-147.

SIOUD, M., WESTBY, P., OLSEN, J. K. E. & MOBERGSLIEN, A. 2015. Generation of new peptide-Fc fusion proteins that mediate antibody-dependent cellular cytotoxicity against different types of cancer cells. *Mol. Ther. Methods Clin. Dev.,* **2,** 15043-15052.

SKERRA, A. & PLUCKTHUN, A. 1988. Assembly of a functional immunoglobulin Fv fragment in Escherichia coli. *Science,* **240,** 1038-1041.

SMITH, S. B., FINZI, L. & BUSTAMANTE, C. 1992. Direct mechanical measurements of the elasticity of single DNA molecules by using magnetic beads. *Science,* **258,** 1122-1126.

SMITS, N. C. & SENTMAN, C. L. 2016. Bispecific T-Cell Engagers (BiTEs) as treatment of B-cell lymphoma. *J. Clin. Oncol.,* **34,** 1131-1133.

SONDERMANN, P., HUBER, R., OOSTHUIZEN, V. & JACOB, U. 2000. The 3.2-Å crystal structure of the human IgG1 Fc fragment-Fc[gamma]RIII complex. *Nature,* **406,** 267-273.

SOSNICK, T. R., BENJAMIN, D. C., NOVOTNY, J., SEEGER, P. A. & TREWHELLA, J. 1992. Distances between the antigen-binding sites of three murine antibody subclasses measured using neutron and x-ray scattering. *Biochemistry,* **31,** 1779-1786.

STANFIELD, R. L., ZEMLA, A., WILSON, I. A. & RUPP, B. 2006. Antibody elbow angles are influenced by their light chain class. *J. Mol. Biol.,* **357,** 1566-1574.

STAPLETON, N. M., ANDERSEN, J. T., STEMERDING, A. M., BJARNARSON, S. P., VERHEUL, R. C., GERRITSEN, J., ZHAO, Y., KLEIJER, M., SANDLIE, I., DE HAAS, M., JONSDOTTIR, I., VAN DER SCHOOT, C. E. & VIDARSSON, G. 2011. Competition for FcRn-mediated transport gives rise to short half-life of human IgG3 and offers therapeutic potential. *Nat. Commun.,* **2,** 599.

STEINER, L. & LOPES, A. D. 1979. The crystallizable human myeloma protein Dob has a hinge-region deletion. *Biochemistry,* **18,** 4054-4067.

TAKAHASHI, N., TETAERT, D., DEBUIRE, B., LIN, L. C. & PUTNAM, F. W. 1982. Complete amino acid sequence of the delta heavy chain of human immunoglobulin D. *Proc. Natl Acad. Sci. USA,* **79,** 2850-2854.

TAN, L. K., SHOPES, R. J., OI, V. T. & MORRISON, S. L. 1990. Influence of the hinge region on complement activation, C1q binding, and segmental flexibility in chimeric human immunoglobulins. *Proc. Natl Acad. Sci. USA,* **87,** 162-166.

TANG, Y., LOU, J., ALPAUGH, R. K., ROBINSON, M. K., MARKS, J. D. & WEINER, L. M. 2007. Regulation of antibody-dependent cellular cytotoxicity by IgG intrinsic and apparent affinity for target antigen. *J. Immunol.,* **179,** 2815-2823.

TANZARELLA, S., RUSSO, V., LIONELLO, I., DALERBA, P., RIGATTI, D., BORDIGNON, C. & TRAVERSARI, C. 1999. Identification of a promiscuous T-cell epitope encoded by multiple members of the MAGE family. *Cancer Res.,* **59,** 2668-2674.

TAO, M. H. & MORRISON, S. L. 1989. Studies of aglycosylated chimeric mouse-human IgG. Role of carbohydrate in the structure and effector functions mediated by the human IgG constant region. *J. Immunol.,* **143,** 2595-2601.

TARELLI, E., SMITH, A. C., HENDRY, B. M., CHALLACOMBE, S. J. & POURIA, S. 2004. Human serum IgA1 is substituted with up to six O-glycans as shown by matrix assisted laser desorption ionisation time-of-flight mass spectrometry. *Carbohydr. Res.,* **339,** 2329-2335.

TERNESS, P., KOHL, I., HÜBENER, G., BATTISTUTTA, R., MORODER, L., WELSCHOF, M., DUFTER, C., FINGER, M., HAIN, C. & JUNG, M. 1995. The natural human IgG anti-$F(ab')_2$ antibody recognizes a conformational IgG1 hinge epitope. *J. Immunol.,* **154,** 6446-6452.

TOMANA, M., NOVAK, J., JULIAN, B. A., MATOUSOVIC, K., KONECNY, K. & MESTECKY, J. 1999. Circulating immune complexes in IgA nephropathy consist of IgA1 with galactose-deficient hinge region and antiglycan antibodies. *J. Clin. Invest.,* **104,** 73-81.

TORRERI, P., CECCARINI, M., MACIOCE, P. & PETRUCCI, T. C. 2005. Biomolecular interactions by surface plasmon resonance technology. *Ann. Ist Super Sanita.,* **41,** 437-441.

TORRES, A. J., HOLOWKA, D. & BAIRD, B. A. 2011. Micropatterned ligand arrays to study spatial regulation in Fc receptor signaling. *Methods Mol. Biol.,* **748,** 195-207.

TROMBETTA, E. S., EBERSOLD, M., GARRETT, W., PYPAERT, M. & MELLMAN, I. 2003. Activation of lysosomal function during dendritic cell maturation. *Science,* **299,** 1400-1403.

TSUCHIYA, S., YAMABE, M., YAMAGUCHI, Y., KOBAYASHI, Y., KONNO, T. & TADA, K. 1980. Establishment and characterization of a human acute monocytic leukemia cell line (THP-1). *Int. J. Cancer,* **26,** 171-176.

TSUZUKIDA, Y., WANG, C. C. & PUTNAM, F. W. 1979. Structure of the A2m(1) allotype of human IgA—a recombinant molecule. *Proc. Natl Acad. Sci. USA,* **76,** 1104-1108.

VALENTINE, R. C. & GREEN, N. M. 1967. Electron microscopy of an antibody-hapten complex. *J. Mol. Biol.,* **27,** 615-617.

VAN DER BRUGGEN, P., TRAVERSARI, C., CHOMEZ, P., LURQUIN, C., DE PLAEN, E., VAN DEN EYNDE, B., KNUTH, A. & BOON, T. 1991. A gene encoding an antigen recognized by cytolytic T lymphocytes on a human melanoma. *Science,* **254,** 1643-1647.

VANSTEENKISTE, J. F., CHO, B. C., VANAKESA, T., DE PAS, T., ZIELINSKI, M., KIM, M. S., JASSEM, J., YOSHIMURA, M., DAHABREH, J., NAKAYAMA, H., HAVEL, L., KONDO, H., MITSUDOMI, T., ZAROGOULIDIS, K., GLADKOV, O. A., UDUD, K., TADA, H., HOFFMAN, H., BUGGE, A., TAYLOR, P., GONZALEZ, E. E., LIAO, M. L., HE, J., PUJOL, J.-L., LOUAHED, J., DEBOIS, M., BRICHARD, V., DEBRUYNE, C., THERASSE, P. & ALTORKI, N. 2016. Efficacy of the MAGE-A3 cancer immunotherapeutic as adjuvant therapy in patients with resected MAGE-A3-positive non-small-cell lung cancer (MAGRIT): a randomised, double-blind, placebo-controlled, phase 3 trial. *Lancet Oncol.,* **17,** 822-835.

VELDE, A. A. T., MALEFIJT, R. D. W., HUIJBENS, R. & FIGDOR, C. 1993. IL-10 stimulates monocyte FcγR surface expression and cytotoxic activity. Distinct regulation of antibody-dependent cellular cytotoxicity by IFNγ, IL-4, and IL-10. *J. Immunol.,* **149,** 4048-4052.

VELDERS, M. P., VAN RHIJN, C. M., OSKAM, E., FLEUREN, G. J., WARNAAR, S. O. & LITVINOV, S. V. 1998. The impact of antigen density and antibody affinity on antibody-dependent cellular cytotoxicity: relevance for immunotherapy of carcinomas. *Br. J. Cancer,* **78,** 478-483.

VIDARTE, L., PASTOR, C., MAS, S., BLÁZQUEZ, A. B., DE LOS RIOS, V., GUERRERO, R. & VIVANCO, F. 2001. Serine 132 is the C3 covalent attachment point on the CH1 domain of human IgG1. *J. Biol. Chem.,* **276,** 38217-38223.

VINCENTS, B., VON PAWEL-RAMMINGEN, U., BJÖRCK, L. & ABRAHAMSON, M. 2004. Enzymatic characterization of the *Streptococcal* endopeptidase, IdeS, reveals that it is a cysteine protease with strict specificity for IgG cleavage due to exosite binding. *Biochemistry,* **43,** 15540-15549.

VINK, T., OUDSHOORN-DICKMANN, M., ROZA, M., REITSMA, J.-J. & DE JONG, R. N. 2014. A simple, robust and highly efficient transient expression system for producing antibodies. *Methods,* **65,** 5-10.

VIRELLA, G. & YEH, C. 1977. The sensitivity to plasmin digestion of human IgG proteins of different heavy chain subclasses. *Experientia,* **33,** 1231-1233.

VON PAWEL-RAMMINGEN, U., JOHANSSON, B. P. & BJÖRCK, L. 2002. IdeS, a novel streptococcal cysteine proteinase with unique specificity for immunoglobulin G. *EMBO J.,* **21,** 1607-1615.

WALKER, M. R., WOOF, J. M., BRÜGGEMANN, M., JEFFERIS, R. & BURTON, D. R. 1989. Interaction of human IgG chimeric antibodies with the human FcRI and FcRII receptors: Requirements for antibody-mediated host cell-target cell interaction. *Mol. Immunol.,* **26,** 403-411.

WARD, E. S., ZHOU, J., GHETIE, V. & OBER, R. J. 2003. Evidence to support the cellular mechanism involved in serum IgG homeostasis in humans. *Int. Immunol.,* **15,** 187-195.

WARMERDAM, P. A., VAN DE WINKEL, J. G., GOSSELIN, E. J. & CAPEL, P. J. 1990. Molecular basis for a polymorphism of human Fc gamma receptor II (CD32). *J. Exp. Med.,* **172,** 19-25.

WATSON, J. D. & CRICK, F. H. C. 1953. Molecular structure of nucleic acids: A structure for deoxyribose nucleic acid. *Nature,* **171,** 737-738.

WEFLEN, A. W., BAIER, N., TANG, Q.-J., VAN DEN HOF, M., BLUMBERG, R. S., LENCER, W. I. & MASSOL, R. H. 2013. Multivalent immune complexes divert FcRn to lysosomes by exclusion from recycling sorting tubules. *Mol. Biol. Cell.,* **24,** 2398-2405.

WOOF, J. M. & BURTON, D. R. 2004. Human antibody-Fc receptor interactions illuminated by crystal structures. *Nat. Rev. Immunol.,* **4,** 89-99.

WOOF, J. M., PARTRIDGE, L. J., JEFFERIS, R. & BURTON, D. R. 1986. Localisation of the monocyte-binding region on human immunoglobulin G. *Mol. Immunol.,* **23,** 319-330.

WOOF, J. M. & RUSSELL, M. W. 2011. Structure and function relationships in IgA. *Mucosal Immunol.,* **4,** 590-597.

YE, L., ZENG, R., BAI, Y., ROOPENIAN, D. C. & ZHU, X. 2011. Efficient mucosal delivery of vaccine using the FcRn-mediated IgG transfer pathway. *Nat. Biotechnol.,* **29,** 158-163.

ZEARFOSS, N. R. & RYDER, S. P. 2012. End-labeling oligonucleotides with chemical tags after synthesis. *Methods Mol. Biol.,* **941,** 181-193.